PERFORMANCE-BASED PLASTIC DESIGN OF EARTHQUAKE RESISTANT REINFORCED CONCRETE MOMENT FRAMES

by

Wen-Cheng Liao

A dissertation submitted in partial fulfillment
of the requirements for the degree of
Doctor of Philosophy
(Civil Engineering)
in The University of Michigan
2010

Doctoral Committee:

Emeritus Professor Subhash C. Goel, Chair
Emeritus Professor Antoine E. Naaman
Professor Anthony M. Waas
Associate Professor Gustavo J. Parra-Montesinos
Assistant Professor Jason P. McCormick

ACKNOWLEDGEMENTS

First and foremost, the author would like to express his deepest gratitude and sincere appreciation to Professor Subhash C. Goel, chairman of the doctoral committee, for his valuable guidance, advice and support during this research. Appreciation is also extended to the members of the dissertation committee, Professors Jason P. McCormick, Antoine E. Naaman, Gustavo J. Parra-Montesinos and Anthony M. Waas, for their valuable suggestions and advice. Special thanks are due to Professor Antoine E. Naaman for his extra encouragement and mentorship.

The author also wishes to thank Professor Shih-Ho Chao at the University of Texas, Arlington, for his advice and help.

In the initial stages of his graduate study the author received Rackham Graduate School Fellowship and financial support from the National Science Foundation Grants CMS 0530383 and CMS 0754505 under the direction of Professors James K. Wight and Gustavo J. Parra-Montesinos. Partial support from the G. S. Agarwal Fellowship Fund is also gratefully acknowledged.

Last but not the least the author would like to thank his beloved Yang-Luen Shih for giving all her affection and support during this entire period. The author would also like to express his gratitude and love to his family for their continuous understanding, encouragement, and support that enabled him to fulfill his dream of completing his doctoral degree at the University of Michigan.

TABLE OF CONTENTS

LIST OF TABLES

LIST OF FIGURES

LIST OF SYMBOLS

C_d Deflection amplification factor

C_s Seismic response coefficient

C_u Coefficient for upper limit on calculated period (ASCE 7-05)

C_{vx} Vertical force distribution factor (ASCE 7-05)

C_y Yield strength coefficient for yield point spectra method

C_2 Modification factor of target design drift (FEMA 440)

e Cyclic degradation energy factor in PERFORM 3D

E_c Energy capacity for energy spectrum method

E_d Energy demand for energy spectrum method

E_e Elastic components of the energy needed to push the structure up to the target drift

EI_{eff} Effective stiffness

E_p Plastic components of the energy needed to push the structure up to the target drift

f'_c Concrete strength

F_i Lateral force at level i

F_{i-PD} Lateral force due to P-Delta at level i

F_n Lateral force at the top level n of the structure

F_L Total required lateral force

g Acceleration due to gravity

h Height, total height of the structure

h_i Height of the first story

I Occupancy factor (ASCE 7-05)

k Exponent related to the structure period, T (ASCE 7-05)

L Span length

L' Distance between plastic hinges in the beam

M Total mass of the system

m Oscillator mass

M_i Seismic mass at level i

M_n Nominal flexural strength

M_{pbi} Required plastic moment strength of the beam at the level i

M_{pbr} Reference plastic moment of beams

M_{pc} Plastic moment of the columns at the base of the structure

P_n Nominal compressive strength

P_u Required axial strength

R Force reduction factor

$R_{\max}$ Minimum strength factor to avoid dynamic instability (FEMA 440; FEMA P440A)

R_μ Ductility reduction factor

R_μ^* Modified ductility reduction factor by C_2 factor method

S_a Elastic design spectral acceleration value

S_{DS} Design spectral response acceleration parameter at short periods (5% damped)

S_{D1} Design spectral response acceleration parameter at period of 1 sec (5% damped)

s_n Rebar buckling coefficient (FEMA P695)

S_v Design pseudo-spectral velocity

S_1 Mapped MCE spectral response acceleration parameter at a period of 1 sec (5% damped)

T Fundamental period of the structure

T_e Effective fundamental period

T_L Long-period transition period

u_r Roof displacement

$u_{r-\max}$ Maximum roof displacement

V Seismic design base shear

V^* Design base shear for one frame

V_i Static story shear at level i

V_n Static story shear at the top level n

V_y Design base shear as determined from the energy balance Equation (3-6)

W Total seismic weight of the structure

w_i Weight of the structure at level i

w_n Weight of the structure at the top level n

x $\left|\frac{M_{pb-negative}}{M_{pb-positive}}\right|$

α Design base shear parameter

α_{sl} Bond-slip indicator (FEMA P695)

β_i Shear proportioning factor

Δ Lateral drift

Δ_{eu} Maximum elastic drift corresponding to C_{eu}

$\Delta_{\max}$ Maximum inelastic drift

Δ_y Yield drift

δ_s Moment magnifier (ACI 318)

γ Modification factor for the energy balance equation

γ^* Modified modification factor for the energy balance equation by C_2 factor method

η Ratio of reduced area of typical hysteretic loop to the corresponding full loop

ρ Longitudinal reinforcement ratio

ρ_{sh} Confinement ratio

λ Cyclic energy dissipation capacity (FEMA P695)

λ_i Proportioning factor of the equivalent lateral force at level i

μ Rotational ductility demand

μ_s Ductility

μ_S^* Modified ductility by C_2 factor method

θ_p Plastic rotation, Inelastic drift

$\theta_{cap,pl}$ Plastic rotation capacity (FEMA P695)

θ_{pc} Post-capping rotation capacity (FEMA P695)

θ_u Target design drift by C_2 factor method

θ_u^* Modified target design drift by C_2 factor method

θ_y Yield rotation

Ω Structural overstrength factor

ξ Overstrength factor of the beam

ABSTRACT

Performance-Based Plastic Design of Earthquake Resistant Reinforced Concrete Moment Frames

by

Wen-Cheng Liao

Chair: Subhash C. Goel

Performance-Based Plastic Design (PBPD) method has been recently developed to achieve enhanced performance of earthquake resistant structures. The design concept uses pre-selected target drift and yield mechanism as performance criteria. The design base shear for selected hazard level is determined by equating the work needed to push the structure monotonically up to the target drift to the corresponding energy demand of an equivalent SDOF oscillator.

This study presents development of the PBPD approach as applied to reinforced concrete special moment frame (RC SMF) structures. RC structures present special challenge because of their complex and degrading ("pinched") hysteretic behavior. In order to account for the degrading hysteretic behavior the FEMA 440 C_2 factor approach was used in the

process of determining the design base shear.

Four baseline RC SMF (4, 8, 12 and 20-story) as used in the FEMA P695 were selected for this study. Those frames were redesigned by the PBPD approach. The baseline frames and the PBPD frames were subjected to extensive inelastic pushover and time-history analyses. The PBPD frames showed much improved response meeting all desired performance objectives, including the intended yield mechanisms and the target drifts. On the contrary, the baseline frames experienced large story drifts due to flexural yielding of the columns.

The work-energy equation to determine design base shear can also be used to estimate seismic demands, called the energy spectrum method. In this approach the skeleton force-displacement (capacity) curve of the structure is converted into energy-displacement plot (E_c) which is superimposed over the corresponding energy demand plot (E_d) for the specified hazard level to determine the expected peak displacement demands.

In summary, this study shows that the PBPD approach can be successfully applied to RC moment frame structures as well, and that the responses of the example moment frames were much improved over those of the corresponding baseline frames. In addition, the drift demands of all study frames as computed by the energy spectrum method were in excellent agreement with those obtained from detailed inelastic dynamic analyses.

CHAPTER 1

INTRODUCTION

1.1. Background and motivation

Reinforced concrete special moment frames (RC SMF) comprise of horizontal framing components (beams and slabs), vertical framing components (columns) and joints connecting horizontal and vertical framing components that are designed to meet the special requirements given in seismic codes (e.g., ACI 318, 2008; ASCE 7-05, 2005). Those special proportioning and detailing requirements are intended to make the frames capable of resisting strong earthquake shaking without significant loss of stiffness or strength. However, the losses due to structural and nonstructural damage in code compliant buildings have led to the awareness that current seismic design methods are not always able to provide the desired and satisfactory performance as can be seen from the example shown in Figure 1-1. Since RC SMF have been widely used as part of seismic force-resisting systems, design methodologies and systematic procedures are needed which require no or little iteration after initial design in order to meet the targeted design objectives.

Figure 1-1 Undesirable (soft story) failure of RC SMF under Chi-Chi earthquake (1999)

In order to achieve targeted design objectives, such as well-controlled interstory drifts and desired yield mechanism under earthquake ground motions, it is essential to develop a complete design methodology for RC SMF. Such design method should consider inelastic behavior of RC SMF from the beginning along with determination of appropriate design base shear and lateral force distribution. A systematic procedure for proportioning members by considering inelastic behavior of the overall structure should be also concluded in the methodology.

1.2. Objectives and scope of this study

The main objective of this study was to develop and validate a seismic design methodology for RC SMF which is able to produce structures with predictable and intended seismic performance. Based on performance limit states of target drift and desired yield mechanism, this design methodology accounts for inelastic structural behavior directly, and practically eliminates the need for assessment or iteration by nonlinear static or time-history analysis after initial design. The methodology for steel frames has been developed by Goel et al., in recent years (1999~2008). It is called Performance-Based Plastic Design (PBPD) method.

The PBPD method explicitly accounts for inelastic state of structures, i.e., pre-selected yield mechanisms. Previous studies on steel moment frames (MF), buckling-restrained braced frame (BRBF), eccentrically braced frames (EBF), special truss moment frames (STMF), and concentrically braced frames (CBF) have demonstrated the superiority of this method over the current elastic design approach (Goel et al., 1999~2008). It is also worth mentioning that results of those prior investigations have led to a PBPD design guide for steel framing systems (Goel and Chao, 2008).

A comprehensive research effort is needed to further advance the PBPD methodology and extend its application to reinforced concrete structures. Seismic design of RC structures

to achieve targeted response presents special challenge mainly due to their complex hysteretic behavior. This study is primarily analytical in nature and focuses on RC moment frames. It is expected that findings from this study will be incorporated in the next generation of performance-based design codes and practice.

This study was comprised of three phases:

1. A series of RC SMF (4, 8, 12 and 20 stories) as used in the FEMA P695 document (ATC-63, 2009) were used as baseline frames for this study. Those buildings were called *"benchmark buildings"* in that report *"in order to obtain a generalized collapse prediction that is representative of RC SMF buildings designed by current building codes in the western United States*". The PBPD methodology was developed and applied to redesign those four frames.

2. For response evaluation purposes, the baseline frames and the PBPD frames were subjected to extensive inelastic pushover and time-history analyses

3. An energy spectrum method based on the same energy concept as used in the PBPD method was developed and validated for prediction of approximate displacement demand, including interstory drifts.

1.3. Organization of the dissertation

This dissertation is comprised of eight chapters:

1. Chapter 1 provides background and motivation, objectives and scope, and organization of the dissertation.

2. Chapter 2 presents a review of the current code procedures for seismic design of RC special moment frames and the weakness of those procedures. Related past studies

that have addressed the problems of current code procedures or recently proposed Performance-Based Seismic Design (PBSD) methods are also reviewed and discussed.

3. Chapter 3 provides energy balance concept in Performance-Based Plastic Design (PBPD), comparison of PBPD and current code design method as well as detailed PBPD design procedures for RC SMF. Necessary modifications of PBPD method for RC frames due to "pinched" and degrading hysteretic characteristics are also discussed. Design flow charts for determination of design base shear, lateral forces and member design forces are also presented.

4. Chapter 4 presents redesign work of 4, 8, 12 and 20-story example RC special moment frame structures with PBPD method.

5. Chapter 5 presents the simulation study, including element-level modeling, structure-level modeling and selection of ground motions in reference to FEMA P695 report. The computer programs used in this study are discussed as well.

6. Chapter 6 provides results of nonlinear static (pushover) and dynamic (time-history) analyses of the baseline and PBPD frames which were carried out by using PERFORM 3D program. The results of inelastic static and dynamic analyses proved the validity of the PBPD methodology as applied to reinforced concrete moment frames.

.

7. Chapter 7 presents estimation of drift demand by the energy spectrum method ($E_c = E_d$). Application of the energy spectrum method to the 4, 8, 12 and 20-story RC moment frames is also discussed. The results are compared with those obtained from detailed time-history analyses.

8. Chapter 8, the final chapter, presents the summary and conclusions of this study. Some suggestions for future study are also presented.

The organization of this research report is summarized in the flow chart shown in Figure 1-2.

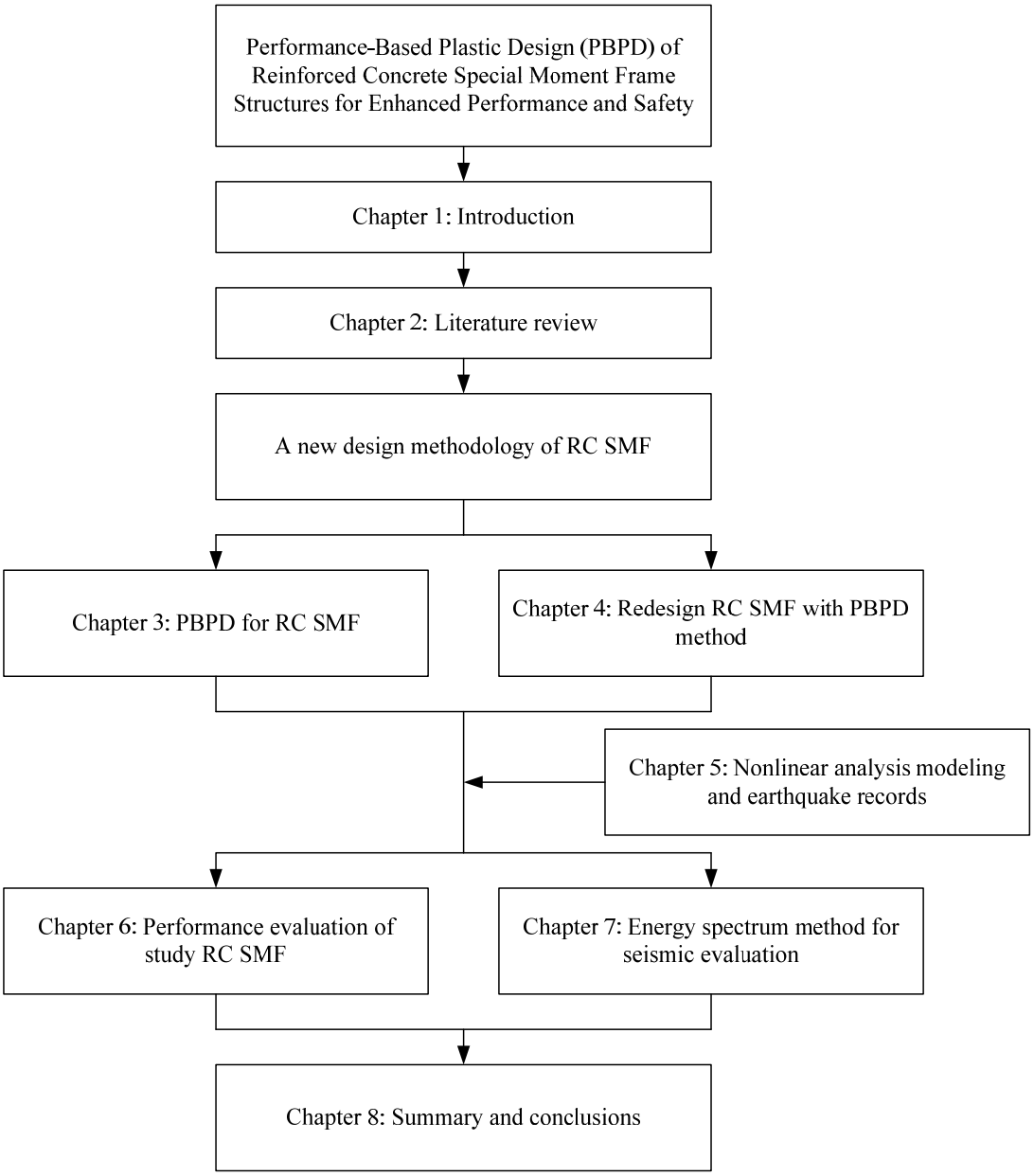

Figure 1-2 Flow chart of the dissertation

CHAPTER 2

LITERATURE REVIEW

2.1. Introduction

The term "Performance-Based Seismic Design (PBSD)" has been widely used by the engineering and research community since the 1994 Northridge Earthquake, perhaps the most costly earthquake in U.S. history, and other major earthquakes around the world which occurred at the end of the 20th century. The goal of PBSD is to develop design methodologies that produce structures of predictable and intended seismic performance under stated levels of seismic hazards (SEAOC, 1995). However, the current trend towards this goal is to use approaches that may be quite complex and iterative for practical application. A general methodology was formulated in an effort to involve all the variables that may affect the performance, such as seismic hazard, damage measures, collapse, financial losses or length of downtime due to damage, engineering demands such as story drifts, floor accelerations, etc., (Krawinkler and Miranda, 2004). The performance evaluation of a structure is carried out by using complex probabilistic formulas, and the design work proceeds by going through several iterations of this process (Hamburger, 2004).

Current seismic design practice around the world (including the U.S.) is generally carried out by elastic method, even though it is well recognized that structures designed by current codes undergo large deformations in the inelastic range when subjected to strong earthquakes. Elastic analysis is carried out for prescribed equivalent static design forces to determine the required strength and deflection demands. Then adequate design strength and detailing are provided to help ensure proper inelastic behavior. Thus, expected inelastic behavior is accounted for in a somewhat indirect manner (BSSC, 2006). As a consequence,

the inelastic activity, which may include severe yielding and buckling of structural members and connections, can be unevenly and widely distributed in the structure designed by elastic methods. This may result in rather undesirable and unpredictable response, total collapse, or difficult and costly repair work at best. There is need for more direct design methods that would fit in the framework of PBSD and produce structures that would perform as desired.

2.2. Current Seismic Design Procedure and Its Weaknesses

Current seismic design in the U.S. and even in most countries in the world, is carried out in accordance with force-based design methodology. The force-based design sequence is given in Figure 2-1.

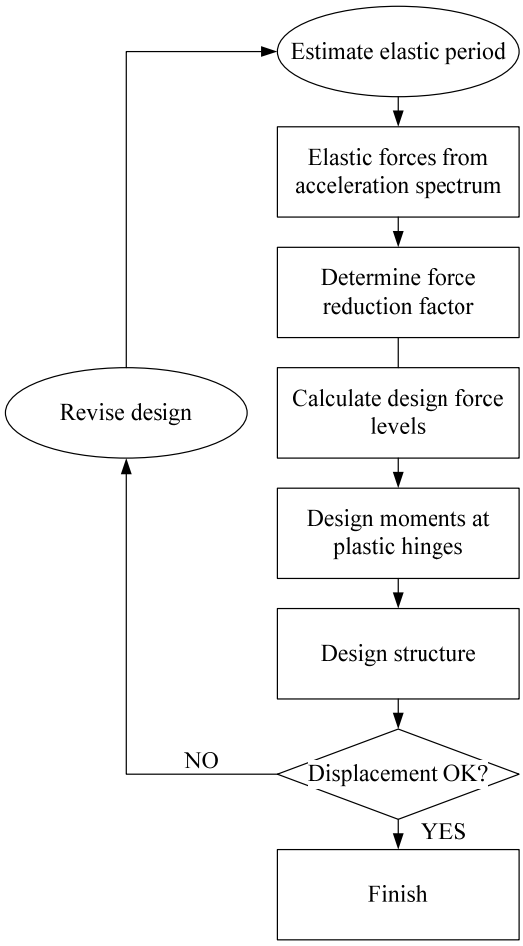

Figure 2-1 Design sequence of force-based design

Figure 2-2 briefly shows the process of determining design base shear as used in the current U.S. practice. The factor *R* represents force reduction factor depending upon assumed ductility of the structural system, and *I* represents occupancy factor to increase the design force for more important buildings. Lateral design forces at the floor levels (along the building height) are then determined according to the prescribed formulas to represent dynamic characteristics of the structure (ATC, 1978; BSSC, 2003; BSSC 2003b). Elastic analysis is performed to determine the required member strengths. After member section design for strength, a deflection amplification factor, C_d, is then used to multiply the calculated drift obtained from elastic analysis to check the specified limits. The process is repeated in an iterative manner until the strength and drift requirements are satisfied.

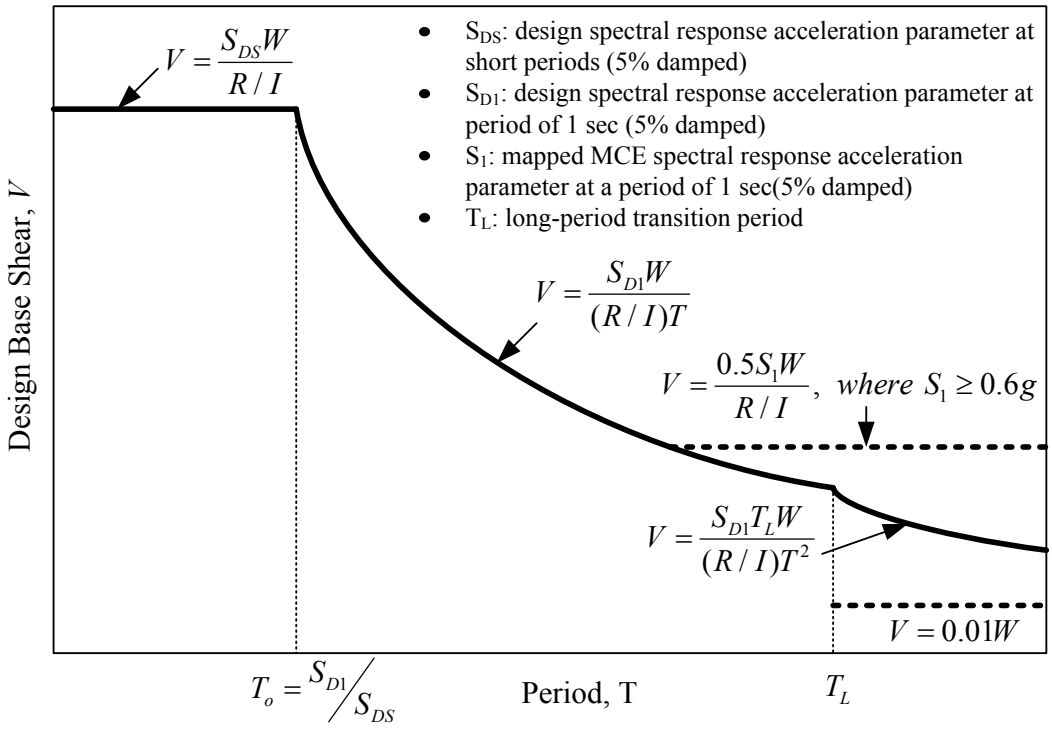

Figure 2-2 Design response spectrum for seismic design (ASCE 7-05, 2006)

Proper detailing provisions are followed in order to meet the expected ductility demands. Certain critical members, such as columns, are designed based on a "partial capacity design approach" to prevent damage that could lead to collapse of structures. For a typical reinforced concrete moment frame, a minimum column-to-beam strength ratio of 1.2

is specified in an effort to eliminate column plastic hinging (ACI 318, 2008). However, it has been found such procedures are not adequate to give the desired results with satisfactory confidence levels. The inelastic activity, which may include severe yielding and buckling of structural members, can be unevenly and widely distributed in the structure (Browning et al., 2000; Deierlein et al., 2007; Eberhard and Sozen, 1989; Sabelli, 2000).

In summary, the major weaknesses of the current code procedure are:

1. Assuming safety could be guaranteed (or damage could be reduced) by increasing the design base shear: it has been observed in many past earthquakes that collapse occurred due to local column damage (Moehle and Mahin, 1991).

2. Assuming design lateral force distribution along the building height based on elastic behavior: Prior studies have shown that the code specified lateral force distribution (thus the story shear) deviates significantly from the nonlinear time-history dynamic analysis results (Chao et al., 2007), which can be partly responsible for non-uniform maximum interstory drifts along the height. Nonlinear dynamic analyses carried out by Villaverde (1991, 1997) also showed that using the code distribution of lateral forces, without accounting for the fact that a structure would enter inelastic state during a major earthquake, could be the primary reason leading to numerous upper story collapses during the 1985 Mexico City Earthquake.

3. Proportioning member sizes based on initial stiffness (i.e. elastic analysis): The magnitude of individual member forces from elastic analysis is obtained based on relative elastic stiffness of structural members. However, when subjected to major earthquakes, stiffness of many members changes significantly due to concrete cracking or yielding in steel, while that of others may remain unchanged. This alters the force distribution in the structural members. Proper proportioning of member sizes cannot be achieved without using a more representative force distribution which takes into account the expected inelastic behavior.

4. Attempting to predict inelastic displacements by using approximate factors and analysis behavior: This has been shown by many prior investigations to be unrealistic, especially for structures having degrading ("pinched") hysteretic behavior and energy dissipation characteristics (Chao and Goel, 2006; Sabelli et al., 2003).

5. Attempting to eliminate column yielding by a single column-to-beam strength ratio: Many prior studies have shown that conventional capacity design approach for designing columns in reinforced concrete moment frames cannot eliminate yielding in the columns (Dooley and Bracci, 2001; Kuntz and Browning, 2003). In fact, the column moment demand is quite often underestimated, because the columns are subjected to moments not only from those delivered from the beams or other members framing into the columns (i.e., conventional capacity design approach), but also from the lateral displacements (Bondy, 1996).

2.3. Current State of Performance-Based Seismic Design in the U.S.

In September 2001, the Applied Technology Council, under the contract with Federal Emergency Management Agency, initiated ATC-58 project to develop the next-generation performance-based seismic design guidelines (2006). Figure 2-3 illustrates the current progress and basic performance-based design process as given in the FEMA-445 report (2006). As indicated in the flowchart, the primary work done in ATC-58 project is found on the "Assess Performance" phase, which includes evaluation of the structural and nonstructural performance, as well as prediction of losses by using nonlinear structural analysis and complex probabilistic approaches (Comartin, 2004; Cornell, 2004; Deierlein, 2004; FEMA, 2006; Hamburger, 2004; Krawinkler et al., 2004). As can been seen in Figure 2-3, the FEMA-445 performance-based design methodology heavily relies on iterative "Assess Performance→ Revise Design→ Asses Performance" process to obtain a structure capable of achieving the intended performance. This is mainly due to inadequacy of the current seismic approaches to produce a good initial design. However, a poor initial design

may be improved through many iterations, but it may never become as good or optimal design as desired (Krawinkler and Miranda, 2004).

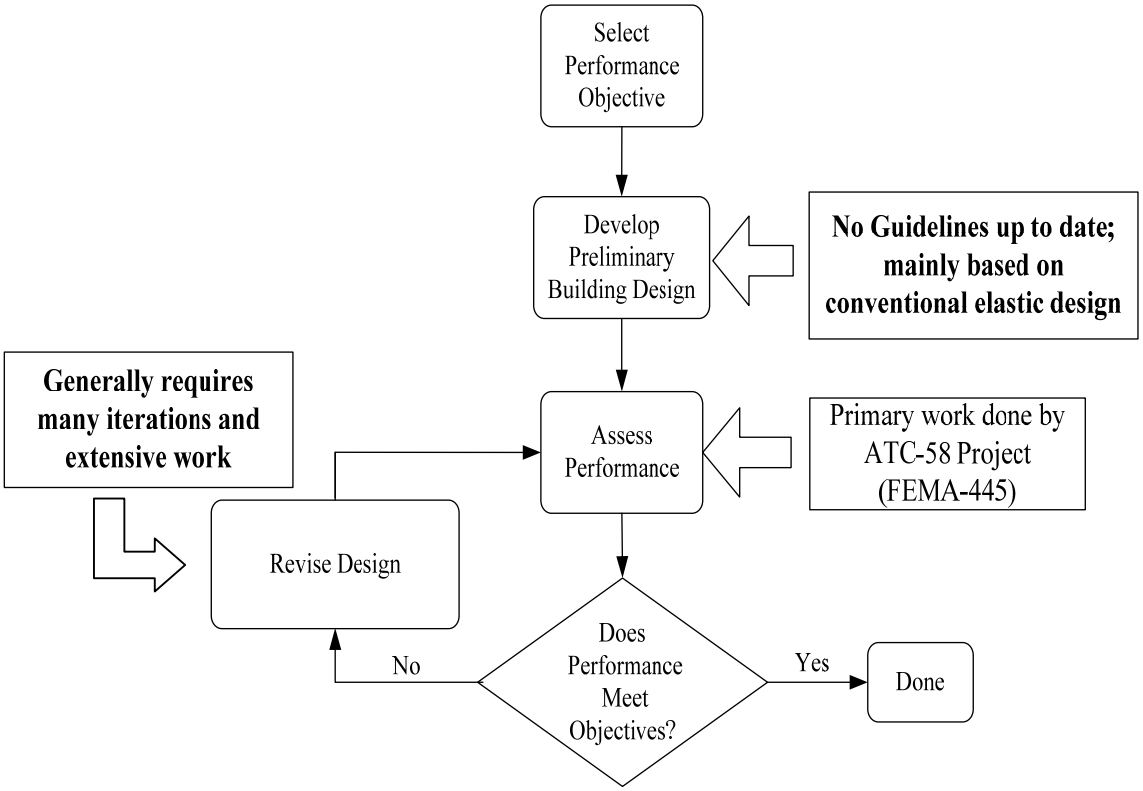

Figure 2-3 FEMA 445 performance-based design flowchart (FEMA, 2006)

A good design should be based on realistic structural behavior under major seismic loading and incorporate intended performance targets directly in the initial design stage. That way subsequent "Assess Performance→ Revise Design→ Assess Performance" process becomes more of a verification process rather than part of the main design process, requiring only minor revisions, if any, to the initial design. The current performance-based design procedures also provide little guidance to the engineers on how to modify the initial design in order to achieve the intended performance. Indeed, as acknowledged in the FEMA-445 report, unless further guidance is provided, engineers will have difficulty developing preliminary designs capable of meeting the desired performance objectives and may find implementation of performance-based deign to be very time-consuming in many cases (FEMA, 2006).

In view of the above, this study provides a bridge between the conventional seismic design and the FEMA performance-based design framework and addresses the need for developing a systematic design methodology that produces structures of predictable and intended seismic performance under stated levels of seismic hazards in a more direct manner as given in Figure 2-4. This in turn considerably reduces the subsequent assessment and redesign work.

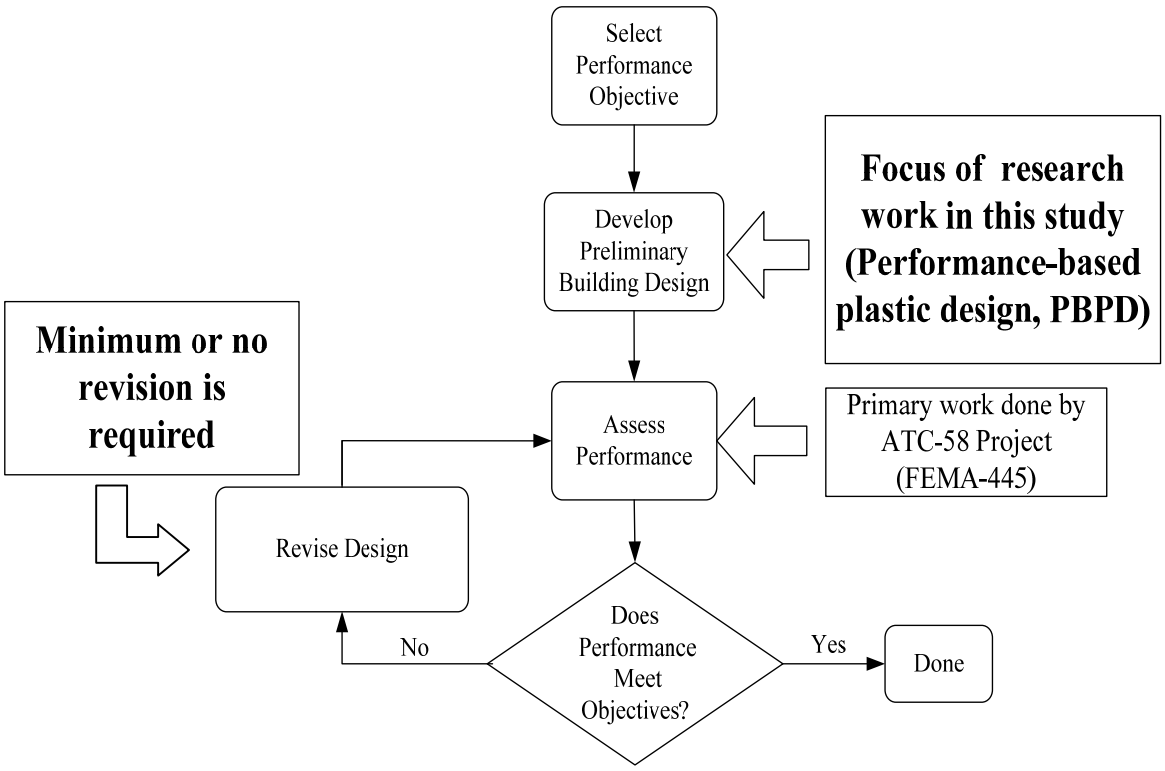

Figure 2-4 Major role of research work in this study in the current performance-based design framework

2.4. Approaches for the Initial Design Proposed by other Researchers

A few approaches have been proposed by other researchers to provide tools in the initial design stage for producing structures meeting the desired performance. These approaches, such as the Yield Point Spectra Method (Aschheim and Black, 2000), the

Modified Lateral Force Procedure (MLFP) (Englekirk, 2003; Panagiotou and Restrepo, 2007), and the Direct Displacement-Based Design (DDBD) approach (Priestley et al., 2003 2007), primarily focus on the development of a suitable design base shear that accounts for higher mode effects, system overstrength, yield displacement, effective stiffness, viscous damping, effective period, or displacement ductility. The design of yielding members (such as beams in moment frames) and design of columns are still based on conventional elastic and capacity design approach or a relatively complex procedure that significantly deviates from the current practice. It has been noted that nonlinear analysis is required for performance assessment and refinement of the design (Aschheim, 2004). Practical applications of these approaches are still under development and improvement.

.

2.4.1 Yield Point Spectra Method

The yield point spectra method uses constant ductility curves by plotting the yield strength coefficient, C_y, as a function of the system's yield displacement. Therefore, the strength required by a SDOF oscillator can be determined from those curves for the given displacement ductility, yield displacement and period as shown in Figure 2-5.

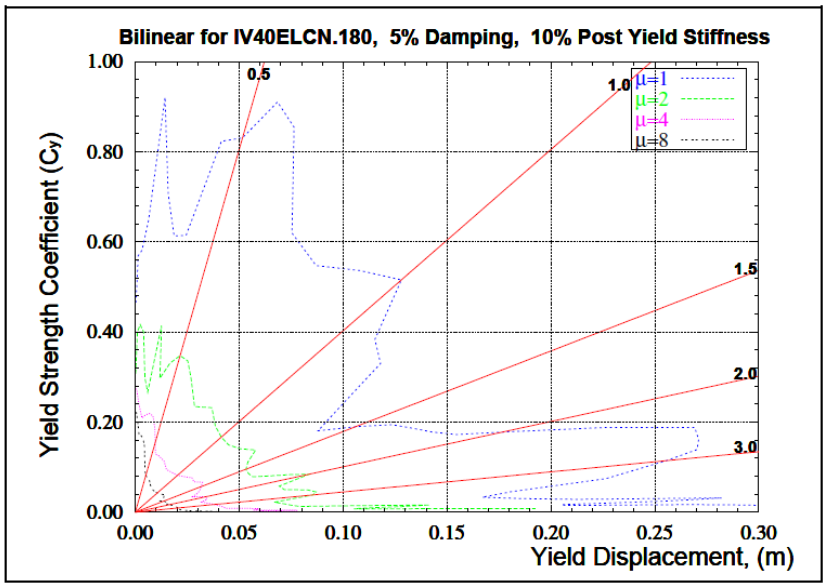

Figure 2-5 Example of yield point spectra of the 1940 record at El Centro (bilinear model; damping 5%)

For design, Yield Point Spectra may be used to determine combinations of strength and stiffness sufficient to limit drift and/or displacement ductility demands to the prescribed values. The yield strength coefficient, C_y, can also be calculated by using simple expressions as shown in the following:

$$V_y = C_y \cdot W = C_y \cdot m \cdot g \tag{2-1}$$

$$T = 2 \cdot \pi \cdot \sqrt{\frac{m}{k}} = 2 \cdot \pi \cdot \sqrt{\frac{m \cdot u_y}{V_y}} = 2 \cdot \pi \cdot \sqrt{\frac{u_y}{C_y \cdot g}} \tag{2-2}$$

$$C_y = \frac{4 \cdot \pi^2 \cdot u_y}{T^2 \cdot g} \tag{2-3}$$

, where W is the oscillator weight, m is the oscillator mass, k is the initial stiffness, T is the initial period and g is the acceleration of gravity.

The yield point spectra method offers practical approach for engineers to have direct control over the strength and stiffness of the structure and reasonable way to determine the design base shear for different ductility demands. However, the subsequent design work still follows the conventional strength-based design approaches instead of systematic performance-based design procedure.

2.4.2 Modified Lateral Force Procedure

The modified lateral force procedure (MLFP) is an extension of the equivalent lateral force design procedure (ELFP) since ELFP ignores the contribution of higher modes. The MLFP approach makes use of capacity design principles and accounts explicitly for section and kinematic overstrength as well as for dynamic effects on the structure. The steps of MLFP method include determination of first mode design lateral forces, calculation of static system overstrength, consideration of dynamic effects and design of elastic regions by following capacity design principles. However, the MLFP is complex and its main focus is on the determination of design base shear.

2.4.3 Direct Displacement-Based Design

In recent years, the displacement based design methodology has been well received by the profession since displacement is deemed as better indicators of damage potential than force. Shibata and Sozen (1976) were the first ones to propose the concept of substitute structure to account for inelastic activity and to determine design forces of RC structures. Based on that concept, direct displacement-based design (DDBD), developed by Priestley et al., (2003, 2007), is one of the more popular methodologies in this category.

Unlike force based design, DDBD starts with selection of the design drift. The structure is then characterized by its effective stiffness and damping at the design drift level so that the necessary design forces can be directly obtained. It is noted that iteration may be required if the assumed level of damping fails to check. The procedure of DDBD can be summarized as shown in Figure 2-6.

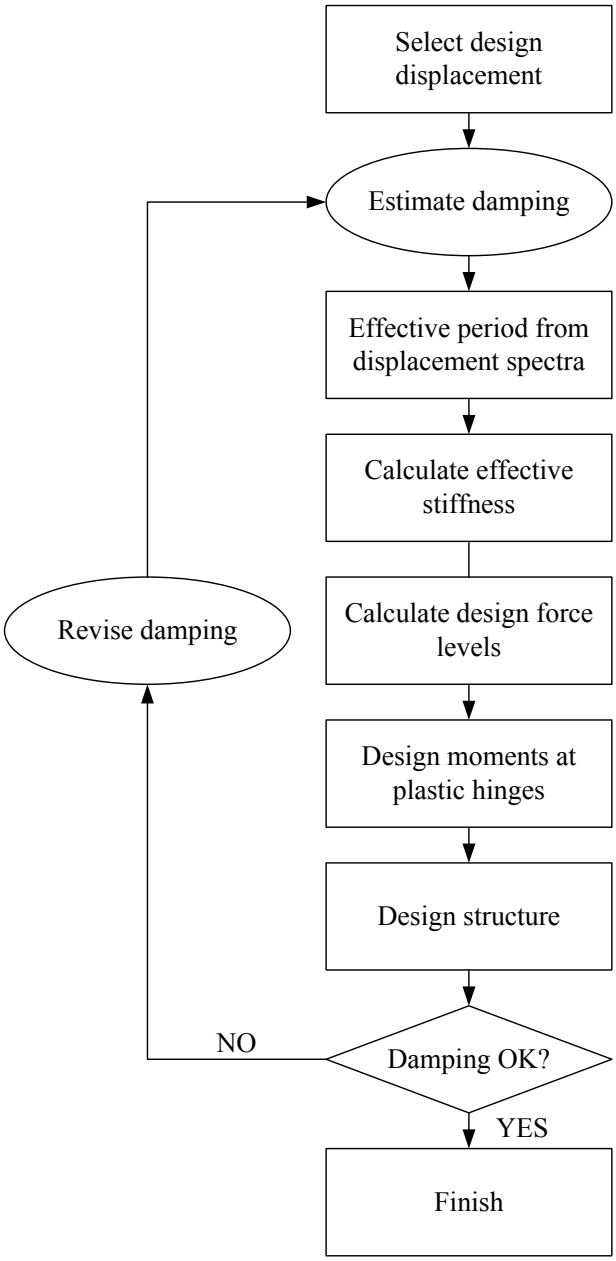

Figure 2-6 Design sequence of direct displacement-based design (Priestley, 2003)

Compared to current conventional seismic design practice, DDBD ensures that the structure responds at the design drift limit. It was also mentioned by Priestley (2003) that use of DDBD would result in more consistent designs than force-based designs and generally reduce the design forces. However, the complexity of DDBD is a major obstacle in broader acceptance of this approach by the profession, especially because iteration for damping check is still needed.

2.5. Summary and Conclusions

Performance-Based Seismic Design (PBSD) has been considered as an essential part of earthquake engineering. New developments and methods for the application of PBSD methodology are needed because most existing PBSD approaches tend to provide guidance and tools for the evaluation of seismic performance of a building that has already been designed. In other words, more research work is needed for development of initial design because there is no guideline provided in current PBSD practice.

Several approaches for the initial design proposed by other researchers have been briefly reviewed in this chapter. These approaches mainly provide a suitable design base shear that accounts for higher mode effects, system overstrength, yield displacement, effective stiffness, viscous damping, effective period, or displacement ductility. However, a major shortcoming of these approaches is that the rest of design work, involving design of yielding members (such as beams in moment frames) and design of columns, is still based on conventional elastic and capacity design approach. Some of the methods even require relatively complex calculations and procedures that significantly deviate from current practice. Additionally, iteration during the design process is still required. Thus, practical methods based on these approaches are still under development and improvement.

CHAPTER 3

PERFORMANCE-BASED PLASTIC DESIGN (PBPD) METHOD FOR RC SMF

3.1. Introduction

Reinforced concrete special moment frames (RC SMF) consist of horizontal framing components (beams and/or slabs), vertical framing components (columns) and joints connecting horizontal and vertical framing components are deemed to satisfy the special requirements in seismic provisions (ACI 318, 2008; ASCE 7-05, 2006). RC SMF are widely used as part of seismic force-resisting systems. In seismic provisions, certain requirements such as special proportioning and detailing requirements result in a frame capable of resisting strong earthquake shaking without significant loss of strength. Nevertheless, structural and nonstructural damage observed in code compliant RC buildings due to undesired failure modes (Moehle and Mahin, 1991) have shown the need to develop alternative methodologies to better ensure the desired performance.

One such complete design methodology, which accounts for inelastic structural behavior directly, and practically requires no or little iteration after initial design, has been developed (Chao and Goel, 2005; Chao and Goel, 2006a; Chao and Goel, 2006b; Chao and Goel, 2006c; Chao et al., 2007; Chao and Goel, 2008a, Chao and Goel, 2008b; Dasgupta et al., 2004; Goel and Chao, 2009; Lee and Goel, 2001; Lee at al., 2004; Leelataviwat et al., 1999; Goel et al, 2009[a], 2009[b], 2010,; Liao and Goel, 2010[a], 2010[b]). It is called Performance-Based Plastic Design (PBPD) method.

By using the concept of energy balance applied to a pre-selected yield mechanism with proper strength and ductility, structures designed by the PBPD method can achieve more predictable structural performance under strong earthquake ground motions. It is important to select a desirable yield mechanism and target drift as key performance limit states for given hazard levels right from the beginning of the design process. The distribution and degree of structural damage are greatly dependent on these two limit states. In addition, the design base shear for a given hazard level is derived corresponding to a target drift limit of the selected yield mechanism by using the input energy from the design pseudo-velocity spectrum: that is, by equating the work needed to push the structure monotonically up to the target drift (Figure 3-1a) to the energy required by an equivalent elastic-plastic single-degree-of-freedom (EP-SDOF) system to achieve the same state (Figure 3-1b). Furthermore, a better representative distribution of lateral design forces is also used in this study, which is based on inelastic dynamic response results (Chao at el, 2007). This lateral design force distribution accounts for higher mode effects and inelastic behavior better than the distribution prescribed by the current codes. Nonlinear dynamic analysis results of a variety of steel structures have shown that this new lateral force distribution leads to more realistic story shears as well as uniform story drifts over the building height (Goel and Chao, 2008).

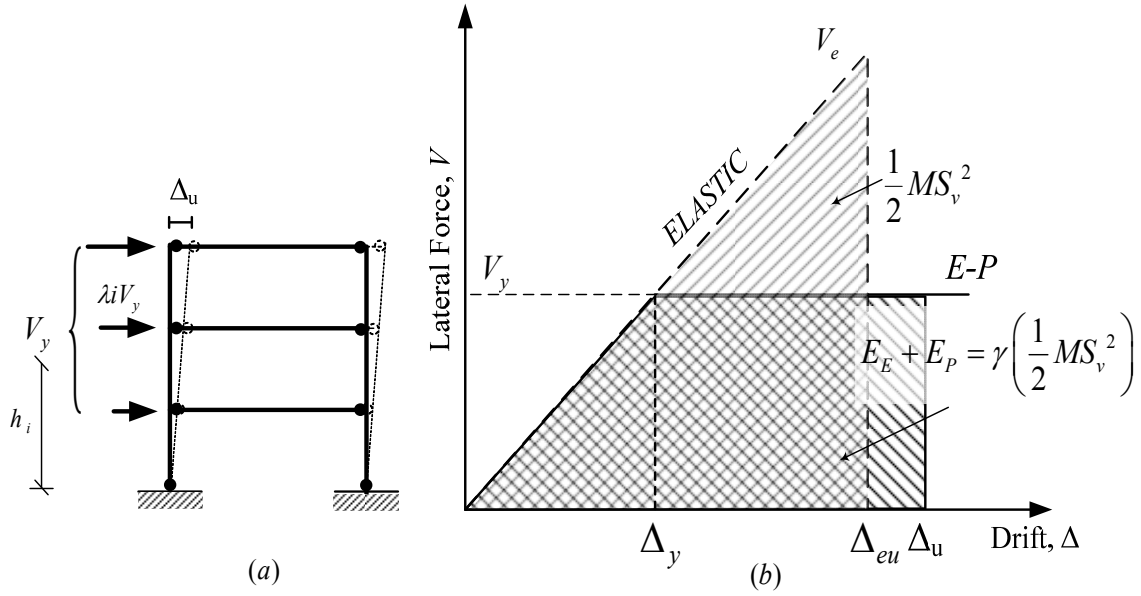

Figure 3-1 PBPD concept

Mechanism based plastic analysis is used to determine the required of the designated yielding frame members, such as beams in RC SMF, to achieve the selected yield mechanism. Design of non-yielding members, such as columns, is then performed by considering the equilibrium of an entire "column tree" in the ultimate limit state to ensure formation of the selected yield mechanism.

3.2. Energy balance concept in PBPD design

The concept of energy balance in conjunction with ultimate limit state design was first used by Housner (1956). Housner (1960) also extended this concept to derive the required design lateral force to prevent structure collapsing due to overturning under extreme drift limits. However, some assumptions were made by Housner in this energy approach for simplicity and due to limited available knowledge about inelastic response spectra at that time.

Housner (1960) noted that shaking structures may collapse in one of several ways under strong ground motions:

> *"One possibility is that the vibrations will cause approximately equal plastic straining in alternate directions and that this will continue until the material breaks because of a fatigue failure. Another possibility is that all of the plastic straining will take place in one direction until the column collapses because of excessive plastic drift. These two possibilities are extreme cases, and the probability of their occurrence is small. The most probable failure is collapse due to greater or lesser amount of energy having been absorbed in plastic straining in the opposite direction. In this case collapse occurs when some fraction of the total energy pE is just equal to the energy required to produce collapse by plastic drift in one direction. In what follows, the factor p will be taken equal to unity as a matter of convenience,…"*

The energy balance concept used in the PBPD method to determine the design base shear is quite similar to the basic approach suggested by Housner (1960). By using suitable inelastic response spectra for EP-SDOF systems, the amount of work needed to push the structure monotonically up to the design target drift is equated to a fraction of the elastic

input energy. The basic energy balance concept is then extended to MDOF systems by using equivalent modal SDOF oscillators along with other appropriate assumptions (Goel and Chao, 2008).

3.3. Comparison of PBPD and current code design method

The design requirements for RC SMF are presented in the American Concrete Institute (ACI) Committee 318 Building Code Requirements for Structural Concrete (ACI 318). The special requirements relate to inspection, materials, framing members (beams, columns, and beam-column joints), and construction procedures. In addition, the pertinent seismic load requirements are specified in the American Society of Civil Engineers (ASCE) publication *ASCE/SEI 7-05 Minimum Design Loads for Buildings and Other Structures* (ASCE 2006). The International Building Code, or IBC, (ICC 2006), which is the code generally adopted throughout the United States, refers to ASCE 7 for the determination of seismic loads. The ACI Building Code includes design requirements according to the Seismic Design Categories designated by the IBC and ASCE 7 and contains the latest information on design of special moment frames. In addition, the design base shear equations of current building codes (e.g., IBC and ASCE 7) was calculated by reducing the elastic strength demands to the inelastic strength demands by incorporating a seismic force-reduction factor R that reflects the degree of inelastic response expected for design-level ground motions, as well as the ductility capacity of the framing system. The *R* factor for special moment frames is 8. Therefore, a special moment frame should be expected to sustain multiple cycles of inelastic response if it experiences a design-level ground motion.

Haselton (2007) observed the major goal of the seismic design in current building codes is

> "*to protect life safety of building inhabitants during extreme earthquakes. First and foremost, this requires controlling the likelihood of structural collapse such that it remains at an acceptably low level. With the implementation of detailing and capacity design requirements in current codes and standards, the assumption is that the building codes will meet this safety goal. However, codes are empirical in nature such that the collapse safety they provide has not been rigorously quantified.*"

As mentioned earlier, the key performance objectives in the PBPD method are pre-selected target drift and yield mechanism. The design lateral forces are determined for the given seismic hazard and selected target drift. Therefore, factors based on engineering judgment, such as R, I, C_d (Fig 3-2) are no longer needed.

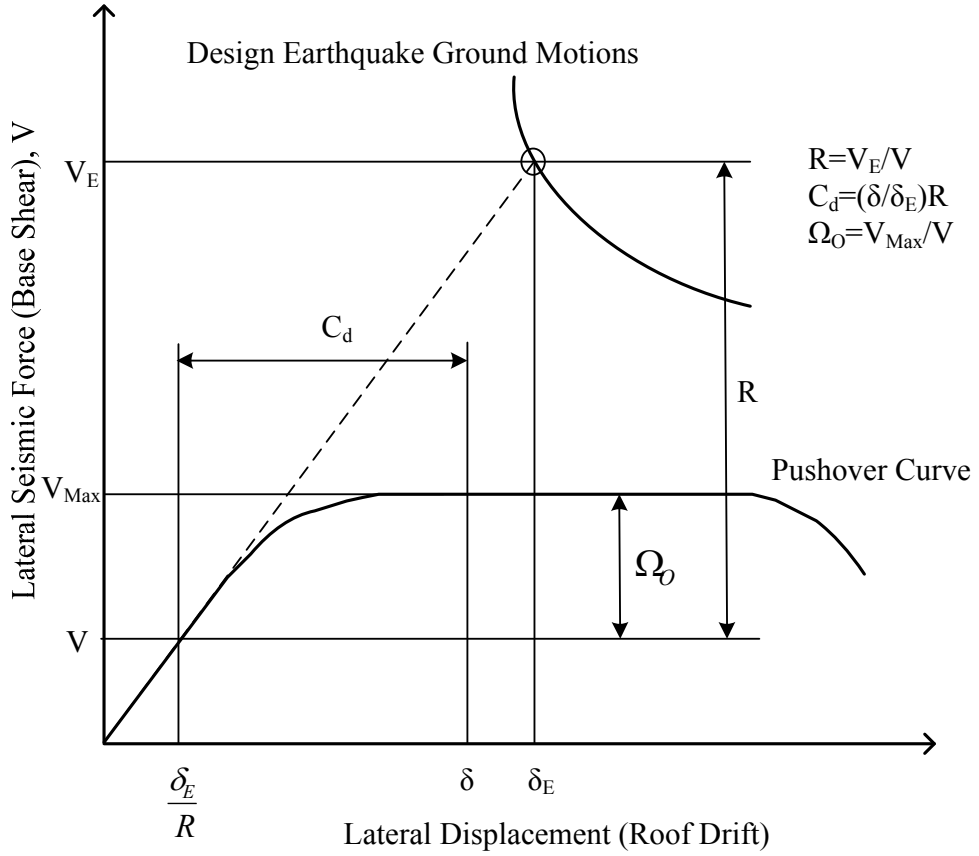

Figure 3-2 Illustration of seismic performance factors (R, Ω_o and C_d) as defined by the commentary to the NEHRP recommended provisions (FEMA P440A, 2009)

In addition, the proportioning and detailing requirements for special moment frames are intended to ensure that inelastic response is ductile. In order to ensure good performance of RC SMF, Moehle el al. (2008) proposed three main goals for design; they are (1) to achieve a strong-column/ weak-beam design that spreads inelastic response over several stories; (2) to avoid shear failures; and (3) to provide details that enable ductile flexural

response in yielding regions. As shown in this study, the first goal to assure strong column/ weak beam design is reached by following the PBPD method since the yielding mechanism is preselected and all non designated yielding members (columns) are designed by capacity-design approach considering an entire "column tree" instead of single joints. The other two goals are related to detailing requirements to achieve the needed ductility capacity.

It is important to note that in the PBPD method control of drift and yielding is built into the design process from the very start, eliminating or minimizing the need for lengthy iterations to arrive at the final design. Other advantages include the fact that innovative structural schemes can be developed by selecting suitable yielding members and/or devices and placing them at strategic locations, while the designated non-yielding members can be detailed lower ductility capacity. All of this would translate into enhanced performance, safety, and economy in life-cycle costs.

3.4. Design procedure

3.4.1 Overview

An outline of the step-by-step Performance-Based Plastic Design (PBPD) procedure is given in the following. The details are then presented in the subsequent sections:

1. Select a desired yield mechanism and target drift for the structure for the design earthquake hazard.

2. Estimate the yielding drift, θ_y, the fundamental period, T, of the structure and determine an appropriate vertical distribution of design lateral forces.

3. Determine the elastic design spectral acceleration value, S_a (Figure 3-3), by multiplying seismic response coefficient, C_s, with R/I, where R=8 and I=1 in the

design of RC SMF. S_a was determined this way for two reasons: (a) for long period the codes prescribe the minimum value of C_s but not for S_a; (b) for consistency and fair comparison with the baseline frames.

4. Calculate the design base shear, V. In order to estimate the ductility reduction factor and the structural ductility factor, an inelastic seismic response of EP-SDOF is needed, such as idealized inelastic response spectra by Newmark-Hall (1985) used in this study.

5. Modify V for RC SMF as needed since the force-deformation behavior is different from the assumed EP behavior and P-Delta effect is not considered in the calculation of V in Step 4.

6. Use plastic method to design the designated yielding members (DYM), such as beams in RC SMF. Members that are required to remain elastic (non-DYM), such as columns, are designed by a capacity design approach.

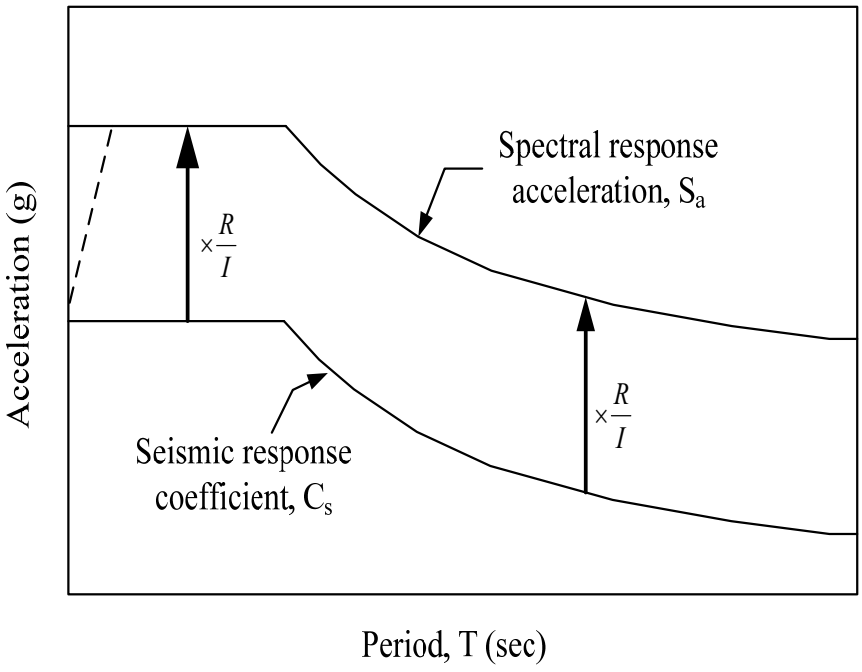

Figure 3-3 Typical spectral response acceleration and seismic response coefficient for calculation of design base shear

3.4.2 Desired yield mechanism and target drift

Figure 3-4 shows a typical moment frame in the yield mechanism state subjected to design lateral forces and pushed to the target plastic drift limit. All inelastic deformations are intended to be confined within DYM, such as plastic hinges in the beams. It is noted that the global yield also includes plastic hinges at the column bases which generally form under major earthquakes.

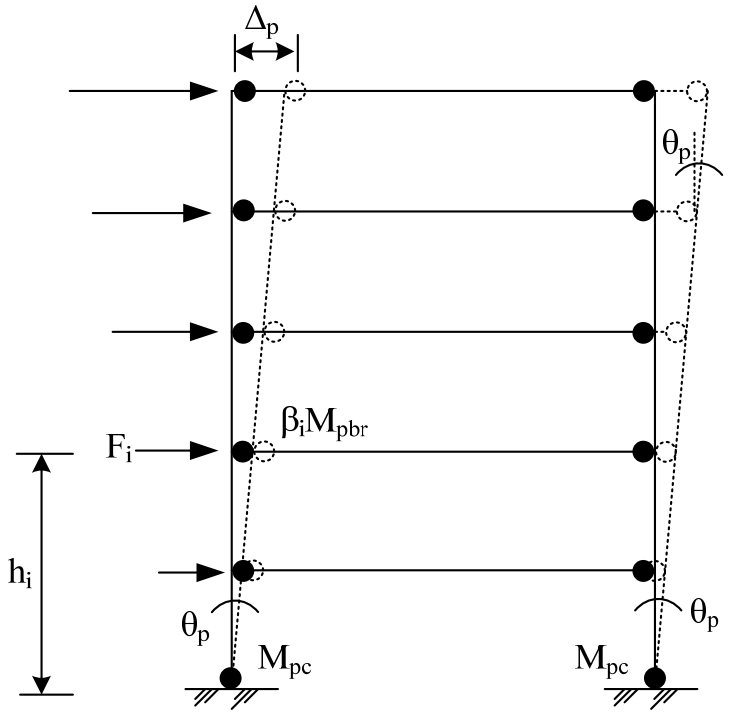

Figure 3-4 Desirable yield mechanisms for typical SMF

As suggested by Goel and Chao (2008), target drifts for the two design hazards are as follows:

1. A 2% maximum story drift ratio for ground motion hazard with 10% probability of exceedance in 50 years (10/50 or 2/3MCE).
2. A 3% maximum story drift ratio for ground motion hazard with 2% probability of exceedance in 50 years (2/50 or MCE).

3.4.3 Determination of fundamental period

The fundamental period, *T*, in seconds, for RC SMF can be determined from the following equation, as given in ASCE 7-05 (2006):

$$T = C_u \cdot T_a = C_u \cdot C_t \cdot h_n^x \text{ if } T_{actural/\mathrm{mod}el} > C_u \cdot C_t \cdot h_n^x \tag{3-1}$$

where T_a is the approximate fundamental period per ASCE 7-05 (2006) section 12.8.2.1; C_u represents the coefficient for upper limit on calculated period, and for $S_{D1} \geq 0.3g$, C_u is 1.4 (Table 12.8-1 in ASCE 7-05); h_n is the height in feet above the base to the highest level of the structure and the coefficient C_t and *x* for concrete moment resistant frames are 0.016 and 0.9 (Table 12.8-2 in ASCE 7-05), respectively. It should be mentioned that for the design cases in FEMA P695, the fundamental periods as calculated from the analysis models were larger than the maximum values permitted in ASCE 7-05 (Equation 3-1). Therefore, the fundamental periods calculated by Equation 3-1 were used.

3.4.4 Design base shear

Determination of the design base shear for a given hazard level is a key element in the PBPD method. It is calculated by equating the work needed to push the structure monotonically up to the target drift to that required by an equivalent elastic-plastic single degree of freedom (EP-SDOF) system to achieve the same state. Assuming an idealized E-P force-deformation behavior of the system (Figure 3-1), the work-energy equation can be written as:

$$(E_e + E_p) = \gamma \cdot \left(\frac{1}{2} M \cdot S_v^{\,2} \right) = \frac{1}{2} \gamma \cdot M \cdot \left(\frac{T}{2\pi} S_a \cdot g \right)^2 \tag{3-2}$$

where E_e and E_p are, respectively, the elastic and plastic components of the energy (work) needed to push the structure up to the target drift. S_v is the design pseudo-spectral velocity; S_a is the pseudo spectral acceleration, which can be obtained from the seismic design response spectrum in ASCE 7-05 (2006) as shown in Figure 3-5 by multiplying the seismic response coefficient, C_s, with R/I ; T is the fundamental period; and M is the total seismic mass of the system.

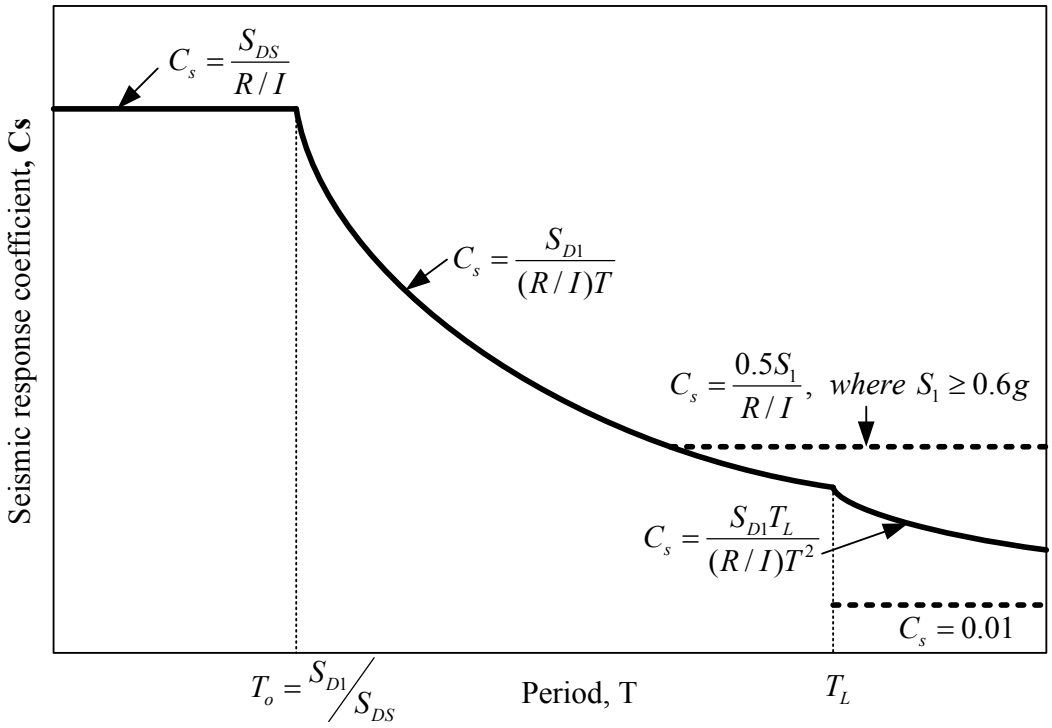

Figure 3-5 Design response spectrum for seismic design (ASCE 7-05, 2006)

With the assumed yield drift θ_y for different structural systems (Table 3-1), the energy modification factor, γ, depends on the structural ductility factor (μ_s) and the ductility reduction factor (R_μ), and can be obtained from the following relationship:

$$\gamma = \frac{2\mu_s - 1}{R_\mu{}^2} \tag{3-3}$$

Because of their simplicity (Table 3-2), idealized inelastic spectra proposed by Newmark and Hall (1982), as shown in Figure 3-6 (a), were used to relate the ductility reduction factor, R_μ, and the structural ductility factor, μ_s, for EP-SDOF. Plots of energy modification factor γ as obtained from Equation (3-3) are also shown in Figure 3-6 (b) (Lee and Goel, 2001). It should be mentioned that it is assumed in this study that the relation is also valid for multi-degree-of-freedom (MDOF) systems. Other inelastic spectra for EP-SDOF systems can also be used as preferred, such as those by Miranda and Bertero (1994).

Table 3-1 Assumed design yield drift ratios

Frame Type	RC	Steel			
	SMF	MF	EBF	STMF	CBF
Yield Drift Ratio, θ_y (%)	0.5	1	0.5	0.75	0.3

Table 3-2 Ductility reduction factor and its corresponding structural period range

Period Range	Ductility Reduction Factor
$0 \le T < \frac{T_1}{10}$	$R_\mu = 1$
$\frac{T_1}{10} \le T < \frac{T_1}{4}$	$R_\mu = \sqrt{2\mu_s - 1} \cdot \left(\frac{T_1}{4T}\right)^{2.513 \cdot \log\left(\frac{1}{\sqrt{2\mu_s - 1}}\right)}$
$\frac{T_1}{4} \le T < T_1'$	$R_\mu = \sqrt{2\mu_s - 1}$
$T_1' \le T < T_1$	$R_\mu = \frac{T\mu_s}{T_1}$
$T_1 \le T$	$R_\mu = \mu_s$

Note: $T_1 = 0.57$ sec.; $T_1' = T_1 \cdot \left(\sqrt{2\mu_s - 1} / \mu_s\right)$ sec.

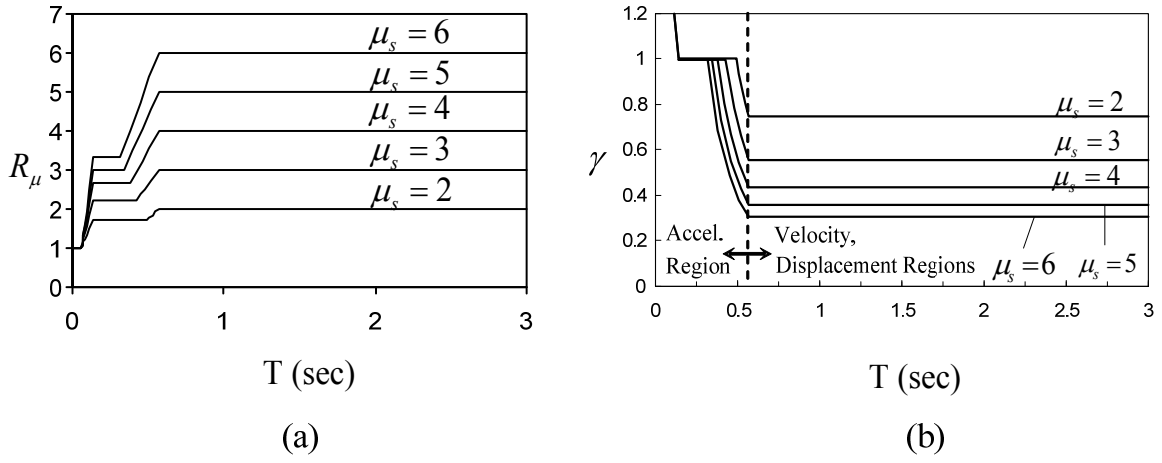

Figure 3-6 (a) Idealized $R_\mu - \mu_s - T$ inelastic spectra by Newmark and Hall for EP-SDOF (1982); (b) Energy modification factor $\gamma - \mu_s - T$ inelastic spectra by Lee and Goel (2001)

The work-energy equation can be re-written in the following form

$$\frac{1}{2}\left(\frac{W}{g}\right)\cdot\left(\frac{T}{2\pi}\frac{V_y}{W}g\right)^2 + V_y\left(\sum_{i=1}^{N}\lambda_i h_i\right)\theta_p = \frac{1}{2}\gamma\left(\frac{W}{g}\right)\cdot\left(\frac{T}{2\pi}S_a g\right)^2 \qquad (3\text{-}4)$$

or,

$$\left(\frac{V_y}{W}\right)^2 + \frac{V_y}{W}\left(h^*\cdot\frac{\theta_p 8\pi^2}{T^2 g}\right)\theta_p - \gamma S_a{}^2 = 0 \qquad (3\text{-}5)$$

The admissible solution of Equation (3-5) gives the required design base shear coefficient, V_y / W :

$$\frac{V_y}{W} = \frac{-\alpha + \sqrt{\alpha^2 + 4\gamma S_a^2}}{2} \qquad (3\text{-}6)$$

where α is a dimensionless parameter given by,

$$\alpha = \left(h^* \cdot \frac{\theta_p 8\pi^2}{T^2 g} \right) \tag{3-7}$$

The term θ_p represents the plastic component of the target drift ratio; that is, $\theta_p = \theta_u - \theta_y$ and $h^* = \sum_{i=1}^{N} (\lambda_i h_i)$.

As mentioned earlier, Equation (3-6) for V_y was derived by assuming ideal elastic-plastic (E-P) force-deformation behavior and "full" hysteretic loops for the system. That is characteristic of a number of ductile steel framing systems, such as MF, EBF, STMF, and BRBF. For systems that do not posses such hysteretic property, such as RC frames or steel braced frames with buckling type braces, some modification is warranted. Two approaches have been tried which show good promise. One approach is to convert target design drift by a C_2 factor to an equivalent non-degrading system for RC SMF. The other one is based on modifying the energy capacity term by a factor η to account for the reduced area of typical hysteretic loops as a fraction of the corresponding "full" loops.

3.4.4.1. C_2 factor method

This approach is based on consideration of the effect of degrading hysteretic behavior on peak (target) displacement. Investigators (Medina, 2002; FEMA 440, 2006) have studied the effect of degrading hysteretic behavior (stiffness and strength degradation, SSD) of SDOF systems on resulting peak displacements. The results show that the peak displacements are larger than those of systems with non-degrading hysteretic behavior (elastic-perfectly-plastic, EPP) in the short period range, but are about equal for longer periods. Approximate expressions have been proposed for modification factors to account for this effect, e.g., factor C_2 in FEMA 440 (2006) (Figure 3-7). The coefficient C_2 is a modification factor to represent the effect of pinched shape of hysteretic loops, stiffness degradation, and strength deterioration on the maximum displacement response according to FEMA 356. Since stiffness degradation and strength deterioration are the major

characteristics of typical RC SMF hysteretic behavior, C_2 is selected for modification of target design drift. Thus, the target design drift for a given structural system with degrading hysteretic behavior can be divided by the C_2 factor which would give design target drift for an equivalent non-degrading system.

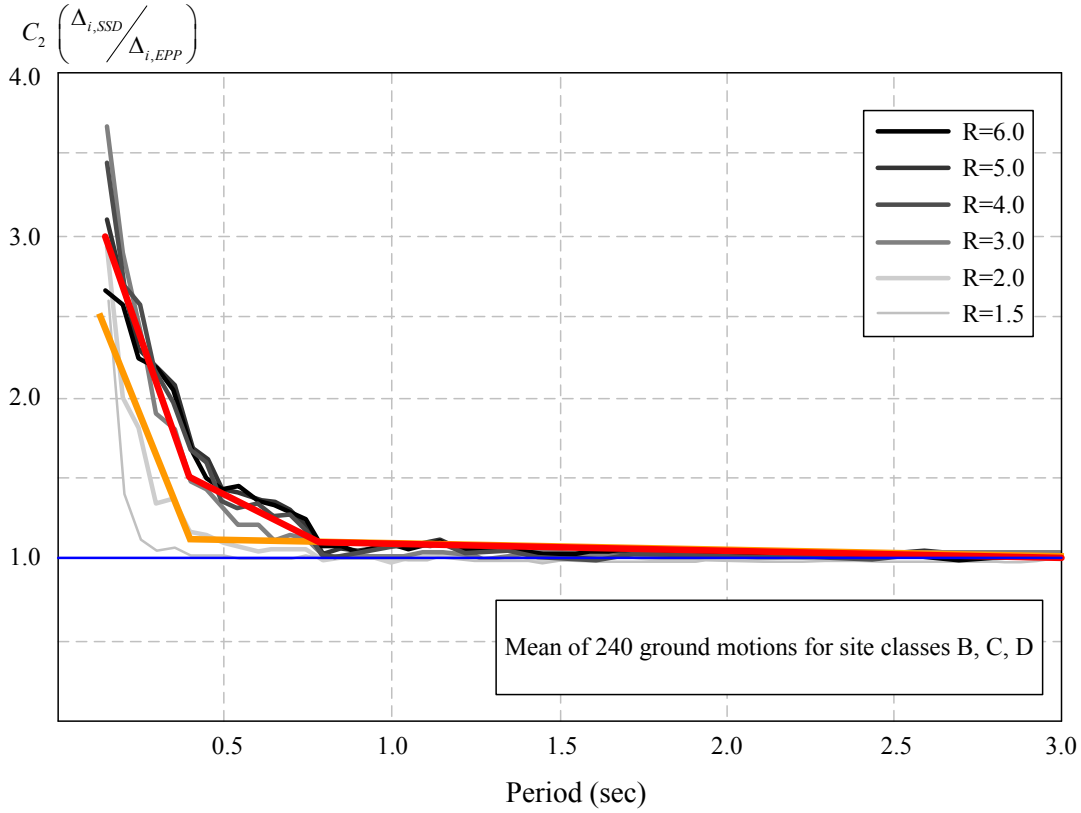

Figure 3-7 Mean displacement ratio (C_2) of SSD to EPP models computed with ground motions recorded on site classes B, C, and D for different force reduction factors, R (FEMA 440, 2006)

The equations of simplified linear regression trendline of C_2 for different force reduction factor, R, are summarized in Table 3-3.

Table 3-3 Values of C_2 factor as function of R and T

	$0.2 \le T < 0.4$	$0.4 \le T < 0.8$	$0.8 \le T$
R= 3.0 ~ 6.0	$3.0 - 7.5 \cdot (T - 0.2)$	$1.5 - 1.0 \cdot (T - 0.4)$	$1.1 - 0.045 \cdot (T - 0.8)$
R= 2.0	$2.5 - 6.5 \cdot (T - 0.2)$	$1.1 - 0.077 \cdot (T - 0.4)$	

After determining the value of C_2, the modified target design drift θ_u^*, ductility μ_S^*, ductility reduction factor R_μ^* and energy modification factor γ^* can be calculated as follows:

$$\theta_u^* = \frac{\theta_T}{C_2} \tag{3-8}$$

$$\mu_s^* = \frac{\theta_u^*}{\theta_y} = \frac{\theta_u}{\theta_y C_2} = \frac{\mu_s}{C_2} \Rightarrow get\ R_\mu^* \text{ from Table 3-2} \tag{3-9}$$

$$\gamma^* = \frac{2\mu_s^* - 1}{(R_\mu^*)^2} \tag{3-10}$$

The design base shear can then be calculated by using this modified energy modification factor γ^* and Equation (3-6) and (3-7). The design base shears calculated by C_2 method for 1 to 20-story typical RC SMF are shown in Table 3-4.

Table 3-4 Design base shears for 1 to 20-story RC SMF for PBPD and Code design method

Target Drift 0.02 **Yield Drift 0.005**											**PBPD**	**Code**
Number of Stories	Height (ft)	Period	C_2	Target drift*	Inelastic drift*	μ*	R_μ *	γ*	α	*Sa*	***V/W***	***V/W***
1	15	0.26	2.34	0.009	0.004	1.71	1.56	1.00	1.99	1.000	0.4162	0.1250
2	28	0.45	1.45	0.014	0.009	2.76	2.13	1.00	2.55	1.000	0.3451	0.1250
4	54	0.81	1.10	0.018	0.013	3.64	3.64	0.47	2.10	0.739	0.1167	0.0924
6	80	1.16	1.08	0.018	0.013	3.69	3.69	0.47	1.54	0.519	0.0781	0.0649
8	106	1.49	1.07	0.019	0.014	3.74	3.74	0.46	1.24	0.403	0.0577	0.0504
10	132	1.81	1.05	0.019	0.014	3.79	3.79	0.46	1.06	0.331	0.0452	0.0413
12	158	2.13	1.04	0.019	0.014	3.85	3.85	0.45	0.94	0.300[a]	0.0416	0.0375 [a]
14	184	2.45	1.03	0.020	0.015	3.90	3.90	0.45	0.85	0.300[a]	0.0451	0.0375 [a]
16	210	2.76	1.01	0.020	0.015	3.96	3.96	0.44	0.78	0.300[a]	0.0482	0.0375 [a]
18	236	3.06	1.00	0.020	0.015	4.00	4.00	0.44	0.72	0.300[a]	0.0512	0.0375 [a]
20	262	3.36	1.00	0.020	0.015	4.00	4.00	0.44	0.66	0.300[a]	0.0549	0.0375 [a]

[a] Sa was calculated by multiplying code *V/W* with R=8; the minimum requirement of *V/W* in ASCE 7-05 is 0.0375 where $S_1 \geq 0.6$g.

A comparison of design base shears calculated by PBPD C_2 factor method for 2% target drift and ASCE7-05 (2006) is shown in Figure 3-8.

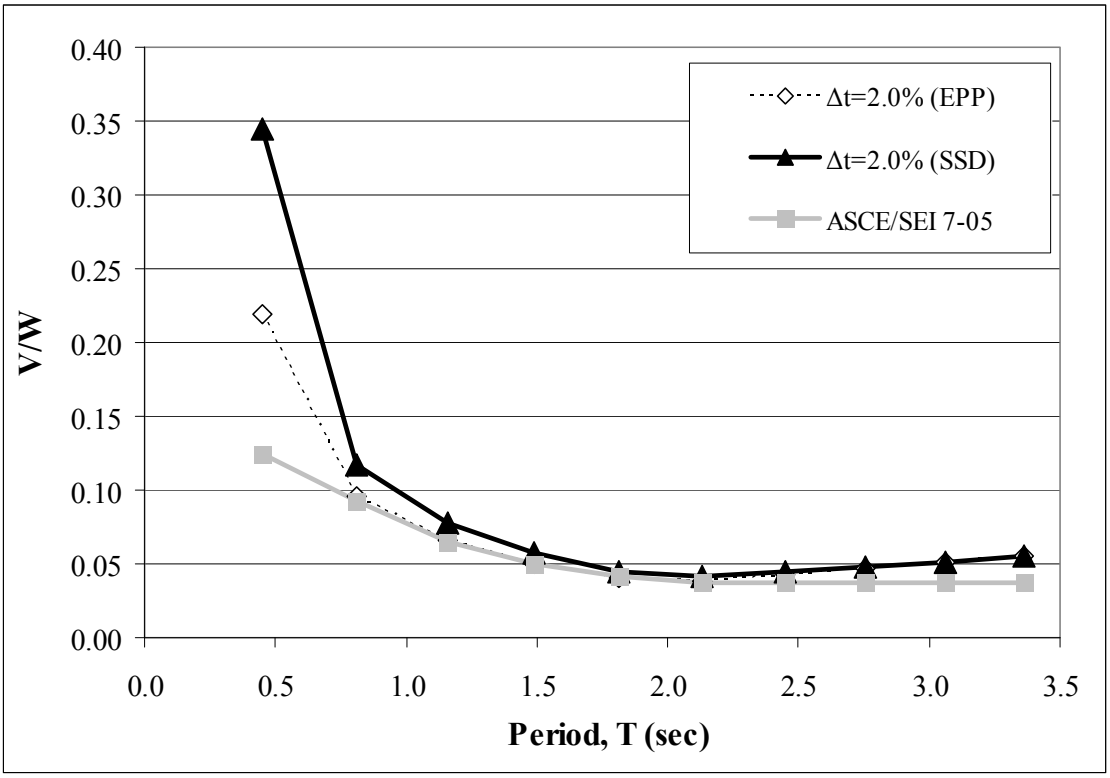

Figure 3-8 Comparison of design base shears calculated by PBPD C_2 method for 2% target drift Δt and ASCE/SE 7-05 (yield drift=0.5%)

As mentioned earlier, the PBPD method uses pre-selected target drift and yield mechanism as key performance limit states. Unlike the conventional code practice to determine design base shear, the PBPD method presents more flexibility to engineers to calculate design base shear of EPP and SSD systems for varying target drift, as shown in Figure 3-9.

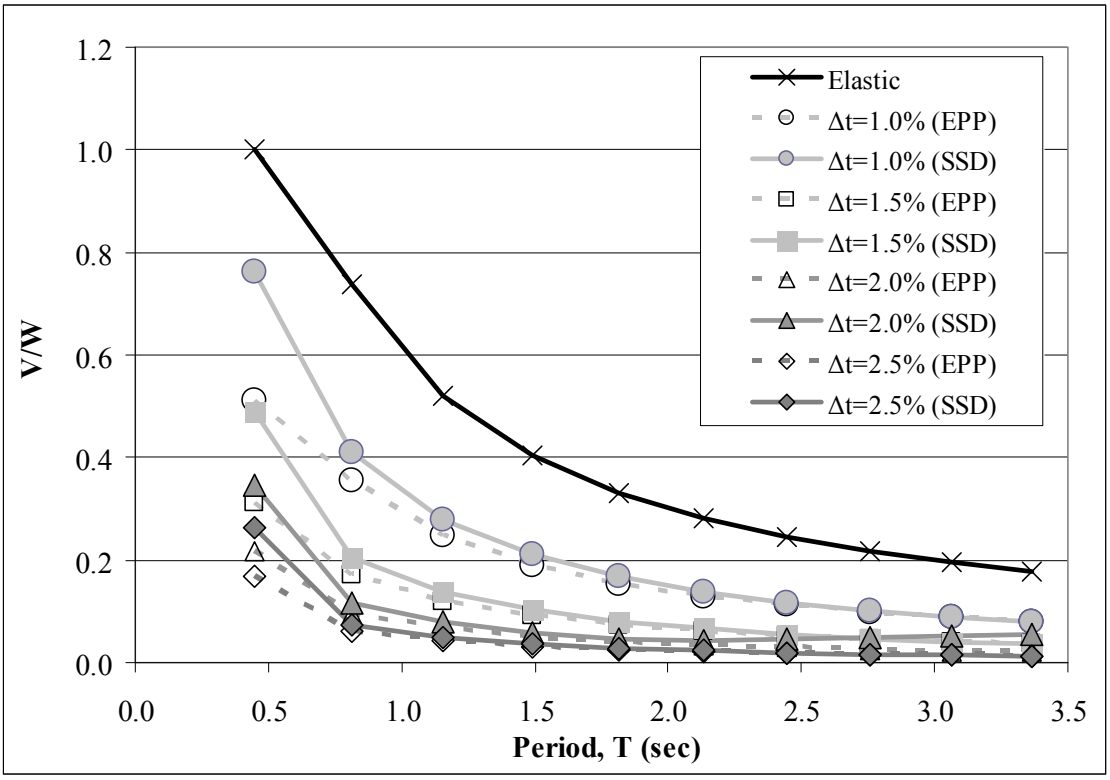

Figure 3-9 The relationship between the PBPD design base shear, design target drift Δt and period for EEP system and SSD system with C_2 factor method (yield drift=0.5%)

3.4.4.2. η factor method

In this approach, the energy capacity term, represented by the left hand side of Equation (3-2), can be modified by a factor η to account for the reduced area of typical hysteretic loops as a fraction of the corresponding "full" loops, Figure 3-10. Thus, Equations (3-2) and (3-6) can be modified as Equations (3-12) and (3-13), respectively:

$$\eta = \frac{Area\ of\ Pinched\ hysteretic\ loop,\ A_1}{Area\ of\ Full\ hysteretic\ loop,\ A_2} \tag{3-11}$$

$$\eta\left(E_e + E_p\right) = \gamma\left(\frac{1}{2}MS_v^{\,2}\right) = \frac{1}{2}\gamma M \cdot \left(\frac{T}{2\pi}S_a g\right)^2 \tag{3-12}$$

$$\frac{V_y}{W} = \frac{-\alpha + \sqrt{\alpha^2 + 4(\gamma/\eta)S_a^2}}{2} \tag{3-13}$$

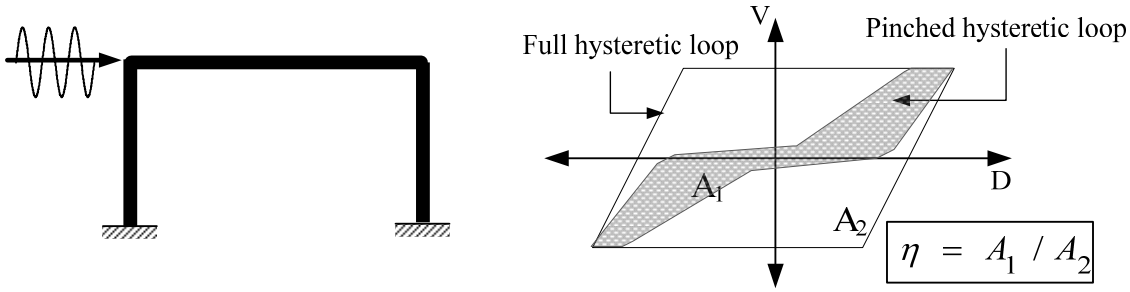

Figure 3-10 Typical full EP and "pinched" hysteretic loops

This method has been successfully applied to steel concentrically braced frames (Goel and Chao, 2008). However, *V/W* values calculated by η factor method may be too conservative with typical value of η =0.2 for RC SMF when compared with those obtained by the C_2 factor method, as can be seen in Table 3-5.

Table 3-5 Design base shears *V/W* calculated by C_2 and η factor method for 4, 8, 12 and 20 story RC SMF

	4-story	8-story	12-story	20-story
C_2 factor method	0.1167	0.0577	0.0416	0.0549
η factor method	0.424	0.224	0.1519	0.0923

3.4.5 Design lateral forces (without P-Delta)

Traditionally, vertical distribution of design lateral forces in modern building codes has been based on elastic fundamental mode response of MDOF systems. Modifications have been made to account for effects, such as contribution of higher modes. Most recently ASCE

7-05 (2006) prescribes the following basic expression for vertical force distribution factor, C_{vx}, at level x :

$$C_{vx} = \frac{w_x h_x^k}{\sum_{i=1}^{n} w_i h_i^k} \tag{3-14}$$

where w_i and w_x are the portion of the total effective seismic weight of the structure located at level i and x respectively; h_i and h_x represent the height (ft or m) from the base to level i and x respectively; and k is an exponent related to the structure period, T, as shown in Table 3-6:

Table 3-6 Exponent *k* for code vertical force distribution factor C_{vx}

	$T < 0.5$ (sec)	$0.5 \le T < 2.5$ (sec)	$2.5 \le T$ (sec)
k	1	2 or linear interpolation between 1 and 2	2

As mentioned previously, a different distribution of lateral design forces is used (Chao at el, 2007) in PBPD design, which is based on relative distribution of maximum story shears consistent with inelastic dynamic response results. The higher mode effects are also well represented in this distribution. It was observed from extensive nonlinear dynamic analyses of various steel structural systems that the new lateral force distribution leads to more realistic story shears and uniform story drifts over the building height. In order to bring the design story shear distribution closer to the inelastic response results an exponent term was used as shown in the following equation:

$$V_i = \left(\frac{\sum_{j=i}^{n} w_j h_j}{\sum_{j=1}^{n} w_j h_j} \right)^{0.75T^{-0.2}} \cdot V_y \tag{3-15}$$

The constants in the exponent term in Equation (3-15) were derived by empirical fit with inelastic response results of a variety of common structural systems (Chao and Goel, 2007). V_y represents the design base shear as determined from Equation (3-6) or (3-13) for use in the PBPD method. For *i=n,* Equation (3-16) gives the value of shear V_n or lateral force F_n at the top level:

$$V_n = F_n = \left(\frac{w_n h_n}{\sum_{j=1}^{n} w_j h_j} \right)^{0.75T^{-0.2}} \cdot V_y \tag{3-16}$$

Combining Equations (3-15) and (3-16), the ratio V_i / V_n, termed as shear distribution factor, β_i , can be expressed as:

$$\frac{V_i}{V_n} = \beta_i = \left(\frac{\sum_{j=1}^{n} w_j h_j}{w_n h_n} \right)^{0.75T^{-0.2}} \tag{3-17}$$

Then, the lateral force at level *i*, F_i, can be obtained as,

$$F_i = \left(\beta_i - \beta_{i+1} \right) \cdot V_n \tag{3-18}$$

or,

$$F_i = \left(\beta_i - \beta_{i+1}\right) \cdot \left(\frac{w_n h_n}{\sum_{j=1}^{n} w_j h_j} \right)^{0.75T^{-0.2}} V_y \qquad (3\text{-}19)$$

3.4.6 Additional lateral forces due to P-Delta effect

It should be mentioned that P-Delta term is not included in basic Equation (3-19). However, P-Delta effect was included in the determination of required moment capacity of beams, particularly for the 12 and 20-story RC SMF, in order to provide necessary strength to counter the overturning due to gravity loads. That was accomplished by adding "P-Delta lateral force", $F_{i\text{-}PD}$, to the basic design force, F_i, in Equation (3-19).

In this method, which can be considered a more direct way of considering P-Delta effect, the "column tree" is considered in an assumed deflected shape at the target drift. A linear deflected shape is assumed herein. The gravity loads can be applied directly on the "column tree" or on a "P-Delta column", which is modeled for this purpose as shown in Figure 3-11.

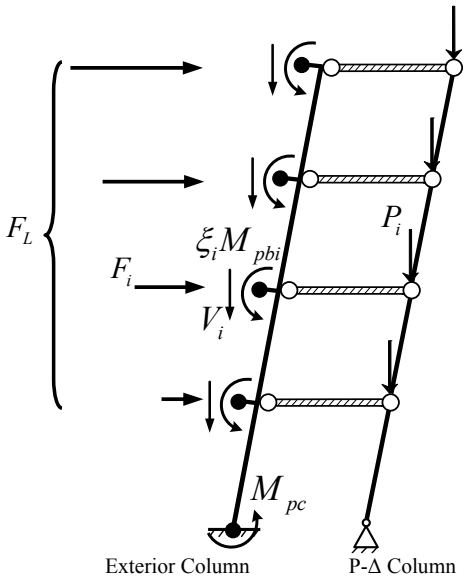

Figure 3-11 Column tree and P-Δ column in direct P-Delta method

Equilibrium equation of the assembly is formulated to calculate the total required lateral force, F_L, and the resulting column moments and shears are obtained as shown in Figure 3-12. The force $F_{i\text{-}PD}$ can be taken equal to $P_i\theta_u$, where P_i represents the tributary gravity load at floor level i and θ_u represents the target design drift ratio which is assumed constant for design purpose.

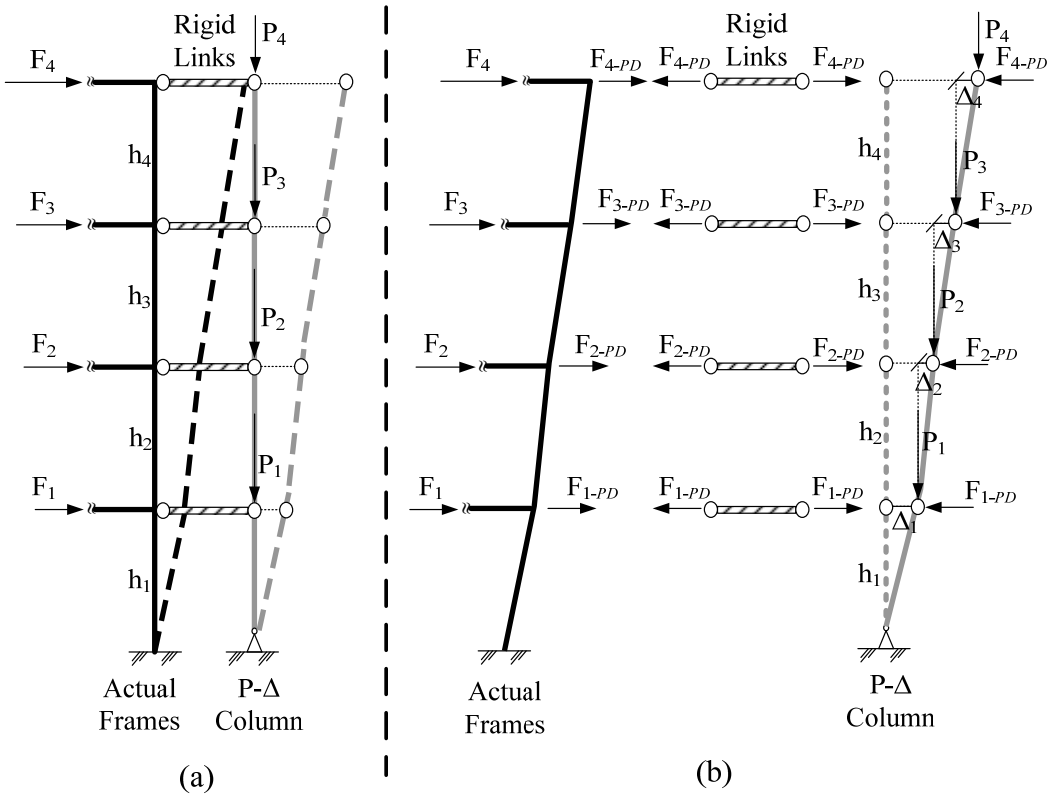

Figure 3-12 Additional lateral forces $F_{i\text{-}PD}$ due to P-Delta effect

Since the pre-selected mechanism for design of RC SMF in this study is complete sway mechanism with the same story drift for each floor (Figure 3-4), the summation of $F_{i\text{-}PD}$ can simply calculated as total weight multiplied by target drift (2% for 2/3MCE; 3% for MCE). The values of $F_{i\text{-}PD}$ for the 4, 8, 12 and 20-story RC SMF are summarized in Table 3-7. Their influence on the total lateral design force can be clearly noticed as it has significant effect on the required frame strength.

Table 3-7 Design base shear with and without P-Delta for PBPD RC SMF

Design Parameters	4-story		8-story		12-story		20-story	
	2/3MCE	MCE	2/3MCE	MCE	2/3MCE	MCE	2/3MCE	MCE
V/W	001167	0.1117	0.0577	0.0552	0.0416	0.0398	0.055	0.054
V w/o *PD* (kips)	242.2 (governs)	231.8	107.1 (governs)	102.5	116.3 (governs)	111.3	255.0 (governs)	248.0
$\Sigma F_{i\text{-}PD}$ (kips)	41.5	62.2	36.9	55.3	55.9	83.7	92.0	138.0
Design Base Shear w/ P-Delta (kips)	**283.7**	**294.0**	**144.0**	**157.8**	**172.2**	**195.0**	**347.0**	**386.0**

It should be noted from the above table that the design base shears with P-Delta for the MCE hazard in all four cases are somewhat greater than the corresponding values for 2/3MCE hazard. However, the latter values were used for the design of PBPD frames in this study because 2/3 MCE is commonly accepted as Design Basis Earthquake (life-safety/drift control objective), whereas MCE is associated with "Collapse Prevention" performance objective in which case strict drift control may not be considered as important as long as collapse is prevented (LATBSDC Alternative Design Criteria, 2008).

3.4.7 Design of designated yielding members (DYMs)

The primary aim of using plastic design method is to provide adequate strength while ensuring formation of the desired yield mechanism. For moment frames, for instance, it is desirable that the plastic hinges form only at the beam ends and column bases.

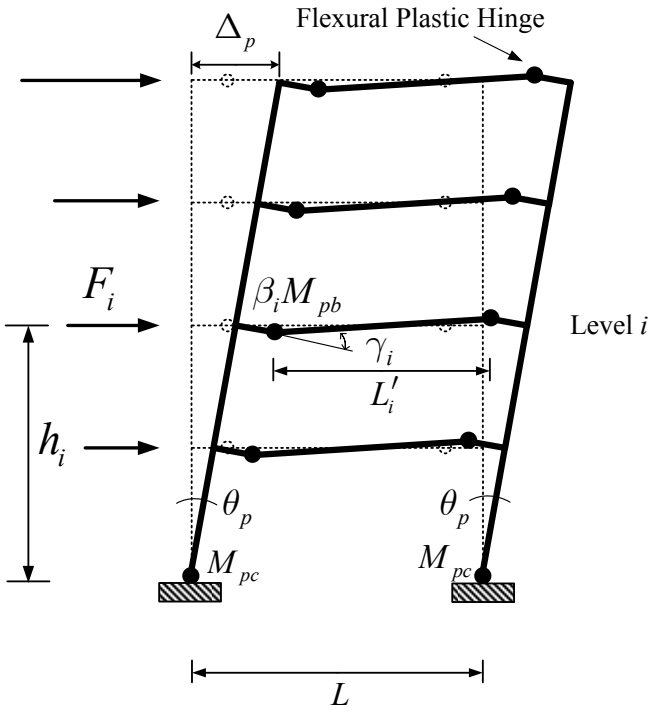

Figure 3-13 Target yield mechanism of moment frame with beam plastic hinges away from column faces

When using the target yield mechanism for moment frames as shown in Figure 3-13, beams become the primary designated yielding members (DYM). The required beam moment capacity at each level can be determined by plastic design approach (external work equals internal work) and referring to Figure 3-13:

$$\sum_{i=1}^{n} F_i h_i \theta = 2M_{pc}\theta + \sum_{i=1}^{n} 2\left(\beta_i M_{pb}\right)\gamma_i \tag{3-20}$$

where θ represents a small kinematic rotation angle of the yield mechanism, and M_{pb} and $\beta_i M_{pb}$ are the required moment strengths at the top floor level and level *i*, respectively. The rotation term $\gamma_i = \left(L / L_i'\right)\theta$, as shown in Figure 3-13. It is noted that the external work done by uniformly distributed gravity loading as the frame is pushed laterally is zero due to anti-symmetrical deformed shape of the beams.

Previous studies (Chao et al, 2007) have shown that it is desirable to have the distribution of structural strength along the building height follow the distribution of design story shears, *i.e.*, $M_{pbi} = \beta_i M_{pb}$. This helps to distribute the yielding more evenly along the height, thereby, preventing yielding from concentrating at a few levels. Thus, the number of unknown terms in Equation (3-20) is reduced to two, i.e., M_{pb}, and M_{pc}. By assuming a suitable value of M_{pc} the required value of M_{pb} (and thus M_{pbi}) can be obtained by solving Equation (3-20). The selection of appropriate beam sections can then be designed by following current building code requirements.

For RC moment frames, in general, because of strength contribution from slabs and non-rectangular beam shapes (ie, T shape beam), as well as the use of different amounts of top and bottom reinforcement, plastic moments in positive and negative direction of DYM may be different. Thus, Equation (3-20) can be further modified as follows:

$$\sum_{i=1}^{n} F_i \cdot h_i \cdot \theta_p = 2 \cdot M_{pc} \cdot \theta_p + \sum_{i=1}^{n} \beta_i \cdot \left(M_{pb-positive} + M_{pb-negative} \right) \cdot \gamma_i \qquad (3\text{-}21)$$

By using a suitable value of x ($x = \left| \frac{M_{pb-negative}}{M_{pb-positive}} \right|$), Equation (3-21) can be simplified as Equation (3-22), which still contains two unknown terms, i.e., $M_{pb-positive}$, and M_{pc}.:

$$\sum_{i=1}^{n} F_i \cdot h_i \cdot \theta_p = 2 \cdot M_{pc} \cdot \theta_p + \sum_{i=1}^{n} (1+x) \cdot \beta_i \cdot \left(M_{pb-positive} \right) \cdot \gamma_i \qquad (3\text{-}22)$$

Selection of appropriate value of x is discussed in Chapter 4 (Section 4.4).

Value of M_{pc} can be determined by using the condition that no soft story mechanism would occur in the first story when a factor ψ (in the order of 1.1 to 1.5) times the design lateral forces are applied on the frame, as shown in Figure 3-14.

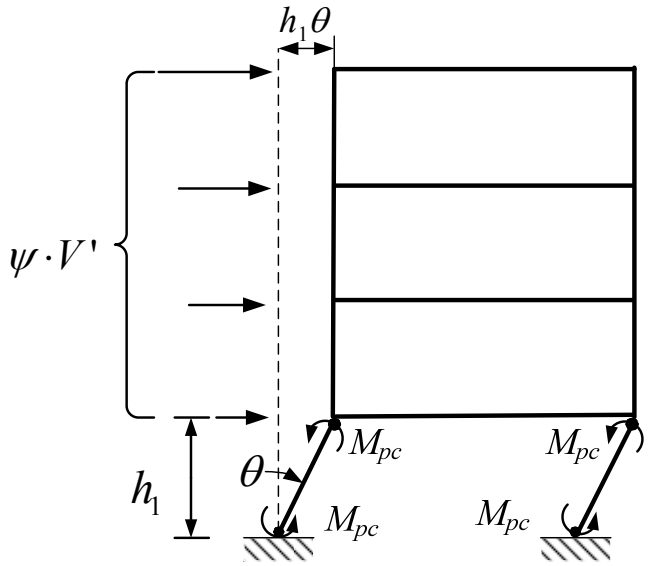

Figure 3-14 Soft story mechanism condition in the first story

Assuming that plastic hinges form at the base and top of the first story columns, the corresponding work equation for a small mechanism deformation, θ, gives

$$M_{pc} = \frac{\psi V' h_1}{4} \tag{3-23}$$

where V' is the base shear (for an equivalent one bay model), which may be taken as V divided by the number of bays; h_1 is the height of the first story; and the factor ψ accounts for over-strength above the design force. A value of 1.1 for the factor ψ in Equation (3-23) was used for 4, 8 and 12- story RC SMF and 1.5 for 20-story RC SMF. It should be noted that a value of 1.1 and 1.5 for the factor ψ for low/medium-rise and high-rise building respectively has given promising results either in RC and steel SMF (Goel and Chao, 2008).

By using Equations (3-22) and (3-23), the required DYM strength at floor level i, $M_{pb-negative}$ and $M_{pb-positive}$, can be determined, and the design can be performed by using applicable specification, such as ACI-318.

3.4.8 Design of non-designated yielding members (Non-DYMs)

Members that are not designated to yield (Non-DYM), such as columns in an RC SMF, must have design strength to resist the combination of factored gravity loads and maximum expected strength of the DYM by accounting for reasonable strain-hardening and material overstrength. For this purpose one approach is to consider the equilibrium of portions of the design yield mechanism in the extreme limit state. In building frames these portions include columns which can be modeled as "column trees". For example, Figure 3-15 shows the free-body diagram of an exterior "column tree" of the frame with maximum expected forces in the limit state.

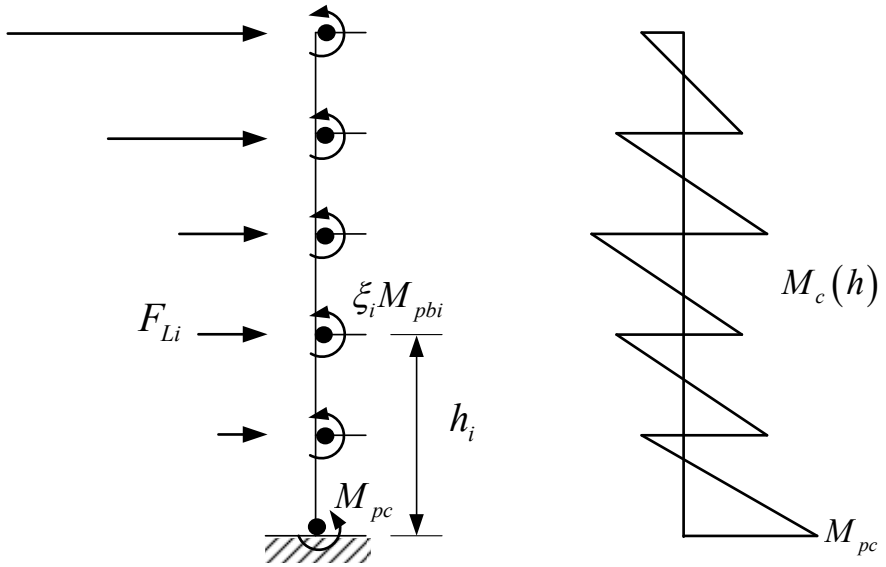

Figure 3-15 Free body diagram of an exterior "column tree"

In order to ensure the formation of intended strong-column weak-beam mechanism, the columns must be designed for maximum expected forces by including gravity loads on beams and columns and by considering a reasonable extent of strain-hardening and material

over-strength in the beam plastic hinges. The columns at the base are also assumed to have reached their maximum capacity, M_{pc}. The moment at a strain-hardened beam plastic hinge can be obtained by multiplying its nominal moment (M_{pb}) by an appropriate over-strength factor (ξ), which accounts for the effect of strain-hardening and material over-strength. In this study, the over-strength factor (ξ) was simply set as 1.25, which was established recognizing all these effects in ACI 318 (Moehle et al, 2008).

At this stage, the required lateral forces (F_{Li}) acting on this free body may be assumed to maintain the distribution as given by Equation (3-17), and their magnitude can be easily obtained by using equilibrium of the entire free body. Then the column end moments and shear force in each story are calculated by applying the expected beam end moments and lateral forces (F_{Li}) applied at each level. Second order effects can be included by using approximate amplification factors as given in design codes to ensure the Non-DYM remain elastic.

In most cases, for the first story, the nominal plastic moment at the column top is usually less than that at the bottom. To ensure base column plastic hinges forming as intended, it is highly desirable to design the base column with M_{pc} even if it may be less than that at the column top in some cases.

3.5. Summary and conclusions

The PBPD method uses pre-selected target drift and yield mechanism as key performance limit states. The design base shear for a specified hazard level is calculated by equating the work needed to push the structure monotonically up to the target drift to the energy required by an equivalent EP-SDOF to achieve the same state.

The PBPD design procedure is easy to follow and can be readily incorporated within the context of broader performance-based design framework given in FEMA-445 (Figure 2-

4). It does differ from the way it is practiced currently, which usually starts with an initial design according to conventional elastic design procedures using applicable design codes, followed by cumbersome and time-consuming iterative assessment process by using inelastic static and dynamic analyses till the desired performance objectives are met. The iterations are carried out in a purely trial-and-error manner. No guidance is provided to the designer as to how to achieve the desired goals, such as controlling drifts, distribution and extent of inelastic deformation. In contrast, the PBPD method is a *direct* design method, which requires no evaluation after the initial design because the nonlinear behavior and key performance criteria are built into the design process from the start. The design procedure is easy to follow and it can be easily programmed as well.

The performance-based plastic design flowcharts for determination of design base shear, lateral forces and member design are shown in Figure 3-16 and Figure 3-17, respectively.

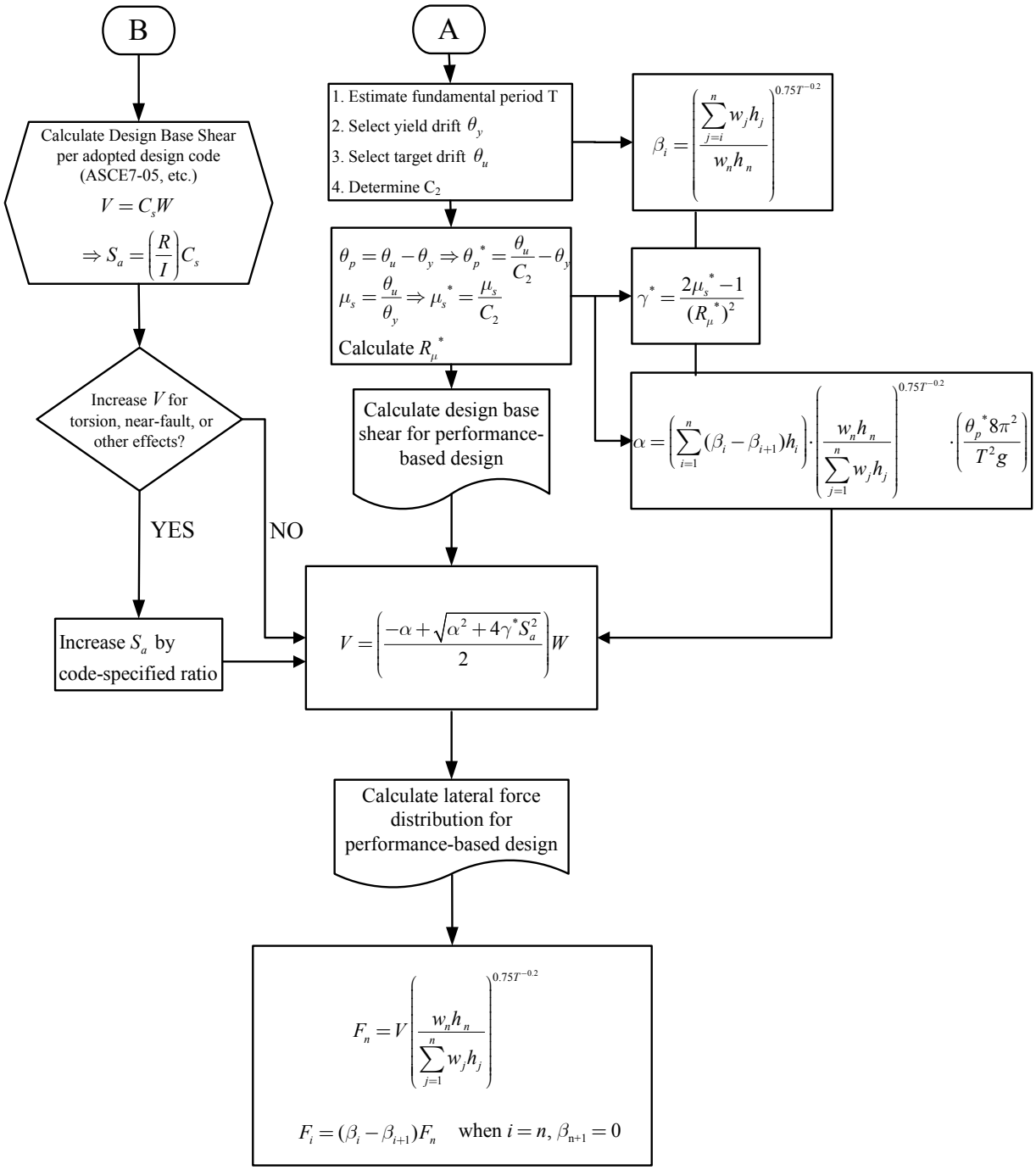

Figure 3-16 Performance-based plastic design flowchart: determination of design base shear and lateral force distribution

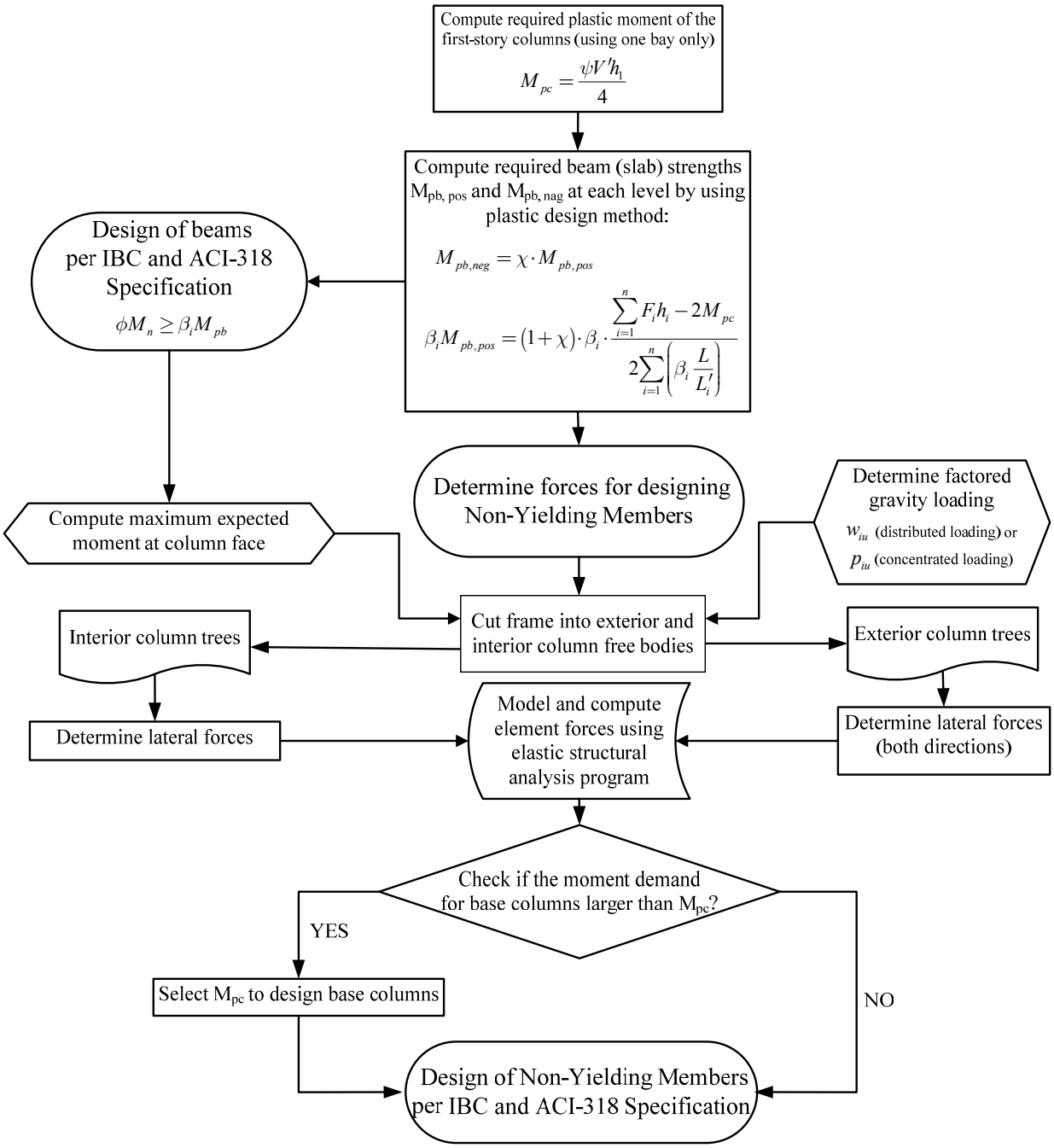

Figure 3-17 Performance-based plastic design flowchart for RC moment frames: member design

CHAPTER 4

REDISGNED RC SMF WITH PERFORMANCE-BASED PLASTIC DESIGN (PBPD) METHOD

4.1. Introduction

Redesign work of four examples of 4, 8, 12 and 20-story RC special moment frame structures with PBPD method is briefly presented in this chapter. All of them were space frames. The baseline space frames were designed to comply with the requirements of ICC (2003), ASCE 7-02 (ASCE, 2002) and ACI 318-02 (ACI, 2002), as reported in FEMA P695 (2009).

The frames were then redesigned by the modified PBPD method. That is, the design base shear and corresponding lateral force distribution were first determined according the flowchart shown in Figure 3-16. Then the design of a typical moment frame can be performed by following the flowchart given in Figure 3-17. In addition, the FEMA 440 (2008) C_2 factor approach and consideration of P-Delta effect as discussed in Chapter 3 were important parts of the redesign work.

4.2. Design decisions of archetype baseline frames

All the selected baseline space frames were taken from FEMA P695 (2009) and belong to the class of reinforced concrete special moment frame buildings designed

according to current building code provisions (ICC 2003, ASCE 2002, ACI 2002). To ensure that each of the archetype designs is representative of current design practice, the design work was checked by a practicing engineer (Hooper 2006), including review of the relevant design assumptions as listed in Table 4-1 to confirm consistency with common design practice.

One important design decision in Table 4-1 is that the strong column/weak beam (SCWB) ratio in FEMA P695 was set at 1.3 instead of 1.2 as specified in ACI 318 (2005). The aim of the strong-column weak-beam (SCWB) design provision is to prevent localized story mechanisms. According to one of the important conclusions in FEMA P695 (2009), it is noted that ACI provision does not fully prevent column hinging and incomplete story mechanisms but only helps to delay column hinging and to spread the damage over more stories of the building. However, further analysis in this study (Chapter 6) showed that even using 1.3 as strong column/ weak beam ratio cannot prevent formation of column hinges and soft story mechanisms under severe earthquake hazard level. On the other hand, designing columns with the concept of "column tree" in PBPD method as described in Chapter 3 automatically fulfills the goal of SCWB without checking every single joint one by one during the design stage.

Table 4-1 Criteria used in the design of the baseline buildings (FEMA P695, 2009)

Design parameter	Design assumption
Beams	$0.5EI_g$ (FEMA 356)
Columns	$0.7EI_g$ for all axial load levels
Slab	Not included in stiffness/strength design
Joint	Elastic joint stiffness
Element flexural and shear strength design	1.15 of required strength
Joint strength design	1.0 of required strength
Strong-column/ weak-beam design	**1.3 instead of 1.2**

Typical floor plan is shown in Figure 4-1, and important design parameters are given in Table 4-2. The second column of Table 4-2 summarizes the range of values these design parameters may typically take on for common engineering practice. Moreover, these parameters and ranges shown in Table 4-2 provide the basis for defining a finite number of design realizations for study using archetype analysis models.

It is noted that these archetypical buildings can provide appropriate predictions not only for a single specific building but also generalized full class of structures (Goulet et al. 2006, Haselton et al, 2007). As mentioned earlier, all baseline frames conform to design requirements for special moment frames (RC SMF) according to IBC (2003) and ACI 318 (2005).

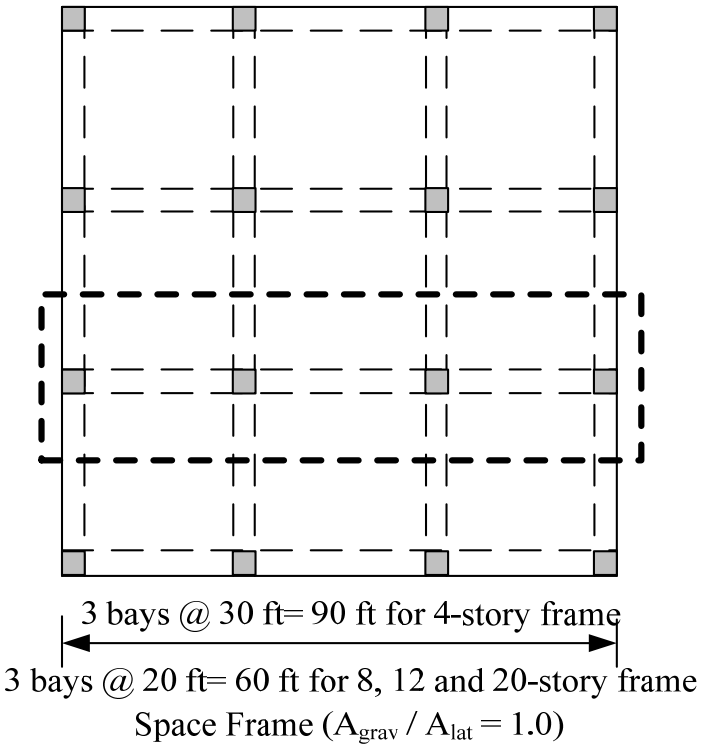

Figure 4-1 Floor plan of RC space moment frame building

Table 4-2 Ranges of design parameters for the archetype model

Design Parameters	Range Considered in Archetype Design
Structural System	
Reinforced Concrete Special Moment Frame (as per 2003 IBC, ACI 318-05)	All designs meet code requirements
Seismic design level	Design Category D
Seismic framing system	Space frames
Configuration	
Building height	Stories: 4, 8, 12, 20
Bay width	20-30 ft
First story and upper story heights	15/13 ft
Element Design	
Confinement ratio (ρ_s) and stirrup spacing (s)	Conforming to ACI 318-05.
Concrete compressive strength	5-7 ksi
Longitudinal rebar diameters (d_b)	#8 and #9 commonly used
Loading	
Ratio of frame tributary areas for gravity and lateral loads (A_{grav}/A_{lat})	1.0 (space frame)
Design floor dead load	175 psf
Lower/upper bounds on design floor dead load (for checking sensitivity)	150 - 200 psf
Design floor live load	Constant 50 psf

Four baseline frames (4, 8, 12 and 20-story space moment frame) were selected from the matrix of 30 archetypical designs provided in FEMA P695 (2009), as summarized in Table 4-3. All of them cover a range of strength and stiffness variations over the building height that are permissible within the ASCE7-02 (ASCE 2002) seismic design provisions.

Table 4-3 Basic design information of selected baseline frames (FEMA P695, 2009)

Design information					
ID	Number of stories	Bay width (ft)	Framing system	First mode period (sec)	Design base shear coefficient, C_s
1010	4	30	space	0.86	0.092
1012	8	20	space	1.80	0.050
1014	12	20	space	2.14	0.044
1021	20	20	space	2.36	0.044

In terms of considerations for further analysis model, a three bay frame was selected by Haselton (2007) for more realistic representation of frame design and behavior, as shown in Figure 4-2. It was mentioned in FEMA P695 (2009) that the three-bay variable story-height configuration is deemed as the simplest model to represent important design features that may affect the structural response. A three-bay model contains both interior and exterior columns. The strong-column weak-beam design provisions can be evaluated as well with the interior and exterior columns. Furthermore, the three-bay frame can capture the additional axial loads due to overturning. It is noted that in FEMA P695 (2009), no nonlinear axial-flexural interaction was considered in the plastic hinge models, whereas it was included in this study. More detail will be given in Chapter 5.

For all designs, P-Delta effect was accounted for by using a combination of gravity loads on the moment frame ("unchecking" P-Delta option for frame member elements in the analysis program) and gravity loads on a "P-Delta column" element ("checking" P-Delta option for P-Delta column element in the analysis program) as shown in Figure 4-2.

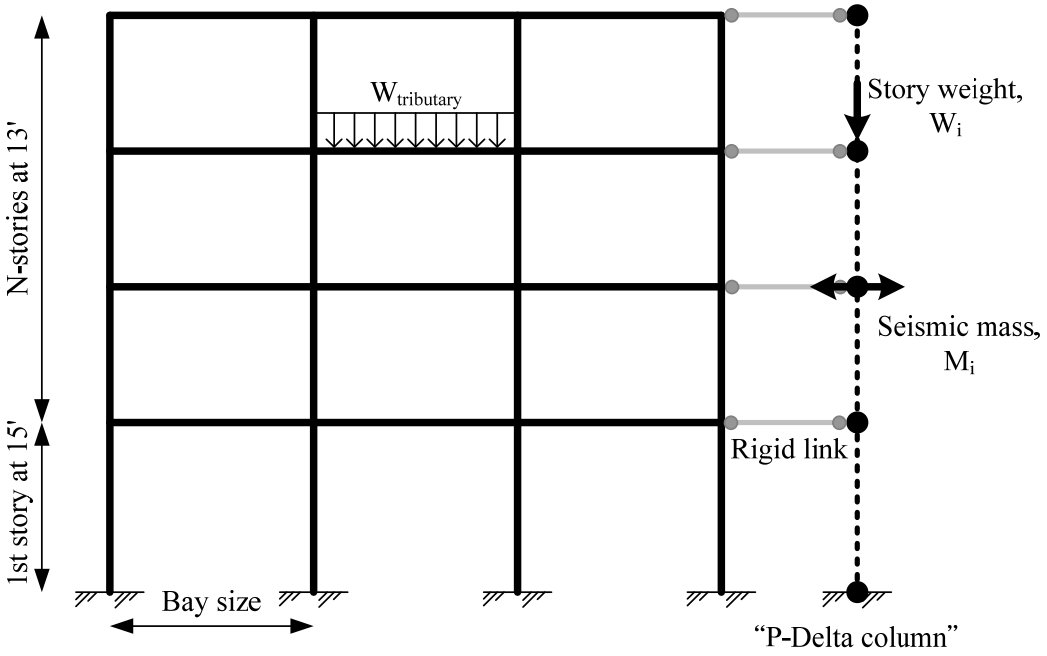

Figure 4-2 Archetype analysis model for RC SMF

In terms of building site, the archetype models listed in Table 4-3 were all designed for a general high seismic site in Los Angeles, California (soil class S_d, S_{ms} = 1.5g, and S_{m1} = 0.9g).

4.3. Software for column design: PCA-Column

For the member section design, PCA-COLUMN was used for designing columns. PCA-COLUMN is a software program for design and evaluation of reinforced concrete sections subject to axial and flexural loads. The section can be rectangular, round or irregular, with any reinforcement layout or pattern. Slenderness effects can be considered as well. The design criteria of PCA-COLUMN also conform to provisions of various code, such as ACI 318-08, ACI 318-05, ACI 318-02, CSA A23.3-04, and CSA A23.3-94. The window interface of PCA-COLUMN is shown in Figure 4-3.

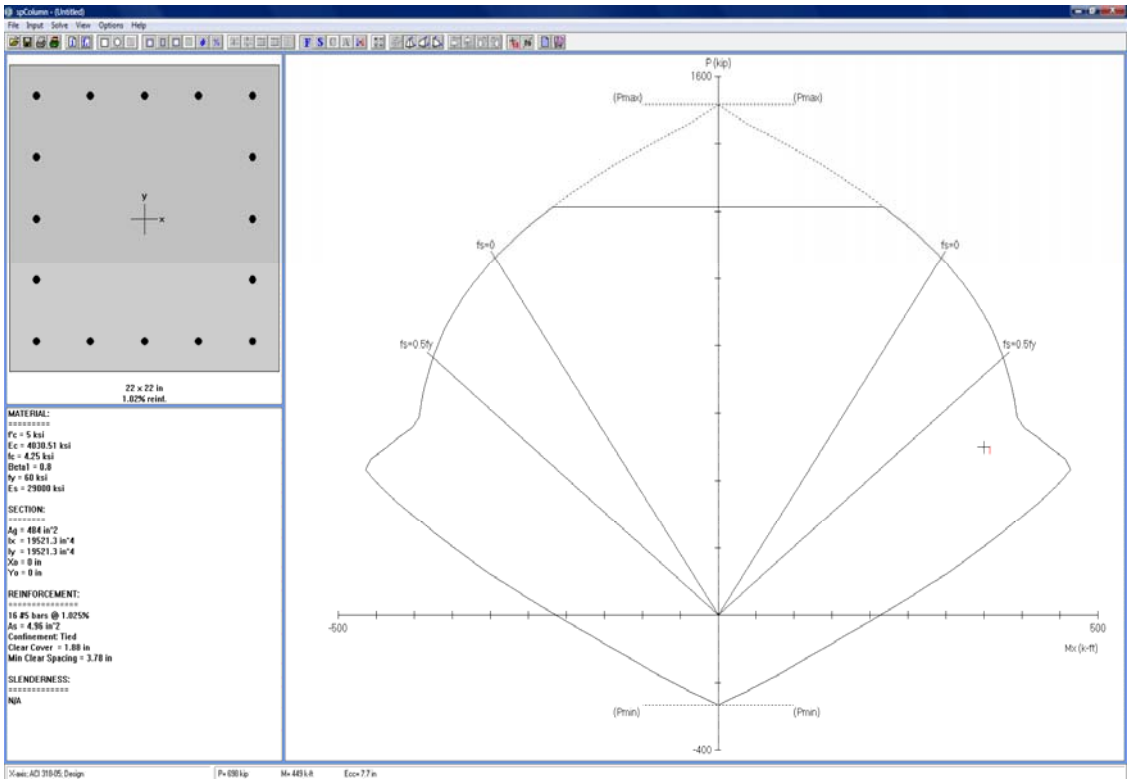

Figure 4-3 Main window of PCA-COLUMN

While the strength demands of column elements were determined by following the PBPD design procedure described in Chapter 3, the column section and reinforcement layout was determined by using PCA-COLUMN.

4.4. Design examples

As mentioned in Chapter 1, the main objectives for this study are to develop PBPD methodology for RC moment frames, to redesign the baseline frames (a series of RC SMF: 4, 8, 12 and 20 story) as used in the FEMA P695 document (2009), and to evaluate the responses under extensive inelastic pushover and time-history analyses for baseline and PBPD RC SMF. Therefore, except for the design methodology, other design assumptions and parameters for redesign work were kept the same as those of the baseline frames for consistency and fair comparison.

In the above context it should be noted that one of the important design parameters in RC SMF is the ratio of $M_{pb—negative}$ to $M_{pb–positive}$ for the design of beams. ACI 318 (Section 21.3.2.2) requires this ratio does not exceed 2.0. However, there is some ambiguity as well as debate regarding this provision as to whether the reinforcement in the slab cast monolithically with the beam ("T-beam behavior") should be included in the design of beams (Moehle et al., 2008). Some designers size the beams by considering reinforcement in the beam web only, whereas some include the slab reinforcement as well. The beam design in "Benchmark frames" was done by following the former approach. Nevertheless, ACI 318 Section 21.4.2.2 is explicit in requiring that slab reinforcement within the effective width at the face of the column be included as beam tension reinforcement in calculating the relative strengths of beams and columns. Therefore for consistency, the approach used in the design of "Benchmark" (baseline) frames was also used to re-design those frames by the PBPD method as developed in this study.

4.4.1 Baseline frames

The baseline moment frames selected from FEMA P695 (2009) were designed by a professional engineer using the current code practice. The 4, 8, 12 and 20-story space frame buildings were designed for base shear coefficient of C_s = 0.092g, 0.050g, 0.044g and 0.044g, respectively.

As mentioned by Haselton (2007), the details of the design were governed by several other aspects of the code provisions. Beam strengths were controlled by gravity and lateral force demands, and column strengths were governed by the strong-column weak-beam provision. That is, the column strengths generally had to be increased in order to satisfy the specified SCWB ratio at every single joint.

It is also worth mentioning that with the exception of the 4-story baseline building, all other taller baseline frame designs were controlled by interstory drift limitations (2% for 2/3MCE and 3% for MCE hazard level). It means that for the taller buildings, more iteration

work was needed to refine the design in order to meet the drift limits requirements, which is not so in the PBPD method.

4.4.2 4-story PBPD RC SMF

As described in Chapter 3, the target drift and desired yield mechanism (Figure 4-4) are selected at the start of design in the PBPD method.

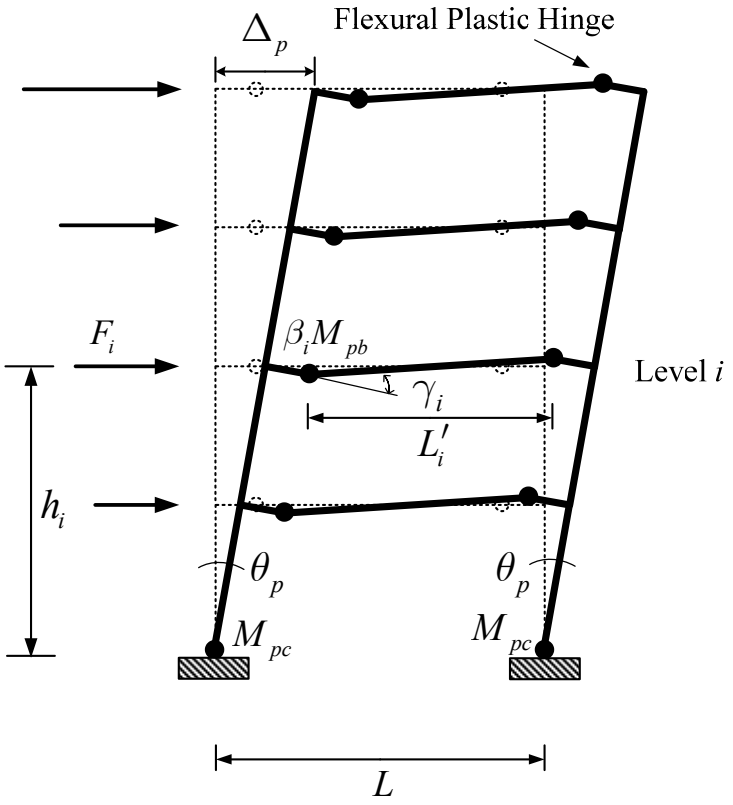

Figure 4-4 Pre-selected yield mechanism of 4-story RC SMF with beam plastic hinges away from the column faces

By following the design flowcharts shown in Figure 3-16 and Figure 3-17, the design base shear, lateral force distribution factors, required moment and shear strengths for DYM and Non-DYM can be systematically calculated.

Design Parameters

Important design parameters were summarized in Table 4-4. It is noted that S_a can be obtained by simply multiplying C_s by R/I for 2/3 MCE hazard level; that is,

$$S_a = C_s \cdot \left(\frac{R}{I}\right) = 0.092 \cdot \left(\frac{8}{1}\right) = 0.74g \,. \tag{4-1}$$

Table 4-4 Important design parameters for 4-story PBPD RC SMF

T (sec) Eq (3-1)	Yield Drift Ratio θ_y	Target Drift Ratio θ_u	S_a (g) Eq (4-1)	L (ft)	L' (ft)	W- tributary (k/ft)	W (kips)
0.81	0.005	0.02 (2/3 MCE) 0.03 (MCE)	0.74 (2/3 MCE) 1.11 (MCE)	30	27.5	5.76	2075

Lateral Force Distribution

The design lateral force distribution in the PBPD method can be determined by Equation (3-17) and the calculation results are given in Table 4-5.

Table 4-5 Important design parameters for 4-story PBPD RC SMF

Floor	h_j (ft.)	w_j (kips)	$w_j h_j$ (k-ft)	$\sum w_j h_j$ (k-ft)	β_i Eq (3-17)	$\beta_i - \beta_{i+1}$	$(\beta_i - \beta_{i+1}) \cdot h_i$
Roof	54	518	28013	28013	1.000	1.000	54.0
4	41	519	21269	49282	1.555	0.555	22.8
3	28	519	14525	63807	1.904	0.348	9.7
2	15	519	7781	71588	2.083	0.179	2.7
Σ		2075			6.542	2.083	89.2

Design Base Shear

The design base shear was determined for two level performance criteria: 1) a 2% maximum story drift ratio (θ_u) for a ground motion hazard with 10% probability of

exceedance in 50 years (10/50 and 2/3MCE); 2) a 3% maximum story drift ratio (θ_u) for 2/50 event (MCE).

A yield drift ratio (θ_y) of 0.5% is used, which can be considered a lower bound for typical of RC moment frames, as listed in Table 4-4. The design base shear is then calculated from Equation (3-6). The calculated values of all significant parameters are listed in Table 4-6. It can be noticed that the design base shears calculated for 2/3 MCE and MCE hazards were quite close. Design base shear for 2/3 MCE hazard was used in this study because 2/3 MCE is commonly accepted as Design Basis Earthquake (life-safety/drift control objective) in which case strict drift control is essential (LATBSDC Alternative Design Criteria, 2008), also discussed earlier in Section 3.4.6 in Chapter 3.

Table 4-6 Design parameters for determination of design base shear of 4-story PBPD RC SMF

Design Parameters		2/3MCE	MCE
Sa	**Eq (4-1)**	0.74g	1.11g
T (sec.)	**Eq (3-1)**	0.81	0.81
C_2	**Table 3-3**	1.1	1.1
Yield Drift Ratio θ_y		0.5%	0.5%
Target Drift Ratio θ_u		2%	3%
Modified Target Drift Ratio θ_u^*	**Eq (3-8)**	1.82%	2.73%
Inelastic Drift Ratio	$\theta_u^* - \theta_y$	1.32%	2.23%
μ_s^*	**Eq (3-9)**	3.64	5.46
R_μ	**Table 3-2**	3.64	5.46
γ^*	**Eq (3-10)**	0.47	0.33
α	**Eq (3-7)**	2.103	3.552
V/W	**Eq (3-6)**	001167	0.1117
V w/o *P-Delta* (kips)		242.2	231.8
$\Sigma F_{i\text{-}PD}$ (kips)	**3.4.6**	41.5	`62.2
Design Base Shear V^*		283.7^+	294.0

Note: V* is design base shear for one frame; + represents the base shear used in design (refer to Section 3.4.6 in Chapter 3)

Design of Designated Yielding Members (DYM)

When using the target yield mechanism for moment frames as shown in Figure 4-4, beams become the primary designated yielding members (DYM). The required beam moment capacity at each level can be determined by plastic design approach (external work equals internal work) and referring to Figure 4-4 and Equation (3-22).

The required plastic moment, M_{pc}, of columns in the first story of the one-bay model as shown in Figure 3-14 can be calculated by Equation (3-23) by setting the factor ψ as 1.1 for 4-story RC SMF. It is noted that V' in Equation (3-23) is the base shear for one-bay frame, which is equal to V divided by the number of bays. The number of bays is equal to 3 in all study RC SMF as shown in Figure 4-2.

It is noted that as the lateral loads are applied the external work done by uniformly distributed gravity loading is zero due to anti-symmetrical deformed shape of the beams. Therefore the required moment strength at level *i* is given by transposing Equation (3-22) as shown in the following:

$$\beta_i \cdot M_{pb-positive} = \beta_i \cdot \frac{\sum_{i=1}^{n} F_i \cdot h_i - 2 \cdot M_{pc}}{(1+x) \cdot \sum_{i=1}^{n} \left(\beta_i \cdot \frac{L}{L_i'} \right)} \tag{4-2}$$

where x is the ratio of the absolute value of $M_{pb-negative}$ to $M_{pb-positive}$ and was taken as 2.1 according to the baseline frame design profile. The design parameters of beams calculated from the above procedure and section design details are summarized in Table 4-7.

Table 4-7 Design parameters and section design details of beams for 4-story PBPD RC SMF

Design parameters								Section design f'_c = 5 ksi			
Floor	F_i (kips)	F_{i-PD} (kips)	$F_i^* = F_i + F_{i-PD}$ (kips)	$\frac{F_i^*}{3}$ (kips)	$\frac{F_i^* \cdot h_i}{3}$	M_{pb-pos} (k-ft)	M_{pb-neg} (k-ft)	h (in)	b (in)	ρ (%)	ρ' (%)
R	116.3	10.4	126.7	42.2	2280.4	148.5	-309.6	24	26	0.35	0.56
4	64.6	10.4	75.0	25.0	1024.6	231.0	-481.6	24	26	0.46	0.89
3	40.5	10.4	50.9	17.0	474.8	282.7	-589.4	24	26	0.41	0.82
2	20.8	10.4	31.2	10.4	156.1	309.4	-644.9	24	26	0.45	0.91
Σ	242.2	41.5	283.7								

Design of Non Designated Yielding Members (Non-DYM)

According to the concept of "column tree" as described in Section 3.4.8, the columns must be designed for maximum expected forces by including gravity loads on beams and columns and by considering a reasonable extent of strain-hardening and material over-strength in the beam plastic hinges. Thus, M_{pr} is given as:

$$M_{pr} = \xi \cdot M_{pb} = 1.25 \cdot M_{pb} \tag{4-3}$$

the over-strength factor (ξ) was taken as 1.25 which was established recognizing all these effects in ACI 318 (Moehle et al, 2008).

The free-body diagrams of beams, exterior column tree and interior column tree are shown in Figure 4-5.

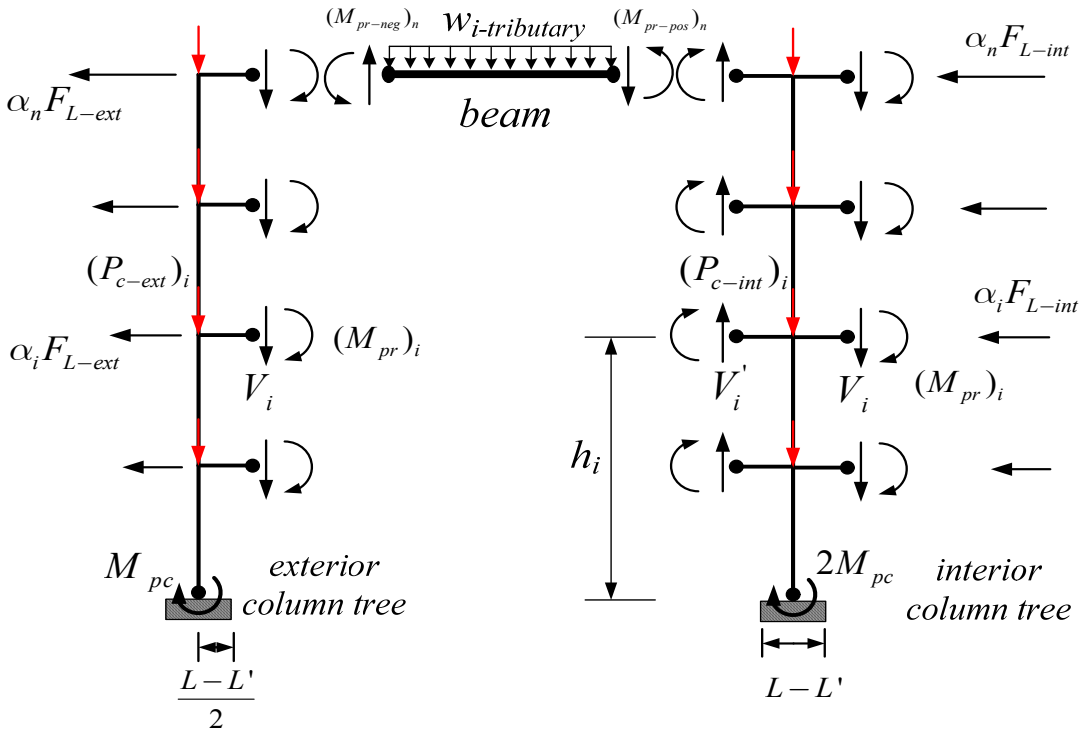

Figure 4-5 The free-body diagrams of beam, exterior column tree and interior column

(i) Exterior Column Tree

As shown in Figure 4-5, when the frame reaches its target drift, the shear force and moment at the desired beam plastic hinge locations at all levels are assumed to reach the expected strengths, V_i or V_i' and $(M_{pr})_i$. V_i or V_i' can be calculated by the following equations:

$$V_i = \frac{\left|M_{pr-positive}\right|_i + \left|M_{pr-negative}\right|_i}{L'} + \frac{w_{i-tributary} \cdot L'}{2} \tag{4-4}$$

$$V_i' = \frac{\left|M_{pr-positive}\right|_i + \left|M_{pr-negative}\right|_i}{L'} - \frac{w_{i-tributary} \cdot L'}{2} \tag{4-5}$$

Additionally, the column at the base is also assumed to have reached its maximum capacity, M_{pc}. At this stage, the required balancing lateral forces can be obtained by using moment equilibrium of the whole column tree while assuming to maintain the same distribution as used earlier. The sum of those forces, F_{L-ext}, can be calculated as:

$$F_{L-ext} = \frac{\sum_{i=1}^{n}\left(M_{pr-negative}\right)_i + \sum_{i=1}^{n} V_i \cdot \left(\frac{L-L'}{2}\right)_i + M_{pc}}{\sum_{i=1}^{n} \alpha_i h_i} \tag{4-6}$$

where $\alpha_i = \frac{(\beta_i - \beta_{i+1})}{\sum_{i=1}^{n}(\beta_i - \beta_{i+1})}$ when $i = n$, $\beta_{n+1} = 0$ (4-7)

(ii) Interior Column Tree

The sum of lateral forces, F_{L-int}, can be similarly calculated as follows:

$$F_{L-int} = \frac{\sum_{i=1}^{n}\left(\left|M_{pr-positive}\right|_i + \left|M_{pr-negative}\right|_i\right) + \sum_{i=1}^{n}\left[V_i + V'_i\right] \cdot \left(\frac{L-L'}{2}\right)_i + 2M_{pc}}{\sum_{i=1}^{n} \alpha_i h_i} \tag{4-8}$$

By assuming a column size of 30 inches, the corresponding summation of required balancing lateral forces for exterior column, F_{L-ext}, and interior column, F_{L-int}, are 85.0 and 118.3 kips, respectively. The important design parameters for the columns are listed in Table 4-8.

Table 4-8 Design parameters of DYM for 4-story PBPD RC SMF

Floor	V_i (kips)	V_i' (kips)	α_i	$\alpha_i \cdot h_i$	Exterior column		Interior column	
					$\alpha_i \cdot F_{L-ext}$ (kips)	Shear (kips)	$\alpha_i \cdot F_{L-ext}$ (kips)	Shear (kips)
Roof	99.9	-58.6	0.48	25.9	40.8	40.8	56.8	56.8
4	114.6	-43.9	0.27	10.9	22.7	63.4	31.5	88.3
3	122.5	-36.0	0.17	4.7	14.2	77.6	19.8	108.1
2	126.6	-31.9	0.09	1.3	7.3	85.0	10.2	118.3
Σ	463.7	-170.3	1.00	42.8	85.0		118.3	

The bending moment diagrams of exterior and interior column trees are presented in Figure 4-6 and detailed column design parameters and results can be found in Table 4-9 and 4-10. It should be mentioned that longitudinal reinforcement for column sections design in this study was based on the minimum required amounts. That was done for the purpose of validated the design procedure, and it worked well. If for practical reasons larger amounts are provided that should make the columns stringer and will make them work even better. The same applies to the minimum reinforcement for columns in the 8, 12 and 20-story PBPD frames as well, i.e., Tables 4-17, 4-24 and 4-31, respectively.

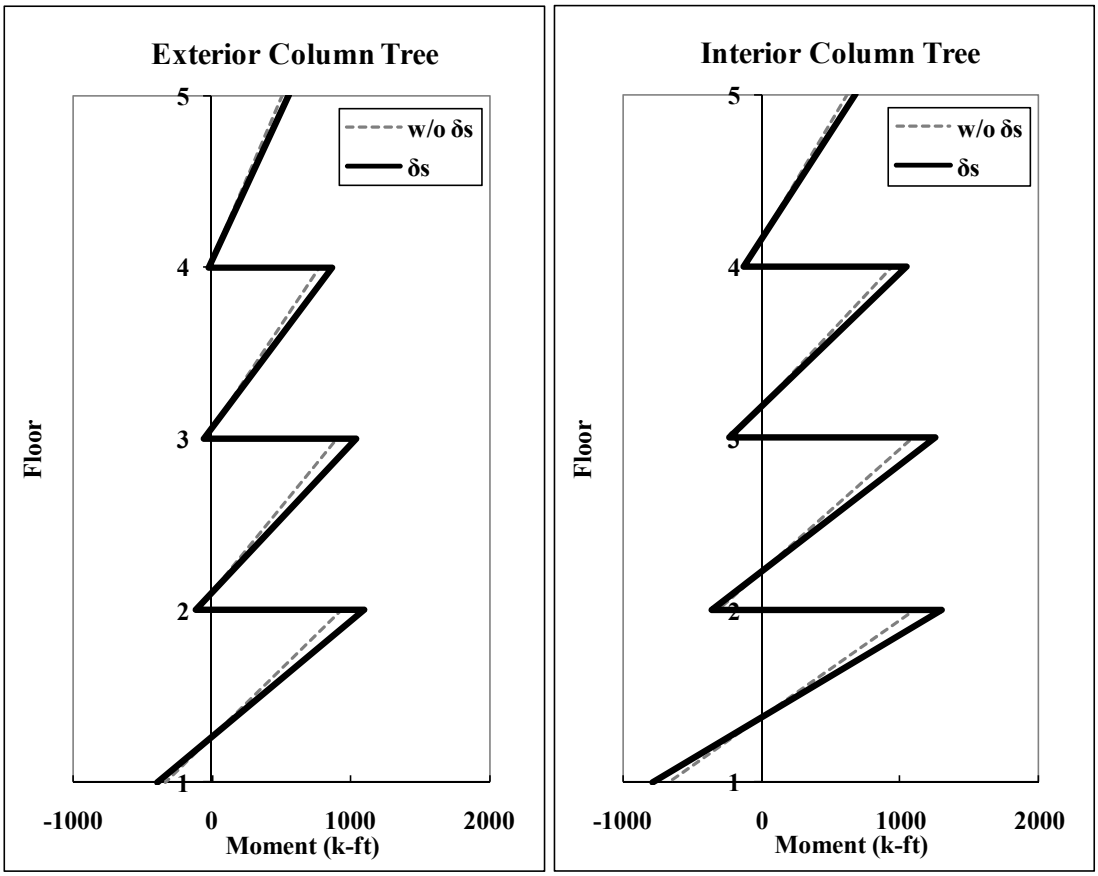

Figure 4-6 Bending moment diagrams of exterior and interior column trees

Table 4-9 Required strength of columns

	Floor	M_{u-top} (k-ft)	M_{u-bot} (k-ft)	δ_s	PCA-COLUMN			
					Magnified M_{u-top} (k-ft)	Magnified M_{u-bot} (k-ft)	Axial force, P_u (kips)	Shear (kips)
Exterior Column	Roof	509.1	-21.2	1.089	554.5	-23.1	99.9	40.8
	4	779.4	-45.4	1.115	868.8	-50.6	214.5	63.4
	3	912.2	-97.2	1.141	1040.4	-110.8	337.1	77.6
	2	941.2	-333.1	1.171	1102.5	-390.2	463.7	85.0
Interior Column	Roof	620.2	-118.2	1.089	675.5	-128.8	158.5	56.8
	4	942.8	-205.6	1.115	1051.0	-229.2	317.0	88.3
	3	1092.9	-312.6	1.141	1246.6	-356.5	475.5	108.1
	2	1108.2	-666.2	1.171	1298.1	-780.3	634.0	118.3

Note: Moment magnifier, δ_s, was calculated according to ACI 318 (2008)

Table 4-10 Column section design results

f'_c = 5 ksi	Floor	d_c (in)	Longitudinal reinforcement size (#)	Longitudinal reinforcement numbers	Reinforcement ratio (%)
Exterior Column	Roof	30	8	12	1.053
	4	30	9	12	1.333
	3	30	11	8	1.387
	2	30	9	12	1.333
Interior Column	Roof	30	8	12	1.053
	4	30	7	24	1.600
	3	30	10	12	1.693
	2	30	7	24	1.600

Note: Refer to the note on page 66 regarding minimum column reinforcement used in design.

4.4.3 8-story PBPD RC SMF

By following exactly the same design procedure as for 4-story PBPD RC SMF, all important parameters and results are summarized in the following tables and figures.

Design Parameters

Important design parameters for 8-story PBPD RC SMF are summarized in Table 4-11. It is noted that S_a can be obtained by multiplying *Cs* by R/I for 2/3 MCE hazard level; that is,

$$S_a = C_s \cdot \left(\frac{R}{I}\right) = 0.050 \cdot \left(\frac{8}{1}\right) = 0.40g \ .$$

Table 4-11 Important design parameters for 8-story PBPD RC SMF

T (sec) Eq (3-1)	Yield Drift Ratio θ_y	Target Drift Ratio θ_u	S_a (g) Eq (4-1)	L (ft)	L' (ft)	W-tributary (k/ft)	W (kips)
1.49	0.005	0.02 (2/3 MCE) 0.03 (MCE)	0.40 (2/3 MCE) 0.60 (MCE)	20	18.2	3.86	1855

Lateral Force Distribution

The design lateral force distribution in the PBPD method can be determined by Equation (3-17) and the calculation results are given in Table 4-12.

Table 4-12 Important design parameters for 8-story PBPD RC SMF

Floor	h_j (ft.)	w_j (kips)	$w_j h_j$ (k-ft)	$\sum w_j h_j$ (k-ft)	β_i Eq (3-17)	$\beta_i - \beta_{i+1}$	$(\beta_i - \beta_{i+1}) \cdot h_i$
Roof	106	231.9	24578.8	24578.8	1.00	1.00	106.0
8	93	231.9	21564.4	46143.1	1.55	0.55	50.9
7	80	231.9	18550.0	64693.1	1.95	0.41	32.6
6	67	231.9	15535.6	80228.8	2.27	0.31	21.1
5	54	231.9	12521.3	92750.0	2.51	0.24	12.9
4	41	231.9	9506.9	102256.9	2.68	0.18	7.2
3	28	231.9	6492.5	108749.4	2.80	0.12	3.3
2	15	231.9	3478.1	112227.5	2.86	0.06	0.9
Σ		1855			17.63	2.86	234.9

Design Base Shear

A yield drift ratio (θ_y) of 0.5% is used. The design base shear is then calculated from Equation (3-6). The calculated values of all significant parameters are listed in Table 4-13.

Table 4-13 Design parameters for determination of design base shear of 8-story PBPD RC SMF

Design Parameters		2/3MCE	MCE
Sa	Eq (4-1)	0.40g	0.60g
T (sec.)	Eq (3-1)	1.49	1.49
C_2	Table 3-3	1.07	1.07
Yield Drift Ratio θ_y		0.5%	0.5%
Target Drift Ratio θ_u		2%	3%
Modified Target Drift Ratio θ_u^*	Eq (3-8)	1.87%	2.81%
Inelastic Drift Ratio	$\theta_u^* - \theta_y$	1.37%	2.31%
μ_s^*	Eq (3-9)	3.74	5.61
R_μ	Table 3-2	3.74	5.61
γ^*	Eq (3-10)	0.46	0.32
α	Eq (3-7)	1.243	2.092
V/W	Eq (3-6)	0.0577	0.0552
V w/o *P-Delta* (kips)		107.1	102.5
$\Sigma F_{i\text{-}PD}$ (kips)	3.4.6	36.9	55.3
Design Base Shear V^* (kips)		144.0^+	157.8

Note: V* is design base shear for one frame; + represents the base shear used in design (refer to Section 3.4.6 in Chapter 3)

Design of Designated Yielding Members (DYM)

The required plastic moment, M_{pc}, of columns in the first story of the one-bay model as shown in Figure 3-14 can be calculated by Equation (3-23) by setting the factor ψ as 1.1 for 8-story RC SMF. In addition, the ratio of the absolute value of $M_{pb-negative}$ to $M_{pb-positive}$, x, was taken as 2.4 according to the baseline frame design profile for consistency and fair comparison.

The design parameters of beams calculated from the above procedure and section design details are summarized in Table 4-14.

Table 4-14 Design parameters and section design details of beams for 8-story PBPD RC SMF

Design parameters								**Section design** f'_c = 5 ksi			
Floor	F_i (kips)	F_{i-PD} (kips)	$F_i^* = F_i + F_{i-PD}$ (kips)	$\frac{F_i^*}{3}$ (kips)	$\frac{F_i^* \cdot h_i}{3}$	M_{pb-pos} (k-ft)	M_{pb-neg} (k-ft)	h (in)	b (in)	ρ (%)	ρ' (%)
Roof	37.4	4.6	42.0	14.0	1485.4	51.5	-122.7	16	16	0.42	0.66
8	20.5	4.6	25.1	8.4	777.8	79.7	-189.9	16	16	0.54	1.13
7	15.3	4.6	19.9	6.6	530.5	100.8	-239.9	16	16	0.71	1.45
6	11.8	4.6	16.4	5.5	366.0	117.0	-278.5	16	16	0.82	1.68
5	9.0	4.6	13.6	4.5	244.9	129.3	-307.9	22	22	0.37	0.75
4	6.6	4.6	11.2	3.7	153.0	138.3	-329.4	22	22	0.40	0.80
3	4.4	4.6	9.0	3.0	84.1	144.4	-343.8	22	22	0.42	0.83
2	2.3	4.6	6.9	2.3	34.7	147.6	-351.3	22	22	0.43	0.87
Σ	107.1	37.1	144.2								

Design of Non Designated Yielding Members (Non-DYM)

By assuming a column size of 24 inches, the corresponding summation of required balancing lateral forces for exterior column, F_{L-ext}, and interior column, F_{L-int}, are 43.6 and 59.9 kips, respectively. The important design parameters for the columns are summarized in Table 4-15.

Table 4-15 Design parameters of DYM for 8-story PBPD RC SMF

Floor	V_i (kips)	V_i' (kips)	α_i	$\alpha_i \cdot h_i$	Exterior column		Interior column	
					$\alpha_i \cdot F_{L-ext}$ (kips)	Shear (kips)	$\alpha_i \cdot F_{L-ext}$ (kips)	Shear (kips)
Roof	47.0	-23.2	0.35	37.0	15.2	15.2	20.9	20.9
8	55.4	-14.9	0.19	17.8	8.3	23.6	11.4	32.4
7	60.7	-9.5	0.14	11.4	6.2	29.8	8.5	40.9
6	64.8	-5.4	0.11	7.4	4.8	34.5	6.6	47.5
5	67.9	-1.6	0.08	4.5	3.6	38.2	5.0	52.5
4	70.2	0.7	0.06	2.5	2.7	40.9	3.7	56.1
3	71.8	2.2	0.04	1.1	1.8	42.6	2.4	58.6
2	72.6	3.0	0.02	0.3	0.9	43.6	1.3	59.9
Σ	510.5	-48.6	1.00	82.05	43.6		59.9	

The bending moment diagrams of exterior and interior column trees are presented in Figure 4-7 and detailed column design parameters and results are shown in Table 4-16 and 4-17.

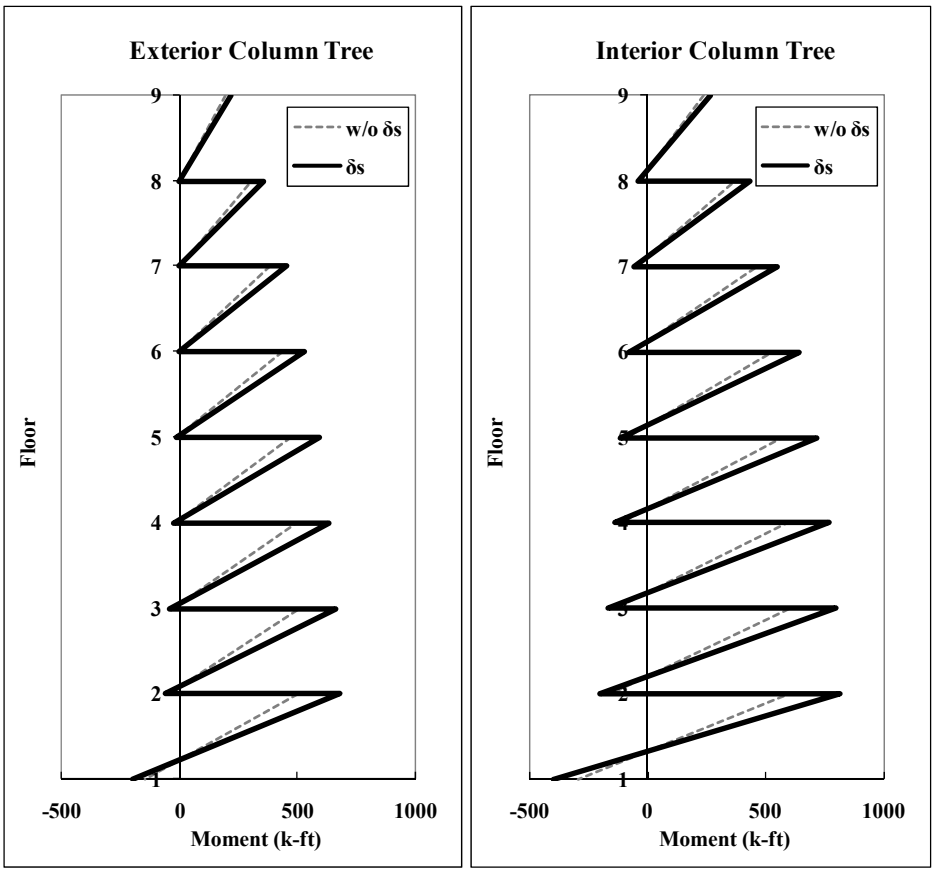

Figure 4-7 Bending moment diagrams of exterior and interior column trees

Table 4-16 Required strength of columns

	Floor	M_{u-top} (k-ft)	M_{u-bot} (k-ft)	δ_s	PCA-COLUMN			
					Magnified M_{u-top} (k-ft)	Magnified M_{u-bot} (k-ft)	Axial force, P_u (kips)	Shear (kips)
Exterior Column	Roof	195.4	-2.6	1.124	219.6	-2.9	47.0	15.2
	8	307.3	1.1	1.160	356.6	1.3	102.4	23.6
	7	384.2	-2.7	1.190	457.3	-3.2	163.1	29.8
	6	436.8	-12.3	1.219	532.2	-15.0	227.9	34.5
	5	475.8	-20.7	1.247	593.4	-25.9	295.8	38.2
	4	499.1	-32.1	1.277	637.5	-41.0	366.0	40.9
	3	508.8	-45.6	1.310	666.5	-59.7	437.8	42.6
	2	506.6	-147.2	1.347	682.1	-198.2	510.5	43.6
Interior Column	Roof	238.1	-33.9	1.124	267.6	-38.1	70.2	20.9
	8	371.2	-49.4	1.160	430.7	-57.3	140.4	32.4
	7	462.5	-69.1	1.190	550.5	-82.2	210.6	40.9
	6	525.1	-91.9	1.219	639.9	-112.0	280.8	47.5
	5	571.1	-111.0	1.247	712.3	-138.4	350.4	52.5
	4	598.3	-131.5	1.277	764.2	-167.9	420.0	56.1
	3	608.8	-152.8	1.310	797.4	-200.2	489.5	58.6
	2	603.7	-294.4	1.347	812.9	-396.5	559.1	59.9

Note: Moment magnifier, δ_s, was calculated according to ACI 318 (2008)

Table 4-17 Column section design results

f'_c = 6 ksi	Floor	d_c (in)	Longitudinal reinforcement size (#)	Longitudinal reinforcement Numbers	Reinforcement ratio (%)
Exterior Column	Roof	22	5	16	1.025
	8	22	6	16	1.455
	7	22	6	20	1.818
	6	22	10	8	2.099
	5	24	9	8	1.389
	4	24	9	8	1.389
	3	24	9	8	1.389
	2	24	5	24	1.292
Interior Column	Roof	22	5	16	1.025
	8	22	6	20	1.818
	7	22	6	24	2.182
	6	22	11	8	2.579
	5	24	10	8	1.764
	4	24	9	12	2.083
	3	24	9	12	2.083
	2	24	9	12	2.083

Note: Refer to the note on page 66 regarding minimum column reinforcement used in design.

4.4.4 12-story PBPD RC SMF

By following exactly the same design procedure as for 4 and 8-story PBPD RC SMF, all important parameters and results are summarized in the following tables and figures.

Design Parameters

Important design parameters are summarized in Table 4-18. S_a can be obtained by multiplying *Cs* with R/I for 2/3 MCE hazard level; that is,

$$S_a = C_s \cdot \left(\frac{R}{I}\right) = 0.0375 \cdot \left(\frac{8}{1}\right) = 0.30g\,.$$

Table 4-18 Important design parameters for 12-story PBPD RC SMF

T (sec) Eq (3-1)	Yield Drift Ratio θ_y	Target Drift Ratio θ_u	S_a (g) Eq (4-1)	L (ft)	L' (ft)	W- tributary (k/ft)	W (kips)
2.13	0.005	0.02 (2/3 MCE) 0.03 (MCE)	0.30 (2/3 MCE) 0.45 (MCE)	20	18.2	3.88	2795

Lateral Force Distribution

The design lateral force distribution in the PBPD method can be determined by Equation (3-17) and the detailed results are given in Table 4-19.

Table 4-19 Important design parameters for 12-story PBPD RC SMF

Floor	h_j (ft.)	w_j (kips)	$w_j h_j$ (k-ft)	$\sum w_j h_j$ (k-ft)	β_i Eq (3-17)	$\beta_i - \beta_{i+1}$	$(\beta_i - \beta_{i+1}) \cdot h_i$
Roof	158	232.9	36800.8	36800.8	1.00	1.00	158.0
12	145	232.9	33772.9	70573.8	1.52	0.52	75.6
11	132	232.9	30745.0	101318.8	1.92	0.40	52.7
10	119	232.9	27717.1	129035.8	2.24	0.32	38.6
9	106	232.9	24689.2	153725.0	2.51	0.27	28.4
8	93	232.9	21661.3	175386.3	2.74	0.22	20.7
7	80	232.9	18633.3	194019.6	2.92	0.18	14.7
6	67	232.9	15605.4	209625.0	3.07	0.15	10.0
5	54	232.9	12577.5	222202.5	3.19	0.12	6.3
4	41	232.9	9549.6	231752.1	3.27	0.09	3.6
3	28	232.9	6521.7	238273.8	3.33	0.06	1.7
2	15	232.9	3493.8	241767.5	3.36	0.03	0.5
Σ					31.08	3.37	410.8

Design Base Shear

A yield drift ratio (θ_y) of 0.5% is used for calculation of design base shear is from Equation (3-6). The calculated values of all significant parameters are listed in Table 4-20.

Table 4-20 Design parameters for determination of design base shear of 12-story PBPD RC SMF

Design Parameters		2/3MCE	MCE
Sa	Eq (4-1)	0.30 g	0.45 g
T (sec.)	Eq (3-1)	2.13	2.13
C_2	Table 3-3	1.04	1.04
Yield Drift Ratio θ_y		0.5%	0.5%
Target Drift Ratio θ_u		2%	3%
Modified Target Drift Ratio θ_u^*	Eq (3-8)	1.92%	2.89%
Inelastic Drift Ratio	$\theta_u^* - \theta_y$	1.42%	2.39%
μ_s^*	Eq (3-9)	3.85	5.77
R_μ	Table 3-2	3.85	5.77
γ^*	Eq (3-10)	0.45	0.32
α	Eq (3-7)	0.937	1.570
V/W	Eq (3-6)	0.0416	0.0398
V w/o *P-Delta* (kips)		116.3	111.3
$\Sigma F_{i\text{-}PD}$ (kips)	3.4.6	55.9	83.7
Design Base Shear V^*		172.2^+	195.0

Note: V* is design base shear for one frame; + represents the base shear used in design (refer to Section 3.4.6 in Chapter 3)

Design of Designated Yielding Members (DYM)

The required plastic moment, M_{pc}, of columns in the first story is calculated by Equation (3-23) by setting the factor ψ as 1.1 for 12-story RC SMF. In addition, the ratio of the absolute value of $M_{pb-negative}$ to $M_{pb-positive}$, x, was set at 2.4 according to the baseline frame design profile for consistency and fair comparison.

The design parameters of beams calculated from the above procedure and section design details are listed in Table 4-21.

Table 4-21 Design parameters and section design details of beams for 12-story PBPD RC SMF

Design parameters								**Section design** f'_c = 5 ksi			
Floor	F_i (kips)	F_{i-PD} (kips)	$F_i^* = F_i + F_{i-PD}$ (kips)	$\frac{F_i^*}{3}$ (kips)	$\frac{F_i^* \cdot h_i}{3}$	M_{pb-pos} (k-ft)	M_{pb-neg} (k-ft)	h (in)	b (in)	ρ (%)	ρ' (%)
Roof	34.6	4.7	39.2	13.1	2065.3	52.4	-123.7	14	16	0.37	0.53
12	18.0	4.7	22.7	7.6	1096.2	79.7	-188.2	14	16	0.46	0.93
11	13.8	4.7	18.5	6.2	812.2	100.6	-237.6	14	16	0.62	1.20
10	11.2	4.7	15.9	5.3	628.9	117.5	-277.7	14	16	0.57	1.12
9	9.3	4.7	13.9	4.6	492.0	131.6	-310.8	16	22	0.36	0.74
8	7.7	4.7	12.4	4.1	383.1	143.2	-338.4	16	22	0.39	0.78
7	6.4	4.7	11.0	3.7	293.7	152.9	-361.1	16	22	0.43	0.85
6	5.2	4.7	9.8	3.3	219.2	160.7	-379.6	16	22	0.54	0.91
5	4.1	4.7	8.7	2.9	156.9	166.8	-394.1	18	26	0.35	0.72
4	3.0	4.7	7.7	2.6	105.0	171.4	-405.0	18	26	0.36	0.74
3	2.0	4.7	6.7	2.2	62.5	174.5	-412.3	18	26	0.40	0.74
2	1.1	4.7	5.7	1.9	28.7	176.1	-416.2	18	26	0.47	0.75
Σ	116.3	55.9	172.2		6343.9						

Design of Non Designated Yielding Member (Non-DYM)

By assuming a column size of 26 inches, the corresponding summation of required balancing lateral forces for exterior column, F_{L-ext}, and interior column, F_{L-int}, are 51.0 and 70.5 kips, respectively. The important design parameters for the columns are summarized in Table 4-22.

Table 4-22 Design parameters of DYM for 12-story PBPD RC SMF

Floor	V_i (kips)	V_i' (kips)	α_i	$\alpha_i \cdot h_i$	Exterior column		Interior column	
					$\alpha_i \cdot F_{L-ext}$ (kips)	Shear (kips)	$\alpha_i \cdot F_{L-ext}$ (kips)	Shear (kips)
Roof	47.3	-23.2	0.30	47.0	15.2	15.2	21.0	21.0
12	55.4	-15.1	0.15	22.5	7.9	23.1	10.9	31.9
11	60.7	-9.9	0.12	15.7	6.1	29.1	8.4	40.3
10	64.9	-5.6	0.10	11.5	4.9	34.1	6.8	47.0
9	68.5	-1.4	0.08	8.4	4.1	38.1	5.6	52.7
8	71.5	1.6	0.07	6.2	3.4	41.5	4.7	57.3
7	73.9	4.0	0.05	4.4	2.8	44.3	3.9	61.2
6	75.9	6.0	0.04	3.0	2.3	46.6	3.1	64.3
5	77.5	8.3	0.03	1.9	1.8	48.3	2.5	66.8
4	78.7	9.5	0.03	1.1	1.3	49.7	1.8	68.6
3	79.5	10.3	0.02	0.5	0.9	50.6	1.2	69.9
2	79.9	10.7	0.01	0.1	0.5	51.0	0.7	70.5
Σ	833.8	-4.7	1.00	122.10	51.0		70.5	

The bending moment diagrams of exterior and interior column trees are presented in Figure 4-8 and detailed column design parameters and results are given in Table 4-23 and 4-24.

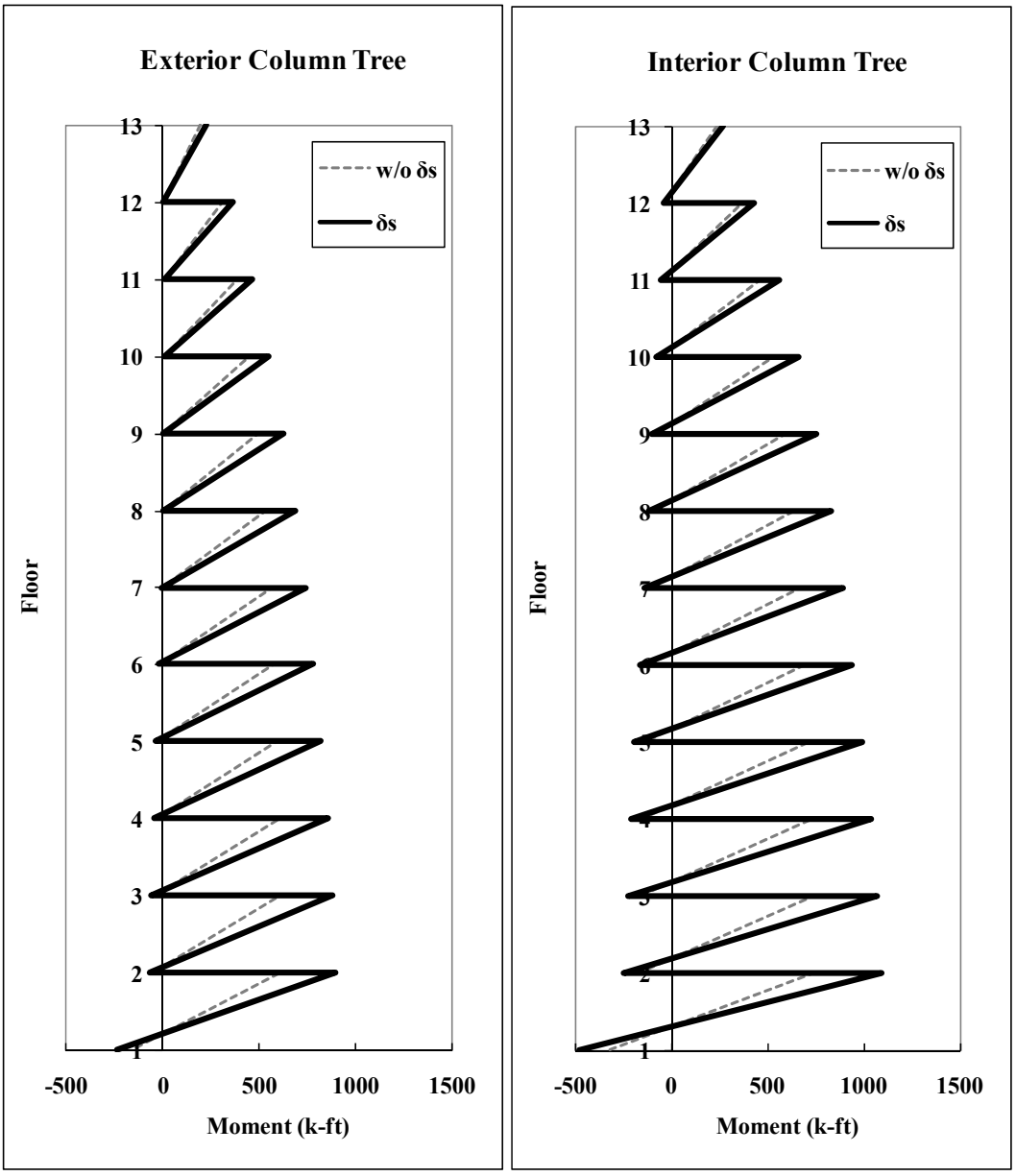

Figure 4-8 Bending moment diagrams of exterior and interior column trees

. It is observed that $M_{u-bot} < M_{u-top}$ in the first story. For 12 and 20 story frames the required moment strength of the first story columns was taken as M_{u-bot} instead of M_{u-top} in order to ensure formation of plastic hinges at the column base as desired, The results of inelastic pushover and time-history analyses also showed that the formation of plastic hinge at the base of columns helped in better distribution of lateral deformation along the height. In contrast, absence of plastic hinges at the base column bases resulted in some concentration of

lateral drift in the middle stories after certain drift level. The results and further discussion are presented in Chapter 6.

Table 4-23 Required strength of columns

	Floor	M_{u-top} (k-ft)	M_{u-bot} (k-ft)	δ_s	PCA-COLUMN			
					Magnified M_{u-top} (k-ft)	Magnified M_{u-bot} (k-ft)	Axial force, P_u (kips)	Shear (kips)
Exterior Column	Roof	196.8	-0.4	1.135	223.3	-0.5	47.3	15.2
	12	307.2	7.1	1.177	361.6	8.4	102.7	23.1
	11	387.0	8.1	1.211	468.4	9.8	163.3	29.1
	10	446.6	3.8	1.240	553.9	4.8	228.3	34.1
	9	496.5	0.9	1.268	629.7	1.1	296.8	38.1
	8	534.2	-5.4	1.296	692.1	-7.0	368.2	41.5
	7	561.4	-14.5	1.323	742.8	-19.2	442.1	44.3
	6	579.5	-25.8	1.351	783.1	-34.9	518.0	46.6
	5	596.1	-32.4	1.381	823.1	-44.7	595.6	48.3
	4	605.6	-40.2	1.412	855.0	-56.7	674.3	49.7
	3	608.7	-48.7	1.445	879.5	-70.4	753.8	50.6
	2	605.9	-159.9	1.481	**897.1**	**-236.7**	833.8	51.0
Interior Column	Roof	240.5	-32.0	1.135	272.9	-36.3	70.5	21.0
	12	370.4	-44.1	1.177	436.1	-51.9	141.0	31.9
	11	464.0	-59.4	1.211	561.7	-71.9	211.6	40.3
	10	534.4	-77.2	1.240	662.8	-95.8	282.1	47.0
	9	593.6	-91.1	1.268	752.8	-115.5	352.0	52.7
	8	639.3	-106.1	1.296	828.3	-137.5	421.8	57.3
	7	673.3	-122.2	1.323	890.9	-161.7	491.7	61.2
	6	697.1	-139.1	1.351	942.1	-188.0	561.6	64.3
	5	719.5	-148.7	1.381	993.5	-205.3	630.8	66.8
	4	733.5	-158.5	1.412	1035.6	-223.8	700.0	68.6
	3	739.6	-168.6	1.445	1068.6	-243.6	769.3	69.9
	2	738.0	-319.7	1.481	**1092.9**	**-473.5**	838.5	70.5

Note: Moment magnifier, δ_s, was calculated according to ACI 318 (2008)

Table 4-24 Column section design results

f'_c = 6 ksi	Floor	d_c (in)	Longitudinal reinforcement size (#)	Longitudinal reinforcement numbers	Reinforcement ratio (%)
Exterior Column	Roof	22	5	16	1.025
	12	22	6	16	1.455
	11	22	8	12	1.959
	10	22	9	12	2.479
	9	24	8	12	1.646
	8	24	10	8	1.764
	7	24	10	8	1.764
	6	24	10	8	1.764
	5	26	5	24	1.101
	4	26	7	12	1.065
	3	26	9	8	1.183
	2	26	9	8	1.183
Interior Column	Roof	22	6	12	1.091
	12	22	6	20	1.818
	11	22	9	12	2.479
	10	22	11	8	2.579
	9	24	9	12	2.083
	8	24	11	8	2.167
	7	24	7	24	2.500
	6	24	11	12	3.250
	5	26	9	12	1.775
	4	26	7	24	2.130
	3	26	11	12	2.769
	2	26	9	8	1.183

Note: Refer to the note on page 66 regarding minimum column reinforcement used in design.

4.4.5 20-story PBPD RC SMF

By following exactly the same design procedure as for 4, 8 and 12-story PBPD RC SMF, all important parameters and results are summarized in the following tables and figures.

Design Parameters

S_a was obtained by multiplying *Cs* with R/I for 2/3 MCE hazard level and important design parameters are summarized in Table 4-25.

$$S_a = C_s \cdot \left(\frac{R}{I}\right) = 0.0375 \cdot \left(\frac{8}{1}\right) = 0.30g\,.$$

Table 4-25 Important design parameters for 20-story PBPD RC SMF

T (sec) Eq (3-1)	Yield Drift Ratio θ_y	Target Drift Ratio θ_u	S_a (g) Eq (4-1)	L (ft)	L' (ft)	W-tributary (k/ft)	W (kips)
3.36	0.005	0.02 (2/3 MCE) 0.03 (MCE)	0.30 (2/3 MCE) 0.45 (MCE)	20	18.2	3.86	4636

Lateral Force Distribution

The design lateral force distribution was determined by Equation (3-17) and the detailed calculation results are given in Table 4-26.

Table 4-26 Important design parameters for 20-story PBPD RC SMF

Floor	h_j (ft.)	w_j (kips)	$w_j h_j$ (k-ft)	$\sum w_j h_j$ (k-ft)	β_i Eq (3-17)	$\beta_i - \beta_{i+1}$	$(\beta_i - \beta_{i+1}) \cdot h_i$
Roof	262	231.8	60731.6	60731.6	1.00	1	262.0
20	249	231.8	57718.2	118449.8	1.48	0.48	119.9
19	236	231.8	54704.8	173154.6	1.85	0.37	87.5
18	223	231.8	51691.4	224846.0	2.16	0.31	68.6
17	210	231.8	48678.0	273524.0	2.42	0.26	55.5
16	197	231.8	45664.6	319188.6	2.65	0.23	45.4
15	184	231.8	42651.2	361839.8	2.86	0.20	37.4
14	171	231.8	39637.8	401477.6	3.04	0.18	30.8
13	158	231.8	36624.4	438102.0	3.20	0.16	25.3
12	145	231.8	33611.0	471713.0	3.34	0.14	20.6
11	132	231.8	30597.6	502310.6	3.47	0.13	16.6
10	119	231.8	27584.2	529894.8	3.58	0.11	13.2
9	106	231.8	24570.8	554465.6	3.67	0.10	10.3
8	93	231.8	21557.4	576023.0	3.76	0.08	7.8
7	80	231.8	18544.0	594567.0	3.83	0.07	5.7
6	67	231.8	15530.6	610097.6	3.89	0.06	3.9
5	54	231.8	12517.2	622614.8	3.93	0.05	2.5
4	41	231.8	9503.8	632118.6	3.97	0.04	1.4
3	28	231.8	6490.4	638609.0	3.99	0.02	0.7
2	15	231.8	3477.0	642086.0	4.01	0.01	0.2
Σ					62.11	4.01	815.4

Design Base Shear

The design base shear was calculated from Equation (3-6); other calculated values of significant parameters are listed in Table 4-27.

Table 4-27 Design parameters for determination of design base shear of 20-story PBPD RC SMF

Design Parameters		2/3MCE	MCE
Sa	Eq (4-1)	0.30 g	0.45 g
T (sec.)	Eq (3-1)	3.36	3.36
C_2	Table 3-3	1.0	1.0
Yield Drift Ratio θ_y		0.5%	0.5%
Target Drift Ratio θ_u		2%	3%
Modified Target Drift Ratio θ_u^*	Eq (3-8)	2%	3%
Inelastic Drift Ratio	$\theta_u^* - \theta_y$	1.5%	2.5%
μ_s^*	Eq (3-9)	4	6
R_μ	Table 3-2	4	6
γ^*	Eq (3-10)	0.44	0.31
α	Eq (3-7)	0.662	1.103
V/W	Eq (3-6)	0.055	0.054
V w/o *P-Delta* (kips)		255.0	248.0
$\Sigma F_{i\text{-}PD}$ (kips)	3.4.6	92.0	138.0
Design Base Shear V^*		347.0^+	386.0

Note: V* is design base shear for one frame; + represents the base shear used in design (refer to Section 3.4.6 in Chapter 3)

Design of Designated Yielding Members (DYM)

By setting the factor ψ as 1.5 for 20-story RC SMF, The required plastic moment, M_{pc}, of columns in the first story of the one-bay model was calculated from Equation (3-23). In addition, the ratio of the absolute value of $M_{pb-negative}$ to $M_{pb-positive}$, x, was set at 2.1 to be consistent with the baseline frame design profile.

The design parameters of beams calculated by following the above procedure and section design details are summarized in Table 4-28.

Table 4-28 Design parameters and section design details of beams for 20-story PBPD RC SMF

Design parameters								Section design f'_c = 5 ksi			
Floor	F_i (kips)	F_{i-PD} (kips)	$F_i^* = F_i + F_{i-PD}$ (kips)	$\frac{F_i^*}{3}$ (kips)	$\frac{F_i^* \cdot h_i}{3}$	M_{pb-pos} (k-ft)	M_{pb-neg} (k-ft)	h (in)	b (in)	ρ (%)	ρ' (%)
Roof	63.6	4.6	68.2	22.7	5956.0	95.9	-205.4	16	22	0.35	0.35
20	30.6	4.6	35.2	11.7	2925.4	142.1	-304.3	16	22	0.37	0.62
19	23.6	4.6	28.2	9.4	2219.5	177.7	-380.5	16	22	0.44	0.79
18	19.6	4.6	24.2	8.1	1799.1	207.2	-443.7	16	22	0.50	0.96
17	16.8	4.6	21.4	7.1	1499.5	232.5	-498.0	16	22	0.54	1.10
16	14.7	4.6	19.3	6.4	1266.9	254.6	-545.3	24	26	0.35	0.69
15	12.9	4.6	17.6	5.9	1077.2	274.1	-587.1	24	26	0.38	0.76
14	11.5	4.6	16.1	5.4	917.5	291.4	-624.2	24	26	0.44	0.81
13	10.2	4.6	14.8	4.9	780.4	306.8	-657.1	24	26	0.48	0.86
12	9.0	4.6	13.7	4.6	661.0	320.4	-686.3	24	26	0.49	0.90
11	8.0	4.6	12.6	4.2	556.0	332.5	-712.1	26	28	0.36	0.69
10	7.0	4.6	11.7	3.9	463.3	343.1	-734.9	26	28	0.38	0.70
9	6.1	4.6	10.8	3.6	381.0	352.4	-754.7	26	28	0.39	0.72
8	5.3	4.6	9.9	3.3	308.1	360.4	-771.9	26	28	0.40	0.74
7	4.5	4.6	9.1	3.0	243.5	367.2	-786.4	26	28	0.41	0.75
6	3.7	4.6	8.4	2.8	186.6	372.8	-798.4	30	28	0.37	0.66
5	3.0	4.6	7.6	2.5	136.9	377.3	-808.0	30	30	0.35	0.62
4	2.2	4.6	6.9	2.3	94.0	380.7	-815.3	30	30	0.36	0.63
3	1.5	4.6	6.2	2.1	57.5	383.0	-820.2	30	30	0.39	0.62
2	0.8	4.6	5.4	1.8	27.2	384.2	-822.8	30	30	0.45	0.62
Σ	254.6	92.7	347.3		21556.5						

Design of Non Designated Yielding Members (Non-DYM)

By assuming a column size of 32 inches, the corresponding summation of required balancing lateral forces for exterior column, F_{L-ext}, and interior column, F_{L-int}, are 100.9 and 148.0 kips, respectively. The important design parameters for the columns are listed in Table 4-29.

Table 4-29 Design parameters of DYM for 20-story PBPD RC SMF

Floor	V_i (kips)	V_i' (kips)	α_i	$\alpha_i \cdot h_i$	Exterior column		Interior column	
					$\alpha_i \cdot F_{L-ext}$ (kips)	Shear (kips)	$\alpha_i \cdot F_{L-ext}$ (kips)	Shear (kips)
Roof	55.3	-13.0	0.250	65.4	25.2	25.2	36.9	36.9
20	68.6	0.4	0.120	29.9	12.1	37.3	17.8	54.7
19	77.2	9.0	0.093	21.9	9.3	46.7	13.7	68.4
18	84.4	16.2	0.077	17.1	7.8	54.4	11.4	79.8
17	90.6	22.3	0.066	13.8	6.7	61.1	9.8	89.6
16	95.9	27.7	0.058	11.3	5.8	66.9	8.5	98.1
15	100.7	32.4	0.051	9.3	5.1	72.0	7.5	105.6
14	105.2	37.6	0.045	7.7	4.5	76.5	6.7	112.3
13	109.0	41.4	0.040	6.3	4.0	80.6	5.9	118.2
12	112.3	44.7	0.036	5.1	3.6	84.2	5.3	123.4
11	115.3	47.7	0.031	4.1	3.2	87.3	4.7	128.1
10	117.9	50.3	0.028	3.3	2.8	90.1	4.1	132.2
9	120.2	52.5	0.024	2.6	2.4	92.5	3.6	135.8
8	122.1	54.5	0.021	1.9	2.1	94.6	3.1	138.8
7	123.8	56.2	0.018	1.4	1.8	96.4	2.6	141.5
6	125.7	58.7	0.015	1.0	1.5	97.9	2.2	143.6
5	126.8	59.8	0.012	0.6	1.2	99.1	1.7	145.3
4	127.6	60.7	0.009	0.4	0.9	100.0	1.3	146.6
3	128.2	61.3	0.006	0.2	0.6	100.6	0.9	147.5
2	128.5	61.6	0.003	0.0	0.3	100.9	0.5	148.0
Σ	2135.3	781.9	1.00	203.6	100.9		148.0	

The bending moment diagrams of exterior and interior column trees are presented in Figure 4-9 and detailed column design parameters and results are given in Table 4-30 and 4-31.

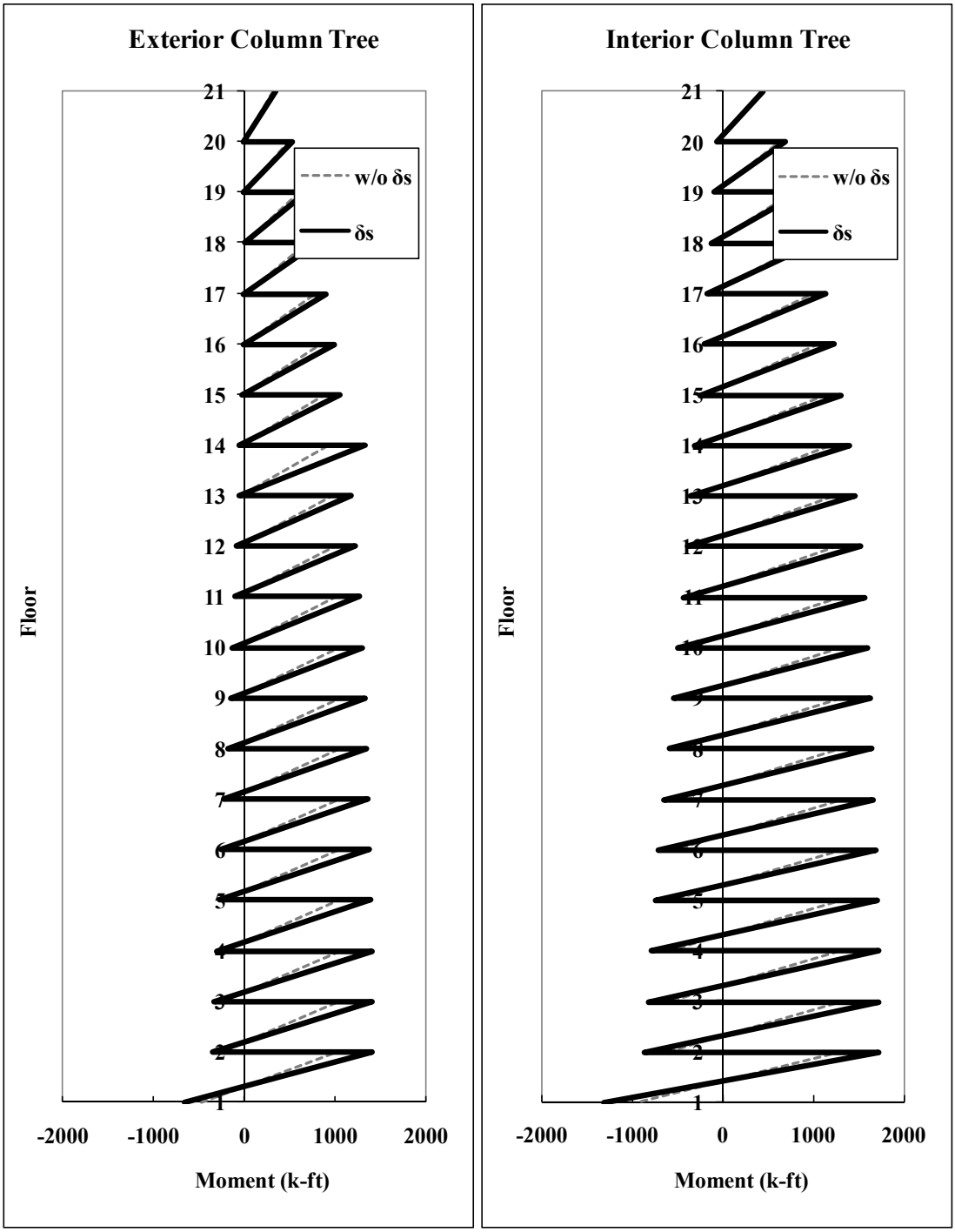

Figure 4-9 Bending moment diagrams of exterior and interior column trees

As for the 12-story frame, it is seen that $M_{u-bot} < M_{u-top}$ in the first story of 20-story PBPD RC SMF. In order to encourage formation of plastic hinges at the column base and thereby more uniform distribution of drift along with the height, the required moment strength for the first story columns was taken as M_{u-bot} instead of M_{u-top}.

Table 4-30 Required strength of columns

	Floor	M_{u-top} (k-ft)	M_{u-bot} (k-ft)	δ_s	PCA-COLUMN			
					Magnified M_{u-top} (k-ft)	Magnified M_{u-bot} (k-ft)	Axial force, P_u (kips)	Shear (kips)
Exterior Column	Roof	319.4	-8.1	1.073	342.6	-8.7	55.3	25.2
	20	487.3	2.2	1.098	535.3	2.4	123.9	37.3
	19	611.7	5.1	1.118	683.9	5.7	201.1	46.7
	18	709.2	1.8	1.135	805.0	2.1	285.6	54.4
	17	787.1	-6.7	1.150	905.6	-7.7	376.1	61.1
	16	849.5	-19.8	1.165	989.6	-23.0	472.1	66.9
	15	899.0	-37.0	1.179	1059.5	-43.6	572.7	72.0
	14	946.4	-48.5	1.192	1128.1	-57.9	677.9	76.5
	13	984.4	-63.0	1.205	1186.5	-75.9	786.9	80.6
	12	1014.1	-79.9	1.218	1235.4	-97.3	899.2	84.2
	11	1036.1	-99.1	1.231	1275.9	-122.0	1014.5	87.3
	10	1051.3	-120.2	1.245	1308.4	-149.6	1132.4	90.1
	9	1060.1	-143.0	1.258	1333.6	-180.0	1252.5	92.5
	8	1063.1	-167.4	1.272	1351.9	-212.8	1374.6	94.6
	7	1060.6	-192.9	1.286	1363.7	-248.1	1498.4	96.4
	6	1064.4	-208.4	1.300	1383.9	-271.0	1624.1	97.9
	5	1063.5	-224.6	1.315	1398.7	-295.3	1750.9	99.1
	4	1058.3	-241.3	1.331	1408.4	-321.1	1878.6	100.0
	3	1049.1	-258.3	1.347	1413.2	-348.0	2006.8	100.6
	2	1036.0	-477.4	1.364	1413.2	-651.3	2135.3	100.9

Interior Column	Roof	423.2	-57.1	1.073	454.1	-61.3	68.3	36.9
	20	632.7	-79.0	1.098	694.9	-86.8	136.5	54.7
	19	783.5	-106.3	1.118	876.0	-118.9	204.8	68.4
	18	899.4	-138.2	1.135	1020.9	-156.9	273.0	79.8
	17	990.4	-174.1	1.150	1139.4	-200.2	341.3	89.6
	16	1062.0	-213.3	1.165	1237.0	-248.4	409.5	98.1
	15	1117.4	-255.5	1.179	1317.0	-301.1	477.8	105.6
	14	1172.6	-286.9	1.192	1397.8	-342.0	545.4	112.3
	13	1216.5	-320.0	1.205	1466.2	-385.6	613.0	118.2
	12	1250.3	-354.5	1.218	1523.2	-431.9	680.6	123.4
	11	1274.9	-390.3	1.231	1570.0	-480.7	748.2	128.1
	10	1291.2	-427.3	1.245	1607.0	-531.8	815.8	132.2
	9	1299.6	-465.3	1.258	1635.0	-585.3	883.4	135.8
	8	1300.9	-504.1	1.272	1654.3	-641.1	951.0	138.8
	7	1295.3	-543.7	1.286	1665.4	-699.1	1018.6	141.5
	6	1300.8	-566.3	1.300	1691.3	-736.3	1085.6	143.6
	5	1300.3	-589.2	1.315	1710.2	-774.9	1152.6	145.3
	4	1294.2	-612.3	1.331	1722.2	-814.8	1219.5	146.6
	3	1282.4	-635.5	1.347	1727.5	-856.1	1286.5	147.5
	2	1265.3	-954.8	1.364	1726.0	-1302.5	1353.5	148.0

Note: Moment magnifier, δ_s, was calculated according to ACI 318 (2008)

Table 4-31 Column section design results

f'_c = 6 ksi	Floor	d_c (in)	Longitudinal reinforcement size (#)	Longitudinal reinforcement numbers	Reinforcement ratio (%)
Exterior Column	Roof	28	9	8	1.020
	20	28	9	8	1.020
	19	28	10	8	1.296
	18	28	10	8	1.296
	17	28	11	8	1.592
	16	28	11	8	1.592
	15	28	11	8	1.592
	14	30	10	8	1.129
	13	30	10	8	1.129
	12	30	10	8	1.129
	11	30	10	8	1.129
	10	30	11	8	1.387
	9	30	11	12	2.080
	8	30	11	12	2.080
	7	30	10	16	2.258
	6	32	11	8	1.219
	5	32	11	8	1.219
	4	32	11	8	1.219
	3	32	10	12	1.488
	2	32	11	8	1.219
Interior Column	Roof	28	9	8	1.020
	20	28	11	8	1.592
	19	28	10	12	1.944
	18	28	10	12	1.944
	17	28	11	12	2.388
	16	28	11	12	2.388
	15	28	11	12	2.388
	14	30	11	12	2.080
	13	30	11	12	2.080

	12	30	11	12	2.080
	11	30	11	12	2.080
	10	30	11	12	2.080
	9	30	11	12	2.080
	8	30	10	16	2.258
	7	30	11	16	2.773
	6	32	11	8	1.219
	5	32	10	12	1.488
	4	32	11	12	1.828
	3	32	10	16	1.984
	2	32	11	8	1.219

Note: Refer to the note on page 66 regarding minimum column reinforcement used in design.

4.5. Design details of baseline and PBPD frames

The member section design and reinforcement layout of the baseline frames (FEMA P695, 2009) and PBPD frames are summarized in this section. The design results were implemented in the calculation of modeling parameters as presented and discussed in Chapter 5. Those design details for beam and column sections of 4, 8, 12 and 20-story baseline and PBPD frames are shown in Figure 4-10 to 4-13, respectively.

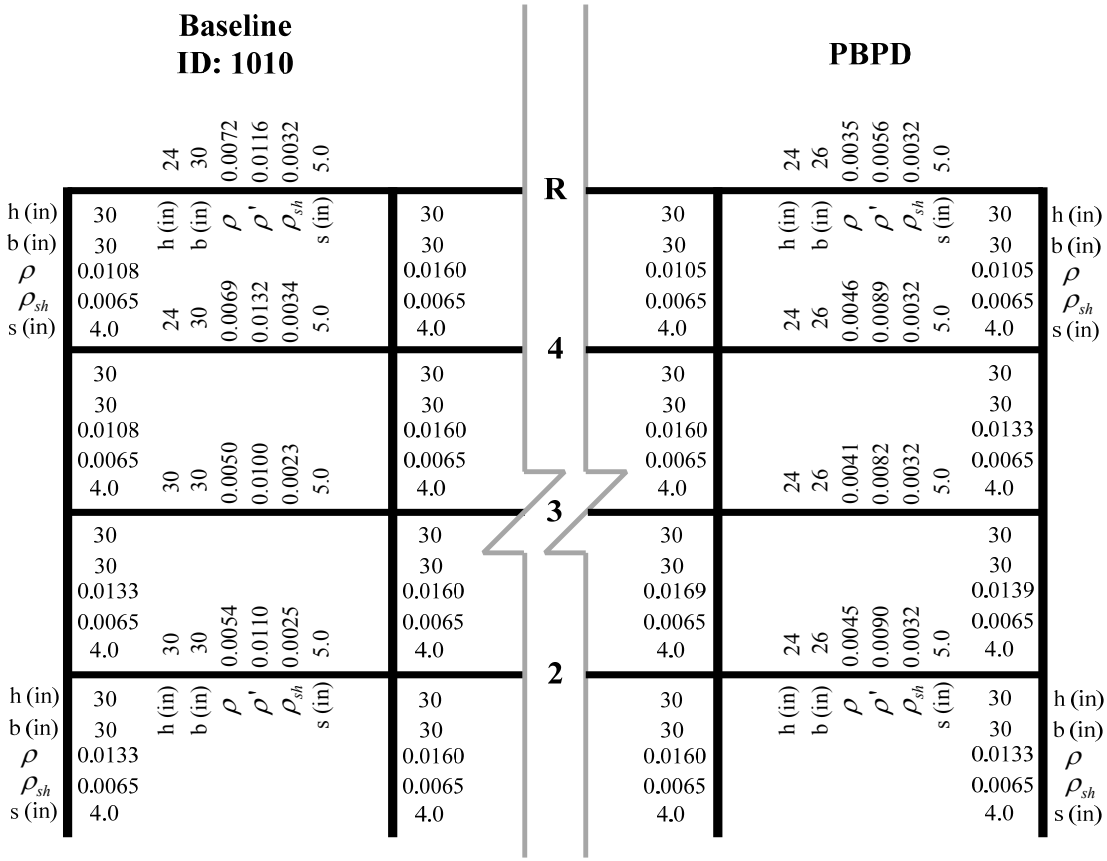

Figure 4-10 Design details of 4-story baseline and PBPD frames

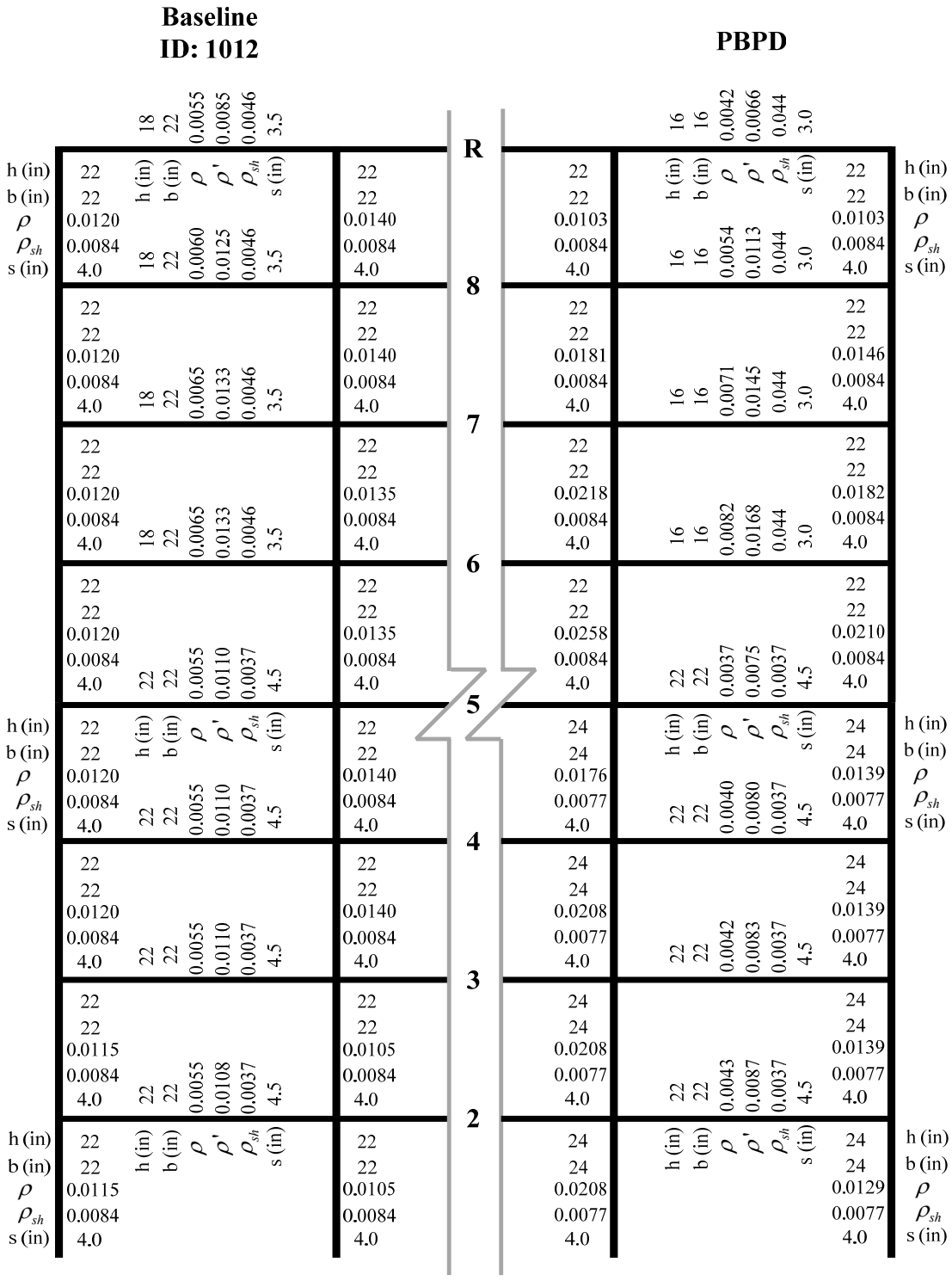

Figure 4-11 Design details of 8-story baseline and PBPD frames

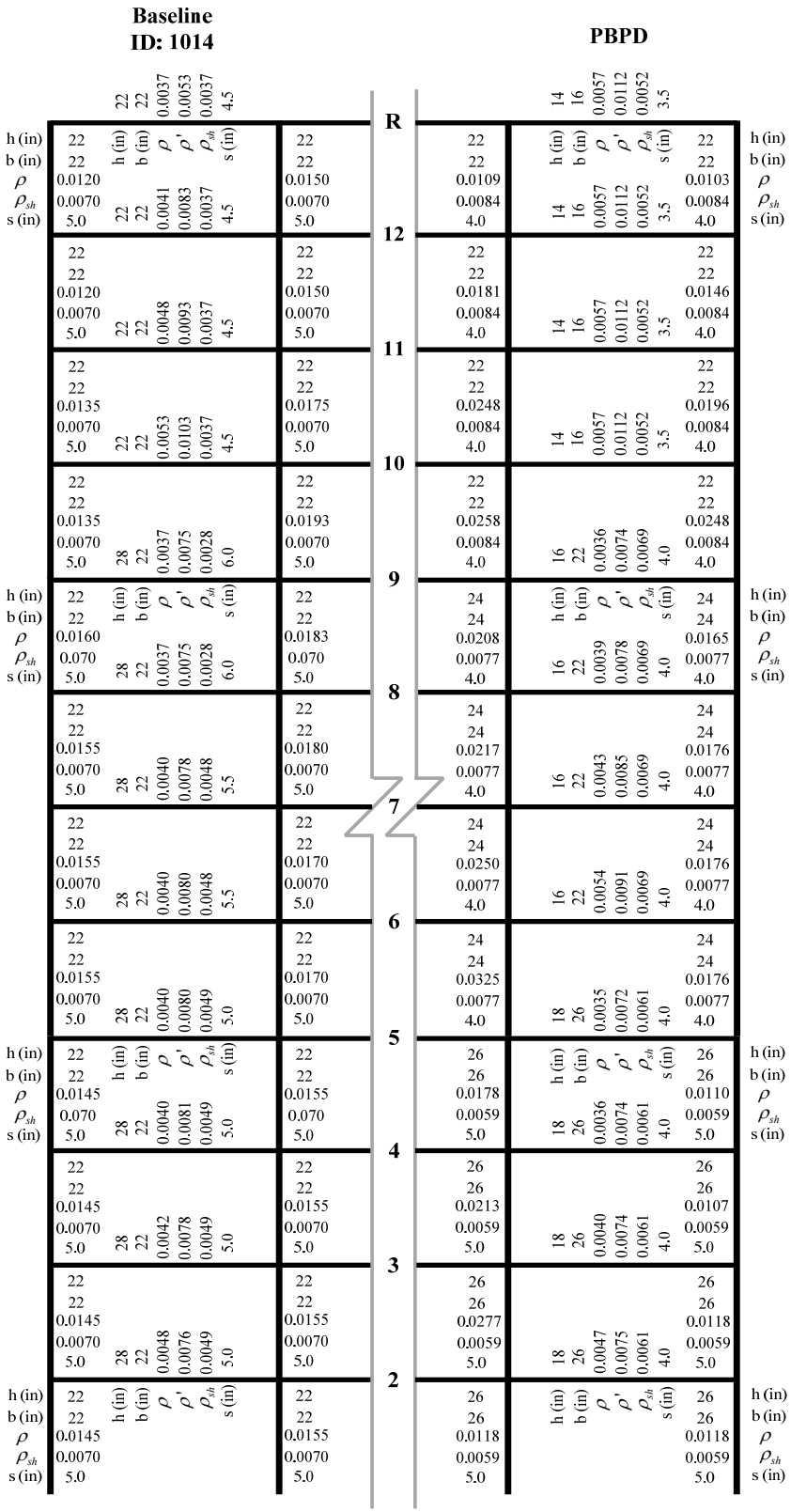

Figure 4-12 Design details of 12-story baseline and PBPD frames

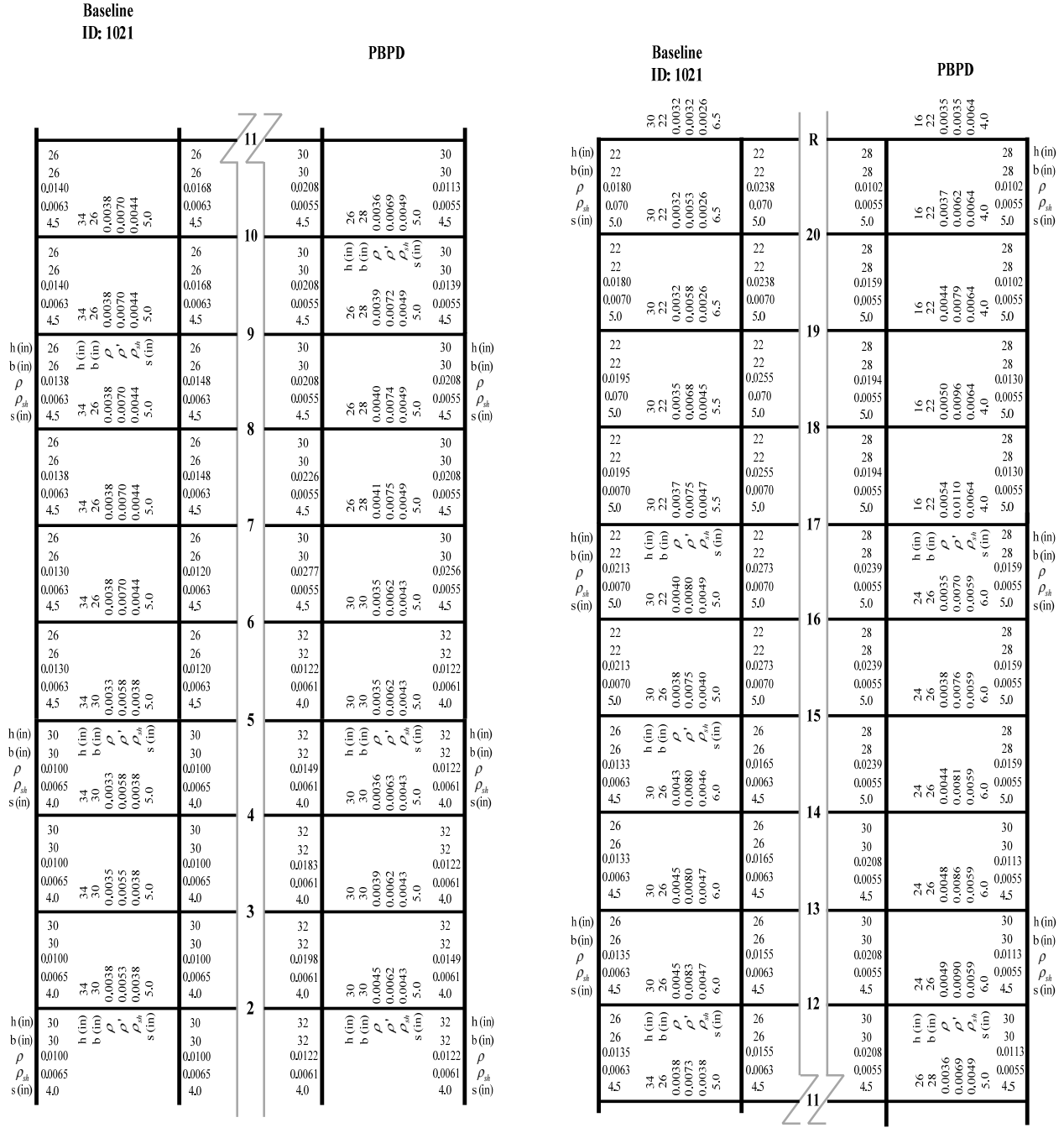

Figure 4-13 Design details of 20-story baseline and PBPD frames

4.6. Summary and conclusions

The main weakness of current seismic design code for RC SMF is lack of guidance to provide the engineers as to how to achieve the desired goals such as, controlling drifts, distribution and extent of inelastic deformation, etc. In contrast, the PBPD method is a *direct* design method, which requires no evaluation after the initial design because the nonlinear behavior and key performance criteria are built into the design process from the start.

For comparison and performance evaluation purposes, the basic design parameters for PBPD RC SMF (4, 8, 12 and 20-story) were kept the same with those of baseline frames. All selected baseline frames which were designed and used in FEMA P695 (2009), were successfully redesigned by the PBPD method. The design details were also presented in this chapter.

CHAPTER 5

NONLINEAR ANALYSIS MODELING AND EARTHQUAKE RECORDS

5.1. General

Nonlinear analysis is widely applied in the studies of seismic response and progressive collapse of structures. A sound nonlinear analysis must consider inelastic material and geometric nonlinear behavior, damping, element type selection, acceptance criteria and properly scaled ground motions. That is, nonlinear analyses based on incorrect modeling/calibration methods will lead to unreliable results.

In this chapter, the element-level modeling, structure-level modeling and selection of ground motions will be presented in reference to FEMA P695 (2009). The computer programs used in this study will be discussed as well. Then the PBPD frames and the baseline frames will be subjected to extensive inelastic pushover and time-history analyses with the same software (PERFORM 3D) for comparison of response and performance evaluation purposes.

5.2. Element-level modeling

5.2.1 Monotonic backbone

A beam-column element was created in order to simulate the behavior of reinforced concrete beams and columns of the study frames. The beam-column element was idealized

using an elastic element and two zero-length lumped flexural plastic hinges at the ends of the element as shown in Figure 5-1.

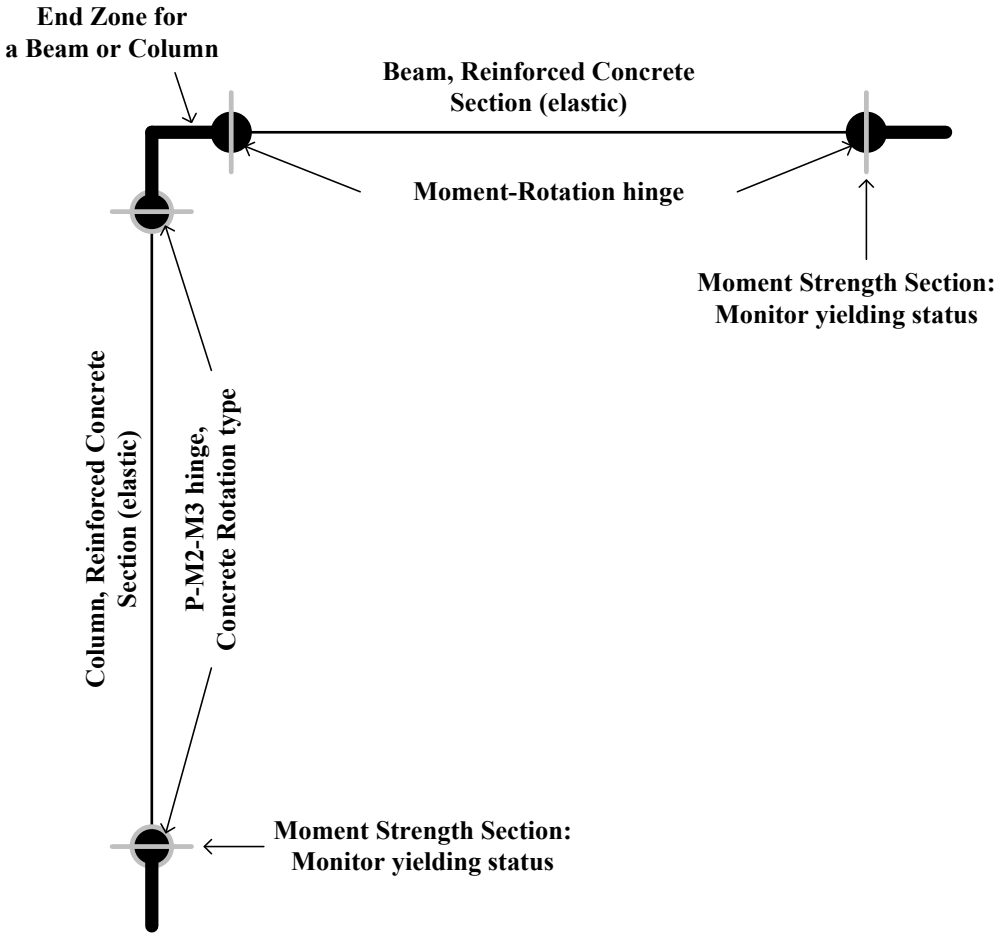

Figure 5-1 Hybrid RC beam and column models in PERFORM 3D program

The monotonic backbone of basic plasticity model developed by Ibarra et al. (2005) was selected for this study as was done in the FEMA P695 (2009) study. To facilitate accurate structural modeling, 255 tests of RC columns were calibrated by Haselton et al., for this proposed RC element model. It is noted that this basic element model was implemented in PEER's open-source structural analysis and simulation software tool, OpenSees.

This model is capable of capturing the important modes of deterioration that lead to global sideway collapse. Using these calibration data, a full set of equations were also

developed for the parameters (mean and uncertainty) of lumped plasticity element model as shown in Figure 5-2.

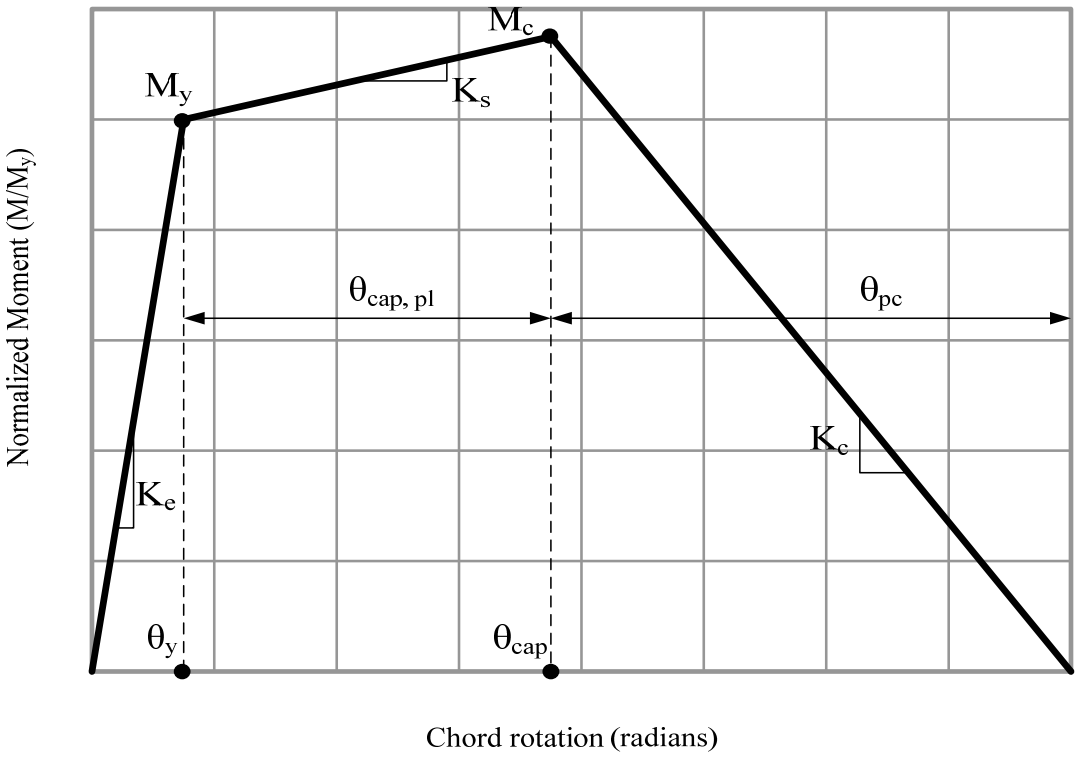

Figure 5-2 Monotonic moment-rotation model

Those parameters include: initial stiffness (K_e), post-yield hardening stiffness (K_s), plastic rotation capacity ($\theta_{cap,pl}$), post-capping rotation capacity (θ_{pc}), and cyclic energy dissipation capacity (λ). The equations, which are applicable to any rectangular RC section element that fails in flexure or flexure-shear will be discussed in more detail in the next section. This portion of the study showed that the median plastic rotation capacity of modern RC elements is larger than reflected in documented such as FEMA 356 (2000).

5.2.2 FEMA P695 equations

Monotonic backbone plot which defines characteristic force deformation relationship of nonlinear structural element model were initially developed in FEMA 273/356 project

(1997, 2003). However, due to its high degree of idealization and conservatism (Haselton, 2007), the backbone curves in FMMA 356 may not be accurate enough for realistic modeling of reinforced concrete beam-column components.

As mentioned earlier, the equations for backbone characteristics of plasticity model as shown in Figure 5-2 were calibrated and proposed by Haselton et al (2007; FEMA P695, 2009) based on an element model developed by Ibarra, Medina, and Krawinkler (2005, 2003), as implemented in OpenSees. The calibration work was based on the data from 255 reinforced concrete column tests assembled by Berry et al. (Berry et al. 2004, PEER 2006a). For ease and consistency of comparison, all the test configurations and force-deflection data were reduced to the case of an equivalent cantilever column as shown in Figure 5-3.

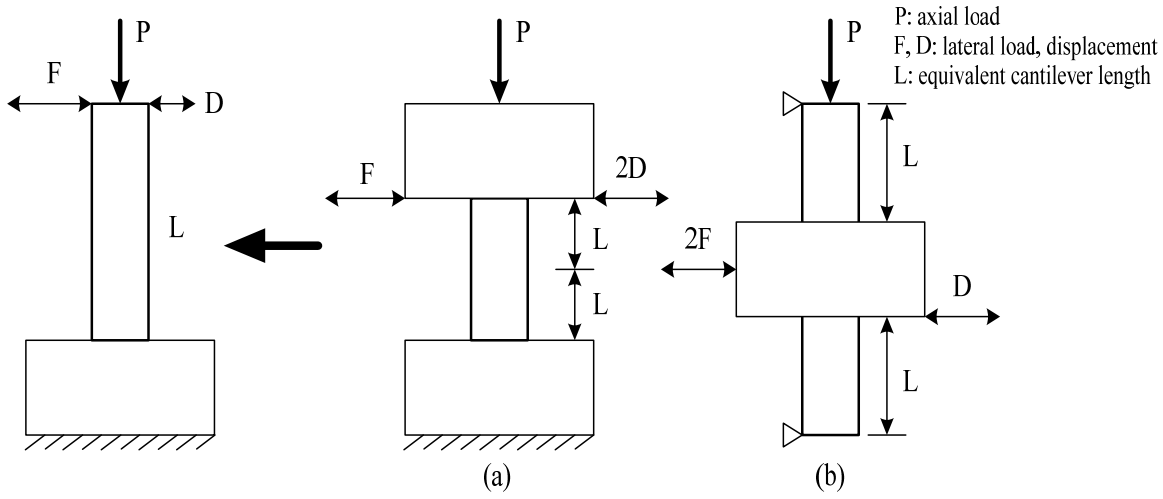

Figure 5-3 Converting (a) double-curvature and (b) double-ended column into equivalent column

For each test, the element model parameters (eg. plastic rotation capacity, cyclic deterioration parameters, etc.) were systematically calibrated such that the analysis results closely matched the experimental results. The mean modeling parameters and the uncertainty were also quantified and detailed discussion can be found in FEMA P695 (2009). The summary of accuracy of proposed equations used in this study is briefly presented in Table 5-1.

Table 5-1 Accuracy of proposed equations used in this study (Haselton, 2007)

Proposed equation	$\frac{predicted}{test\ data}$ **Median**	$\frac{predicted}{test\ data}$ **Mean**	logarithmic standard deviation
Effective stiffness, EI_{eff}	0.98	1.52	0.33
Plastic rotation capacity, $\theta_{cap,pl}$	0.99	1.18	0.54
Post-capping rotation capacity, θ_{pc}	1.00	1.20	0.72
Post-yield hardening stiffness, $\frac{M_c}{M_y}$	0.97	1.01	0.10
Cyclic energy dissipation capacity, λ	1.01	1.25	0.49

The empirical equations proposed in FEMA P695 (2009) are briefly presented and discussed in the following.

Effective stiffness, EI_{eff}

The effective initial stiffness is defined by the secant stiffness at 40% of yield force since it was observed that the stiffness changes noticeably in most tests. The equation for effective stiffness is given as follows:

$$\frac{EI_{eff}}{EI_g} = -0.02 + 0.98\frac{P}{A_g f'_c} + 0.09\frac{L_s}{H},\ and\ \ 0.35 \le \frac{EI_{eff}}{EI_g} \le 0.8 \tag{5-1}$$

, where $\frac{P}{A_g f'_c}$ is the axial load ratio and $\frac{L_s}{H}$ is the column aspect ratio. It is noted that in FEMA 356, EI_{eff} is permitted to be simply set as $0.5 \cdot EI_g$ or $0.7 \cdot EI_g$ while $\frac{P}{A_g f'_c} < 0.3$ or

$0.5 < \frac{P}{A_g f'_c}$, respectively, which is generally 2.5 times higher than that calculated by Equation 6-1. Elwood and Eberhard (2006) showed that most of this difference can be accounted for by significant bond-slip and shear deformations, which were not incorporated in FEMA 356.

Plastic rotation capacity, $\theta_{cap,pl}$

The plastic rotation capacity, $\theta_{cap,pl}$, is mainly affected by the axial load ratio ($\frac{P}{A_g f'_c}$) and confinement ratio (ρ_{sh}), while other parameters, such as concrete strength (f'_c unit: MPa), rebar buckling coefficient (s_n) and longitudinal reinforcement ratio (ρ) also have statistically significant influence. The equation for $\theta_{cap,\ pl}$ is as follows:

$$\theta_{cap,pl} = 0.12 \cdot (1 + 0.55 \cdot \alpha_{sl}) \cdot 0.16^{\frac{P}{A_g f'_c}} \cdot (0.02 + 40 \cdot \rho_{sh})^{0.43} \cdot (0.54)^{0.01 \cdot f'_c} \cdot 0.66^{0.1 \cdot s_n} \cdot 2.27^{10 \cdot \rho} \quad \text{(5-2)}$$

, where α_{sl} is bond-slip indicator variable and can be assumed as 1 or 0 depending on whether slip is possible or not.

It is also worth mentioning that Wight and Sozen (1975) indicated that the transverse reinforcement must be proportioned to carry the total shear required to develop the ultimate moment capacity of the column. That is, confinement ratio (ρ_{sh}), has a significant effect on the plastic rotation capacity. Table 5-2 shows the effects of ρ_{sh} on plastic rotation capacity, $\theta_{cap,pl}$.

Table 5-2 Effects of ρ_{sh} on plastic rotation capacity, $\theta_{cap,pl}$ (Haselton, 2007)

confinement ratio ρ_{sh}	Plastic rotation capacity, $\theta_{cap,pl}$ *
0.002	0.033
0.0075	0.055
0.01	0.062
0.02	0.082

*: f'_c=30 MPa; $\frac{P}{A_g f'_c}$ = 0.1; α_{sl}=1; s_n = 12.7; ρ = 0.02

It is noted that a value of 1 is used for α_{sl} in the analysis model of baseline frames in FEMA P695. That accounts for 35% of the plastic rotation capacity (Haselton, 2007). Haselton (2007) also observed that low axial load ratio, adequate transverse reinforcement, and bond-slip deformations result in relatively large plastic rotation capacities.

Post-capping rotation capacity, θ_{pc}

In the proposed equation for post-capping response shown below, axial load ratio ($\frac{P}{A_g f'_c}$) and transverse steel ratio (ρ_{sh}) are considered as key parameters.

$$\theta_{pc} = 0.76 \cdot 0.1031^{\frac{P}{A_g f'_c}} \cdot (0.02 + 40 \cdot \rho_{sh})^{1.02} \leq 0.1 \quad (5\text{-}3)$$

Post-yield hardening stiffness, $\frac{M_c}{M_y}$

Post-yield hardening stiffness ($\frac{M_c}{M_y}$) is defined by the ratio of the maximum moment capacity and the yield moment capacity. According to regression analysis, two major factors

in determining $\frac{M_c}{M_y}$ are concrete strength (f'_c unit: MPa) and axial load ratio ($\frac{P}{A_g f'_c}$). The predictive equation for $\frac{M_c}{M_y}$ is given as follows.

$$\frac{M_c}{M_y} = 1.25 \cdot 0.89^{\frac{P}{A_g f'_c}} \cdot (0.91)^{0.01 \cdot f'_c} \tag{5-4}$$

Cyclic energy dissipation capacity, λ

Cyclic energy dissipation capacity (λ) was most closely related to both the axial load level ($\frac{P}{A_g f'_c}$) and the degree of confinement of the concrete core. In terms of quantifying the effect of confinement, the ratio of stirrup spacing to column depth ($\frac{s}{d}$) was found as a better predictor than transverse steel ratio (ρ_{sh}) by Haselton (2007). A more detailed discussion of cyclic energy dissipation capacity is given in the next section. The simplified predictive equation of cyclic energy dissipation capacity is given in the following.

$$\lambda = 170.7 \cdot 0.27^{\frac{P}{A_g f'_c}} \cdot (0.10)^{\frac{s}{d}} \tag{5-5}$$

In summary, all these empirical equations developed in FEMA P695 (2009) give element modeling parameters which are based on design section parameters of RC column. Even though there are still limitations of these equations due to limited availability of test data, for fair comparison purpose, the input modeling parameters of all RC SMF, including baseline frames and PBPD frames, were mainly calculated by these equations.

5.2.3 Cyclic behavior

Based on the studies of Comité Euro-International du Béton (1996), it is noted that cyclic degradation is most closely related to both the axial load level and the degree of confinement of the concrete core. That is, the cyclic energy dissipation capacity decreases with increasing axial load and decreasing confinement. As mentioned earlier, certain key parameters can be calculated based on the equations presented in FEMA P695 (2009), including cyclic energy dissipation capacity, λ, developed by Ibarra (2003). By considering ratio of stirrup spacing to column depth ($\frac{s}{d}$) and axial loading ratio ($\frac{P}{A_g f'_c}$), Ibarra presented a good equation for cyclic energy dissipation factor, λ. This cyclic energy dissipation factor was also implemented in OpenSees as "pinching material model" by Altoontash (2005).

To model strength and stiffness degrading hysteretic loops the PERFORM 3D program uses cyclic degradation energy factor, *e*, defined as the ratio of the area of degrading hysteretic loop to the area of elastic perfectly-plastic hysteretic loop. Therefore for this study a proper value of the factor *e* was needed, which was determined by a process of transformation as shown in Figure 5-4. With given section properties the value of factor λ was calculated and the hysteretic loops were constructed for a SDOF system with pinching material model in the OpenSees program. Then the value of the factor *e* was calculated from the area ratio of hysteretic loops to corresponding fully EPP loops. Figure 5-5 shows a typical comparison of the hysteretic loops obtained by this transformation process. The values of the factor *e* were found in this study to vary from 0.15 to 0.25 depending on the section properties.

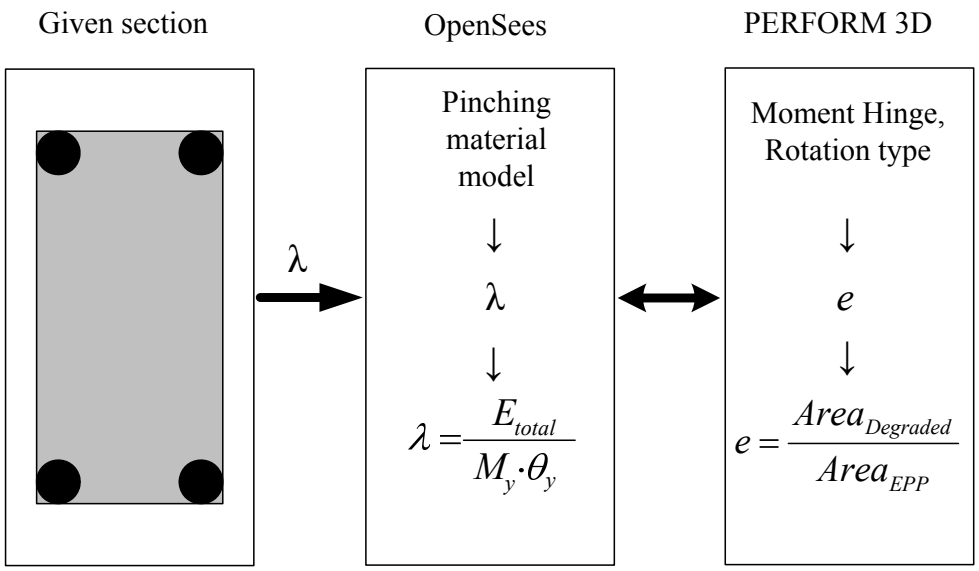

Figure 5-4 Transformation of λ and *e*

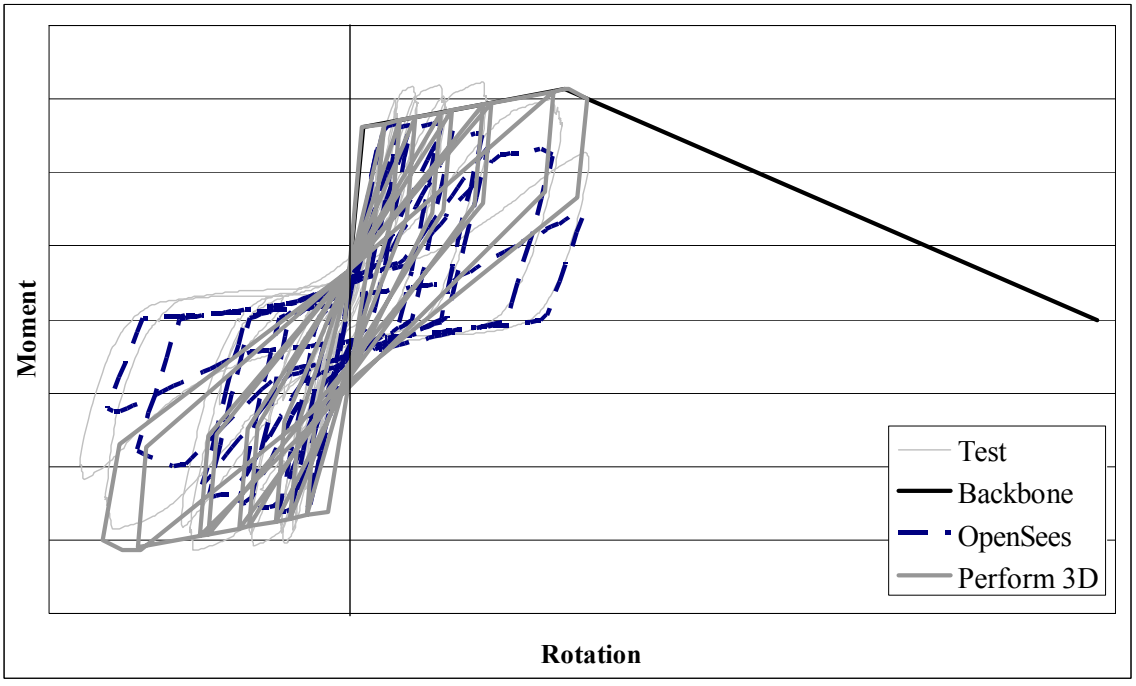

Figure 5-5 Comparison of hysteretic loops obtained by transformation procedure

It is noted that OpenSees was used in FEMA P695 (2009) instead of PERFORM 3D. Although OpenSees is considered to be more accurate to model the hysteretic characteristics as seen in Figure 5-5, the nonlinear axial-flexural interaction was not considered in the

plastic hinge models used in FEMA P695 (2009). In contrast, axial-flexural interaction has been quite accurately modeled in the formulation of column elements in this study.

5.2. Structure-level modeling

As mentioned in Chapter 4, a three-bay frame was selected as main archetype structure model in this study as shown in Figure 5-6. A three-bay model contains both interior and exterior columns. The interior and exterior columns are important for capturing the effects of strong-column weak-beam design provisions as well. Furthermore, the three-bay frame can capture the additional axial loads due to overturning, which influences both the column design and behavior.

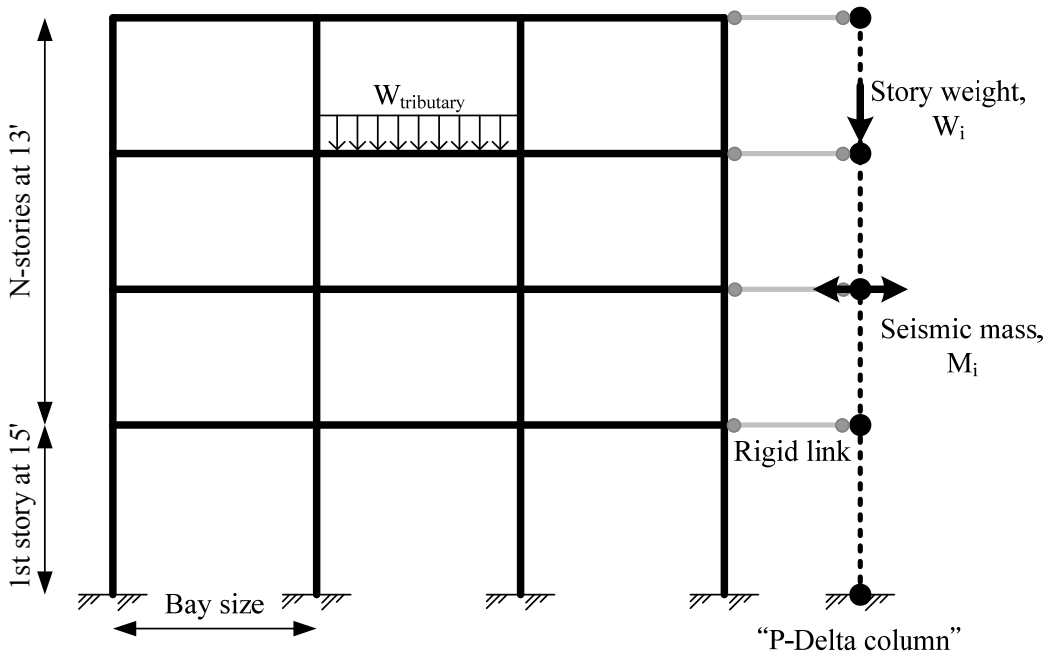

Figure 5-6 Archetype analysis model for RC SMF

It should be noted that the P-Delta effect is captured by applying the story gravity loads on a "P-Delta column" element (columns not part of the lateral force resisting frame), which is connected to the main frame by rigid links. The seismic mass for each floor is equal to corresponding story weight since every study frame is designed as space frame.

The damping ratio is set as 6.5% for RC SMF as suggested in the research by Chopra (1995) and Miranda (2005).

5.3. Simulation software

5.3.1 Overview

In this study, PERFORM 3D (CSI, 2007) was selected as the main analysis program. PERFORM 3D is a highly focused nonlinear software tool for seismic analysis and design. Complex structures and element models can be analyzed nonlinearly using a wide variety of deformation-based and strength-based limit states. Nonlinear analysis can be static and/or dynamic, and can be run on the same model in PERFORM 3D. Loads can be applied in any sequence, such as a dynamic earthquake loading followed by a static pushover. The output includes pushover diagrams, energy balance displays, as well as mode shapes, deflected shapes, and time history records of displacements and forces (CSI, 2007).

As mentioned earlier, PCA-COLUMN was used for designing the columns. Once the section size and reinforcement layouts were obtained, XTRACT (Chadwell and Imbsen, 2002) was applied to get P-M interaction diagrams as input parameters for P-M-M column lumped plastic hinge properties in PERFORM 3D as shown in Figure 5-1. The application sequence of software for simulation of column P-M-M plastic hinges is shown in Figure 5-7.

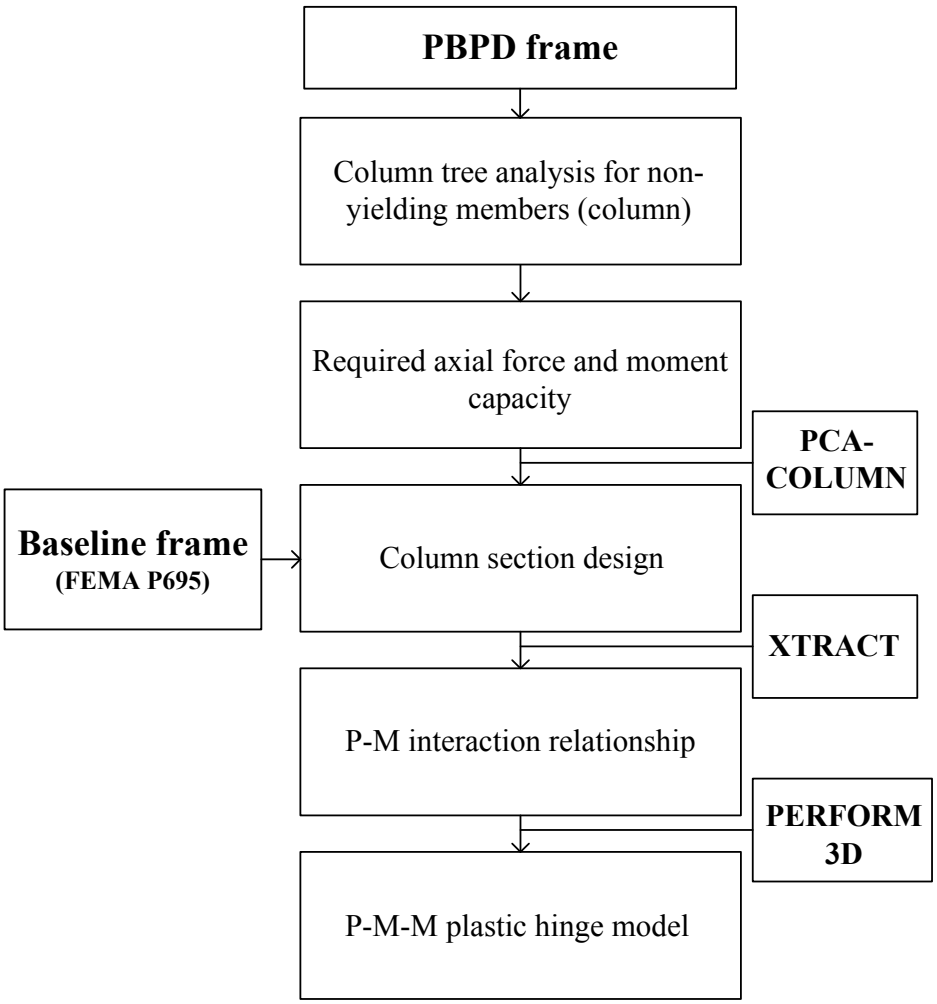

Figure 5-7 Sequence of software use for simulation of column P-M-M plastic hinges

5.3.2 XTRACT

XTRACT (Chadwell and Imbsen, 2002) was developed originally at the University of California at Berkeley by Dr. Charles Chadwell. XTRACT is a general cross section analysis software for analysis of any section shape and material subject to any force based loading as shown in Figure 5-8.

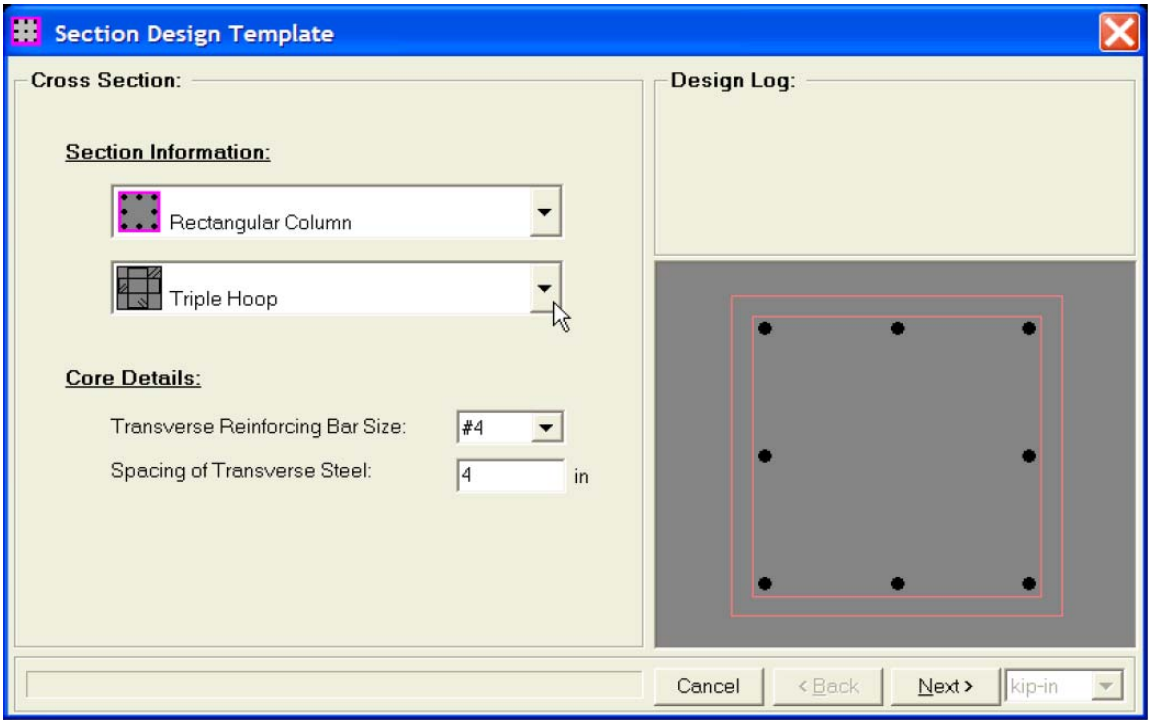

Figure 5-8 Column section input window in XTRACT

Analysis of XTRACT begins with the specification of nonlinear material models, and the cross section will be cut into fibers so that the moment curvature and axial force-moment interactions can be generated. For reinforced concrete, three typical material models must be defined: steel, unconfined concrete and confined concrete (Figure 5-9). Confined concrete mathematical models incorporate effects of increased compressive strain capacity in addition to an increased compressive strength as a function of passive confinement from transverse reinforcing steel. An axial force-moment interaction surface for a typical rectangular reinforced concrete cross section is given in Figure 5-10.

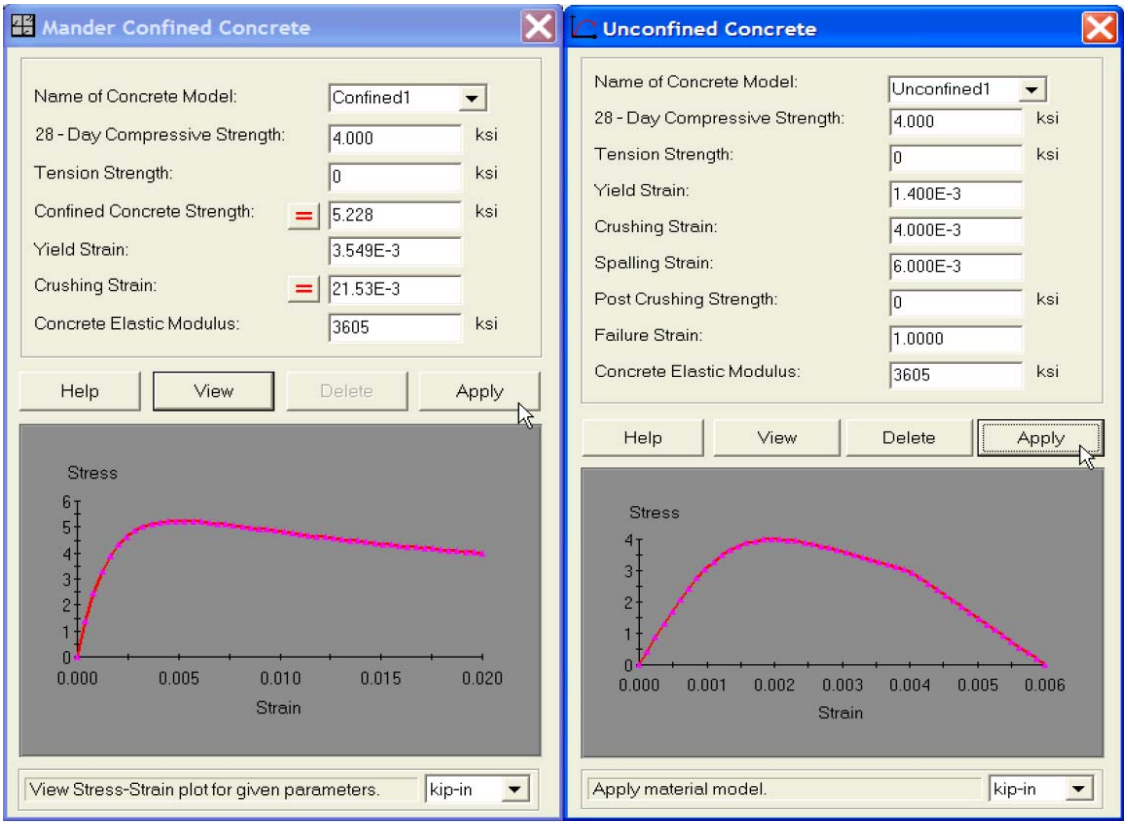

Figure 5-9 Confined concrete (left) and unconfined concrete (right) material models

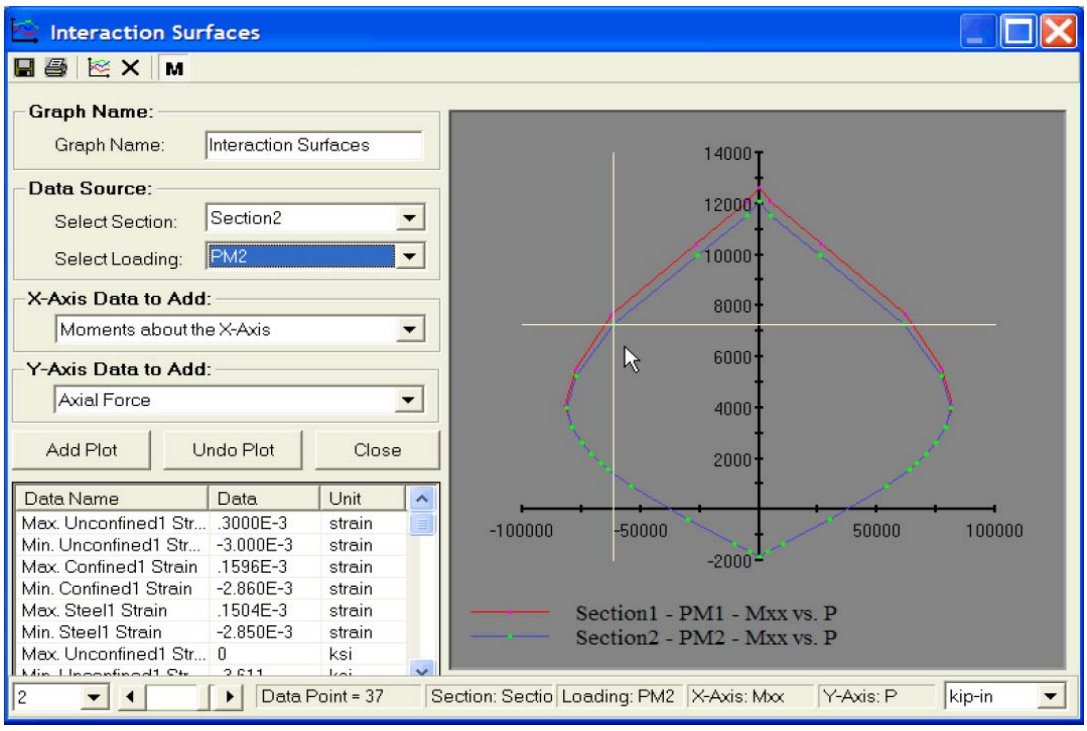

Figure 5-10 Axial force-moment interaction surface

5.3.3 PERFORM 3D

The computer program PERFORM-3D (CSI, 2007) is a highly focused nonlinear software tool for earthquake resistant design. Figure 5-11 and 5-12 show that the backbone curve of all plastic hinge models in PERFORM 3D can be determined by parameters, such as basic force-deformation relationship, strength loss, deformation capacity and cyclic degradation, which are calculated according to the equations presented in Section 5.2.2.

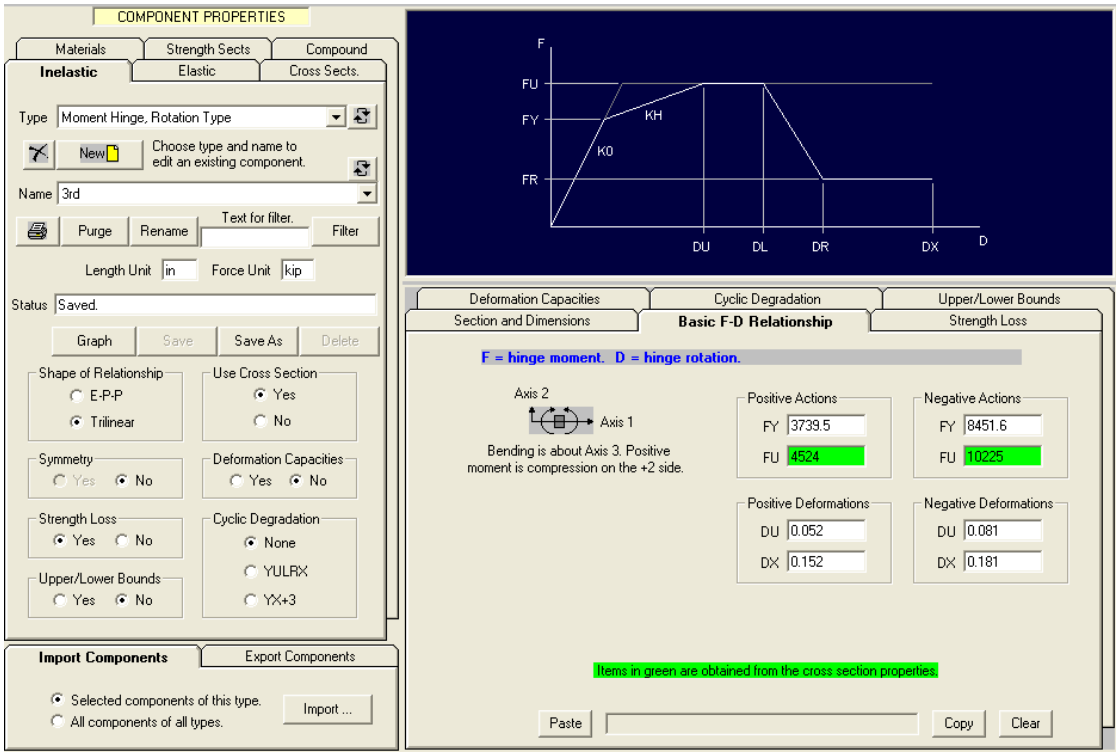

Figure 5-11 Backbone curve of moment hinge of beam

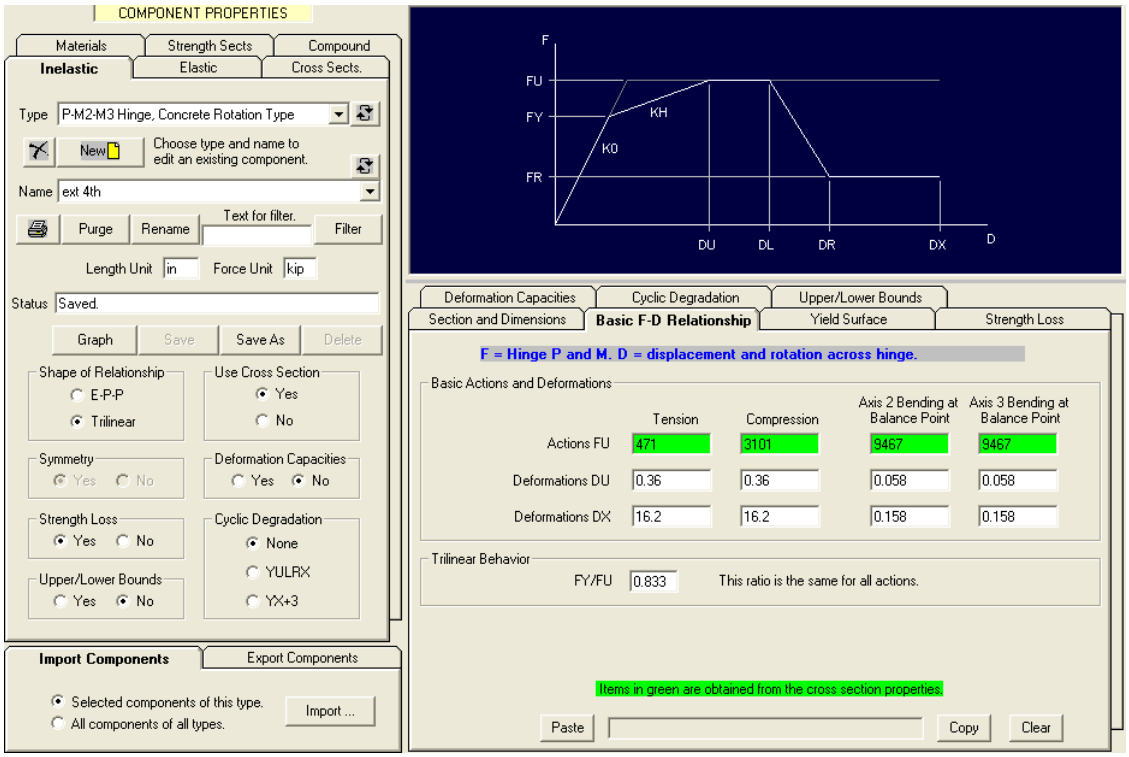

Figure 5-12 Backbone curve of P-M-M moment hinge of column

As mentioned earlier, in terms of column element, there is no nonlinear axial-flexural interaction considered in the plastic hinge models in FEMA P695, while it was indeed considered in this study by using PERFORM 3D. Certain characteristics of P-M diagram obtained from XTRACT can be well implemented in PERFORM 3D as shown in Figure 5-13. The maximum axial forces in compression and tension, moment and axial force at balance point, flexural moment without axial loading are required for column section model in PERFORM 3D.

The window interface is one of the advantages of PERFORM 3D. Occurrences, locations and sequences of plastic hinges can be easily monitored and tracked by color change of elements during static pushover or dynamic time history analyses. Animation is also available to provide better picture about how a structure behaves subjected to earthquakes. Thus, all nonlinear analyses in this study were performed by mainly using the PERFORM 3D program.

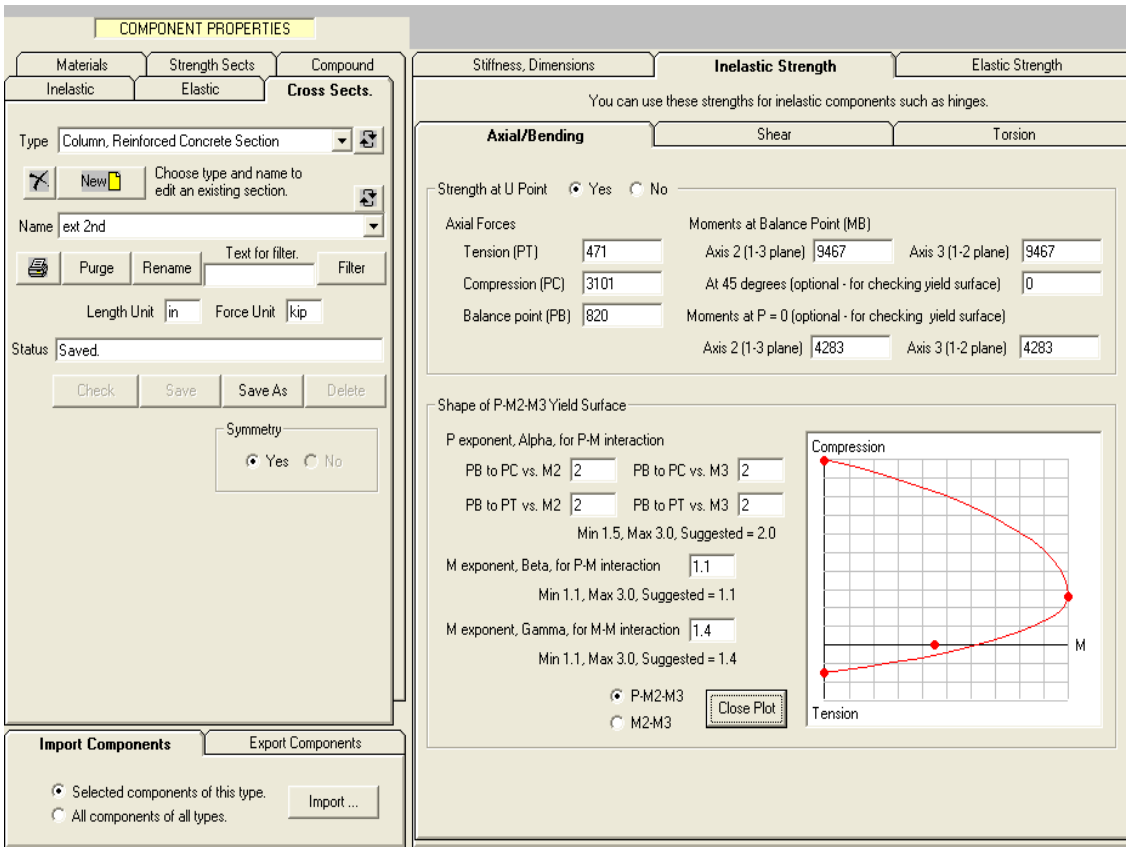

Figure 5-13 Determination of P-M interaction of column sections

5.4. Nonlinear analysis

Structures generally deform far beyond the elastic range while subjected to strong earthquakes. For properly accounting for the nonlinear behavior, a more sophisticated analysis is required.

Nonlinear analyses can offer greater insight into the behavior of the structure and to determine if the structures satisfy performance requirements. Two types of nonlinear analysis, static pushover and dynamic time history analyses, are the most comprehensive and common tools to be used in accordance with several guidelines.

5.4.1 Nonlinear static pushover analyses

Nonlinear static pushover analyses are carried out by applying increasing monotonic lateral forces and pushing the structure models to large displacements. The lateral loads which are statically applied to the model should be properly distributed as defined by the design standard. In this study, the pushover analyses were performed using a static lateral force distribution derived from the equivalent lateral force procedure in the PBPD method (Chao et al., 2007) as mentioned in Chapter 3 instead of that given by the seismic design provisions (ASCE 2005).

The lateral loads are incrementally increased and the resulting force-displacement plot for the structure is obtained. This plot can be assumed to represent the inelastic structural response to earthquake ground motions. In general, displacement control instead of force control is used to study the formation of mechanisms and structural behavior characteristics after mechanism formation.

5.4.2 Nonlinear dynamic time history analyses

Despite the complexity and computational effort, dynamic time history analysis is generally deemed as the most accurate analysis method provided accurate models are used. By applying series of base acceleration records to the study structures, the response can be directly determined. Multiple, representative and properly scaled earthquake records must be used for dynamic analyses in order to ensure that the range of possible responses is properly captured instead of only single loading case considered in static pushover analysis.

In FEMA P695 (2009), a more general method compared to FEMA 356 (2000) was proposed and used in this study as well. That is, to select 10-30 earthquake ground motions, scale the ground motions to different hazard levels, and estimate both the mean and the variability in response due to the variability between different earthquake ground motions.

The detailed description of how this method accounts for the effects of uncertainties in structural design and structural modeling can be found in FEMA P695.

5.5. Site hazard and ground motions

5.5.1 MCE and DE Demand (ASCE/SEI 7-05)

Maximum considered earthquake (MCE) ground motion is the most severe earthquake effect considered by ASCE /SEI 7-05. The site specific MCE response spectra for ASCE 7-05 design evaluations should be determined in accordance with Chapter 21 of ASCE 7-05. MCE ground motions are generally described with the probabilistic criteria specified corresponding to the risk of a 2 percent probability of exceedance within a 50-year period, which is equivalent to a return period of 2,475 years.

On the other hand, design earthquake (DE or 2/3MCE) ground motion is defined as the earthquake ground motion that is two-thirds of the corresponding MCE ground motion. The site specific DE response spectra and the DE design acceleration parameters S_{DS} and S_{D1} should be determined in accordance with Sections 21.3 and 21.4 of ASCE 7-05. The DE (2/3MCE) ground motions are adopted for practical purposes which correspond to the risk of a 10 percent probability of a 50-year period, also meaning a return period of 475 years.

5.5.2 Record Selection Criteria

As mentioned earlier, selection of proper ground motions is essential for reliable dynamic time history analysis. For considering variety of earthquake records, the PEER NGA database is an update and extension to the PEER Strong Motion Database and provides a larger set of records, more extensive meta-data, with some corrections made to information in the original database. It is noted that the NGA site includes only acceleration time history files so far.

In FEMA P695 (2009), by considering unique spectral shapes of some rare earthquakes which are much different from that the shape of a typical building code spectrum, a set of far field strong ground motions were selected. This typically occurs at rather extreme levels of ground motion. So this ground motion set was selected to represent these extreme motions to the extent possible.

Minimum limits on event magnitude, as well as peak ground velocity and acceleration were imposed to ensure that all records represent strong motions. The selection criteria are summarized in Table 5-3.

Table 5-3 Far field ground motion records selection criteria (FEMA P695)

Selection criteria
Magnitude > 6.5
Distance from source to site > 10 km
Peak ground acceleration > 0.2g and peak ground velocity > 15 cm/sec
Soil shear wave velocity, in upper 30m of soil, greater than 180 m/s (NEHRP soil types A-D; note that all selected records happened to be on C/D sites)
Limit of six records from a single seismic event
Lowest useable frequency < 0.25 Hz
Strike-slip and thrust faults
No consideration of spectral shape
No consideration of station housing

5.5.3 Far-Field Record Set

According to the selection criteria described in the previous section, a set of far-field ground motion records was selected by Haselton (2007); it contains 44 records composed of 22 horizontal motions in both perpendicular direction components (x and y). The pseudo acceleration elastic spectra of this ground motion set (only x-direction) is shown in Figure 5-14.

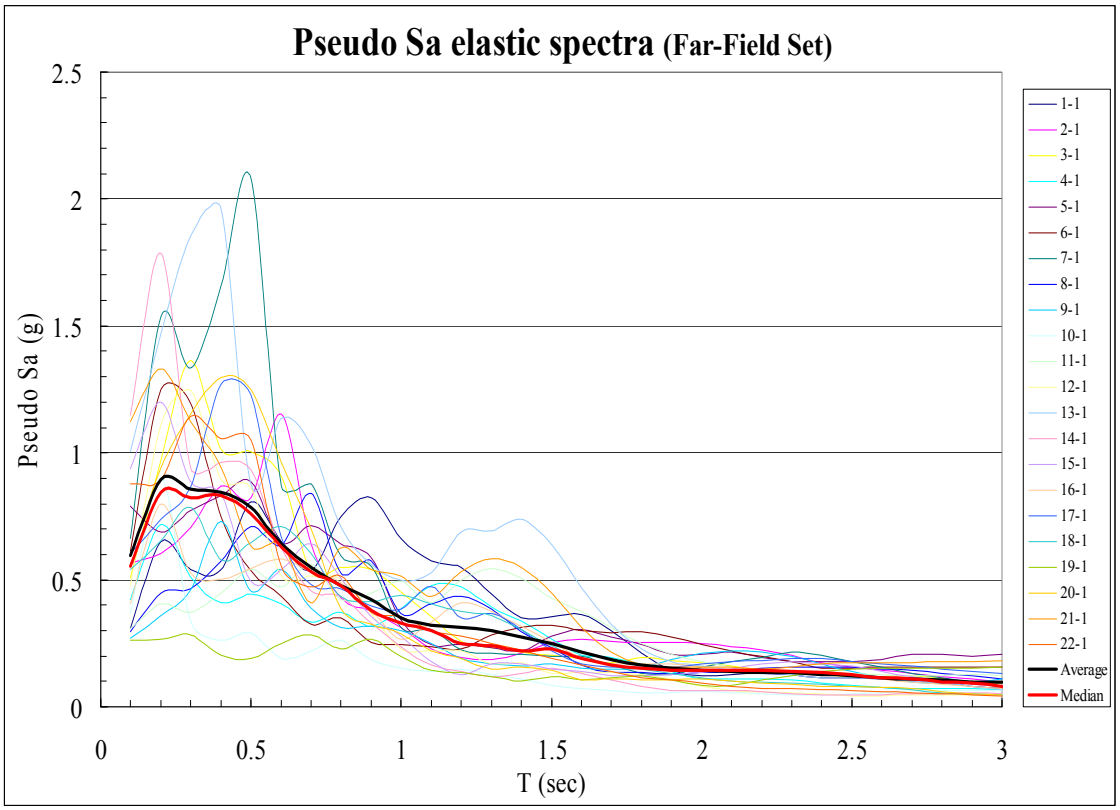

Figure 5-14 Pseudo acceleration elastic spectrum of 22 selected ground motion records

For this study, 11 ground motions were selected from the 44 far-field ground motion records. These 11 ground motions were picked by anchoring the corresponding periods of 4, 8, 12 and 20-story RC frame (0.86,1.80, 2.14 and 2.36 second) and then the 4, 4, and 3 ground motions which represent the highest, closest, and lowest from the median curves were selected. The set of ground motions used in this study is shown in Table 5-4.

Table 5-4 Far field ground motion records used in this study

Earthquake records used in this study				PEER-NGA Record	
ID	Name	M	Year	Sequence No.	File Name
PEER 1-1	Northridge	6.7	1994	953	NORTHR/MUL009
PEER 5-1	Imperial Valley	6.5	1979	169	IMPVALL/H-DLT262
PEER 8-1	Kobe, Japan	6.9	1995	1116	KOBE/SHI000
PEER 9-1	Kocaeli, Turkey	7.5	1999	1158	KOCAELI/DZC180
PEER 10-1	Kocaeli, Turkey	7.5	1999	1148	KOCAELI/ARC000
PEER 11-1	Landers	7.3	1992	900	LANDERS/YER270
PEER 12-1	Landers	7.3	1992	848	LANDERS/CLW-LN
PEER 13-1	Loma Prieta	6.9	1989	752	LOMAP/CAP000
PEER 17-1	Superstition Hills	6.5	1987	725	SUPERST/B-POE270
PEER 19-1	Chi-Chi, Taiwan	7.6	1999	1244	CHICHI/CHY101-E
PEER 22-1	Friuli, Italy	6.5	1976	125	FRIULI/A-TMZ000

It is noted that each individual record of this far-field set was normalized by its peak ground velocity. The detailed normalization process can be found in FEMA P695 (2009).

5.5.4 Scaling Method

To scale the records to the 2/3 MCE and MCE levels, all normalized records were multiplied by the same scale factor. The scaling factor was obtained by the ratios of 2/3 MCE and MCE pseudo acceleration elastic spectrum to the median of all 44 normalized ground motion set. The detailed calculation is given in Table 5-5. The median and mean of pseudo acceleration elastic spectrum curves of these 22 selected ground motions as well as the code design spectrum for 2/3 MCE and MCE hazard level are shown in Figure 5-15.

Table 5-5 Scaling factors of selected ground motion set

ID	File Names		Normalized Factor (1)	Anchor MCE factor (2)	Anchor 2/3 MCE factor (3)	Scaling factor MCE (1)*(2)	Scaling factor 2/3MCE (1)*(3)
1	NORTHR/MUL009	NORTHR/MUL279	0.65	2.59	1.73	1.68	1.12
2	NORTHR/LOS000	NORTHR/LOS270	0.83			2.15	1.43
3	DUZCE/BOL000	DUZCE/BOL090	0.63			1.63	1.09
4	HECTOR/HEC000	HECTOR/HEC090	1.09			2.82	1.88
5	IMPVALL/H-DLT262	IMPVALL/H-DLT352	1.31			3.39	2.26
6	IMPVALL/H-E11140	IMPVALL/H-E11230	1.01			2.62	1.74
7	KOBE/NIS000	KOBE/NIS090	1.03			2.67	1.78
8	KOBE/SHI000	KOBE/SHI090	1.1			2.85	1.90
9	KOCAELI/DZC180	KOCAELI/DZC270	0.69			1.79	1.19
10	KOCAELI/ARC000	KOCAELI/ARC090	1.36			3.52	2.35
11	LANDERS/YER270	LANDERS/YER360	0.99			2.56	1.71
12	LANDERS/CLW -LN	LANDERS/CLW -TR	1.15			2.98	1.99
13	LOMAP/CAP000	LOMAP/CAP090	1.09			2.82	1.88
14	LOMAP/G03000	LOMAP/G03090	0.88			2.28	1.52
15	MANJIL/ABBAR--L	MANJIL/ABBAR--T	0.79			2.05	1.36
16	SUPERST/B-ICC000	SUPERST/B-ICC090	0.87			2.25	1.50
17	SUPERST/B-POE270	SUPERST/B-POE360	1.17			3.03	2.02
18	CAPEMEND/RIO270	CAPEMEND/RIO360	0.82			2.12	1.42
19	CHICHI/CHY101-E	CHICHI/CHY101-N	0.41			1.06	0.71
20	CHICHI/TCU045-E	CHICHI/TCU045-N	0.96			2.49	1.66
21	SFERN/PEL090	SFERN/PEL180	2.1			5.44	3.63
22	FRIULI/A-TMZ000	FRIULI/A-TMZ270	1.44			3.73	2.49

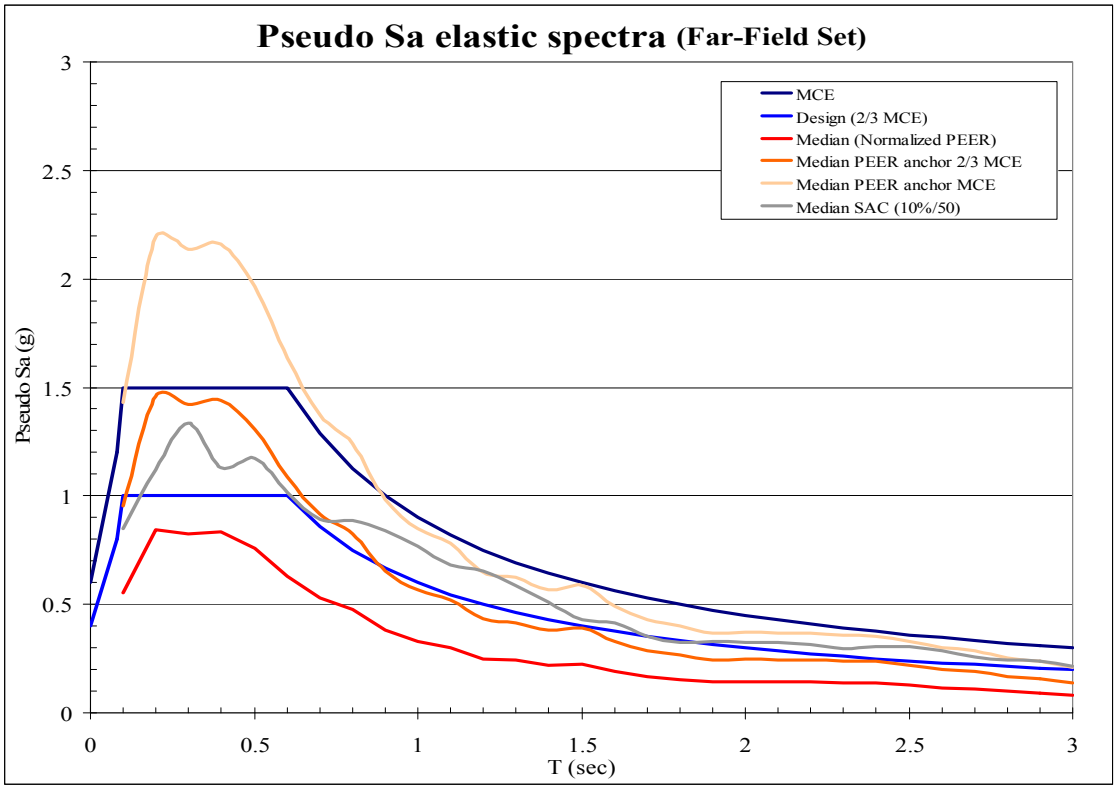

Figure 5-15 Pseudo acceleration elastic spectrum of mean and median of selected 22 ground motions as well as 2/3 MCE and MCE design spectrum

5.6. Structural modeling documentation for the study RC SMF

For this study, the baseline frames and PBPD frames were subjected to extensive inelastic pushover and time-history analyses by using PERFORM 3D. This section provides the documentation of the modeling parameters used for the structural models of each study frame. The modeling parameters of 4, 8, 12 and 20-story baseline and PBPD RC SMF are shown in Figure 5-16 to 5-19 respectively. The units are in US system (kip and in).

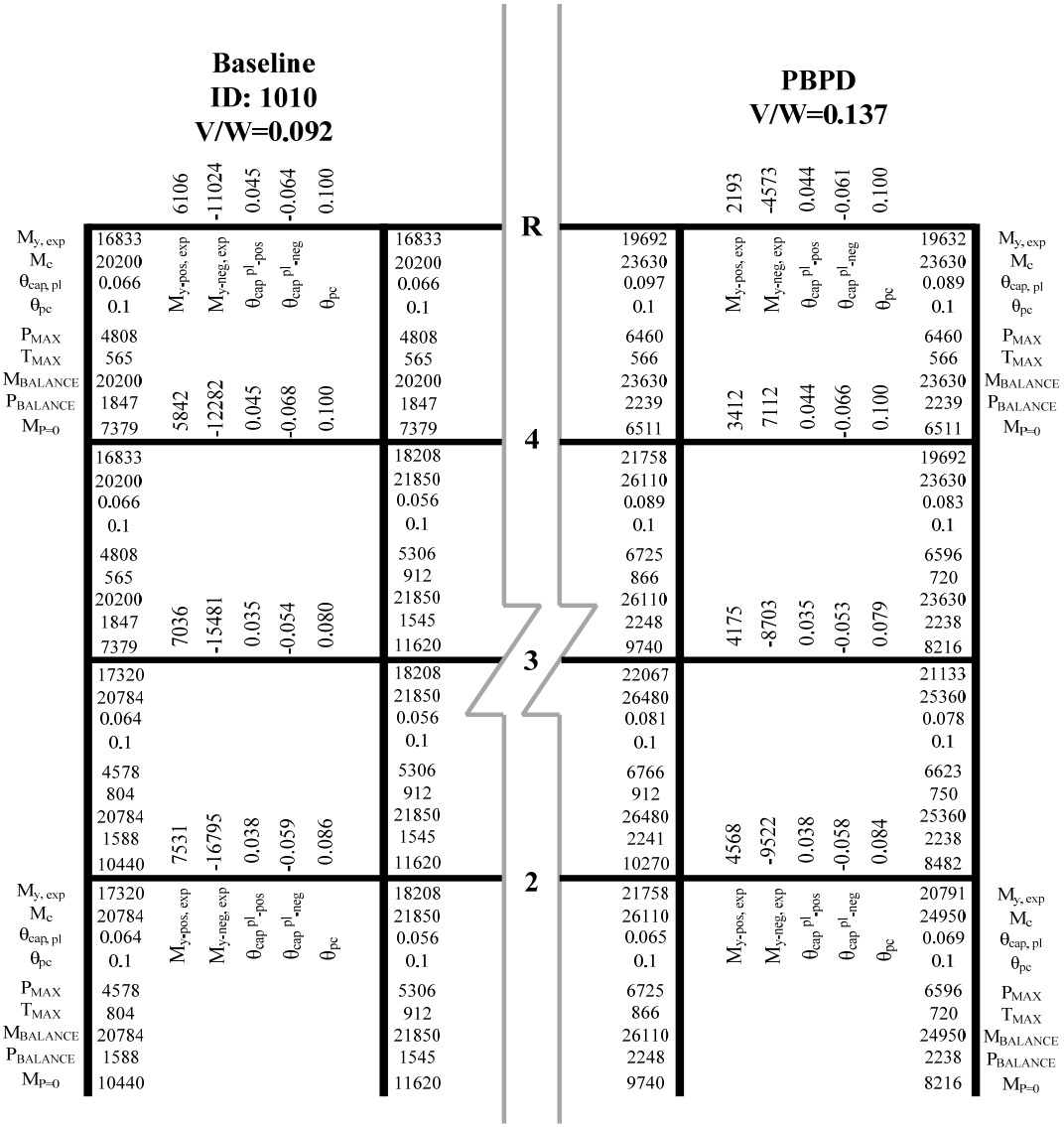

Figure 5-16 Modeling documentation of 4-story baseline and PBPD frames

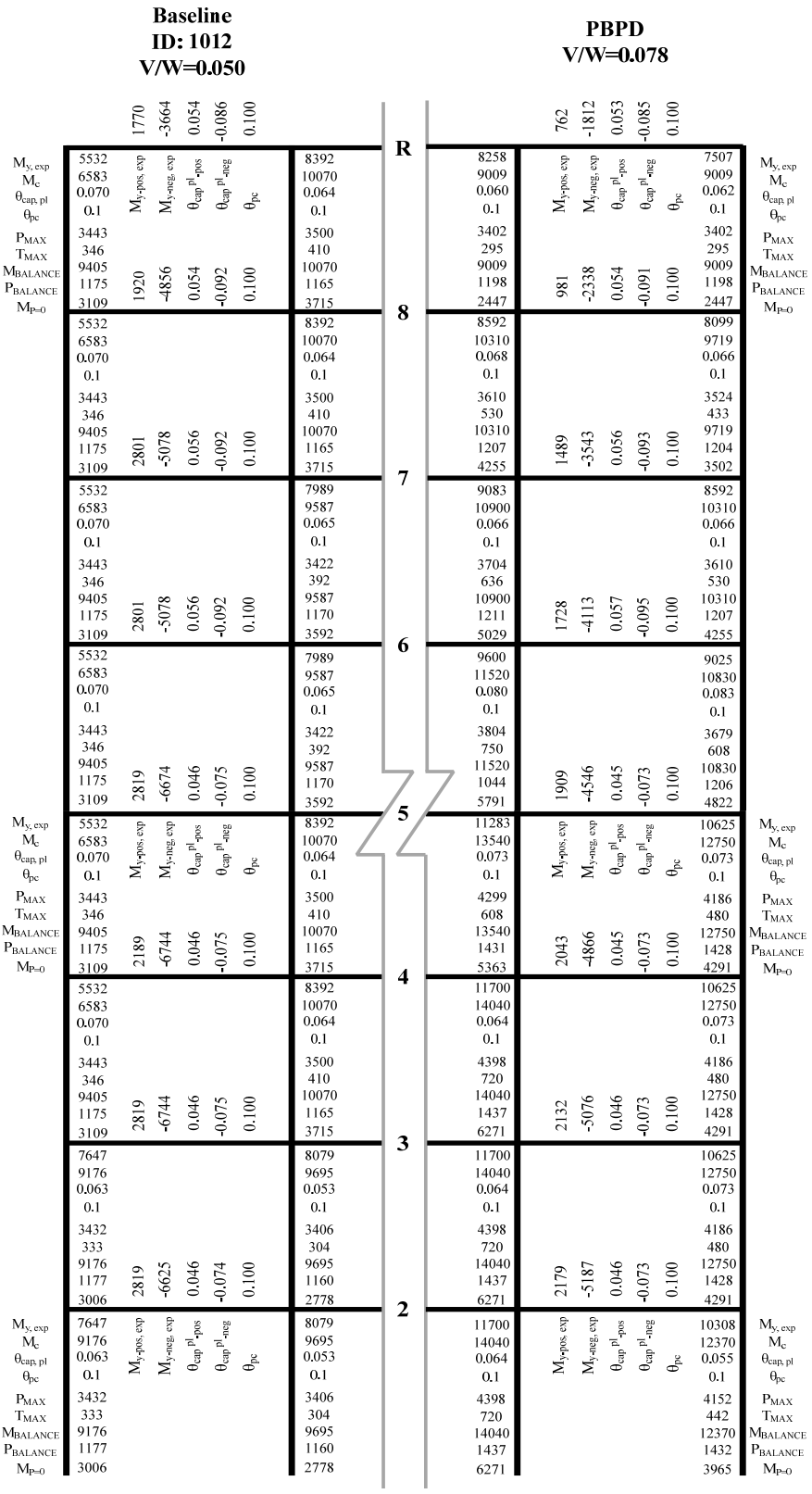

Figure 5-17 Modeling documentation of 8story baseline and PBPD frames

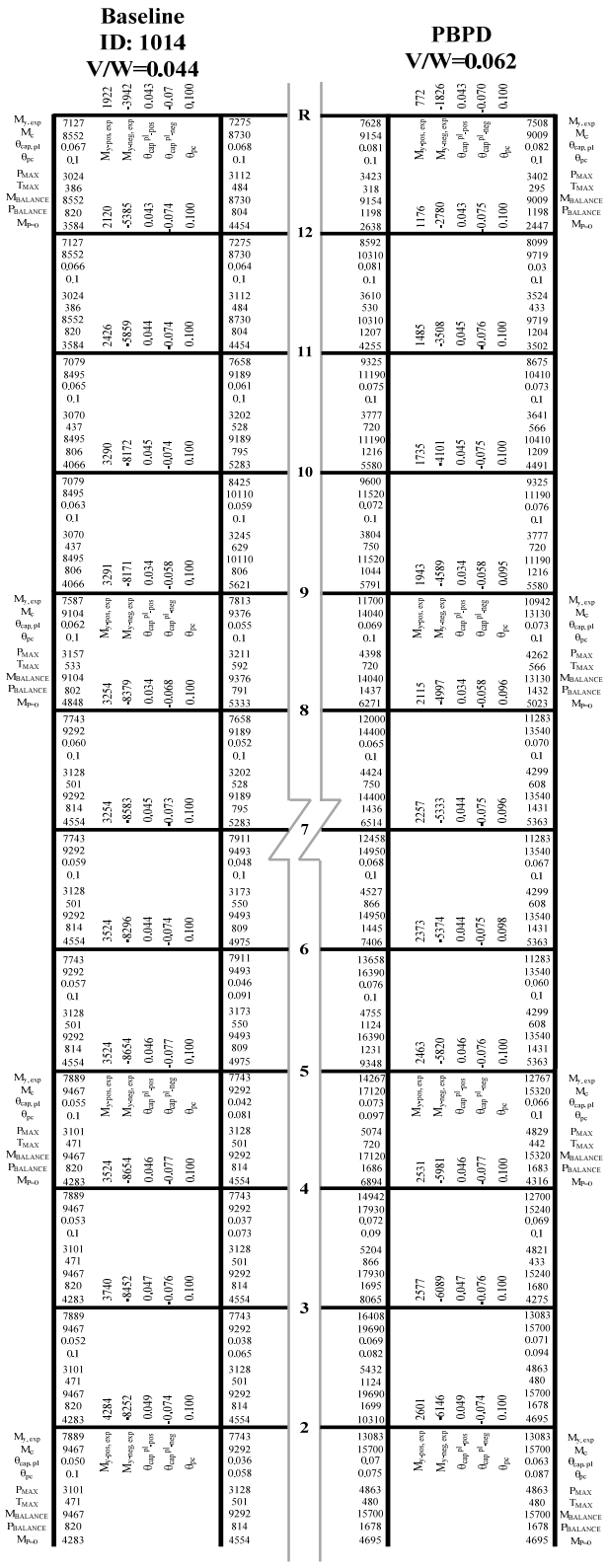

Figure 5-18 Modeling documentation of 12tory baseline and PBPD frames

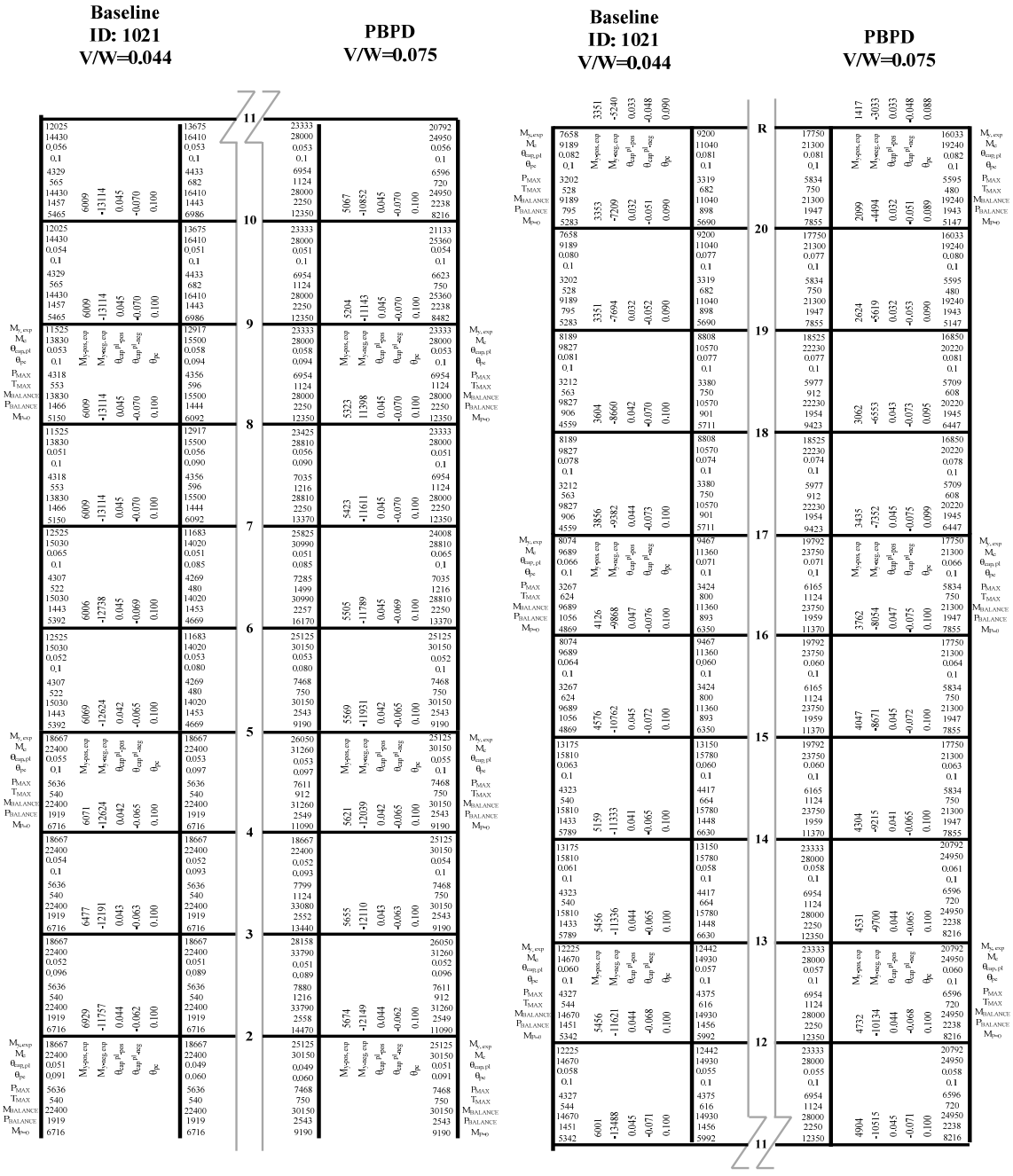

Figure 5-19 Modeling documentation of 20tory baseline and PBPD frames

5.7. Summary and conclusions

The element-level modeling, structure-level modeling and selection of ground motions were presented in reference to FEMA P695 (2009). The computer programs used in this study was discussed as well. It is noted that OpenSees was used in FEMA P695 (2009) instead of PERFORM 3D. Although OpenSees is considered to be more accurate to model the hysteretic characteristics, the nonlinear axial-flexural interaction was not considered in the plastic hinge models used in FEMA P695 (2009). In contrast, axial-flexural interaction has been quite accurately modeled in the formulation of column elements in this study. Thus, all nonlinear analyses in this study were performed by mainly using the PERFORM 3D program.

CHAPTER 6

PERFORMANCE EVALUATION OF STUDY RC SMF

6.1. Introduction

Nonlinear static (pushover) and dynamic (time-history) analyses of the baseline and PBPD frames were carried out by using PERFORM 3D program (CSI, 2007). A lumped "P-Delta column" with pin connections at the floor levels was added which enabled the model to capture the P-Delta effect. Stiffness, strength and cyclic degradation of moment-rotation behavior of plastic hinges were properly modeled to account for the pinched hysteretic behavior as was described in Chapter 5. The results are presented and discussed in this chapter with a view to evaluate the performance of the study frames and to draw some design implications.

6.2. Nonlinear static pushover analyses

6.2.1 Pushover curves

The pushover curves for the 4-story RC SMF in Figure 6-1 show that, PBPD frame presents much higher ductility compared to the baseline frame. Similar observation can also be made for 8, 12 and 20-story frames as shown in Figure 6-2, 6-3 and 6-4, respectively. Moreover, as it can be seen from these pushover plots, the yield drift for RC SMF is quite close to 0.5% which was the assumed for design (Chapter 3).

It is worth mentioning that compared to 8, 12 and 20-story baseline frames, the 4-story baseline frame performed in a more ductile manner, i.e., larger drift capacity before loss

of lateral strength. That is quite reasonable because of lesser influence of P-Delta effect in shorter frames than the taller ones. It is also noted that the 8, 12 and 20-story baseline frames failed before the roof drift reached 3.5%, even though all these taller frame designs were iteratively refined through nonlinear time-history dynamic analyses in order to meet the code specified interstory drift limitation. In contrast, all PBPD frames have about 2 times deformation capacity compared to the baseline frames. This remarkable difference can be attributed to the deformed shapes and location/distribution of plastic hinges as discussed in the following section.

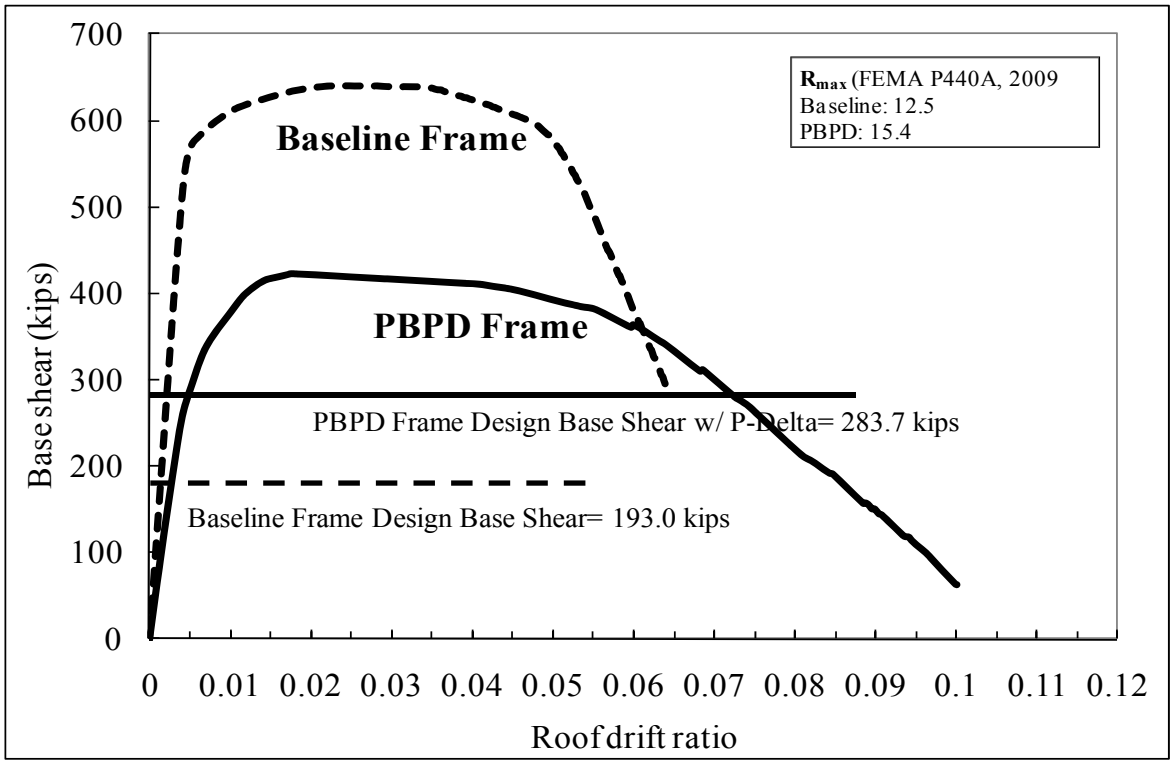

Figure 6-1 Pushover curves of 4-story baseline and PBPD RC SMF

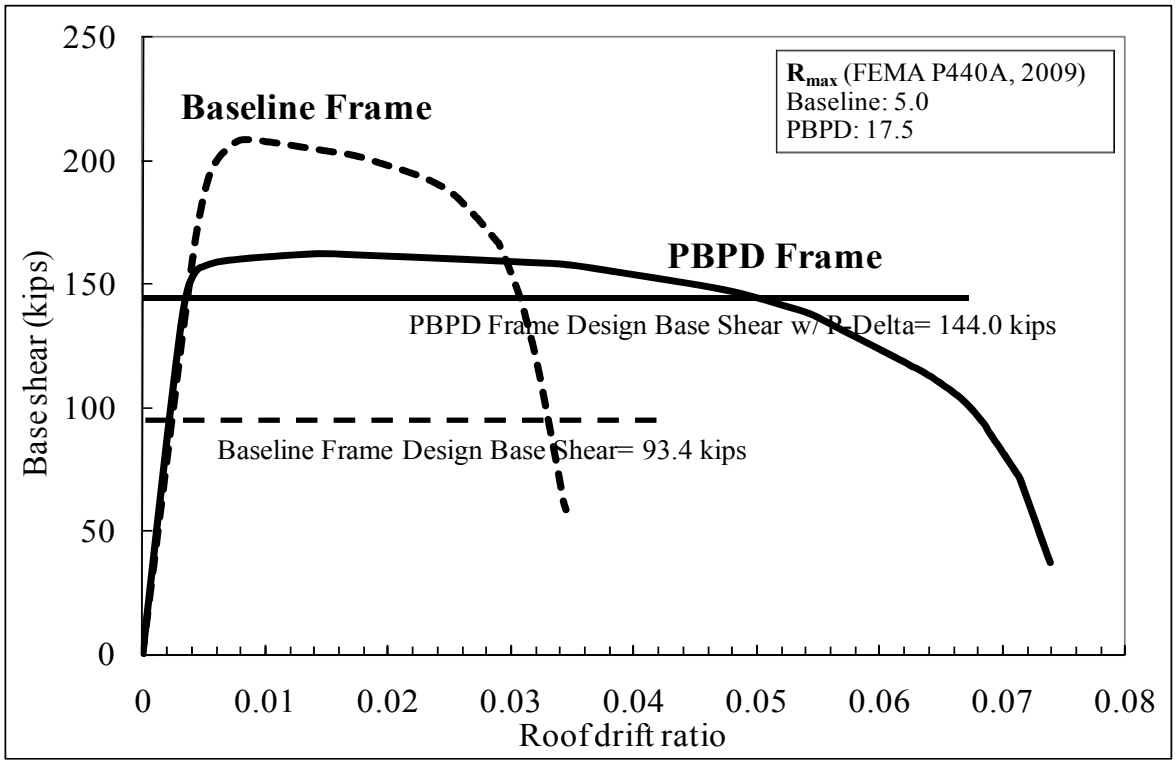

Figure 6-2 Pushover curves of 8-story baseline and PBPD RC SMF

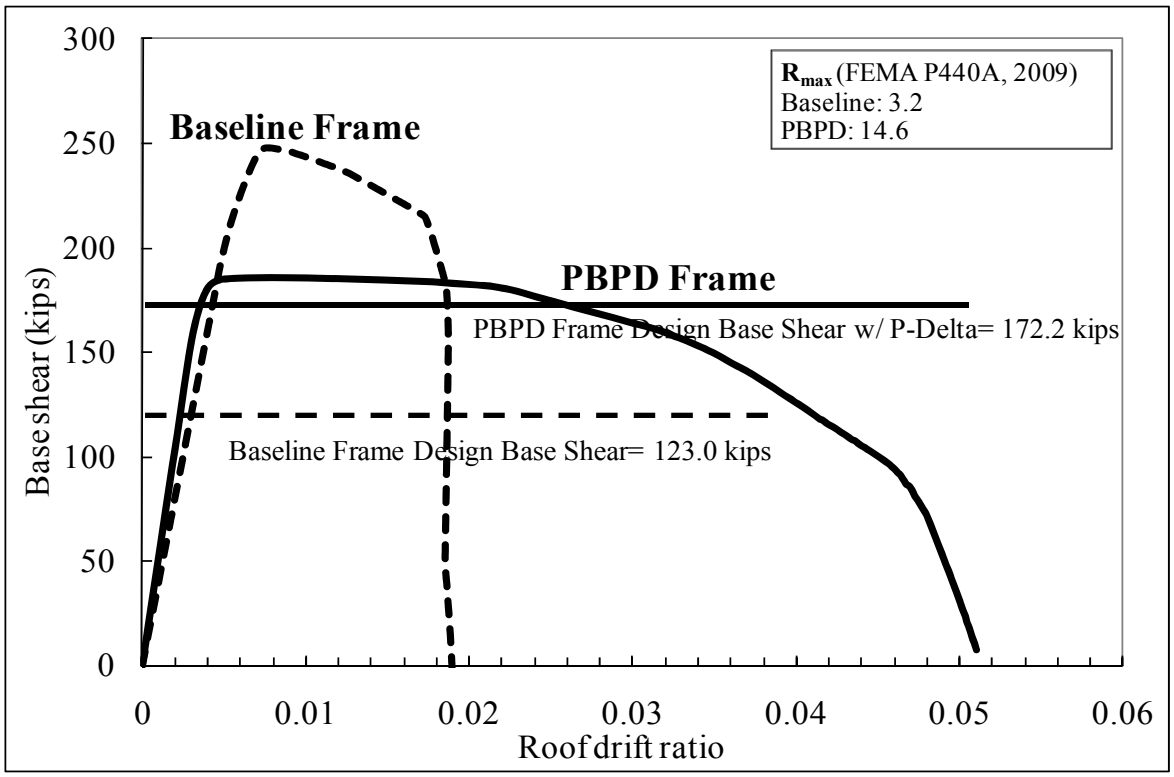

Figure 6-3 Pushover curves of 12-story baseline and PBPD RC SMF

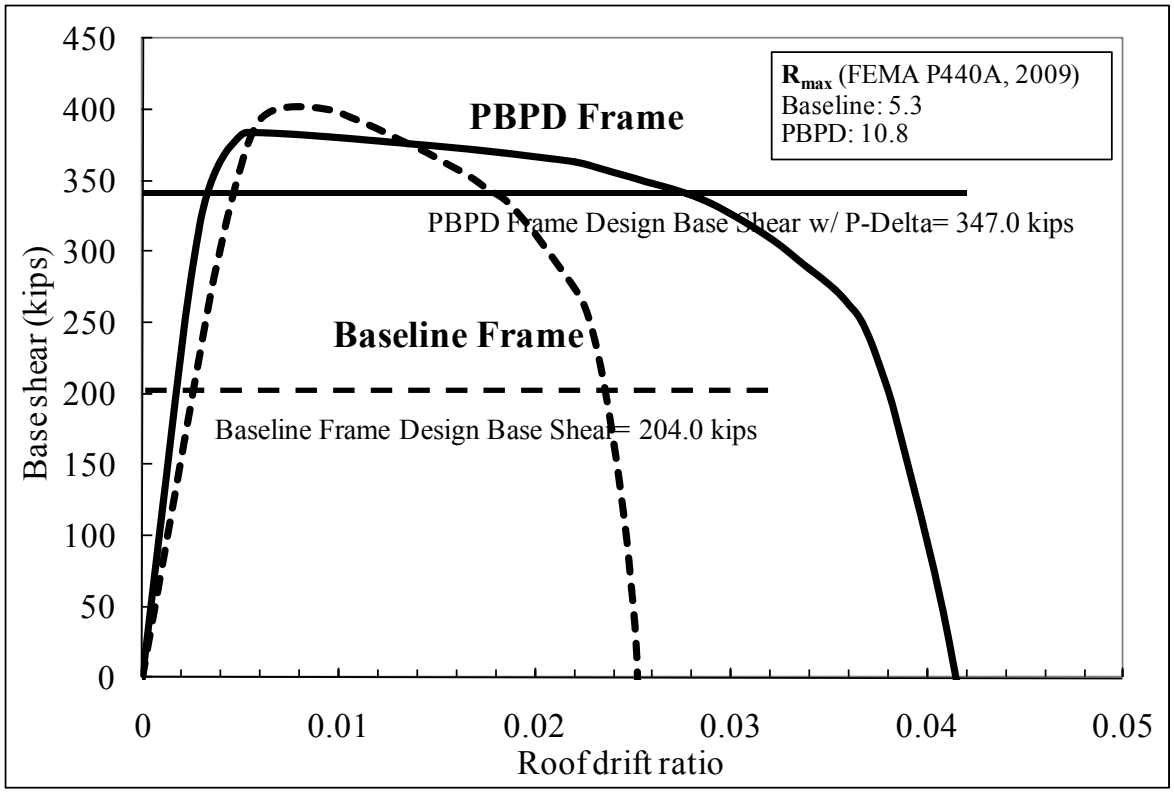

Figure 6-4 Pushover curves of 20-story baseline and PBPD RC SMF

6.2.2 Validation with simulation results in FEMA P695

As noted in Chapter 5, all the simulation work reported in FEMA P695 (2009) was carried out by using OpenSees rather than PERFORM 3D. For validation of the static pushover curves of baseline frames provided in FEMA P695 are compared with those obtained in this study. The pushover curves obtained by using PERFORM 3D (dash line) were superimposed on those obtained by using OpenSees (solid line) as shown in Figure 6-5.

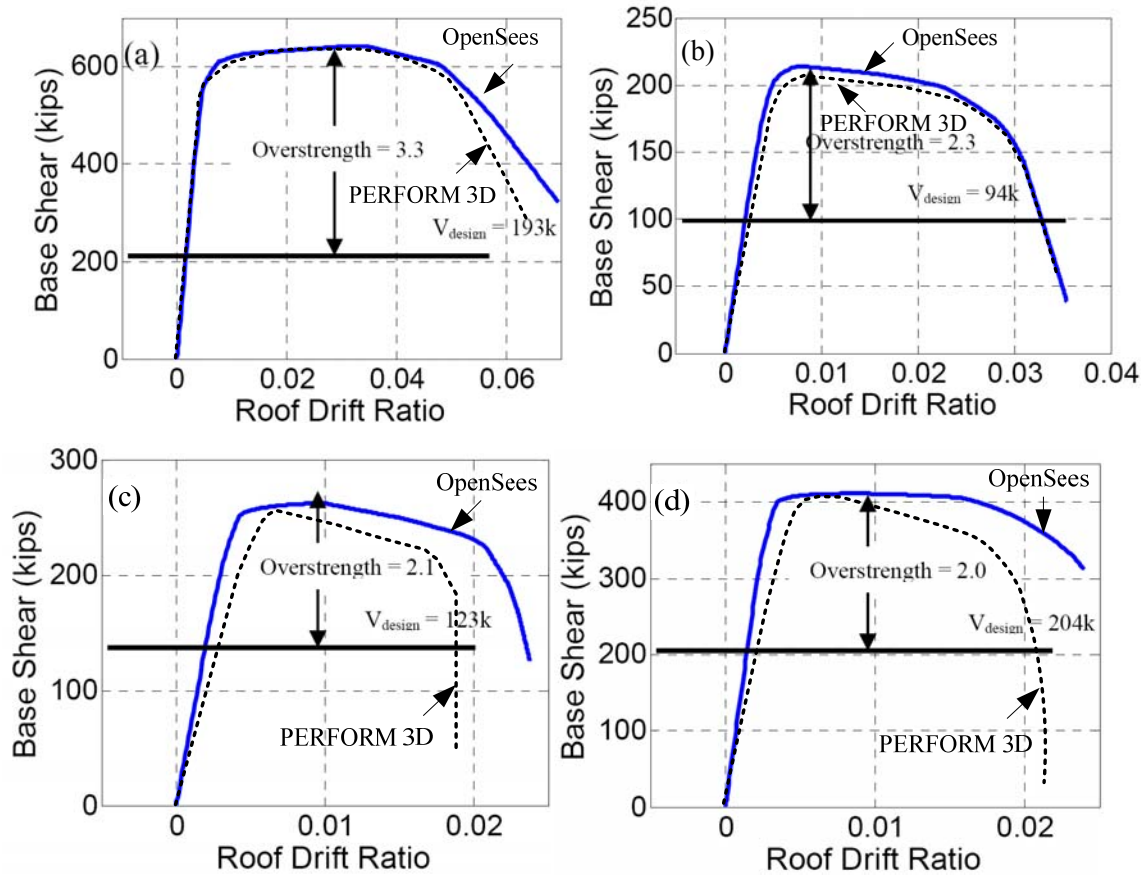

Figure 6-5 Comparisons of pushover curves obtained by OpenSees and PERFORM 3D for (a) 4-story, (b) 8-story, (c) 12-story and (d) 20-story baseline frame

The two pushover curves in each case are seen to be in good agreement as shown in Figure 6-5. Overall, the simulation results obtained by using OpenSees and PERFORM 3D match quite well, particularly for 4 and 8-story frames. The ultimate strengths are almost the same by using the two programs. While obvious divergence can be observed in the tail end of pushover curves for 12 and 20-story frames, this could be due to differences in column plastic hinge model.

As mentioned earlier, no nonlinear axial-flexural interaction was considered in the plastic hinge models by using OpenSees in FEMA P695 (2009) while it was properly considered and modeled in PERFORM 3D in this study. The taller the frame, higher

additional axial loading due to overturning will be, which leads to severe strength loss as the roof drift increases.

6.2.3 Deformed shape and location of yield activity

Figure 6-6 shows the deformed shape and location of plastic hinges of the baseline and PBPD frames at 4%, 3%, 2% and 2.5% roof drift under pushover, for the 4, 8, 12, 20-story frames, respectively. It can be said that formation of plastic hinges in the columns, large plastic hinge rotations, and story mechanism in the lower part of the baseline frames resulted in complete loss of strength at much smaller roof drifts than the corresponding PBPD frames.

As mentioned in Chapter 4, column designs of baseline frames were all governed by SCWB provision. The results show that the soft story mechanisms still formed even though all baseline frames had higher SCWB value of 1.3 instead of 1.2 as required in ACI 318 (2008). This implies that determination of column strength according to current SCWB provision is not only time consuming, i.e., checking every single joint one by one, but it does not safeguard against flexural yielding.

On the other hand, the concept of "column tree" as used in the PBPD method for column design considers the equilibrium of the entire column from top to bottom in the limit state. It gives a very good estimation of maximum column moment demands when the structures respond to severe ground motions and deform up to the extreme limit condition. It can be seen that in PBPD frames all yielding occurred at the intended locations only. There are no unintended plastic hinges in the columns of the PBPD frame, resulting in more favorable deformed shape and yield pattern as intended in the design process.

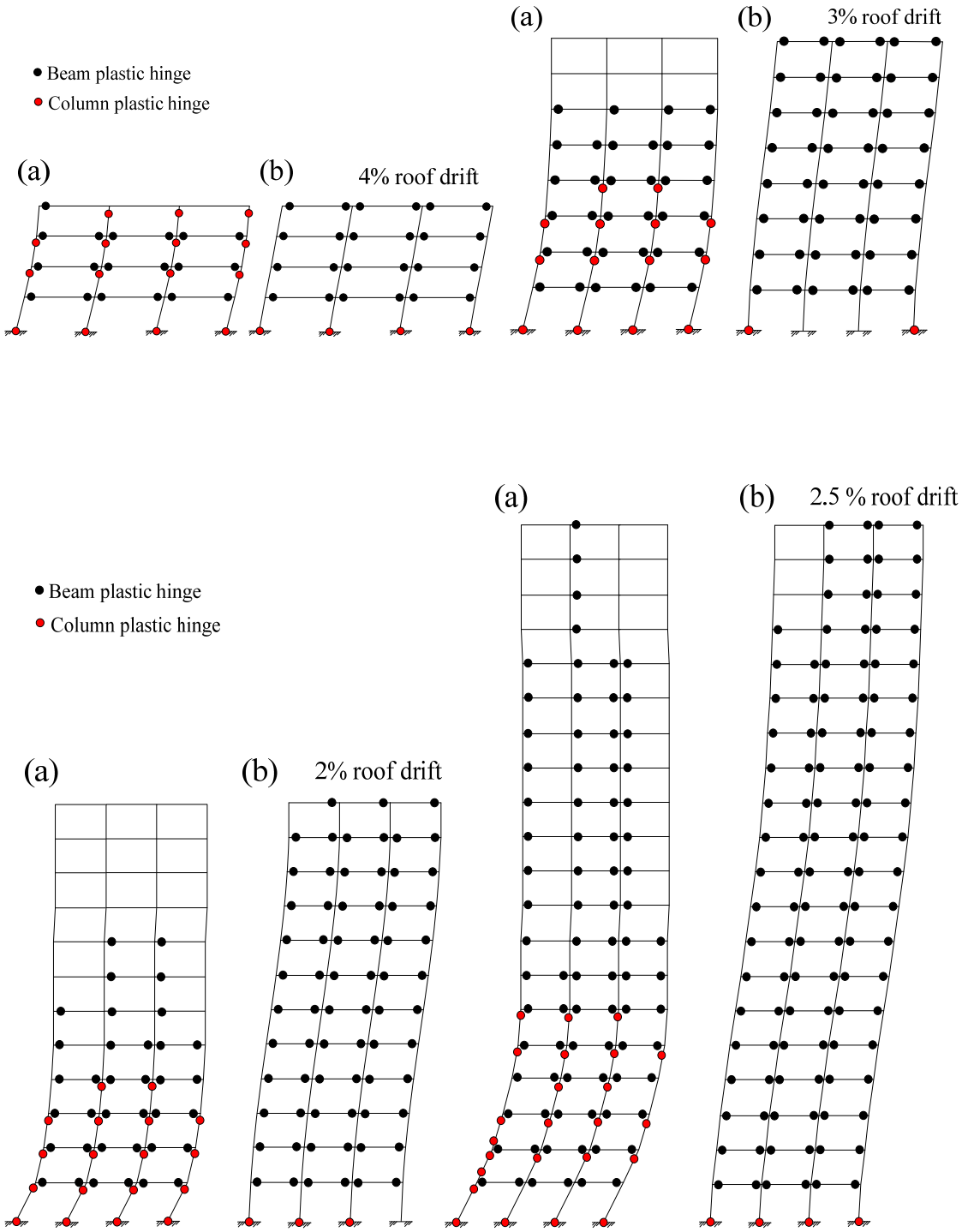

Figure 6-6 Deformed shapes and plastic hinge locations of 4, 8, 12 and 20-story for (a) baseline and (b) PBPD RC SMF under static pushover analysis.

6.2.4 Plastic rotation demands and capacities

Tables 6-1 to 6-4 summarize the plastic rotation demands and capacities of beams in the baseline and PBPD frames at 4%, 3%, 2% and 2.5% roof drift under pushover, for the 4, 8, 12, 20-story frames, respectively. In general, the plastic rotation demands in the PBPD frames are lower than the respective capacities below the capping point, $\theta_{cap,pl}$, indicating no significant strength decay in the PBPD frames. It can be also observed that the plastic rotation demands in PBPD frames are quite uniform along the height. On the other hand, the plastic rotation demands in the baseline frames are mostly concentrated in the lower stories, especially for the taller frames. In the case of 20-story frame, the plastic rotation demands from 2nd to 16th stories are about 1% to 4.5% for the PBPD frame; whereas for the baseline frame all plastic rotations are concentrated at the 2nd to 7th floor. The rotation demands at the 2nd floor are even more than 14%.

Table 6-1 Plastic rotation demands and capacities (in radians) of beams at 4% roof drift under pushover analysis of 4-story baseline and PBPD SMF

	Baseline Frame					PBPD Frame				
	Demand		Capacity			Demand		Capacity		
	End i (+)	End j (-)	$\theta_{cap,pl}$ (+)	$\theta_{cap,pl}$ (-)	θ_{pc}	End i (+)	End j (-)	$\theta_{cap,pl}$ (+)	$\theta_{cap,pl}$ (-)	θ_{pc}
Floor	0.012	0.000	0.045	0.064	0.100	0.029	0.045	0.044	0.061	0.100
4	0.022	0.023	0.045	0.068	0.100	0.032	0.044	0.044	0.066	0.100
3	0.043	0.040	0.035	0.054	0.080	0.041	0.045	0.035	0.053	0.079
2	0.057	0.053	0.038	0.059	0.086	0.039	0.043	0.038	0.058	0.084

Table 6-2 Plastic rotation demands and capacities (in radians) of beams at 3% roof drift under pushover analysis of 8-story baseline and PBPD SMF

	Baseline Frame					PBPD Frame				
	Demand		Capacity			Demand		Capacity		
	End i (+)	End j (-)	$\theta_{cap,pl}$ (+)	$\theta_{cap,pl}$ (-)	θ_{pc}	End i (+)	End j (-)	$\theta_{cap,pl}$ (+)	$\theta_{cap,pl}$ (-)	θ_{pc}
Floor	0.000	0.000	0.054	0.086	0.100	0.023	0.027	0.053	0.085	0.100
8	0.000	0.000	0.054	0.092	0.100	0.028	0.032	0.054	0.091	0.100
7	0.002	0.001	0.056	0.092	0.100	0.032	0.034	0.056	0.093	0.100
6	0.008	0.007	0.056	0.092	0.100	0.036	0.036	0.057	0.095	0.100
5	0.015	0.013	0.046	0.075	0.100	0.038	0.039	0.045	0.073	0.100
4	0.027	0.026	0.046	0.075	0.100	0.036	0.036	0.045	0.073	0.100
3	0.046	0.044	0.046	0.075	0.100	0.030	0.030	0.046	0.073	0.100
2	0.077	0.073	0.046	0.074	0.100	0.020	0.019	0.046	0.073	0.100

Table 6-3 Plastic rotation demands and capacities (in radians) of beams at 2% roof drift under pushover analysis of 12-story baseline and PBPD SMF

	Baseline Frame					PBPD Frame				
	Demand		Capacity			Demand		Capacity		
	End i (+)	End j (-)	$\theta_{cap,pl}$ (+)	$\theta_{cap,pl}$ (-)	θ_{pc}	End i (+)	End j (-)	$\theta_{cap,pl}$ (+)	$\theta_{cap,pl}$ (-)	θ_{pc}
Floor	0.000	0.000	0.043	0.070	0.100	0.000	0.004	0.043	0.070	0.100
12	0.000	0.000	0.043	0.074	0.100	0.002	0.006	0.043	0.075	0.100
11	0.000	0.000	0.044	0.074	0.100	0.007	0.009	0.045	0.076	0.100
10	0.000	0.000	0.045	0.074	0.100	0.014	0.015	0.045	0.075	0.100
9	0.001	0.000	0.034	0.058	0.096	0.024	0.024	0.034	0.058	0.095
8	0.002	0.000	0.034	0.058	0.096	0.028	0.027	0.034	0.058	0.096
7	0.003	0.000	0.044	0.073	0.100	0.031	0.029	0.044	0.073	0.096
6	0.005	0.001	0.044	0.074	0.100	0.031	0.029	0.044	0.075	0.098
5	0.010	0.006	0.046	0.077	0.100	0.029	0.027	0.046	0.076	0.100
4	0.023	0.018	0.046	0.077	0.100	0.025	0.023	0.046	0.077	0.100
3	0.038	0.034	0.047	0.076	0.100	0.019	0.017	0.047	0.076	0.100
2	0.057	0.054	0.049	0.074	0.100	0.012	0.010	0.049	0.074	0.100

Table 6-4 Plastic rotation demands and capacities (in radians) of beams at 2.5% roof drift under pushover analysis of 20-story baseline and PBPD SMF

	Baseline Frame					PBPD Frame				
	Demand		Capacity			Demand		Capacity		
	End i (+)	End j (-)	$\theta_{cap,pl}$ (+)	$\theta_{cap,pl}$ (-)	θ_{pc}	End i (+)	End j (-)	$\theta_{cap,pl}$ (+)	$\theta_{cap,pl}$ (-)	θ_{pc}
Floor	0.000	0.000	0.033	0.048	0.090	0.005	0.004	0.033	0.048	0.088
20	0.002	0.000	0.032	0.051	0.090	0.006	0.005	0.032	0.051	0.089
19	0.002	0.000	0.032	0.052	0.090	0.006	0.005	0.032	0.053	0.090
18	0.003	0.000	0.042	0.070	0.100	0.007	0.006	0.043	0.072	0.095
17	0.003	0.000	0.044	0.073	0.100	0.008	0.008	0.045	0.075	0.099
16	0.004	0.001	0.047	0.076	0.100	0.011	0.010	0.047	0.075	0.100
15	0.004	0.001	0.045	0.072	0.100	0.015	0.014	0.045	0.072	0.100
14	0.004	0.001	0.041	0.065	0.100	0.020	0.019	0.041	0.065	0.100
13	0.004	0.001	0.044	0.067	0.100	0.025	0.023	0.044	0.067	0.100
12	0.004	0.002	0.044	0.068	0.100	0.030	0.028	0.044	0.068	0.100
11	0.004	0.001	0.045	0.071	0.100	0.035	0.033	0.045	0.071	0.100
10	0.004	0.002	0.045	0.070	0.100	0.039	0.038	0.045	0.070	0.100
9	0.005	0.003	0.045	0.070	0.100	0.043	0.041	0.045	0.070	0.100
8	0.008	0.006	0.045	0.070	0.100	0.045	0.044	0.045	0.070	0.100
7	0.012	0.011	0.045	0.070	0.100	0.046	0.044	0.045	0.070	0.100
6	0.023	0.024	0.045	0.069	0.100	0.046	0.044	0.045	0.069	0.100
5	0.064	0.062	0.042	0.065	0.100	0.044	0.042	0.042	0.065	0.100
4	0.076	0.075	0.042	0.065	0.100	0.039	0.038	0.042	0.065	0.100
3	0.101	0.103	0.043	0.063	0.100	0.033	0.032	0.043	0.063	0.100
2	0.147	0.148	0.044	0.062	0.100	0.025	0.024	0.044	0.062	0.100

6.2.5 Static overstrength

All pushover curves in Figure 6-1 to Figure 6-4 show that even though the design base shear for each baseline frame is smaller than that of the corresponding PBPD frame, the ultimate strength of the baseline frame is higher than that of the corresponding PBPD frame. That is mainly due to the fact that the design of the baseline frame was governed by drift which required major revision of the member sizes after having been designed for strength. That iteration step is not needed in the PBPD method. The static overstrength ratio of ultimate strength to design base shear for all frames are summarized in Table 6-5.

Table 6-5 Static overstrength

	4-story	8-story	12-story	20-story
Baseline frame	3.3	2.3	2.1	2.0
PBPD frame	1.4	1.1	1.1	1.1

6.2.6 R_{max} factor

The concept of minimum strength factor to avoid dynamic instability, $R_{\max}$, was originally proposed in FEMA 440 (2006). In FEMA P440A (2009), the expression for $R_{\max}$ has been improved by using the database of results from the focused analytical studies. This improved expression for $R_{\max}$ was recommended for inclusion in ASCE/SEI 41-06 procedures for nonlinear static analysis. If this minimum strength requirement is not met, the system of interest is subject to potential dynamic instability, and a nonlinear dynamic analysis including component strength degradation is required for further evaluation (FEMA P440A, 2009).

The value of R_{max} can be calculated based on the characteristics of the idealized static pushover plot as shown in Figure 6-7, where T_e is the effective fundamental period and f has a the constant value of 4 for structures with stiffness degradation.

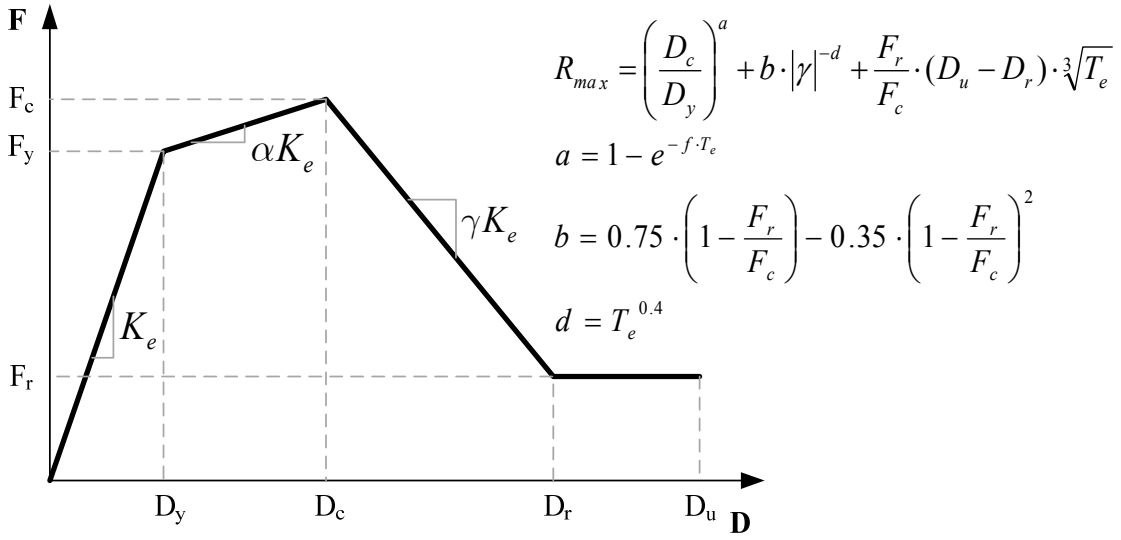

Figure 6-7 Force-displacement capacity boundary parameters for use with revised equation to determine R_{max}

Even though there are still some debate regarding the validity of R_{max}, it is still useful for preliminary performance evaluation purposes. Calculated values of R_{max} for the baseline and PBPD frames are listed in Table 6-6, which reflect much enhanced margin against dynamic instability (collapse) of PBPD frame over the baseline frames.

Table 6-6 R_{max} for the baseline and PBPD RC SMF

	4-story	8-story	12-story	20-story
Baseline frame	12.5	5.0	3.2	5.3
PBPD frame	15.4	17.5	14.6	10.8

6.3. Nonlinear time history dynamic analyses

6.3.1 Maximum interstory drifts

Figure 6-8 shows comparison of maximum interstory drifts of the baseline and PBPD frames obtained from time-history analyses using appropriately scaled ground motion records representative of 2/3 MCE and MCE hazard levels. For clarity and brevity only the mean values of maximum interstory drifts are shown in Figure 6-9. Other detailed maximum interstory drifts of every subjected ground motion for all frames are shown in Figure 6-10 to 6-12.

The results show that the mean maximum interstory drifts of the PBPD frames are well within the corresponding target values, i.e., 2% for 2/3 MCE and 3% for MCE. Moreover, the story drifts of the PBPD frames are more evenly distributed over the height as compared with those of the baseline frames where undesirable "softness" in the lower stories is evident, which is caused mainly by plastic hinges in the columns. Formation of plastic hinges in the columns and story mechanism in the lower part of the baseline frames can be clearly noticed. In contrast, there are no unintended plastic hinges in the columns of the PBPD frame, resulting in more favorable deformed shape and yield pattern.

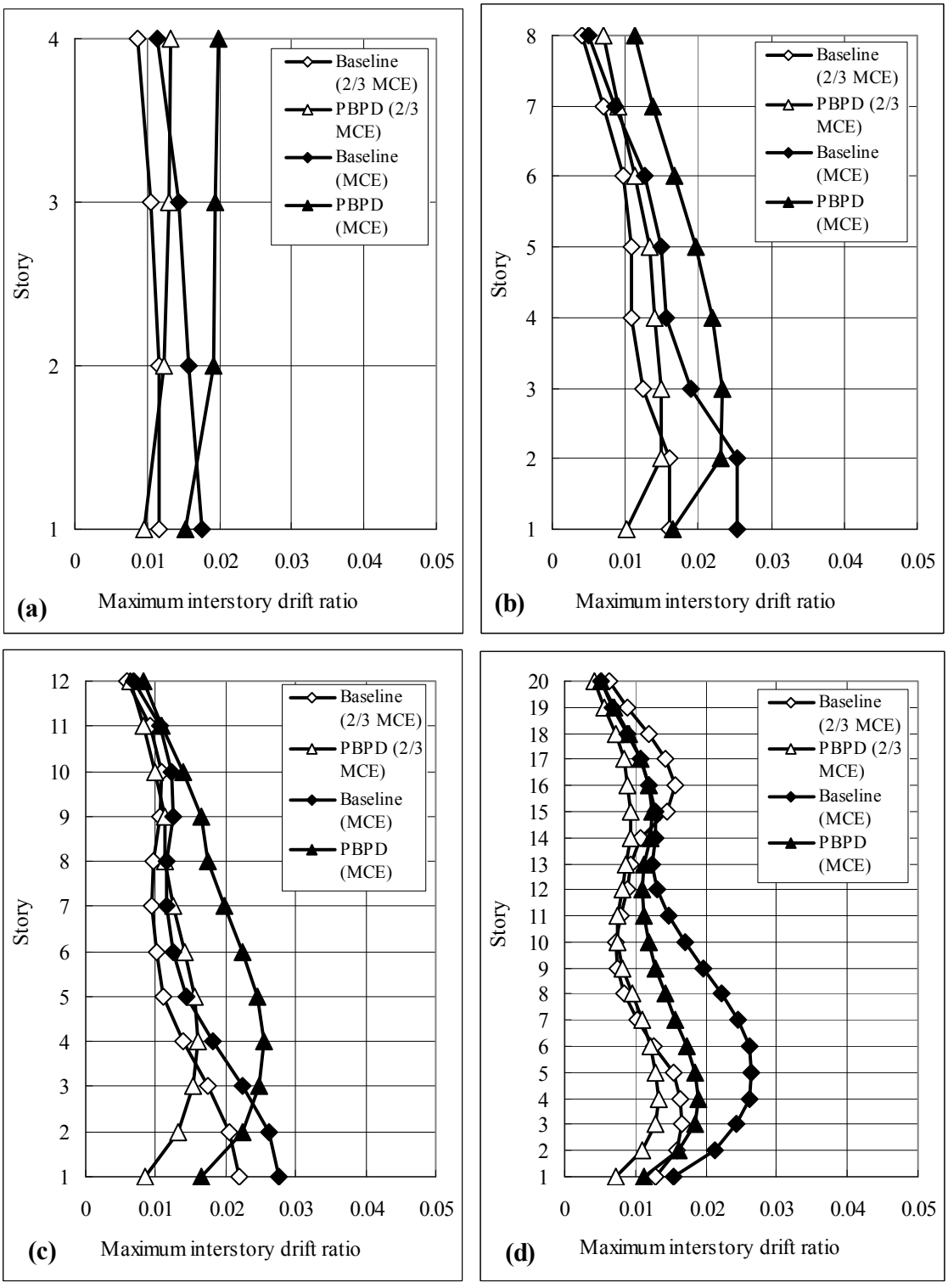

Figure 6-8 Comparison of maximum interstory drifts from time-history analyses of baseline and PBPD frames for 2/3 MCE and MCE hazard levels (a) 4-story, (b) 8-story, (c) 12-story and (d) 20-story.

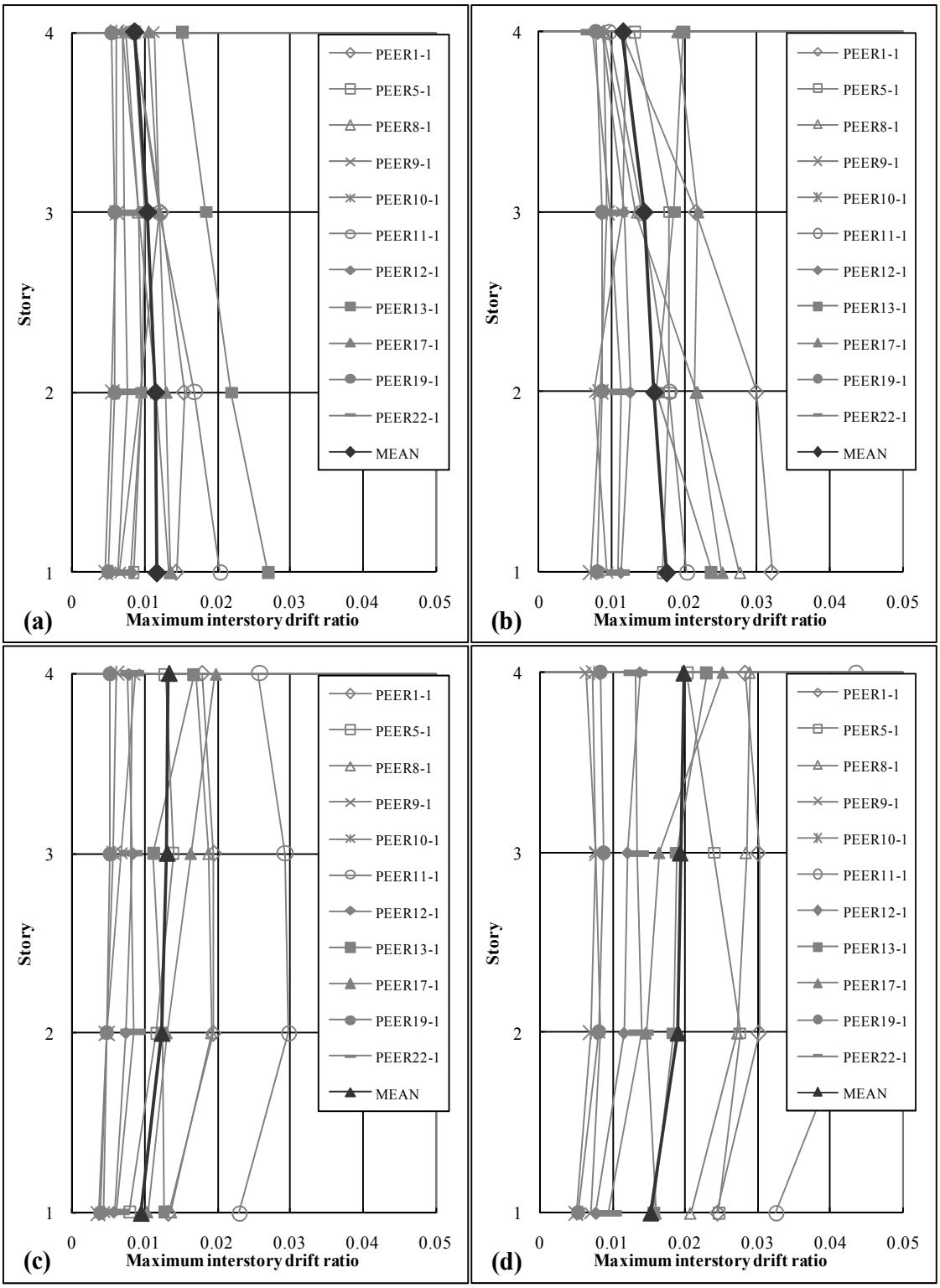

Figure 6-9 4-story RC SMF: comparison of maximum interstory drifts by time-history analyses (a) baseline for 2/3 MCE (b) baseline for MCE (c) PBPD for 2/3 MCE and (d) PBPD for MCE hazard level

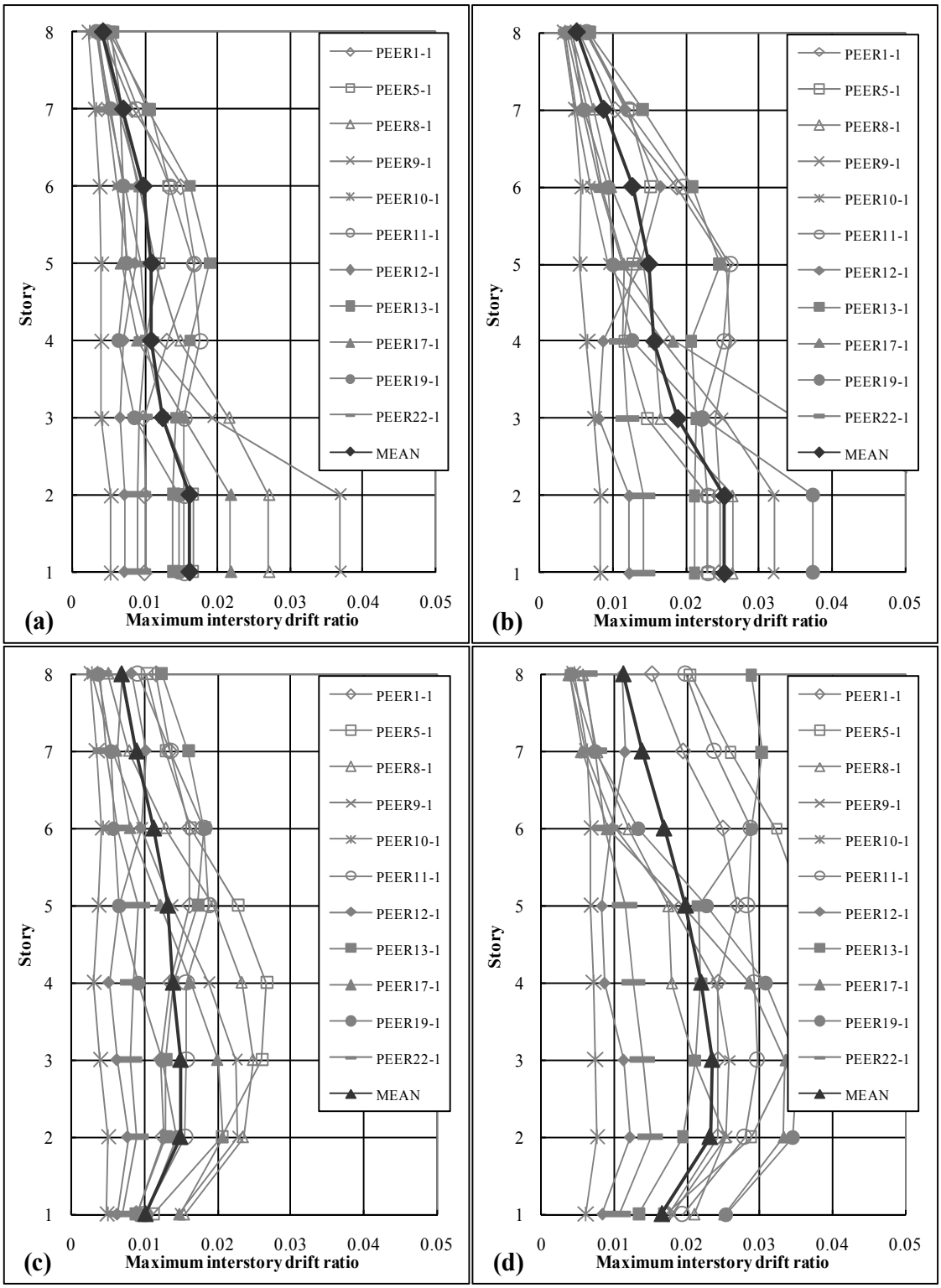

Figure 6-10 8-story RC SMF: comparison of maximum interstory drifts by time-history analyses (a) baseline for 2/3 MCE (b) baseline for MCE (c) PBPD for 2/3 MCE and (d) PBPD for MCE hazard level

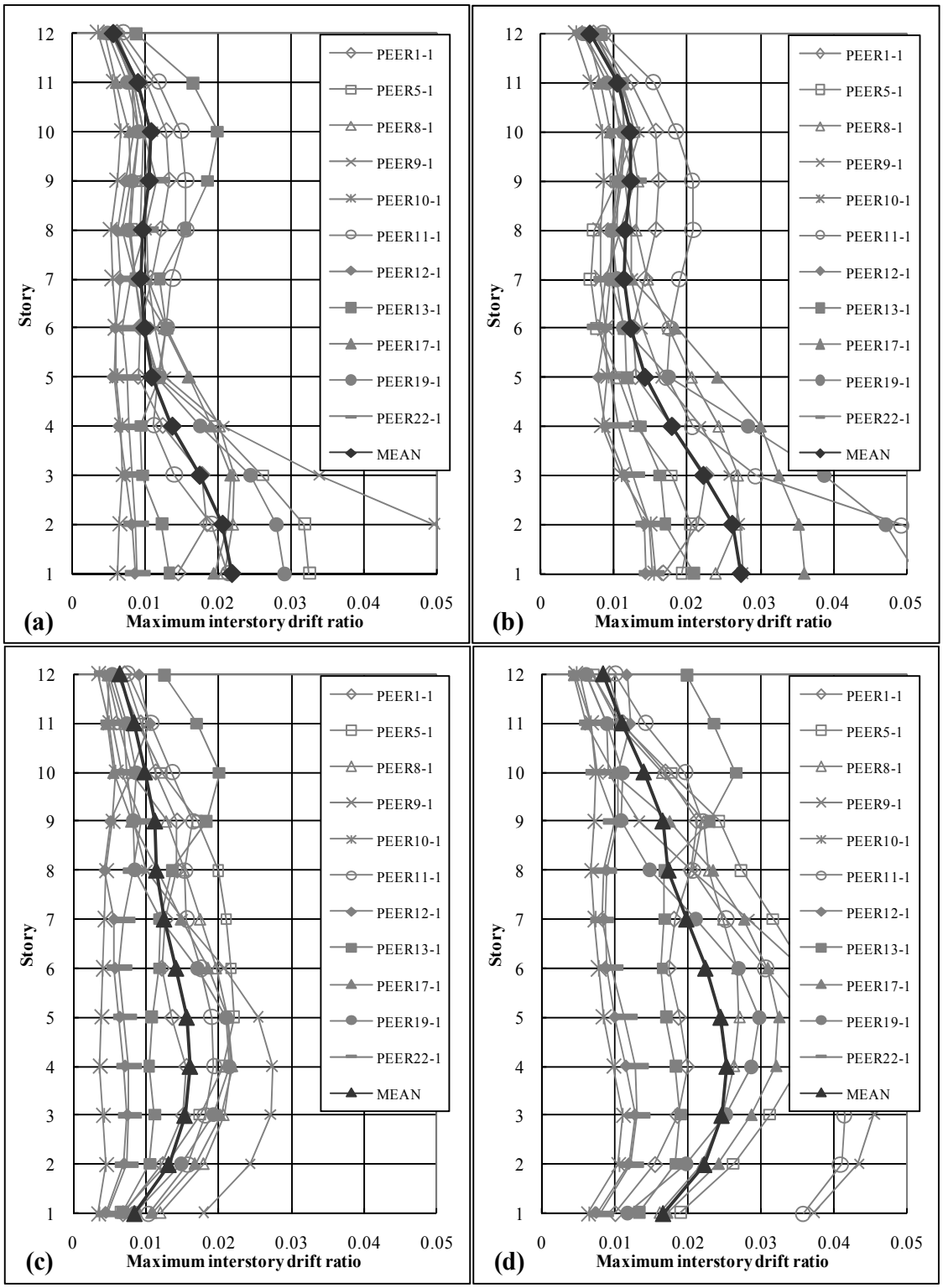

Figure 6-11 12-story RC SMF: comparison of maximum interstory drifts by time-history analyses (a) baseline for 2/3 MCE (b) baseline for MCE (c) PBPD for 2/3 MCE and (d) PBPD for MCE hazard level

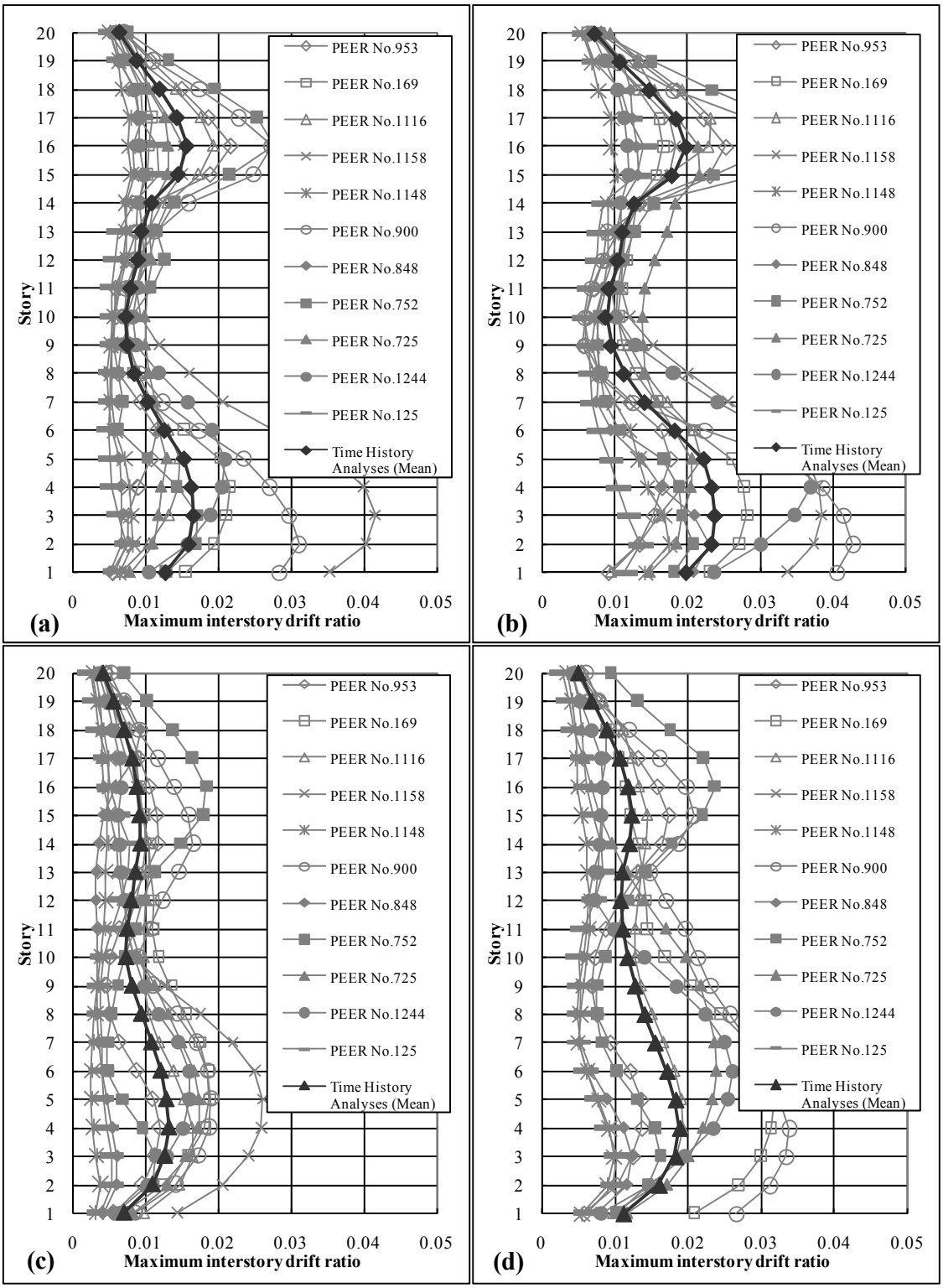

Figure 6-12 20-story RC SMF : comparison of maximum interstory drifts by time-history analyses (a) baseline for 2/3 MCE (b) baseline for MCE (c) PBPD for 2/3 MCE and (d) PBPD for MCE hazard levels

6.3.2 Deformed shape and location of yield activity

Figures 6-13 to 6-16 show the deformed shapes and plastic rotation demands at maximum roof drift under selected 2/50 ground motions from the time history analyses for the 4, 8, 12, 20-story baseline and PBPD frames, respectively. It can be observed that no plastic hinges formed in the columns of the PBPD frames except at the base as intended in design. In contrast, significant plastic hinging occurred in the lower story columns of the baseline frames, leading to soft story formations in those regions and concentration of story drifts. Nevertheless, the plastic rotation demands in the columns are generally smaller than those in the beams. It should also be noted that the story drifts and plastic rotation demands in the beams of PBPD frames are more uniform along the height than those of corresponding baseline frames.

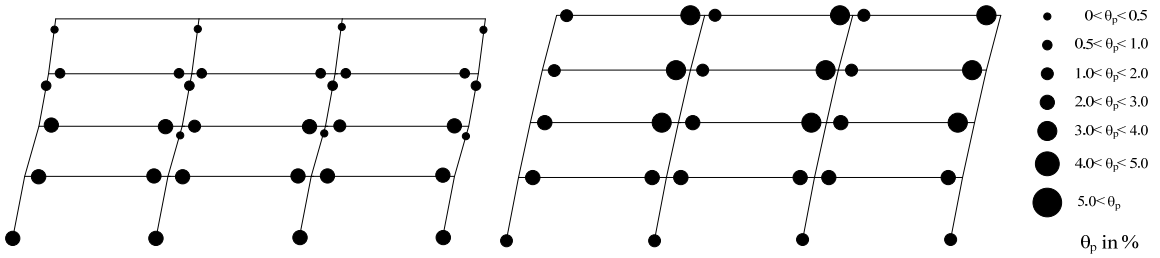

Figure 6-13 Plastic hinge distributions for 4-story (a) Baseline (b) PBPD frames under PEER 1-1 ground motion

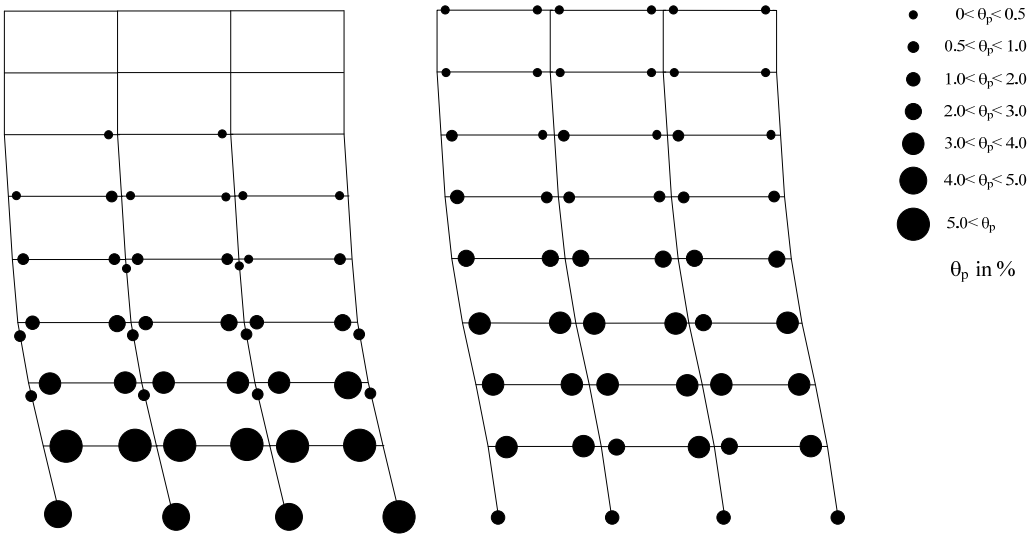

Figure 6-14 Plastic hinge distributions for 8-story (a) Baseline (b) PBPD frames under PEER 17-1 ground motion

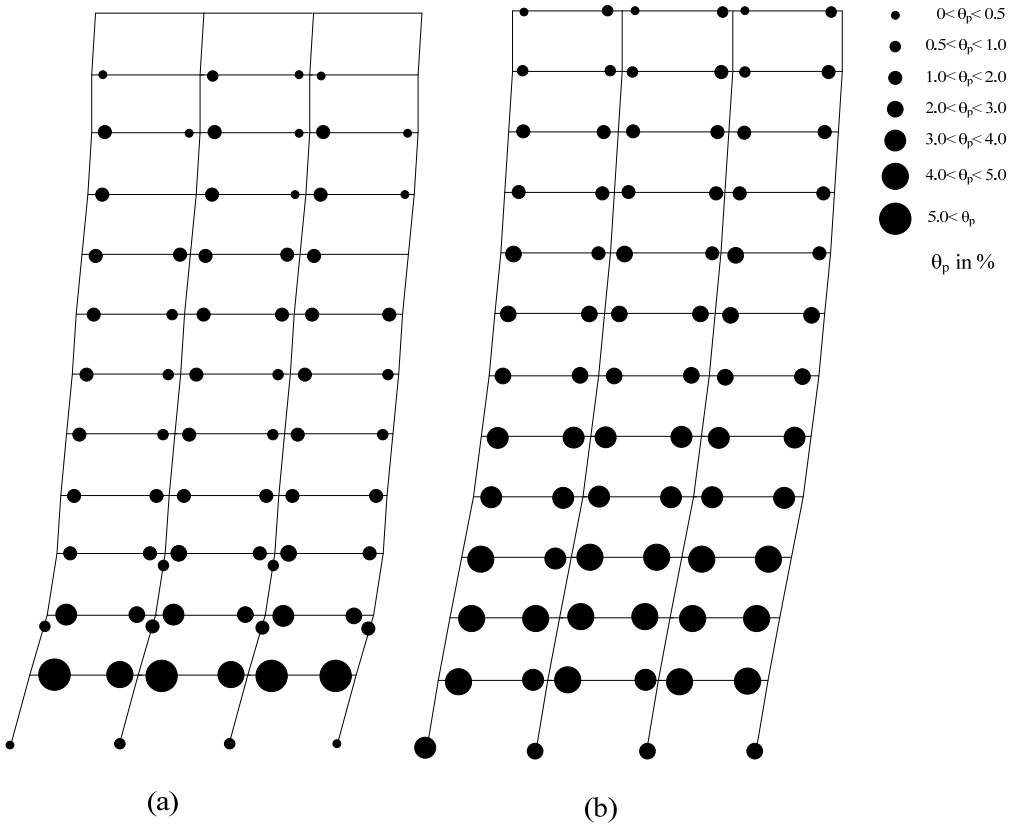

Figure 6-15 Plastic hinge distributions for 12-story (a) Baseline (b) PBPD frames under PEER 11-1 ground motion

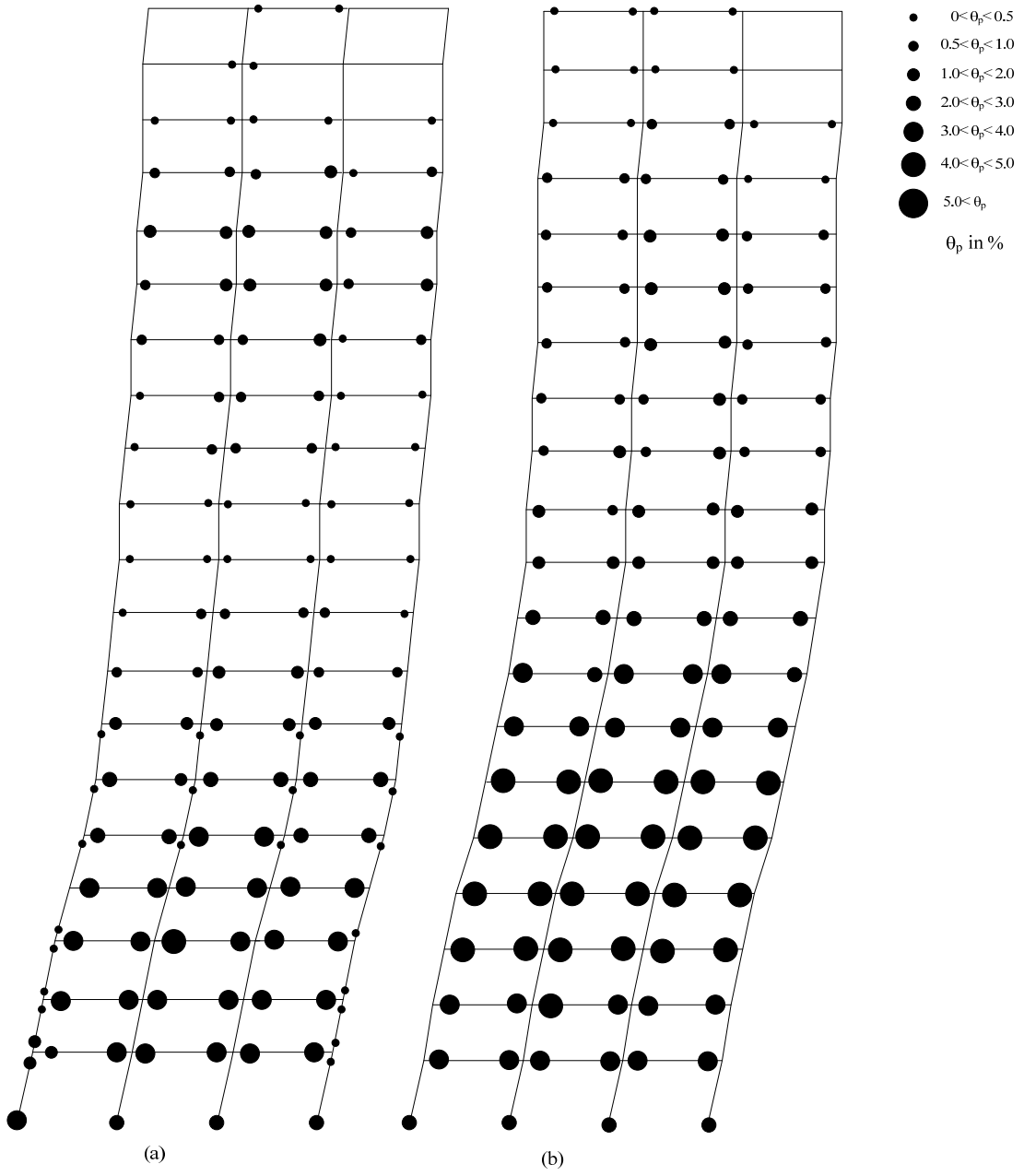

Figure 6-16 Plastic hinge distributions for 20-story (a) Baseline (b) PBPD frames under PEER 9-1 ground motion

6.3.3 Maximum relative story shear distributions

As noted earlier, using a realistic force distribution based on inelastic response is one of the important steps in a comprehensive seismic design methodology. The maximum relative story shear distributions were obtained by extensive nonlinear dynamic analyses. It can be seen in Figure 6-17 to Figure 6-20 that the PBPD lateral force distribution has excellent agreement with maximum relative story shear distributions obtained from time history analyses for the baseline as well as PBPD frames, particularly for taller frames. On the contrary, maximum story shear distributions as given in the codes, which are based on first-mode elastic behavior, deviate significantly from the time-history dynamic analysis results. Higher mode effects are also well reflected in the PBPD design lateral force distribution

Additionally, as discussed earlier, frames designed by using the PBPD lateral force distribution experienced more uniform maximum interstory drifts along the height than the frames designed by using current code distributions.

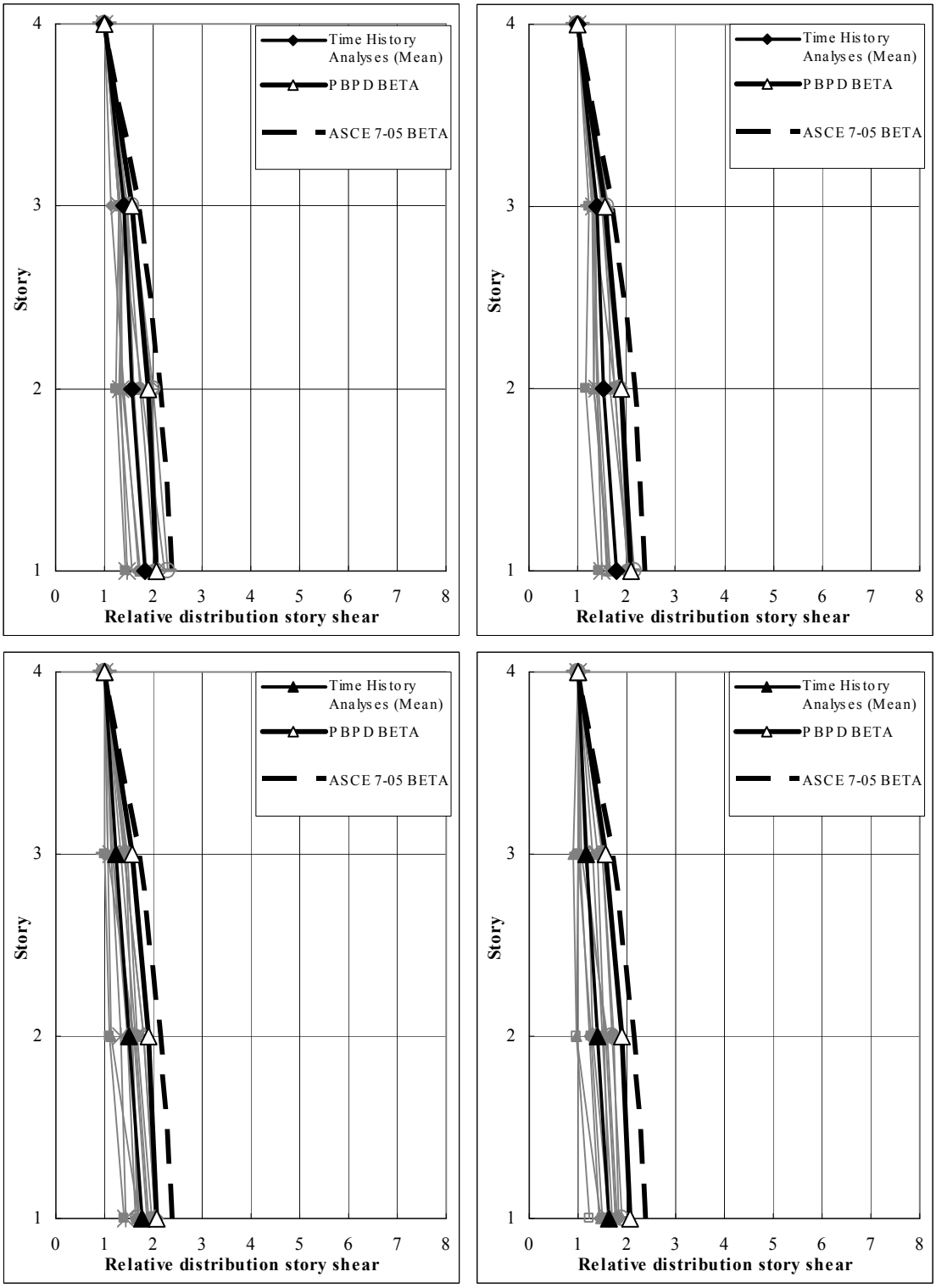

Figure 6-17 4-story RC SMF : maximum relative story shear distributions (a) baseline for 2/3 MCE (b) baseline for MCE (c) PBPD for 2/3 MCE and (d) PBPD for MCE hazard levels

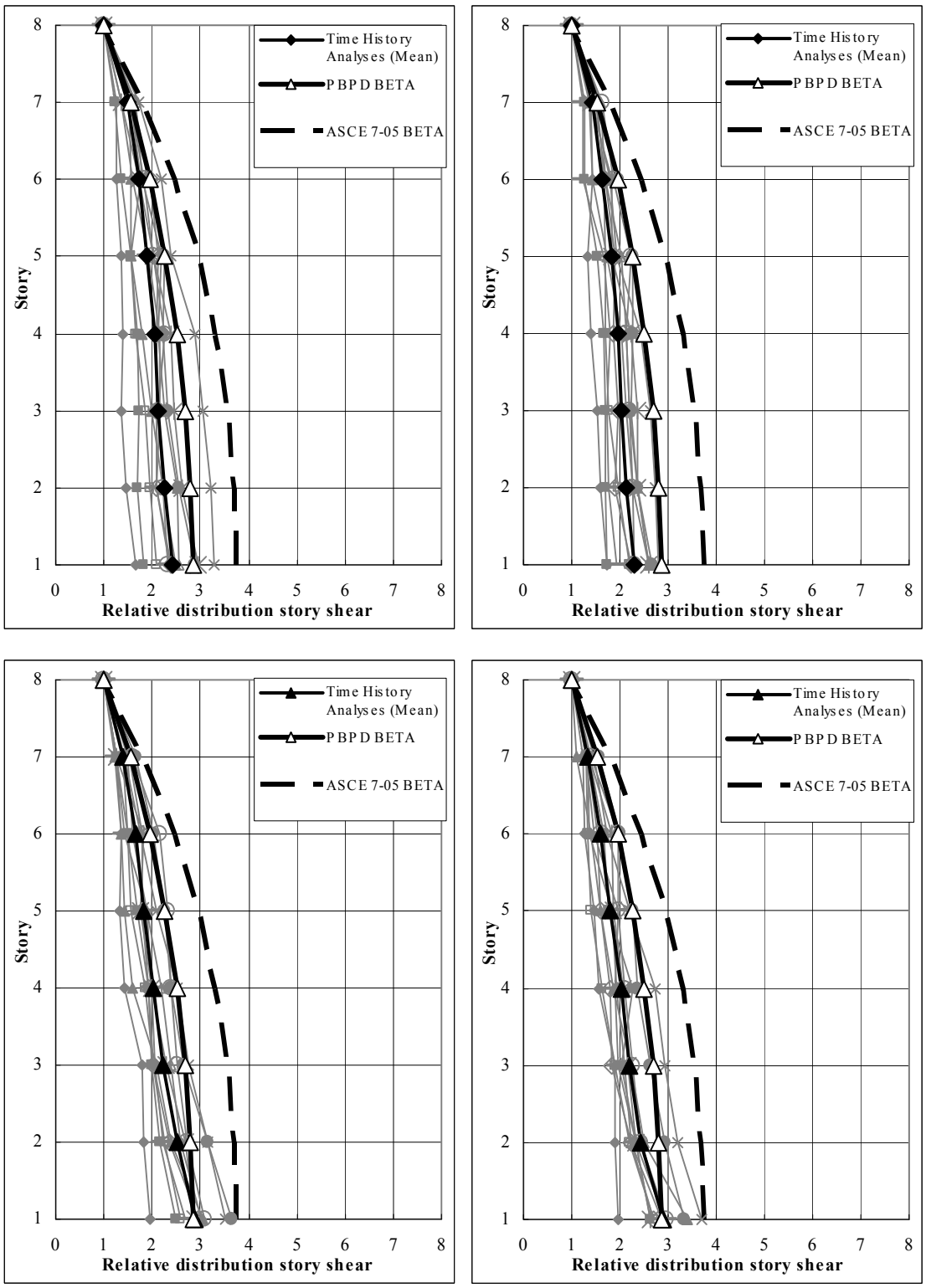

Figure 6-18 8-story RC SMF : maximum relative story shear distributions (a) baseline for 2/3 MCE (b) baseline for MCE (c) PBPD for 2/3 MCE and (d) PBPD for MCE hazard levels

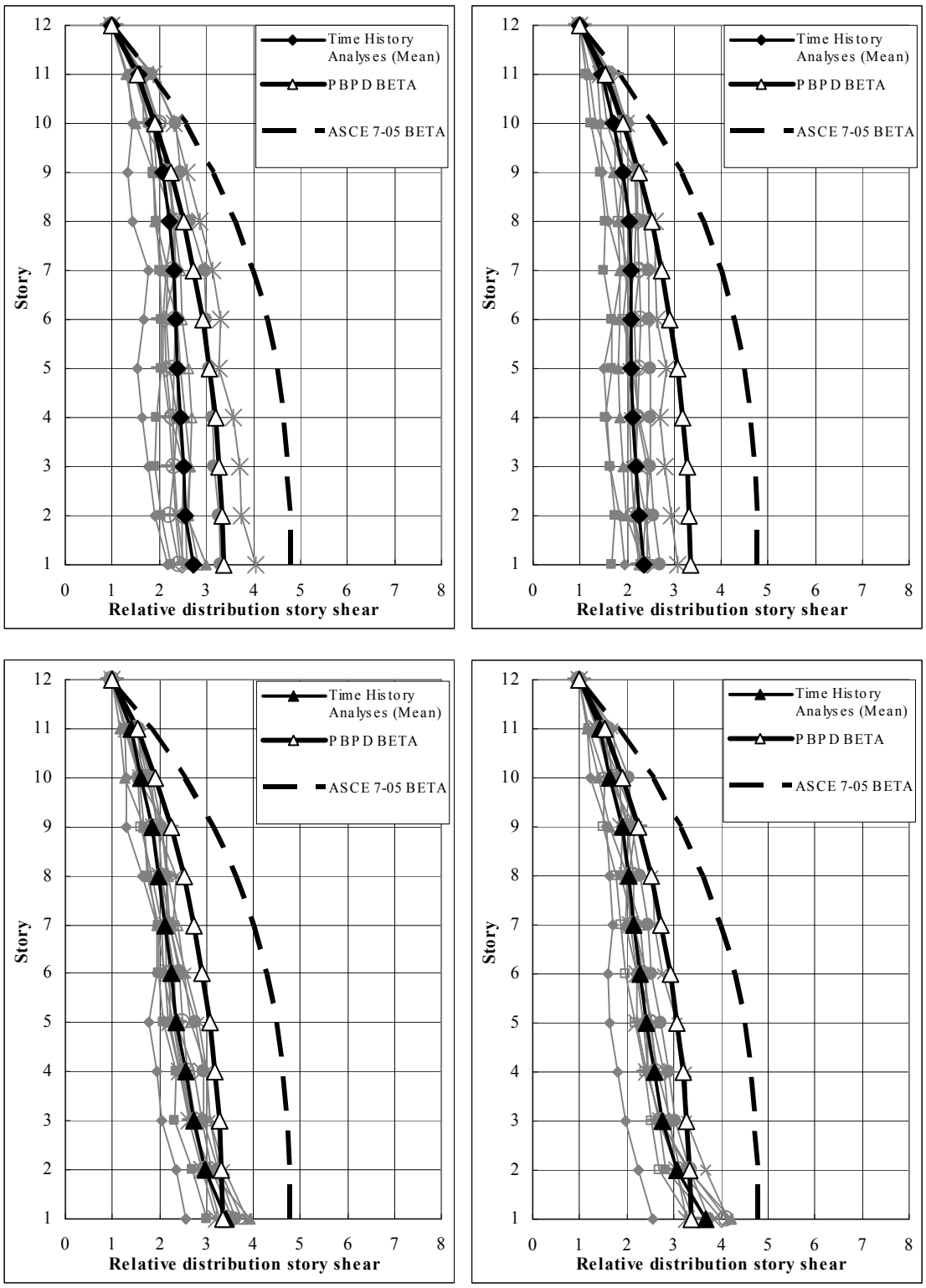

Figure 6-19 12-story RC SMF : maximum relative story shear distributions (a) baseline for 2/3 MCE (b) baseline for MCE (c) PBPD for 2/3 MCE and (d) PBPD for MCE hazard levels

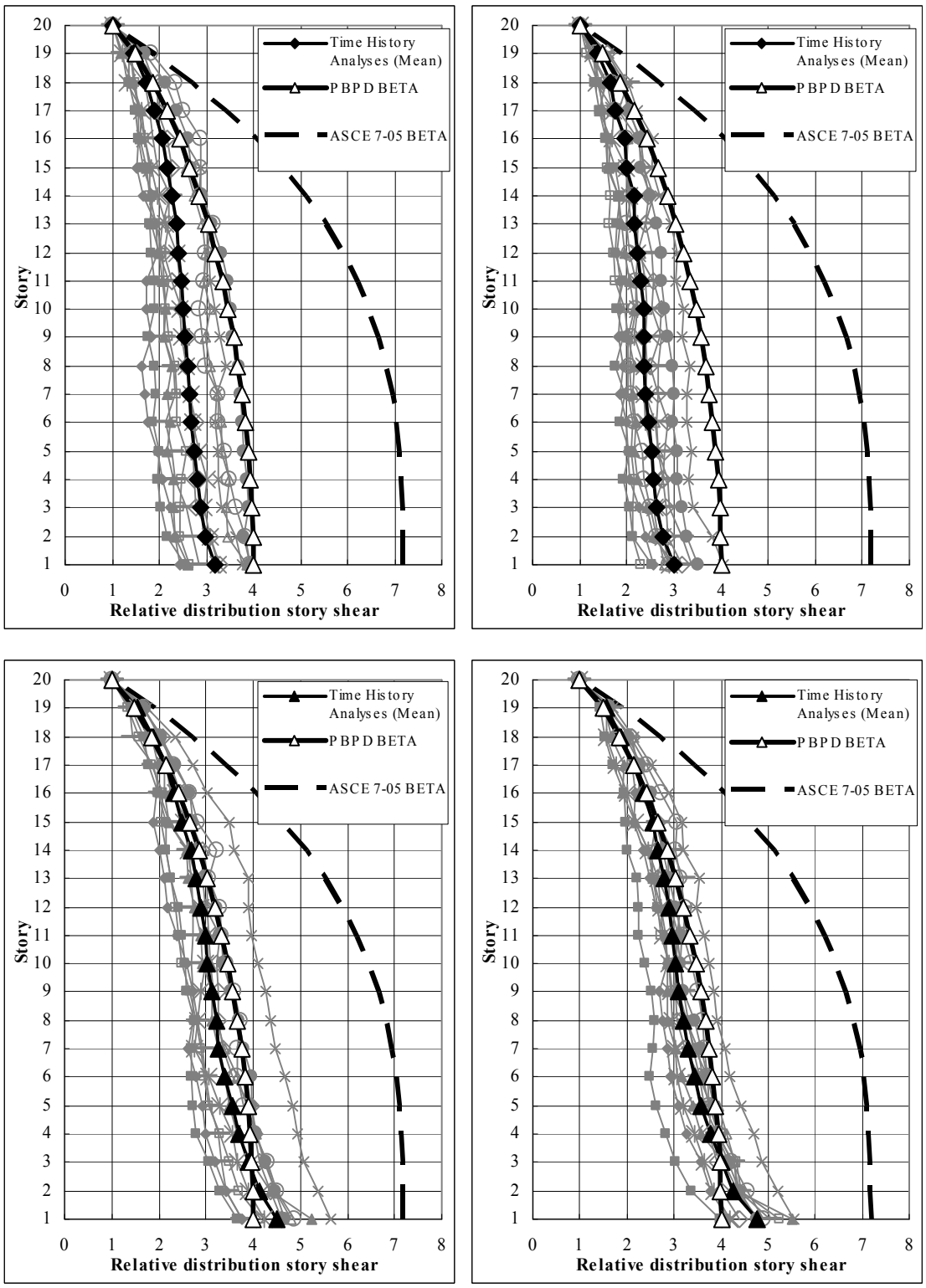

Figure 6-20 20-story RC SMF : maximum relative story shear distributions (a) baseline for 2/3 MCE (b) baseline for MCE (c) PBPD for 2/3 MCE and (d) PBPD for MCE hazard levels

6.4. Further discussion of results

6.4.1 Strong column weak beam provision

The aim of the strong-column weak-beam (SCWB) design provision is to avoid localized story mechanisms and thus attain more global yield mechanisms. Thus, the strong column/ weak beam ratio in FEMA P695 was set at 1.3 instead of 1.2 specified in ACI 318 (2005). However, still in baseline frames plastic hinges formed in the columns, leading to soft story mechanisms both in static pushover and dynamic time history analyses.

One of the major advantages of the PBPD method is that design of columns by using "column tree" concept automatically satisfies the SCWB requirement in code without checking every single joint after the initial design. The simulation results also showed that all plastic hinges formed at intended locations. SCWB ratios of exterior and interior columns for all frames are summarized in Table 6-7 and Table 6-8.

It is noted that smaller standard deviation in baseline frames was caused by the fact that the strength of most columns was increased to meet the applicable SCWB provision. Furthermore, it can also be observed that SCWB ratios of PBPD frames are about 20% to 50% higher than those of corresponding baseline frames. The detailed comparisons of member strengths between baseline and PBPD frames are discussed in the following section.

Table 6-7 SCWB ratios of exterior columns for baseline and PBPD frames

Story	4-story		8-story		12-story		20-story	
	PBPD	Baseline	PBPD	Baseline	PBPD	Baseline	PBPD	Baseline
Floor							1.49	1.03
20							2.04	1.48
19							1.87	1.49
18							1.81	1.40
17							1.81	1.37
16							1.83	1.37
15							1.73	1.35
14							1.71	1.38
13					1.21	0.93	1.69	1.41
12					1.93	1.36	1.66	1.40
11					2.05	1.38	1.63	1.24
10					2.22	1.40	1.63	1.30
9			1.22	0.98	2.14	1.21	1.91	1.31
8			1.91	1.50	2.00	1.31	2.16	1.31
7			1.98	1.51	1.98	1.30	2.22	1.29
6			2.02	1.58	1.93	1.30	2.03	1.30
5	1.32	0.74	1.90	1.24	1.78	1.29	1.79	1.46
4	1.92	1.38	1.76	1.28	1.66	1.28	1.80	1.60
3	1.82	1.27	1.74	1.30	1.73	1.34	1.94	1.66
2	1.74	1.32	1.70	1.35	1.82	1.39	1.97	1.71
Ave. w/o roof	1.82	1.32	1.86	1.39	1.93	1.32	1.85	1.41
Standard derivation	0.23	0.26	0.24	0.18	0.25	0.12	0.18	0.15
$\frac{PBPD}{Baseline}$	1.38		1.34		1.46		1.31	

Table 6-8 SCWB ratios of interior columns for baseline and PBPD frames

Story	4-story		8-story		12-story		20-story	
	PBPD	Baseline	PBPD	Baseline	PBPD	Baseline	PBPD	Baseline
Floor							1.08	0.79
20							1.83	1.30
19							1.94	1.34
18							1.85	1.30
17							1.84	1.29
16							1.86	1.30
15							1.77	1.29
14							1.78	1.31
13					0.98	0.77	1.81	1.30
12					1.66	1.25	1.77	1.31
11					1.86	1.30	1.75	1.21
10					1.89	1.41	1.73	1.31
9			0.93	0.79	1.87	1.20	1.73	1.31
8			1.61	1.32	1.87	1.24	1.77	1.30
7			1.76	1.36	1.93	1.24	1.95	1.29
6			1.82	1.47	2.20	1.26	1.81	1.30
5	0.99	0.54	1.78	1.21	2.17	1.30	1.64	1.52
4	1.55	1.27	1.79	1.31	2.05	1.33	1.84	1.74
3	1.58	1.29	1.88	1.31	2.38	1.40	2.01	1.81
2	1.55	1.30	1.91	1.33	2.15	1.43	1.88	1.87
Ave. w/o roof	1.56	1.29	1.79	1.33	2.00	1.31	1.82	1.39
Standard derivation	0.23	0.26	0.24	0.18	0.25	0.12	0.18	0.15
$\frac{PBPD}{Baseline}$	1.21		1.35		1.53		1.31	

6.4.2 Member strength comparison

As shown earlier, the response of PBPD frames was much improved over that of the corresponding baseline frames in terms of yield mechanism, and more uniform distribution of story drifts and inelastic activities along the height. Relative column to beam moment strengths are one of the important factors responsible for the improvement. For the column strengths, the maximum moment, that is the moment at the balance point (Figure 5-13), were taken for the calculations.

From Figure 6-21 it can be seen that in the case of 4-story frame, the column strengths of baseline and PBPD frames are almost the same (even in section sizes and reinforcement ratios). However, the pushover curves and yield activities shown in Figure 6-1, 6-6 and 6-7 reflect that the performance of baseline frame is quite poor even though it had almost 50% ~ 100% stronger beams compared to the PBPD design. This further shows the importance of PBPD lateral force distribution. That is, frames designed by using the PBPD lateral force distribution resulted in better performance even with less construction material.

In general, the baseline frames had 0% ~ 100% stronger beams and 0% ~ 50% weaker columns compared to the PBPD frames. For the lower stories of the taller frames, the column strengths of the baseline frames are only about half of those of the PBPD frames.

It can be concluded that the baseline frames have much stronger beams but weaker columns compared to the corresponding PBPD frames. Better distribution of strength of beams and capacity design for columns with “column tree” concept are an effective way to help prevent formation of soft story mechanisms.

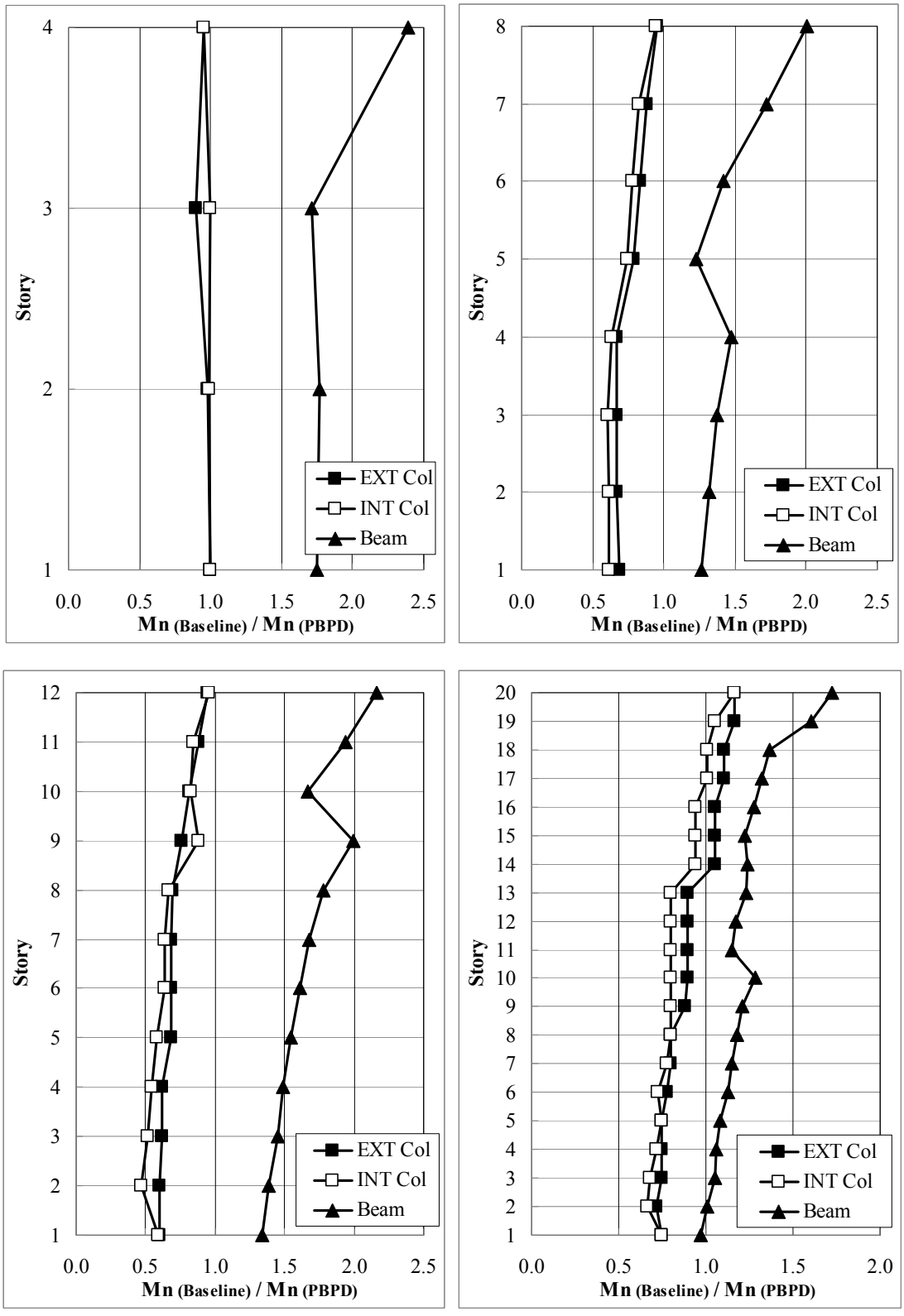

Figure 6-21 Element strength comparisons of baseline and PBPD frames (a) 4-story (b) 8-story (c) 12-story and (d) 20-story

6.4.3 Verification of base column design

As mentioned in Section 3-4, 4-4-4 and 4-4-5, in terms of the design of the first story columns for 12 and 20-story PBPD frames, it is suggested to take M_{u-bot} instead of M_{u-top} even though $M_{u-bot} < M_{u-top}$ in the first story. By using M_{u-bot}, formation of plastic hinges at the column base as desired can be ensured. Figure 6-22 shows the results of inelastic pushover analysis of 12-story PBPD frame: one where the first story columns were designed for M_{u-top} and the other where the first columns were designed for M_{u-bot}. It is noticed that the first frame shows somewhat more ductile behavior. However, it can be seen from the deformed shape and location of plastic hinges of these two frames at 4.5% roof drift that absence of plastic hinges at the base column bases resulted in formation of other plastic hinges at undesired column locations and concentration of lateral drift in the middle stories, Figure 6-23.

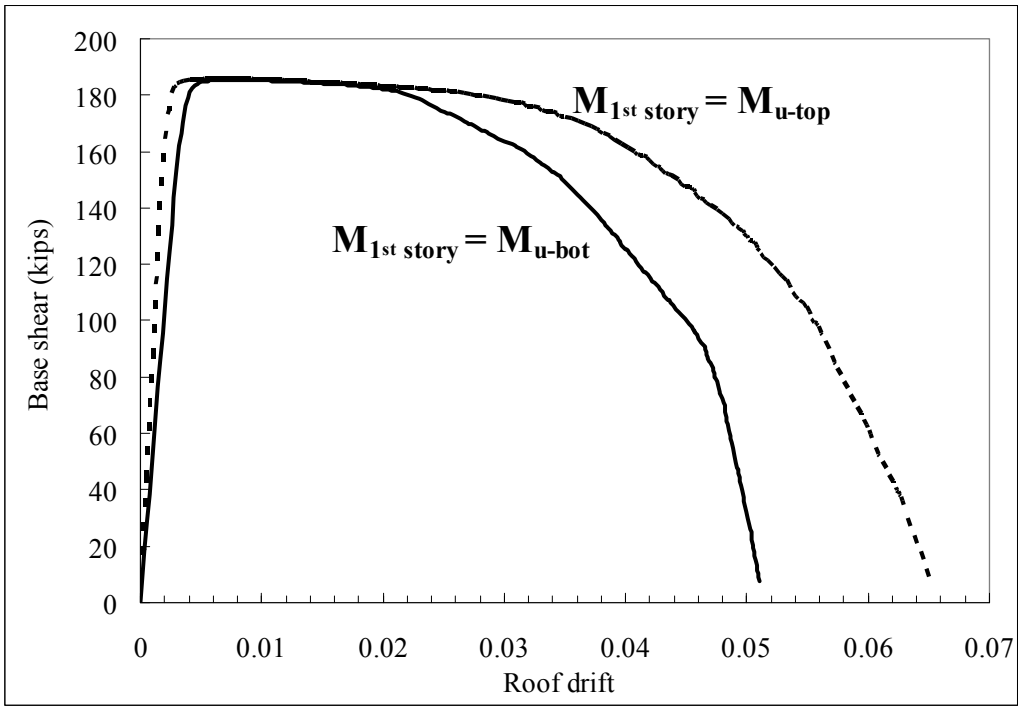

Figure 6-22 Pushover curves of two 12-story PBPD frames with different first story column strengths

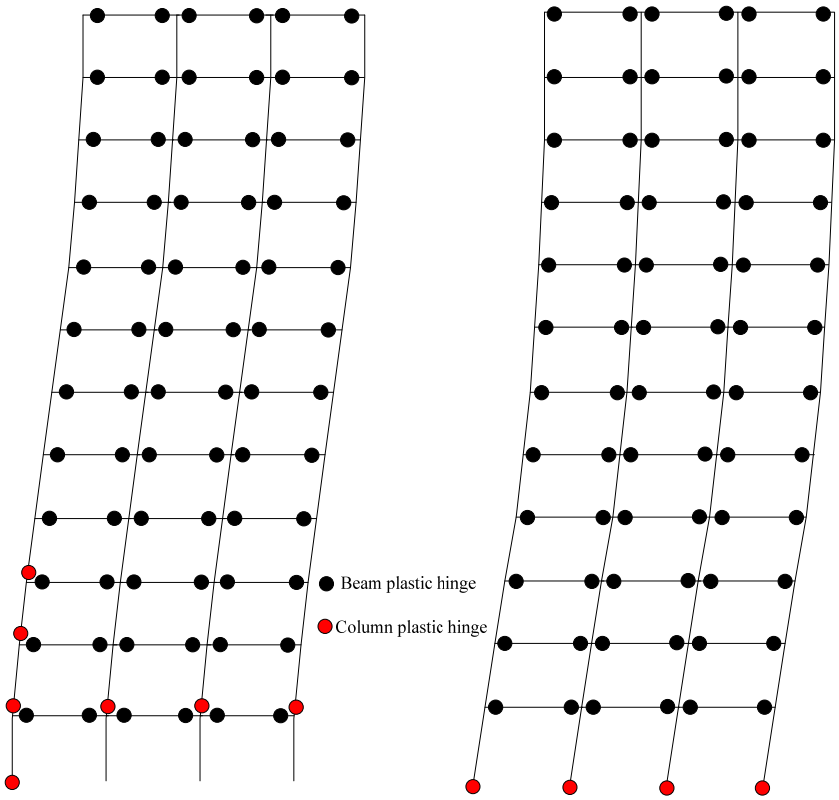

Figure 6-23 Plastic hinge distributions at 4.5% roof drift under static pushover analysis for 12-story PBPD frames (a) $M_{1st\ story} = M_{u-top}$ **(b)** $M_{1st\ story} = M_{u-bot}$

6.5. Summary and conclusions

The baseline frames and the PBPD frames were subjected to extensive inelastic pushover and time-history analyses. The PBPD frames responded as intended in design with much improved performances over those of the corresponding baseline frames.

In both nonlinear static pushover and dynamic analyses, the story drifts of the PBPD frames were more evenly distributed over the height as compared with those of the baseline frame where undesirable "softness" in the lower stories was evident, which is caused mainly by plastic hinges in the columns. Formation of plastic hinges in the

columns and story mechanism in the lower part of the baseline frames could be clearly noticed. In contrast, there were no unintended plastic hinges in the columns of the PBPD frame, resulting in more favorable deformed shape and yield pattern as intended in the design process.

Furthermore, PBPD lateral force distribution also showed excellent agreement with maximum relative story shear distributions obtained from time history analyses in baseline as well as PBPD frames, particularly for taller structures. “Column tree” concept of column design and PBPD lateral force distribution are both successfully validated by proposed nonlinear analyses.

In summary, the results of inelastic static and dynamic analyses proved the validity of the PBPD methodology as applied to reinforced concrete moment frames.

CHAPTER 7

ENERGY SPECTRUM METHOD FOR SEISMIC EVALUATION

7.1. Introduction

Static pushover method has been widely accepted as a useful tool for performance-based seismic design and evaluation of structures (FEMA 440, 2006). Since its introduction to the engineering community, the pushover analysis method has been a subject of extensive research and several new approaches have been proposed. Recent notable modifications include adaptive load patterns and multiple modal analysis procedures. In most cases, the behavior of the structure is characterized by the capacity curve which is represented by a plot of the base shear versus the roof displacement. The capacity curve is used to establish an equivalent SDOF system. The expected peak displacement demand can then be estimated by using one of the methods such as the capacity spectrum approach, the modification factor approach, or the direct use of inelastic constant ductility spectra. The peak displacement can then be projected back to the roof displacement from which the story and member demands can be extracted (Leelataviwat et al, 2007; Goel et al, 2009[b]).

After a brief description of the proposed energy spectrum method, its application to 4, 8, 12 and 20-story RC moment frame is presented. The results are compared with those obtained from detailed time-history analyses.

7.2. Energy Spectrum Evaluation Method

As mentioned earlier, the design base shear in the PBPD method for a specified hazard is calculated by equating the work needed to push the structure monotonically up to the target drift to the energy required by an equivalent EP-SDOF to achieve the same state. Thus, the work-energy equation can be written as described in Chapter 3:

$$(E_e + E_p) = \gamma \cdot \left(\frac{1}{2} M \cdot S_v{}^2 \right) = \frac{1}{2} \gamma \cdot M \cdot \left(\frac{T}{2\pi} S_a \cdot g \right)^2 \qquad (7\text{-}1)$$

where E_e and E_p are, respectively, the elastic and plastic components of the energy (work) needed to push the structure up to the target drift. S_v is the design pseudo-spectral velocity; S_a is the pseudo spectral acceleration; T is the fundamental period; and M is the total mass of the system.

In order to use the energy concept for evaluation purposes, the right hand side of Equation (7-1) can be viewed as energy demand for the given hazard, E_d, and the left hand side as energy capacity of the given structure, E_c. Both these quantities vary with displacement. The value of the desired maximum reference displacement can be obtained by either solving the work-energy equation analytically, or graphically by constructing the two energy curves as a function of the reference displacement and determining their point of intersection. The graphical method is preferred over the analytical one because the two energy plots present a good visual picture of the capacity and demand as a function of the reference displacement.

The energy balance equation can be extended to MDOF systems by using the concept of equivalent simple oscillator. Neglecting coupling between the modes (Chopra and Goel 2002) and assuming constant mode shapes after yielding, Leelataviwat et al. (2007) stated that the energy demand of the *n*-th mode of the MDOF system can be calculated by the equivalent simple oscillator as well. In this study, for simplicity purpose, the total mass is

used for the energy demand instead of summation of individual modal masses and the results also showed excellent promise, which will be further discussed in the following sections.

Figure 7-1 presents a graphical illustration of the evaluation process. Lateral force-displacement plot for the given structure is shown in Figure 7-1(a), where V represents the total force (base shear), and u_r the roof displacement, used as reference displacement. This plot can be obtained by a static pushover analysis by applying either an appropriately selected force or displacement pattern. It is common to plot total force versus roof displacement, but it can be done for any other floor or story level from which the force or displacement at other levels can be determined. The energy capacity curve, E_c-u_r, can be generated as a function of u_r, by calculating the work done by lateral forces up to the displacement at each level corresponding to u_r, Figure 7-1(b). Next, the energy demand, E_d, can be calculated for varying values of u_r, and plotted as shown in Figure 7-1(c). The point of intersection of the two curves, where the energy demand and capacity become equal, gives the desired maximum roof displacement, as shown in Figure 7-1(d).

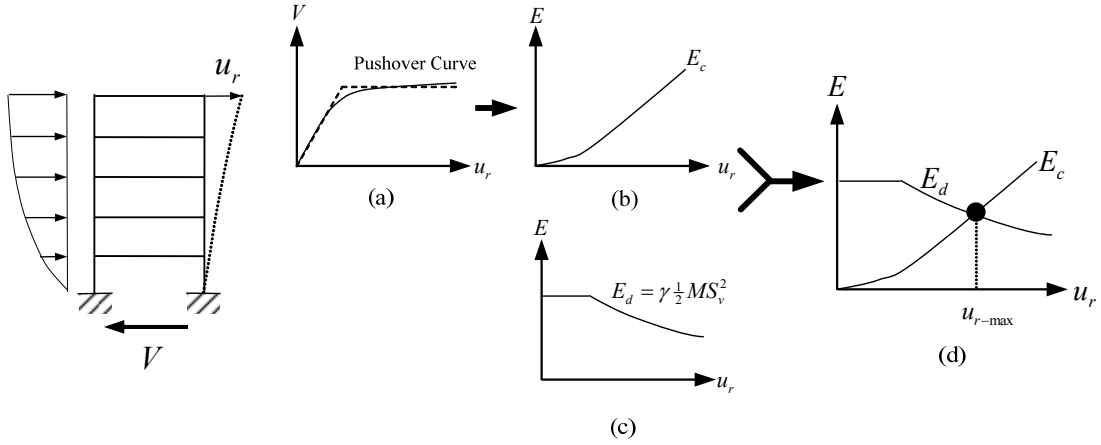

Figure 7-1 Proposed energy-based evaluation method for MDOF systems: (a) Push-over curve, (b) Energy-displacement capacity diagram, (c) Energy demand diagram, and (d) Determination of displacement demand

Evaluation of RC structures presents special problem due to their complex and degrading ("pinched") hysteretic behavior. This aspect is taken care of by making appropriate modification in constructing the energy demand curve, E_d. As described in Section 3.4.4.1 for design purpose, C_2 factor method was also implemented in Equation (7-1)

for modification of design target drift for an equivalent non-degrading system. Thus, the energy demand for the given hazard for a RC structure, E_d, can be expressed as shown in Equation (7-2).

$$E_d = \frac{1}{2}\gamma^* \cdot M \cdot \left(\frac{T}{2\pi} S_a \cdot g\right)^2 = \frac{1}{2} \cdot \frac{2\dfrac{u_r / u_y}{C_2} - 1}{(R_\mu^*)^2} \cdot M \cdot \left(\frac{T}{2\pi} S_a \cdot g\right)^2 \qquad (7\text{-}2)$$

where R_μ^* can be obtained from Table 3-2 for corresponding $\dfrac{u_r / u_y}{C_2}$.

7.3. Verification by nonlinear dynamic (time history) analyses

In terms of energy spectrum method for evaluation purpose, the energy capacity and demand curves of 4, 8, 12 and 20-story RC SMF are presented in this section.

For each frame, the capacity curve was obtained by calculating the work done by the applied forces in the pushover analysis. The energy capacity corresponding to each roof drift was calculated by numerically integrating the lateral load-deflection values at the floor levels. The energy demand curve was obtained based on the total seismic mass. The peak roof drift demand was determined from the intersection point of the corresponding demand and capacity curves. In addition, the maximum interstory drifts of baseline and PBPD frames as calculated by the energy spectrum method are compared with those obtained from the time-history analyses using appropriately scaled ground motion records representative of 2/3 MCE and MCE hazard levels. The scale factors were determined by anchoring to 2/3 MCE and MCE hazard levels at the fundamental period of the structure being analyzed as summarized in Table 7-1.

Table 7-1 Scale factors for all study frames

	4-story		8-story		12-story		20-story	
	Code	PBPD	Code	PBPD	Code	PBPD	Code	PBPD
T (sec)	1.09	1.09	1.80	1.69	2.54	2.18	2.8	2.3
Scale factors	2.54	2.54	2.98	2.84	3.23	3.08	3.53	3.13

7.3.1 4-story RC SMF

The energy capacity and demand curves of the 4-story baseline and PBPD RC SMF are shown in Figure 7-2. The peak roof drift demand for 2/3 MCE and MCE hazard can be easily obtained from the interceptions of capacity and demand curves.

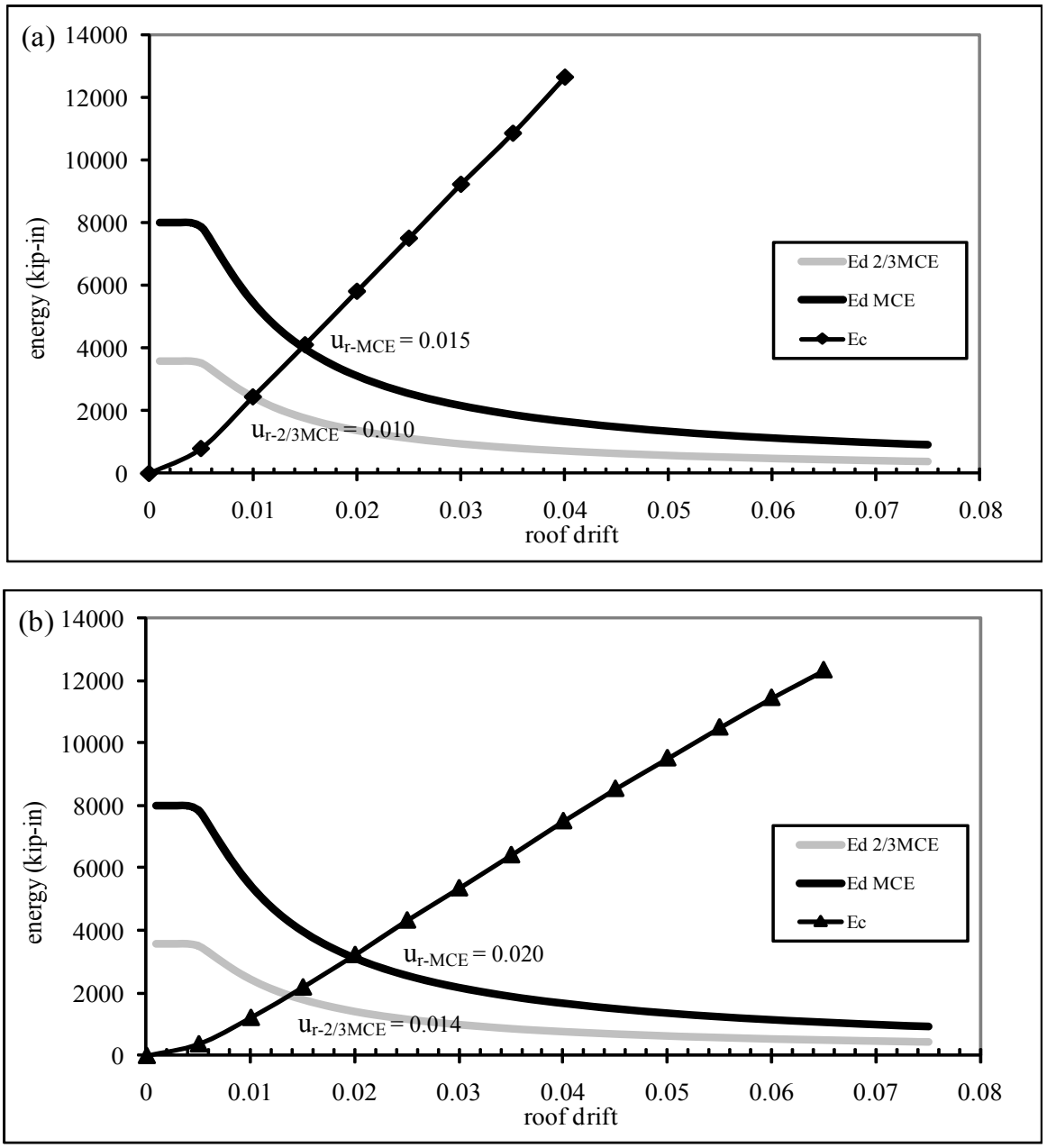

Figure 7-2 The energy capacity and demand curves for 2/3 MCE and MCE hazard of 4-story (a) baseline and (b) PBPD RC SMF

After the peak roof drift is determined, the corresponding deformed shape from static pushover is used to obtain the story drifts, which are then compared with those obtained from the time-history analyses using appropriately scaled ground motion records as shown in Figure 7-3.

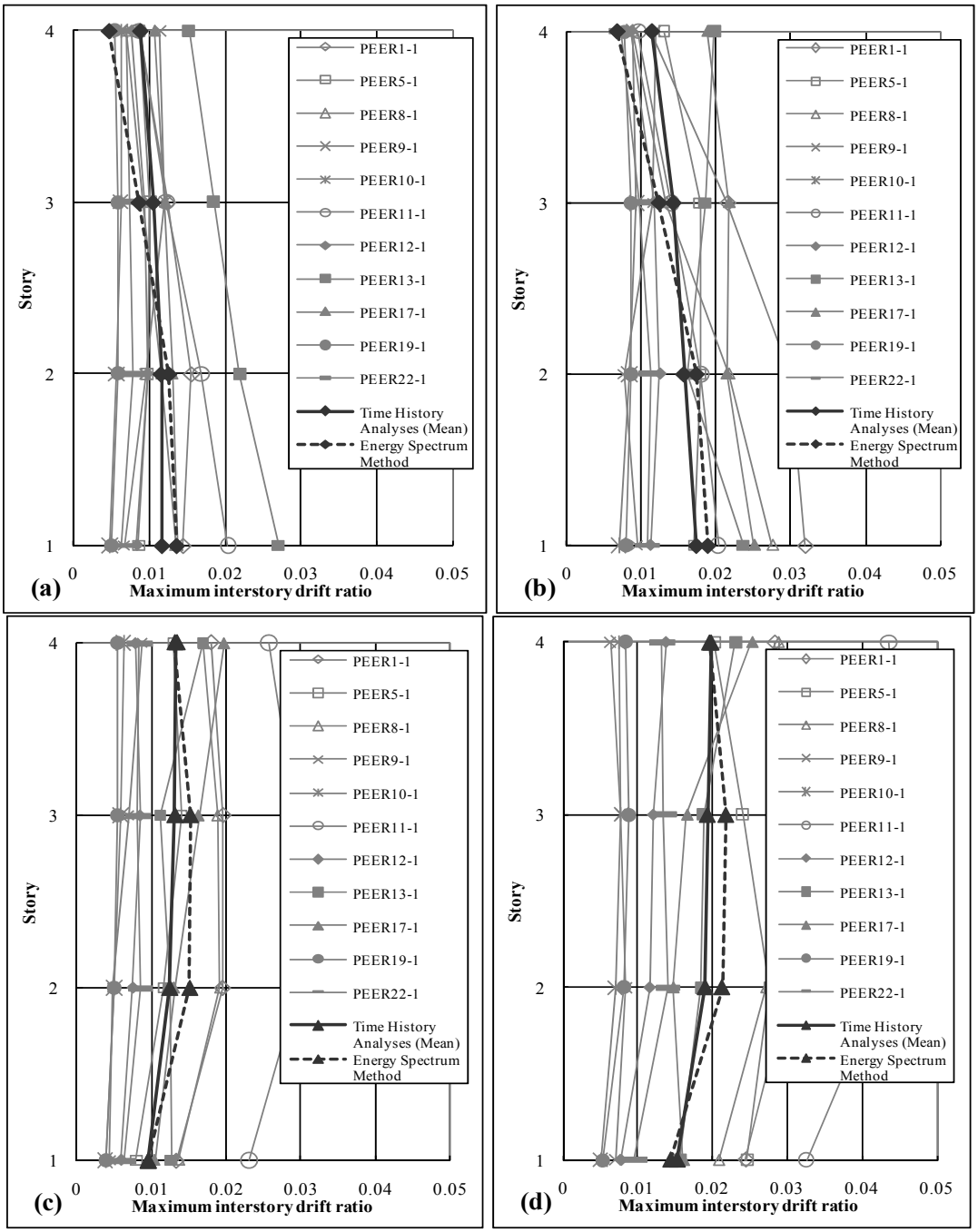

Figure 7-3 Comparison of maximum interstory drifts by the energy spectrum method and time-history analyses for a) baseline frame for 2/3 MCE, b) baseline frame for MCE, c) PBPD frame for 2/3 MCE, d) PBPD frame for MCE hazard levels.

7.3.2 8-story RC SMF

The energy capacity and demand curves of the 8-story baseline and PBPD RC SMF are shown in Figure 7-4. The peak roof drift demand for 2/3 MCE and MCE hazard are obtained from the points of intersection of the corresponding capacity and demand curves.

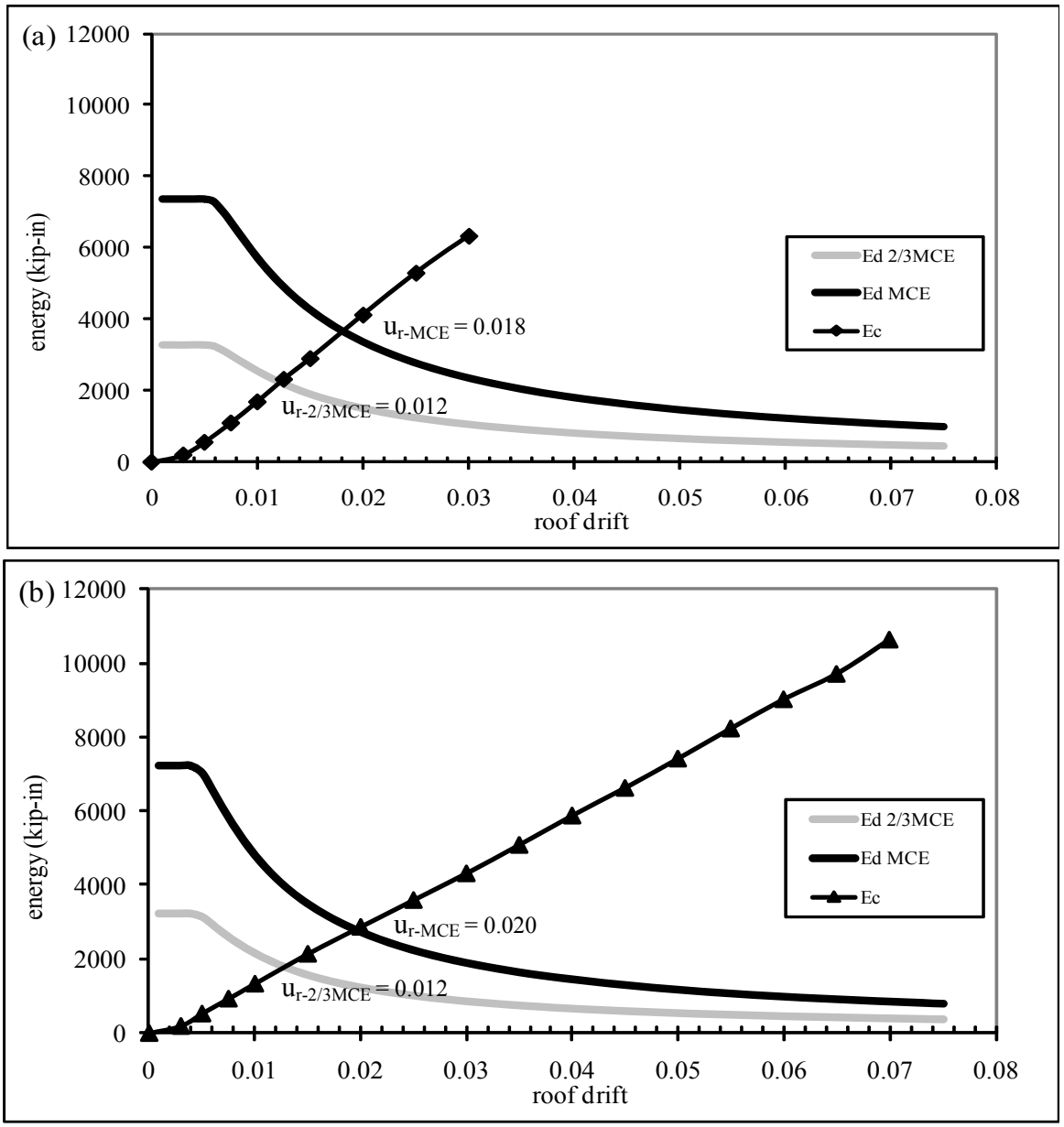

Figure 7-4 The energy capacity and demand curves for 2/3 MCE and MCE hazard of 8-story (a) baseline and (b) PBPD RC SMF

After the peak roof drift is determined, the corresponding deformed shape from static pushover is used to obtain the story drifts, which are then compared with those obtained from the time-history analyses using appropriately scaled ground motion records as shown in Figure 7-5.

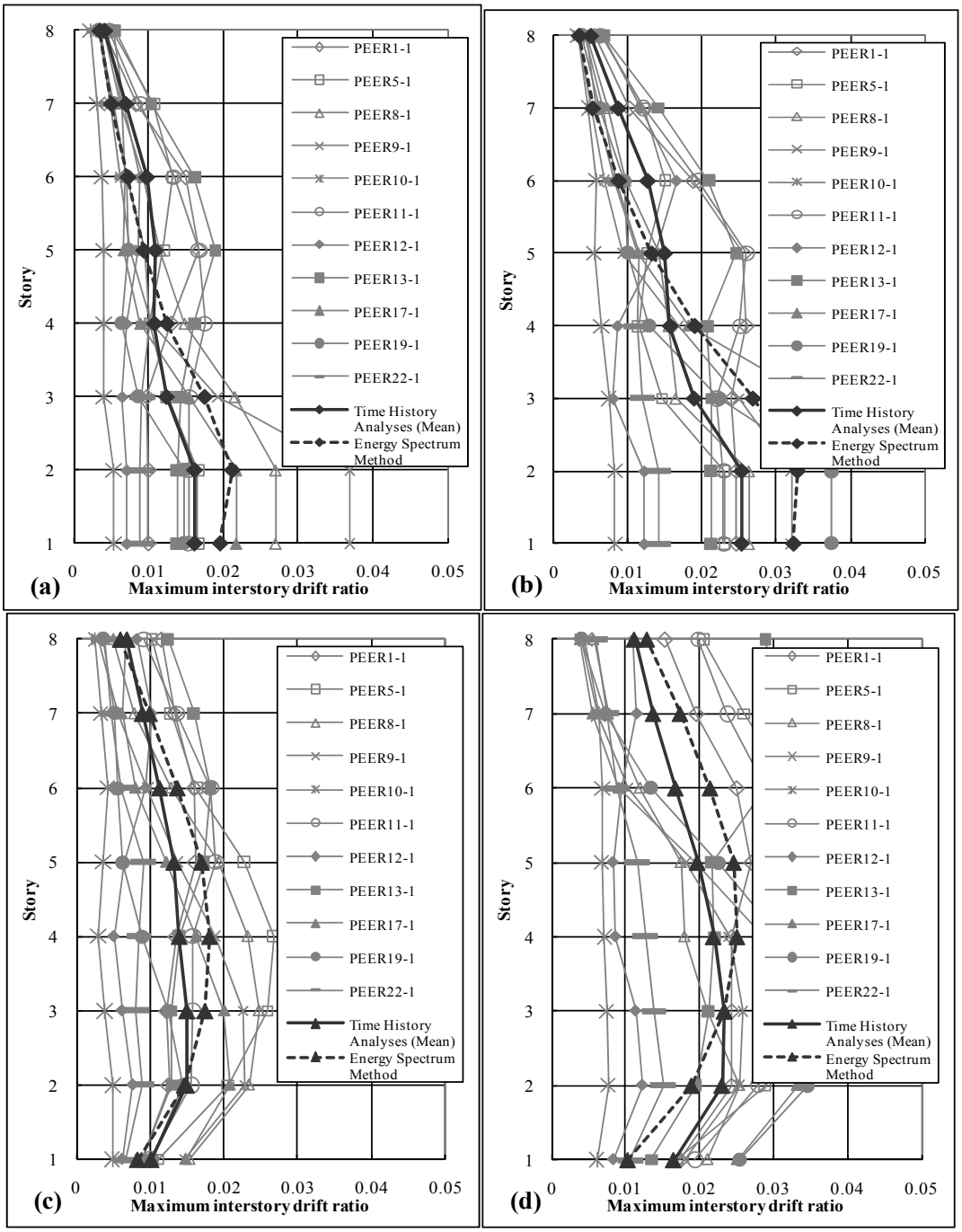

Figure 7-5 Comparison of maximum interstory drifts by the energy spectrum method and time-history analyses for a) baseline frame for 2/3 MCE, b) baseline frame for MCE, c) PBPD frame for 2/3 MCE, d) PBPD frame for MCE hazard levels.

7.3.3 12-story RC SMF

The energy capacity and demand curves of the 12-story baseline and PBPD RC SMF are shown in Figure 7-6. The peak roof drift demand for 2/3 MCE and MCE hazard are obtained from the points of intersection of the corresponding capacity and demand curves.

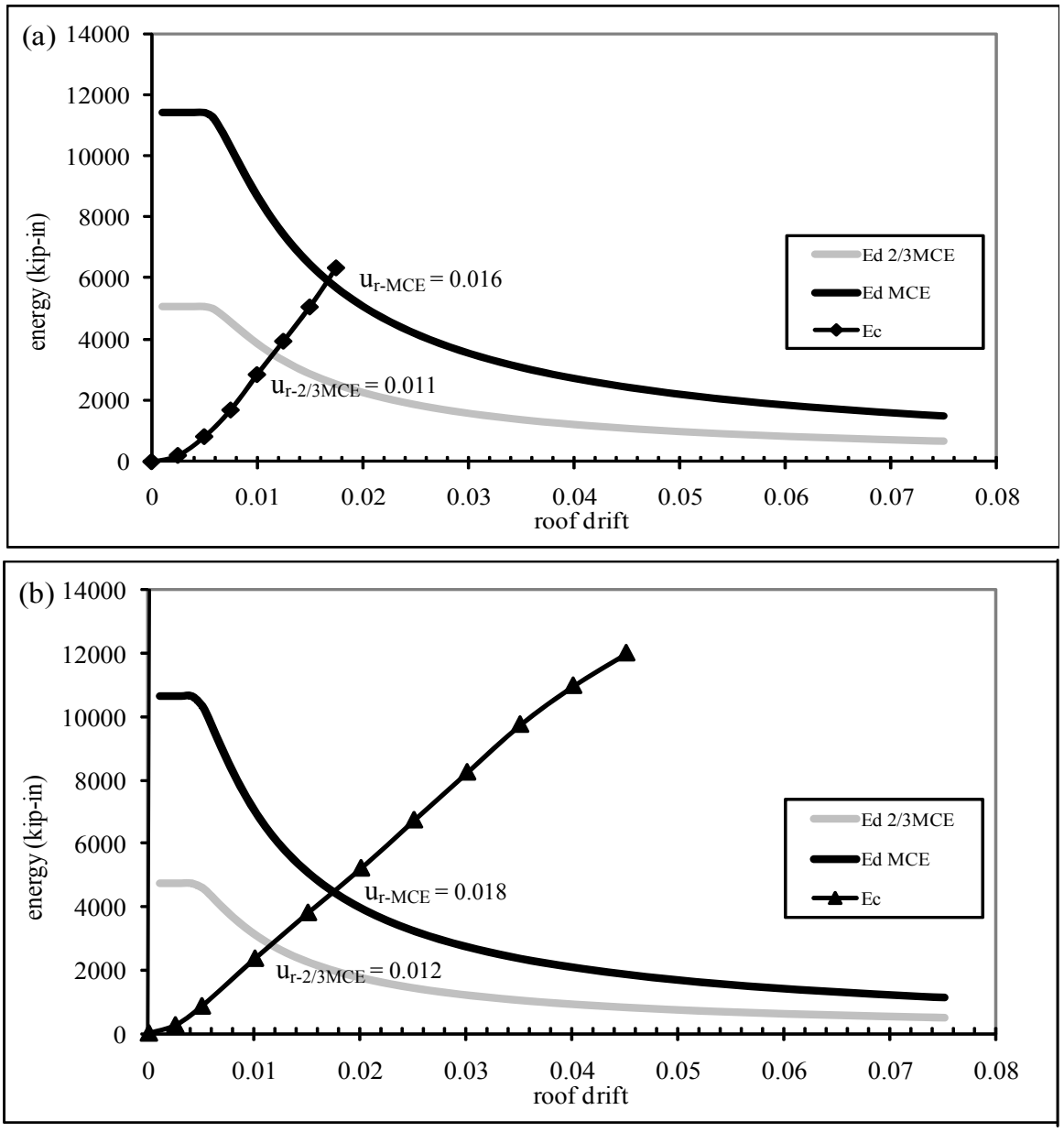

Figure 7-6 The energy capacity and demand curves for 2/3 MCE and MCE hazard of 12-story (a) baseline and (b) PBPD RC SMF

After the peak roof drift is determined, the corresponding deformed shape from static pushover is used to obtain the story drifts, which are then compared with those obtained from the time-history analyses using appropriately scaled ground motion records as shown in Figure 7-7.

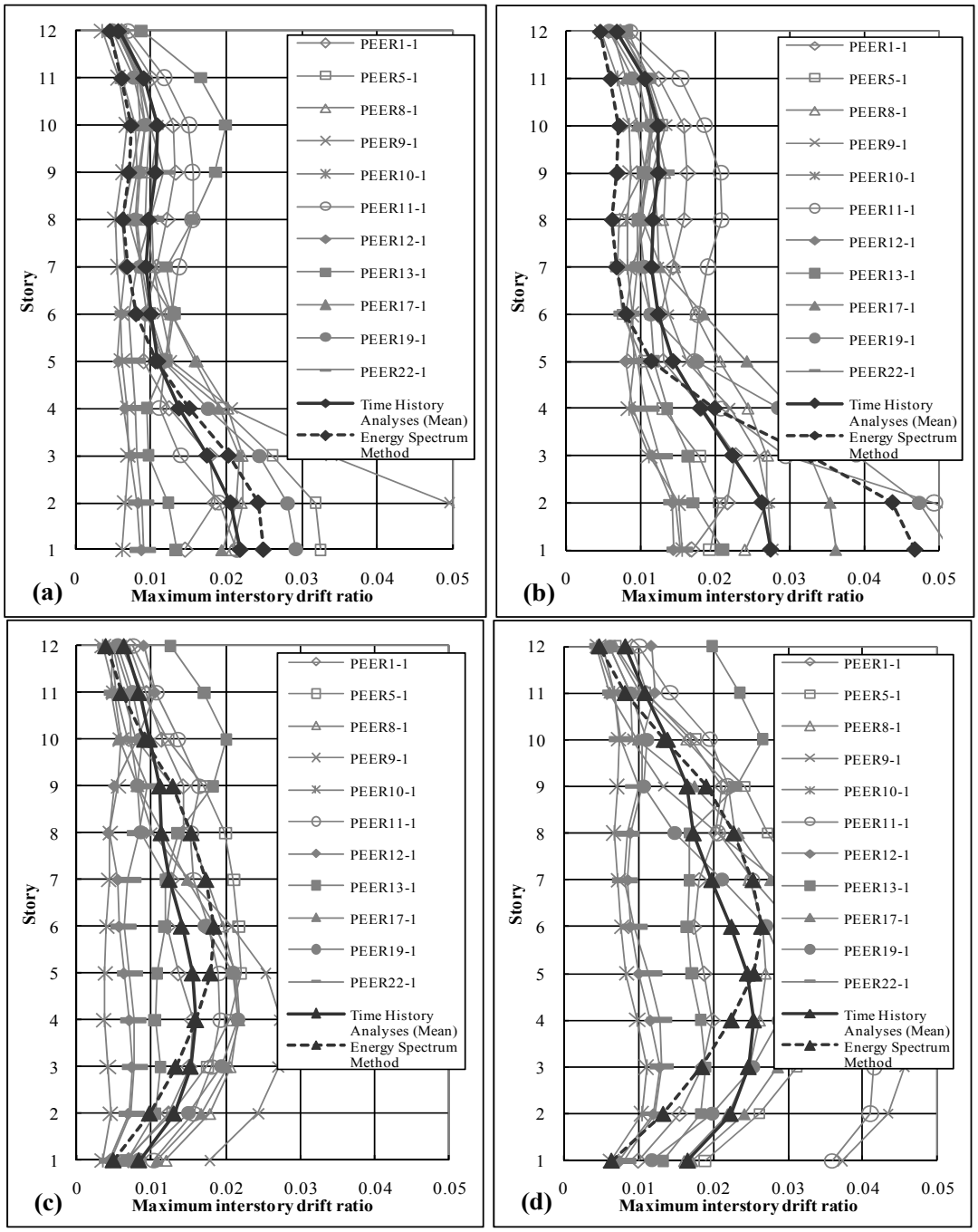

Figure 7-7 Comparison of maximum interstory drifts by the energy spectrum method and time-history analyses for a) baseline frame for 2/3 MCE, b) baseline frame for MCE, c) PBPD frame for 2/3 MCE, d) PBPD frame for MCE hazard levels.

7.3.4 20-story RC SMF

The energy capacity and demand curves of the 20-story baseline and PBPD RC SMF are shown in Figure 7-8. The peak roof drift demand for 2/3 MCE and MCE hazard are obtained from the points of intersection of the corresponding capacity and demand curves.

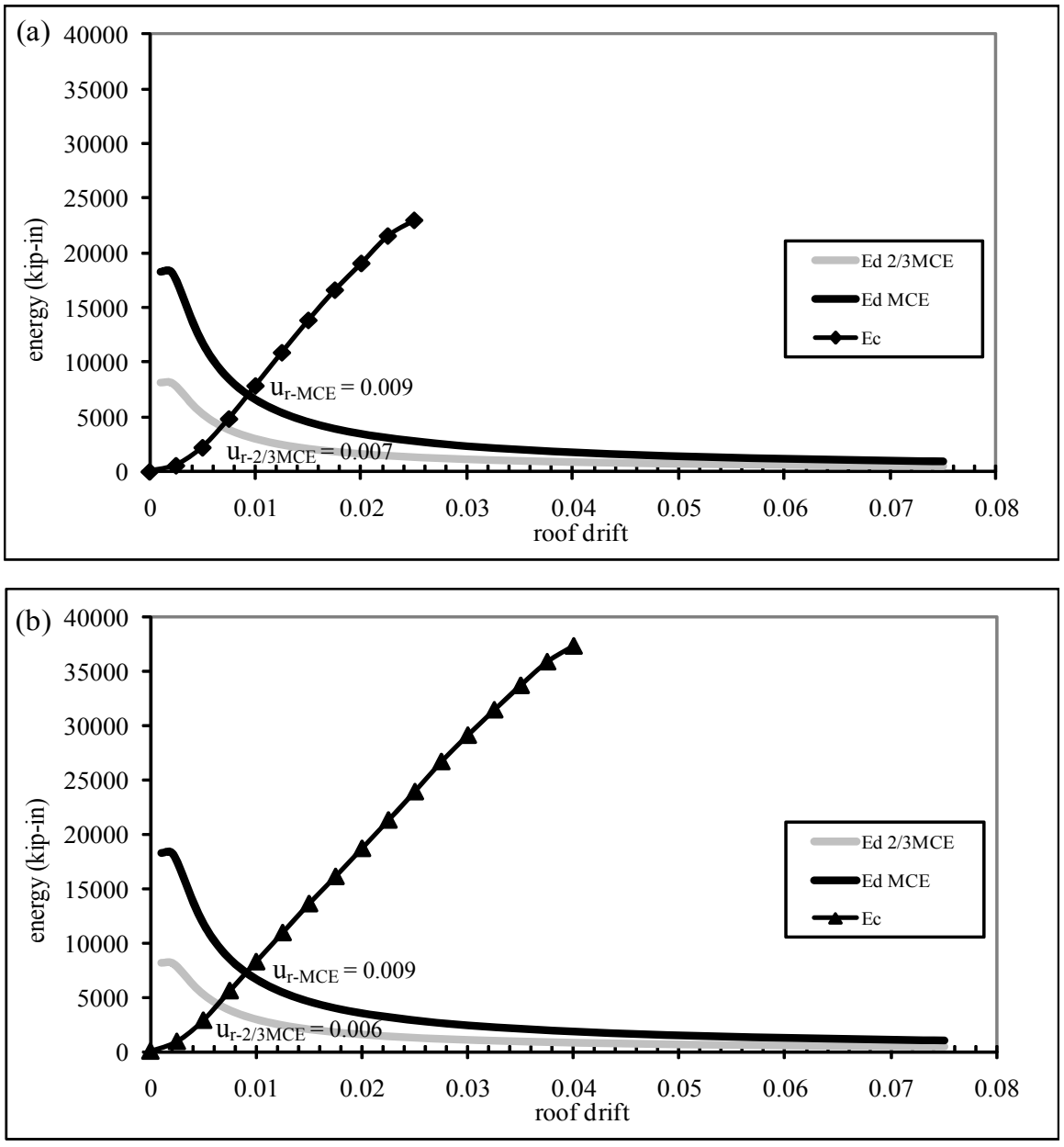

Figure 7-8 The energy capacity and demand curves for 2/3 MCE and MCE hazard of 20-story (a) baseline and (b) PBPD RC SMF

After the peak roof drift is determined, the corresponding deformed shape from static pushover is used to obtain the story drifts, which are then compared with those obtained from the time-history analyses using appropriately scaled ground motion records as shown in Figure 7-9.

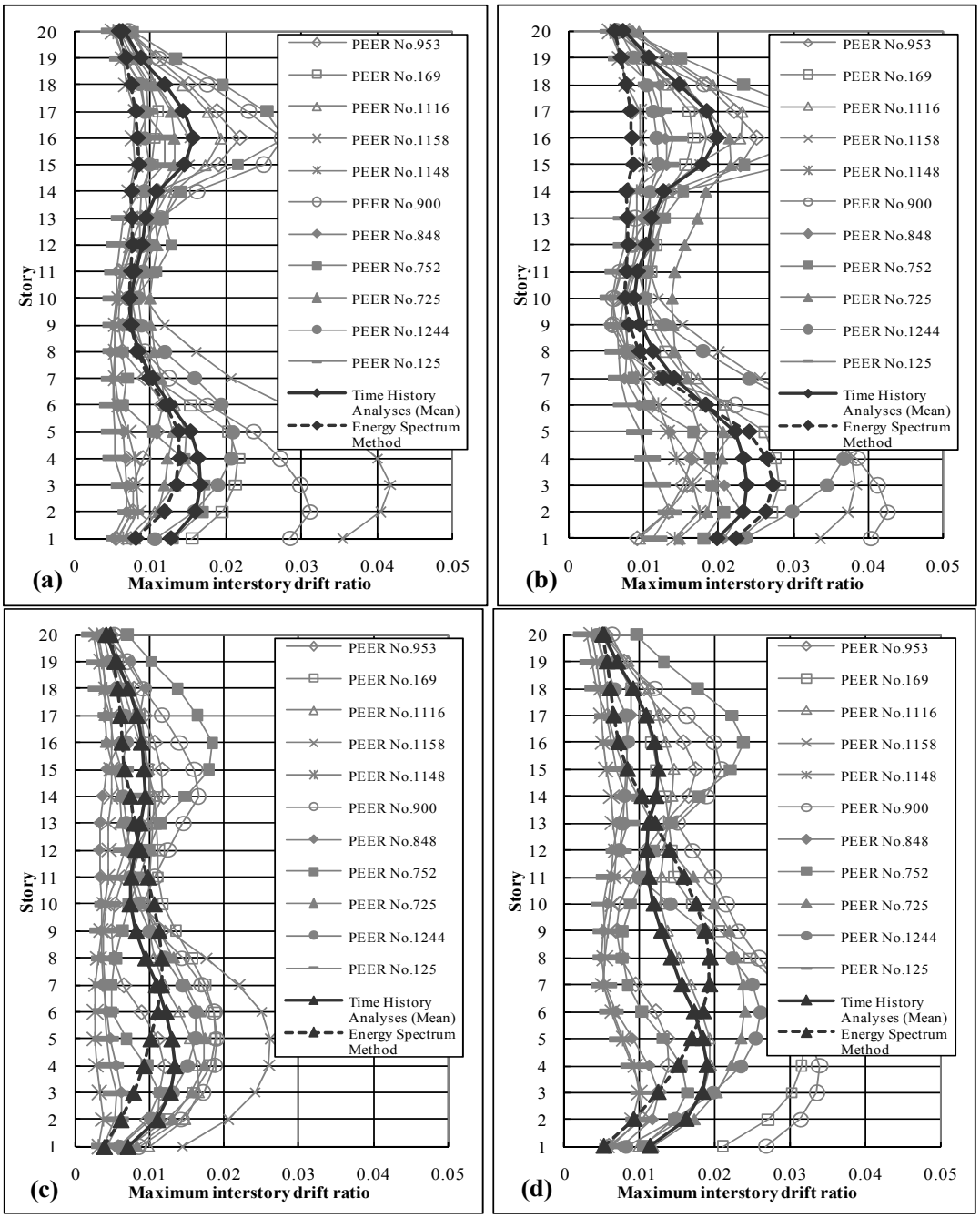

Figure 7-9 Comparison of maximum interstory drifts by the energy spectrum method and time-history analyses for a) baseline frame for 2/3 MCE, b) baseline frame for MCE, c) PBPD frame for 2/3 MCE, d) PBPD frame for MCE hazard levels.

7.4. Discussion of results

Overall, the drift demand estimates given by the energy spectrum method ($E_c = E_d$) were generally quite close to those obtained from time-history analyses using representative ground motion records. This can be considered as a very good correlation between the results given by an approximate method with those from more precise time-history analysis.

It should be noted that the deformed shape of the frames as used in the energy spectrum method were obtained from the static pushover analysis. Thus, if a soft story mechanism forms, as in the case of 12-story baseline frame, the deformation will tend to concentrate in the soft story part while the whole structure is pushed under increasing roof drift. Therefore, the floor displacement and story drift estimates were less accurate as compared to those obtained from the time history analyses but were still within the acceptable limit.

For the case of taller frames (12 and 20-story), the energy spectrum method provides less accurate prediction in the upper stories as well where the influence of higher modes is more significant. Moreover, since the story drifts of the PBPD frames are more evenly distributed over the height because of non yielding columns as compared with those of the baseline frames (i.e., increase in story drifts), it can also be said that the effect of higher modes is much more prominent for the baseline frames than for the PBPD frames.

Further, it should be noted that the Newmark and Hall's idealized R_μ - μ_s - T inelastic spectra as described in Chapter 3 were used. Those spectra were developed to represent response for a wide range of ground motions. The accuracy of results from the energy spectrum method could be improved by using more specific R_μ - μ_s - T spectra for the ground motions used in this study.

It is also worth noting that the interstory drifts calculated by the energy spectrum method are in excellent agreement with those obtained from the dynamic analyses for baseline and PBPD frames. The agreement is better for the PBPD frames. The results also

show that the mean maximum interstory drifts of the PBPD frames are well within the corresponding target values, i.e., 2% for 2/3 MCE and 3% for MCE.

7.5. Summary and conclusions

Seismic evaluation of structures generally involves determination of displacement demands from which story drifts, and component forces and deformations for specified hazard levels can be obtained for comparison with available capacities. A number of methods have been proposed by investigators in the past some of which are also used in current practice, such as MPA, FEMA 440, and Capacity Spectrum. The basic work-energy equation used in the PBPD method for determination of design base shear for new structures can also be used for seismic evaluation purposes where the goal is to determine expected displacement demand for a given structure and earthquake hazard. The results of 4, 8, 12 and 20-story baseline and PBPD RC moment frames as presented in this chapter showed excellent agreement with those obtained from more elaborate inelastic time-history analyses. In summary, the energy spectrum method can be considered as a good and easy evaluation tool for prediction of approximate displacement demand, including interstory drift and deformed shape, of a given structure.

CHAPTER 8

SUMMARY AND CONCLUSIONS

8.1. General

This study is analytical in nature involving further development of the PBPD methodology for most common reinforced concrete framing type i.e., moment frame, performing the design work, and validating the results by performing nonlinear static and time-history analyses. The following major components of the study are listed below:

1. Modeling of reinforced concrete members
2. Determination of design base shear
3. Formulation of design procedure
4. Validation through inelastic static and dynamic analyses
5. Energy spectrum method for seismic evaluation

8.2. Summary

The PBPD method is a direct design method which uses pre-selected target drift and yield mechanism as key performance objectives, which determine the degree and distribution of expected structural damage. The design base shear for a specified hazard level is calculated by equating the work needed to push the structure monotonically up to the target drift to the energy required by an equivalent EP-SDOF to achieve the same state. Plastic

design is performed to detail the frame members in order to achieve the intended yield mechanism and behavior.

By modifying the method for determination of design base shear due to "pinched" hysteretic behavior and P-Delta effect, the PBPD method was developed and successfully applied to the design of RC moment frames. The 4, 8, 12 and 20-story baseline frames used in FEMA P695 (2009) study were redesigned by the modified PBPD method. Then the PBPD frames and the baseline frames were subjected to extensive inelastic pushover and time-history analyses with the same software (PERFORM 3D) for comparison of response and performance evaluation purposes.

From the results of nonlinear static pushover and dynamic analyses it was found that the story drifts of the PBPD frames were more evenly distributed over the height as compared with those of the baseline frames where undesirable "softness" in the lower stories was evident, which is caused mainly by plastic hinges in the columns. Formation of plastic hinges in the columns and story mechanism in the lower part of the baseline frames could be clearly noticed. The PBPD frames responded as intended in design with much improved performances over those of the corresponding baseline frames.

Furthermore, PBPD lateral force distribution also showed excellent agreement with maximum relative story shear distributions obtained from time history analyses in baseline as well as PBPD frames, particularly for taller frames.

In addition, the basic work-energy equation used in the PBPD method for determination of design base shear for new structures can also be used for seismic evaluation purposes where the goal is to determine expected displacement demand for a given structure and earthquake hazard. The results of 4, 8, 12 and 20-story baseline and PBPD RC moment frames showed excellent agreement with those obtained from more elaborate inelastic time-history analyses. That is, the energy spectrum method can be considered as a good and easy evaluation tool for prediction of approximate displacement demand, including interstory drift and deformed shape of a given structure.

8.3. Conclusions

Following main conclusions are drawn from this study:

1. The PBPD design procedure is easy to follow and can be readily incorporated within the context of broader performance-based design framework given in the FEMA-445.

2. Without cumbersome and time-consuming iteration in current conventional elastic design procedures, the PBPD method is a direct design method, which requires little or no evaluation after the initial design because the nonlinear behavior and key performance criteria are built into the design process from the start.

3. Since stiffness degradation and strength deterioration are the major characteristics of typical RC SMF hysteretic behavior, C_2 factor is selected for modification of target design drift. C_2 factor method is based on consideration of the effect of degrading hysteretic behavior on peak (target) displacement. By converting target design drift by the C_2 factor to an equivalent non-degrading system, the design base shear for RC SMF can be reasonably determined.

4. Due to strength degradation at beam plastic hinges of RC SMF, it is necessary to include P-Delta effect in the determination of required moment capacity of beams, particularly for taller frames.

5. In terms of column design in the first story, in order to ensure column base plastic hinge formation as desired, the required moment strength of the first story columns should be taken as M_{u-bot} instead of M_{u-top} even when $M_{u-bot} < M_{u-top}$. The formation of plastic hinge at the column base can help distribute the deformation better along the height of the frame.

6. Although OpenSees, which was used in FEMA P695 study, is considered to be more accurate to model the hysteretic characteristics, the nonlinear axial-flexural interaction was not considered in the plastic hinge models. In contrast, axial-flexural

interaction was quite accurately modeled in the formulation of column elements in this study by using PERFORM 3D program.

7. The results of nonlinear static pushover and dynamic analyses showed that the PBPD frames responded as intended in design with much improved performances over those of the corresponding baseline frames.

8. The strong column-weak beam (SCWB) design provision as used in the current practice is not adequate to prevent localized story mechanisms. In comparison, the use of "column tree" concept to achieve strong column-weak beam yield mechanism gave excellent results as expected.

9. Better distribution of strength of beams and capacity design for columns using "column tree" concept are an effective way to help prevent formation of soft story mechanisms.

10. The lateral force distribution factors used in the PBPD method agreed very well with the relative distributions of the maximum story shears induced by the selected ground motions. On the contrary, maximum story shear distributions as given in the codes, which are based on first-mode elastic behavior, deviated significantly from the time-history dynamic analysis results. Higher mode effects are also well reflected in the PBPD design lateral force distribution.

11. The energy spectrum method showed excellent agreement with the results of inelastic time-history analyses. It can be considered as a good and easy evaluation tool for prediction of approximate displacement demand, including interstory drift and deformed shape, of a given structure.

12. The PBPD method can be successfully applied to the design of RC SMF.

8.4. Suggestions for future study

1. The modified PBPD design procedure for RC SMF as developed in this study should be further validated by more parametric studies, including different frame types (e.g., perimeter frames), various target drifts and soil types.

2. It was assumed in this study that the idealized $R_\mu - \mu_s - T$ inelastic spectra by Newmark and Hall for EP-SDOF systems are also valid for MDOF systems. This needs further study.

3. More accurate model of flexural plastic hinge which considers both axial-flexural interaction and more precise hysteretic characteristics would be desirable for future analyses.

4. The modal shape of higher mode is significant for taller structures. P-Delta effect in the determination of required moment capacity of beams may be overestimated since the inclusion of P-Delta effect in this study was based on first mode shape (linear deformation pattern). Further refinement is needed for taller frames where higher modes can influence the deflected shape significantly.

5. A computer program to perform the entire design process would be helpful for practical design office use.

6. The PBPD design methodology should be extended to other RC structural systems, such as shear wall buildings.

7. Energy spectrum method can be further improved by using modal pushover analysis.

BIBLIOGRAPHY

1. ACI Committee 318, "Building Code Requirements for Reinforced Concrete and Commentary (ACI318-08/ACI318R-08)," American Concrete Institute, Detroit, 2008.
2. Altoontash, A., "Simulation and Damage Models for Performance Assessment of Reinforced Concrete Beam-Column Joints," Dissertation, Department of Civil and Environmental Engineering, Stanford University, 2004.
3. ASCE. "Minimum Design Loads for Buildings and Other Structures (ASCE 7-05)." American Society of Civil Engineers, Reston, Virginia, 2005.
4. ASCE, "Seismic Rehabilitation of Existing Buildings," ASCE/SEI 41-06, American Society of Civil Engineers, 2006.
5. Aschheim, M., and Black, E. F., "Yield Point Spectra for Seismic Design and Rehabilitation," Earthquake Spectra, 16 (2), 2000, pp. 317-335.
6. Aschheim, M., "A Pragmatic Approach for Performance-Based Seismic Design," Performance-Based Seismic Design Concepts and Implementation, Proceedings of The International Workshop, Bled, Slovenia, 28 June-1 July, 2004 and PEER Report 2004/05, September 2004, pp. 481-492.
7. Bondy, K. D., "A more Rational Approach to Capacity Design of Seismic Moment Frame Columns," Earthquake Spectra, 12 (3), 1996, pp. 395-406.
8. Browning, J., Li, R., Lynn, A., and Moehle, J. P., "Performance Assessment for a Reinforced Concrete Frame Building," EERI Spectra, V. 16, No. 3, August 2000, pp. 541-555.
9. Building Seismic Safety Council (BSSC), "National Earthquake Hazard Reduction Program (NEHRP) Recommended Provisions for Seismic Regulations for New Buildings and Other Structures—Part 1: Provisions (FEMA 450-1)," Federal Emergency Management Agency, Washington, D. C., 2003a.
10. Building Seismic Safety Council (BSSC), "National Earthquake Hazard Reduction Program (NEHRP) Recommended Provisions for Seismic Regulations for New Buildings and Other Structures—Part 2: Commentary (FEMA 450-2)," Federal Emergency Management Agency, Washington, D. C., 2003b.
11. Building Seismic Safety Council (BSSC), "NEHRP Recommended Provisions: Design Examples (FEMA 451)," Federal Emergency Management Agency, Washington, D. C., 2006.

12. Chadwell, C.B., Imbsen & Associates, "XTRACT-Cross Section Analysis Software for Structural and Earthquake Engineering". http://www.imbsen.com/xtract.htm, 2002

13. Chao, S.-H., and Goel, S. C., "Performance-Based Seismic Design of EBF Using Target Drift and Yield Mechanism as Performance Criteria," Report No. UMCEE 05-05, Department of Civil and Environmental Engineering, University of Michigan, Ann Arbor, MI., 2005.

14. Chao, S.-H., and Goel, S. C., "Performance-Based Design of Eccentrically Braced Frames Using Target Drift and Yield Mechanism," AISC Engineering Journal, 3rd Quarter, 2006, pp. 173-200., 2006a.

15. Chao, S.-H., and Goel, S.C., "Performance-Based Plastic Design of Seismic Resistant Special Truss Moment Frames (STMF)", Report No. UMCEE 06-03, Department of Civil and Environmental Engineering, University of Michigan, Ann Arbor, MI., 2006b.

16. Chao, S.-H., and Goel, S.C., "A Seismic Design Method for Steel Concentric Braced Frames (CBF) for Enhanced Performance," Paper No. 227, 4th International Conference on Earthquake Engineering, Taipei, Taiwan, October 12-13, 2006c.

17. Chao, S.-H., Goel, S. C., and Lee, S.-S., "A Seismic Design Lateral Force Distribution Based on Inelastic State of Structures," Earthquake Spectra, Earthquake Engineering Research Institute, Vol. 23, No. 3, August 2007, pp. 547-569., 2007.

18. Chao, S.-H., and Goel, S. C., "A Modified Equation for Expected Maximum Shear Strength of the Special Segment for Design of Special Truss Moment Frames," AISC Engineering Journal, second quarter, pp. 117-125, 2008a.

19. Chao, S.-H., and Goel, S. C., "Performance-Based Plastic Design of Special Truss Moment Frames," AISC Engineering Journal, second quarter, pp. 127-150, 2008b.

20. Comartin, C. D., "Applications of Performance-Based Engineering to Risk Management Decisions," Performance-Based Seismic Design Concepts and Implementation, Proceedings of The International Workshop, Bled, Slovenia, 28 June-1 July, 2004 and PEER Report 2004/05, September 2004, pp. 101-112.

21. Comité Euro-International du Béton (CEB), "RC Frames Under Earthquake Loading State of the Art Report," Comité Euro-International du Bénton, Convenor Michael N. Fardis, Published by Thomas Telford, LondonM 1996.

22. Cornell, A., "Hazard, Ground Motions and Probabilistic Assessments for PBSD," Performance-Based Seismic Design Concepts and Implementation, Proceedings of The International Workshop, Bled, Slovenia, 28 June-1 July, 2004 and PEER Report 2004/05, September 2004, pp. 39-52.

23. CSI, "PERFORM-3D v.4.0 User Manual." Computers & Structures Inc, 2007

24. Dasgupta, P., Goel, S.C., and Parra-Montesinos, G., "Performance-Based Seismic Design and Behavior of a Composite Buckling Restrained Braced Frame (BRBF)", Paper No. 497, Proceedings of 13 WCEE, Vancouver, BC, August 1-6, 2004.

25. Deierlein, G. G., "Overview of A Comprehensive Framework for Earthquake Performance Assessment," Performance-Based Seismic Design Concepts and

Implementation, Proceedings of The International Workshop, Bled, Slovenia, 28 June-1 July, 2004 and PEER Report 2004/05, September 2004, pp. 15-26.

26. Deierlein, G. G., Liel, A. B., Haselton, C. B., and Kircher, C. A., "Assessing Building System Collapse Performance and Associated Requirements for Seismic Design," SEAOC Convention Proceedings, September 26-29, 2007, Squaw Creek, California, pp. 43-56.
27. Dooley, K. L., and Bracci, J. M., "Seismic Evaluation of Column-to-Beam Strength Ratios in Reinforced Concrete Frames," ACI Structural Journal, V. 98, No. 6, November-December, 2001, pp. 843-851.
28. Eberhard, M. O., and Sozen, M. A., "Experiments and Analyses to Study the Seismic Response of Reinforced Concrete Frame-Wall Structures with Yielding Columns," Structural Research Series No. 548, Civil Engineering Studies, University of Illinois, Urbana, I11., 1989, 128 pp.
29. Englekirk, R. E., 2003, "Seismic Design of Reinforced and Precast Concrete Buildings", John Wiley & Sons, Inc., Hoboken, New Jersey.
30. FEMA, "Recommended Seismic Evaluation and Upgrade Criteria for Existing Welded Steel Moment Frame Buildings—FEMA 351," Federal Emergency Management Agency, Washington D.C., 2000.
31. FEMA, "Prestandard and Commentary for the Seismic Rehabilitation of Buildings", Report No. FEMA 356, Washington, DC., 2000.
32. FEMA, NEHRP Recommended Provisions for Seismic Regulations for New Buildings and Other Structures, FEMA 450, Part 2: Commentary, Federal Emergency Management Agency, Washington, D.C., 2003.
33. FEMA, "Next-Generation Performance-Based Seismic Design Guidelines: Program Plan for New and Existing Buildings," FEMA-445, Washington, D. C., August 2006.
34. FEMA, "Improvement of Nonlinear Static Seismic Analysis Procedures." FEMA 440, Federal Emergency Management Agency, Washington D.C., 2008.
35. FEMA, "Quantification of Building Seismic Performance Factors (ATC-63 Project)," FEMA P695, Federal Emergency Management Agency, Washington D.C., 2009.
36. FEMA, "Effects of Strength and Stiffness Degradation on Seismic Response (ATC-62 Project)," FEMA P440A, Federal Emergency Management Agency, Washington D.C., 2009.
37. Goel, S. C., Leelataviwat, S., Lee, S.-S., and Chao, S.-H., "Theoretical Justification of Performance-Based Plastic Design and Evaluation Method for Earthquake-Resistant Structures," Earthquake Spectra (under review), 2008.
38. Goel, S. C., and Chao, S.-H., "Performance-Based Plastic Design—Earthquake Resistant Steel Structures," International Code Council (ICC), 2009, 261 pp
39. Goel, S. C., Liao, W.-C., Mohammad, R. B and Chao, S.-H, "Performance-based plastic design (PBPD) method for earthquake-resistant structures: an overview", The Structural Design of Tall and Special Buildings, CTBUH, 2009[a]

40. Goel, S. C., Liao, W.-C., Mohammad, R. B, and Leelataviwat, S., "An Energy Spectrum Method for Seismic Evaluation of Structures", Conference on improving the seismic performance of existing buildings and other structures, ATC & SEI Conference, San Francisco, CA., 2009[b]

41. Hamburger, R. O., "Development of Next-Generation Performance-Based Seismic Design Guidelines," Performance-Based Seismic Design Concepts and Implementation, Proceedings of The International Workshop, Bled, Slovenia, 28 June-1 July, 2004 and PEER Report 2004/05, September 2004, pp. 89-100.

42. Haselton, C. B. and Deierlein, G. G., "Assessing Seismic Collapse Safety of Modern Reinforced Concrete Moment Frame Buildings," Report No. 156, The John, A. Blume Earthquake Engineering Center, Department of Civil and Environmental Engineering, Stanford University, February 2007.

43. Ibarra, L.F., Medina, R.A., and Krawinkler, H., "Hysteretic models that incorporate strength and stiffness deterioration," Earthquake Engineering and Structural Dynamics, Vol. 34, pp. 1489-1511, 2005.

44. Krawinkler, H., and Miranda, E., "Performance-Based Earthquake Engineering," Earthquake Engineering—from Engineering Seismology to Performance-Based Engineering, Edited by Bozorgnia, Y. and Bertero, V. V., CRC Press, 2004.

45. Kuntz, G. L., and Browning, J., "Reduction of Column Yielding During Earthquakes for Reinforced Concrete Frames," ACI Structural Journal, V. 100, No. 5, September-October, 2003, pp. 573-580.

46. Lee, S.-S., and Goel, S. C., "Performance-Based Design of Steel Moment Frames Using Target Drift and Yield Mechanism," Report No. UMCEE 01-17, Department of Civil and Environmental Engineering, University of Michigan, Ann Arbor, MI., 2001.

47. Lee, S.-S., Goel, S. C., and Chao, S.-H., "Performance-Based Design of Steel Moment Frames Using Target Drift and Yield Mechanism," Proceedings, 13th World Conference on Earthquake Engineering, Paper No. 266, Vancouver, B. C., Canada., 2004.

48. Leelataviwat, S., Goel, S. C., and Stojadinović, B., "Toward Performance-Based Seismic Design of Structures," Earthquake Spectra, Vol. 15, No. 3, 1999, pp. 435-461.

49. Leelataviwat, S., Saewon, W., and Goel, S.C., "An Energy Based Method for Seismic Evaluation of Structures." Proceedings of Structural Engineers Association of California Convention SEAOC 2007, Lake Tahoe, California, 21-31.

50. Liao, W.-C. and Goel S. C., "Performance-Based Plastic Design (PBPD) of Reinforced Concrete Special Moment Frame Structures", The 3rd Congress of the International Federation for Structural Concrete (fib), Washington DC, 2010[a]

51. Liao, W.-C. and Goel S. C., "Performance-Based Plastic Design (PBPD) of Reinforced Concrete Special Moment Frame Structures", 9th US National and 10th Canadian Conference on Earthquake Engineering (9USN/10CCEE), Toronto, Canada, 2010[b]

52. Medina, R.A., “Seismic Demands for Nondeteriorating Frame Structures and Their Dependence on Ground Motions,” Ph.D. Dissertation, Department of Civil and Environmental Engineering, Stanford University, 2002.

53. Miranda, E. and Bertero, V. V., “Evaluation of Strength Reduction Factors for Earthquake-Resistant Design.” Earthquake Spectra, Vol. 10, No. 2, 2004, pp. 357-379

54. Moehle J. P., Hooper, J. D. and Lubke C. D., “Seismic Design of Reinforced Concrete Special Moment Frames: A Guide for Practicing Engineers,” NEHRP Seismic Design Technical Brief No. 1. 2008.

55. Moehle J. P. and Mahin S. A., “Observations on the Behavior of Reinoforced Concrete Buildings during Earthquakes,” American Concrete Institute publication SP-127, Earthquake-Resistant Concrete Structures - Inelastic Response and Design, (S.K.Ghosh, editor), 1991.

56. Newmark, N. M., and Hall, W. J., “Earthquake Spectra and Design,” Earthquake Engrg. Res. Inst., El Cerrito, California, 1982.

57. Panagiotou, M. and Restrepo, J. I., "A modification of the equivalent lateral force procedure for use in performance based seismic design of high rise buildings," 12th U.S.-Japan Workshop on Structural design and Construction Practices, September 10 - 12, Hawaii, 2007.

58. PEER, Pacific Earthquake Engineering Research Center: PEER NGA Database,University of California, Berkeley, http://peer.berkeley.edu/nga/, 2006.

59. Priestley, M. J. N., Calvi, G. M., and Kowalsky, M. J., “Displacement-Based Seismic Design of Structures,” IUSS Press, Pavia, Italy, 2007, 720 pp.

60. Sabelli, R., “Research on Improving the Design and Analysis of Earthquake Resistant Steel Braced Frames,” FEMA/EERI Report, 2000.

61. Sabelli, R., Mahin, S., and Chang, C., “Seismic Demands on Steel Braced Frame Buildings with Buckling-Restrained Braces,” Engineering Structures, Vol. 25, 2003, pp. 655-666.

62. Scribner, C. F., and Wight, J. K., “Strength decay in R.C. beams under load reversals.” Journal of the Structural Division. Div., 106 (4), 1980, 861–876.

63. SEAOC., “Vision 2000—Performance Based Seismic Engineering of Buildings,” Structural Engineers Association of California, Sacramento, California, 1995.

64. Shibata, A., and Sozen, M., “Substitute Structure Method for Seismic Design in Reinforced Concrete,” Journal of Structural Engineering, American Society of Civil Engineers, V. 102, No. 12, pp. 3548-3566.

65. Villaverde, R., “Explanation for The Numerous Upper Floor Collapses During The 1985 Mexico City Earthquake,” Earthquake Engineering and Structural Dynamics, 20 (8), 1991, pp. 223-241.

66. Villaverde, R., “Discussion of “A More Rational Approach to Capacity Design of Seismic Moment Frame Columns”, Earthquake Spectra, 13 (2), 1997, pp. 321-322.

67. Wight, J. K., and Sozen, M. A., “Strength decay of RC columns under shear reversals.” Journal of the Structural Division. Div., 101 (5), 1975, pp. 1053–1065.